EPIGENETIC REGULATION IN RENAL DEVELOPMENT, PHYSIOLOGY AND DISEASE

EDITED BY: Xiao-ming Meng and Haiyong Chen
PUBLISHED IN: Frontiers in Physiology, Frontiers in Genetics and Frontiers in Cell and Developmental Biology

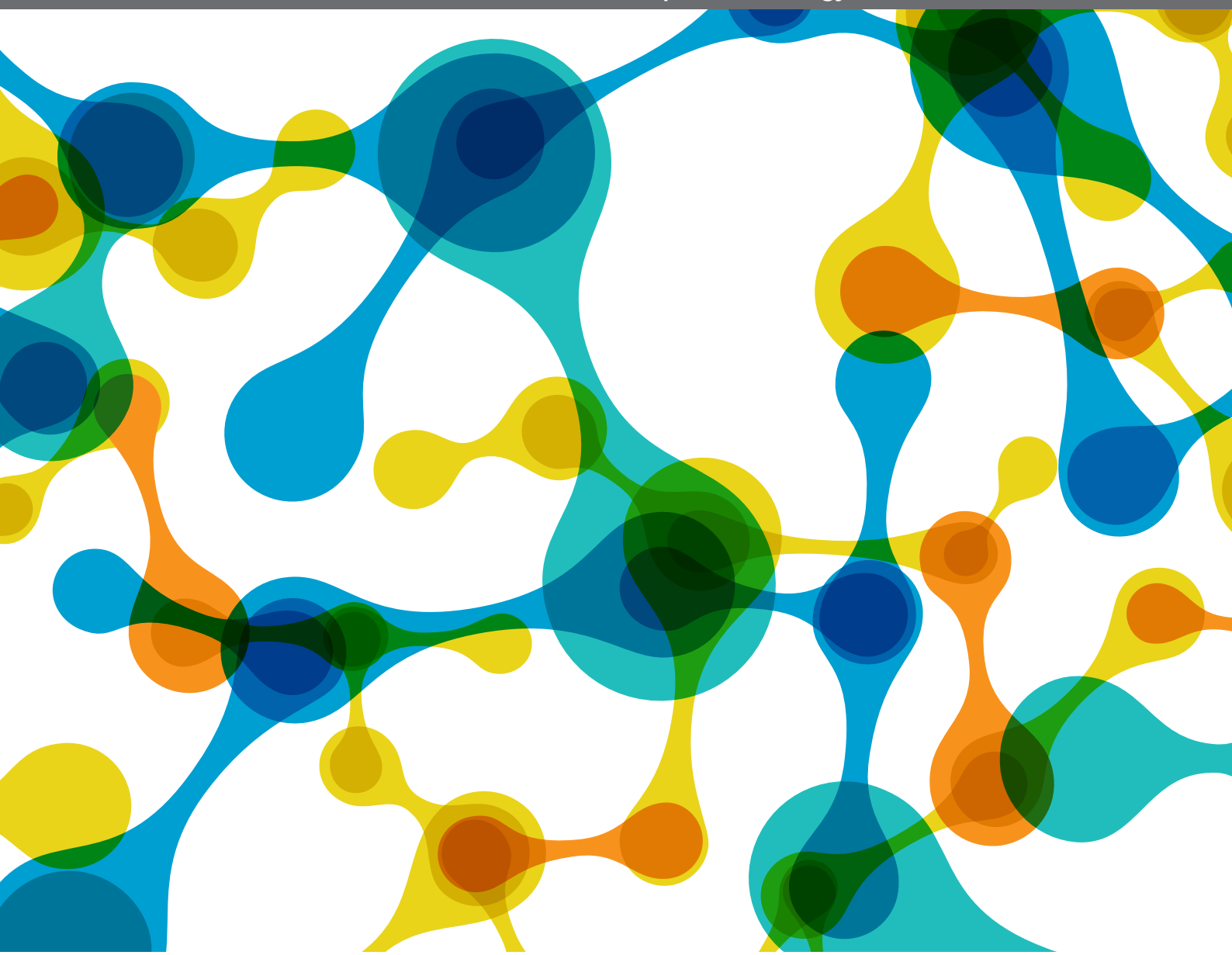

frontiers Research Topics

frontiers

ISSN 1664-8714
ISBN 978-2-88974-396-4
DOI 10.3389/978-2-88974-396-4

About Frontiers

Frontiers is more than just an open-access publisher of scholarly articles: it is a pioneering approach to the world of academia, radically improving the way scholarly research is managed. The grand vision of Frontiers is a world where all people have an equal opportunity to seek, share and generate knowledge. Frontiers provides immediate and permanent online open access to all its publications, but this alone is not enough to realize our grand goals.

Frontiers Journal Series

The Frontiers Journal Series is a multi-tier and interdisciplinary set of open-access, online journals, promising a paradigm shift from the current review, selection and dissemination processes in academic publishing. All Frontiers journals are driven by researchers for researchers; therefore, they constitute a service to the scholarly community. At the same time, the Frontiers Journal Series operates on a revolutionary invention, the tiered publishing system, initially addressing specific communities of scholars, and gradually climbing up to broader public understanding, thus serving the interests of the lay society, too.

Dedication to Quality

Each Frontiers article is a landmark of the highest quality, thanks to genuinely collaborative interactions between authors and review editors, who include some of the world's best academicians. Research must be certified by peers before entering a stream of knowledge that may eventually reach the public - and shape society; therefore, Frontiers only applies the most rigorous and unbiased reviews.
Frontiers revolutionizes research publishing by freely delivering the most outstanding research, evaluated with no bias from both the academic and social point of view. By applying the most advanced information technologies, Frontiers is catapulting scholarly publishing into a new generation.

What are Frontiers Research Topics?

Frontiers Research Topics are very popular trademarks of the Frontiers Journals Series: they are collections of at least ten articles, all centered on a particular subject. With their unique mix of varied contributions from Original Research to Review Articles, Frontiers Research Topics unify the most influential researchers, the latest key findings and historical advances in a hot research area! Find out more on how to host your own Frontiers Research Topic or contribute to one as an author by contacting the Frontiers Editorial Office: frontiersin.org/about/contact

EPIGENETIC REGULATION IN RENAL DEVELOPMENT, PHYSIOLOGY AND DISEASE

Topic Editors:
Xiao-ming Meng, Anhui Medical University, China
Haiyong Chen, The University of Hong Kong, Hong Kong, SAR China

Citation: Meng, X.-m., Chen, H., eds. (2022). Epigenetic Regulation in Renal Development, Physiology and Disease. Lausanne: Frontiers Media SA.
doi: 10.3389/978-2-88974-396-4

Table of Contents

frontiers in Physiology

EDITORIAL
published: 05 January 2022
doi: 10.3389/fphys.2021.818190

Editorial: Epigenetic Regulation in Renal Development, Physiology and Disease

Juan Jin[1,2], *Haiyong Chen*[3]* *and Xiao-Ming Meng*[1]*

[1] Inflammation and Immune Mediated Diseases Laboratory of Anhui, The Key Laboratory of Anti-inflammatory of Immune Medicines, Ministry of Education, School of Pharmacy, Anhui Institute of Innovative Drugs, Anhui Medical University, Hefei, China, [2] School of Basic Medicine, Anhui Medical University, Hefei, China, [3] Li Ka Shing Faculty of Medicine, School of Chinese Medicine, The University of Hong Kong, Pokfulam, Hong Kong SAR, China

Keywords: epigenetics, DNA methylation, histone modification, N6-methyladenosine (m6A) RNA methylation, long non-coding RNAs

Editorial on the Research Topic

Epigenetic Regulation in Renal Development, Physiology and Disease

Epigenetic mechanisms regulate heritable phenotype changes without altering DNA sequence. In this manner, fine-tuning of biological processes is usually achieved in response to environmental stimuli. Epigenetic regulations not only contribute to kidney physiological functions but also kidney diseases (Guo et al., 2019). This Research Topic aimed to summarize the current knowledge of epigenetic modifications on renal development, physiology and pathology in kidneys, as well as epigenetic regulations on cellular metabolism, inflammation and apoptosis, and intracellular signals.

Epigenetic regulations involve covalent modification of DNA or histone proteins, and RNA interference by non-coding RNAs which modulate gene/protein expression. DNA methylation is a common type of epigenetic modification that reversibly affects gene expression without changes in the sequence of nucleotides (Ginder and Williams, 2018; Grimm et al., 2019). Chen et al. recently demonstrated that DNA methylation occurring in peripheral immune cells profoundly contributes to development of kidney diseases (Mok et al., 2016; Chen et al., 2019; Klumper et al., 2020). Chen et al. reviewed that change of DNA methylation sustains for a long time in immune cells and modulates gene expression in the circulating immune cells even after the cells migrate from the circulation into the affected kidney. The aberrant DNA methylation in the immune cells was summarized in different kidney diseases, including lupus nephritis, IgA nephropathy, hypertensive nephropathy, and diabetic kidney diseases. Potential treatment of CKD targeting on DNA methylation is highlighted in the article.

Histones are highly conserved proteins with positive charge which package with negatively charged DNA into highly condensed and ordered chromatin structure units called nucleosomes (Kimura, 2013). Methylation is one of the major forms of histone modification (Kooistra and Helin, 2012). Li et al. focused on the functions of a histone methyltransferase in renal diseases. They thoroughly reviewed histone methyltransferase EZH2 that catalyzes the addition of methyl groups to histone H3 at lysine 27 and leads to gene silencing in different kidney injuries, such as acute kidney injury (AKI), renal fibrosis, diabetic nephropathy, lupus nephritis, and renal transplantation rejection. Their article summarizes the pathological roles of EZH2 in kidney diseases and highlights EZH2 as a potential therapeutic target for kidney diseases.

Epigenetic changes of functional proteins could serve as epigenetic markers to predict the progression and prognosis of a disease progression. You et al. identified a set of clinically relevant

OPEN ACCESS

Edited and reviewed by:
Carolyn Mary Ecelbarger, Georgetown University, United States

***Correspondence:**
Haiyong Chen
haiyong@hku.hk
Xiao-Ming Meng
mengxiaoming@ahmu.edu.cn

Specialty section:
This article was submitted to Renal and Epithelial Physiology, a section of the journal Frontiers in Physiology

Received: *19 November 2021*
Accepted: *10 December 2021*
Published: *05 January 2022*

Citation:
Jin J, Chen H and Meng X-M (2022) Editorial: Epigenetic Regulation in Renal Development, Physiology and Disease. Front. Physiol. 12:818190. doi: 10.3389/fphys.2021.818190

cancer-associated fibroblasts-related methylation-driven genes, NAT8, TINAG, and SLC17A1 in kidney renal clear cell carcinoma (KIRC). Methylation levels of these genes are highly correlated with the severity of KIRC. Methylation levels of the gene panel could be used as promising biomarkers to predict the progression and prognosis of KIRC.

N6-methyladenosine (m6A) is the most abundant modification which regulates post-transcriptional RNA on mRNAs. It is involved in various physiological and pathological processes, such as metabolism, inflammation, and apoptosis. Shen et al. presented that differentially m6A methylated genes are enriched in cisplatin-induced kidney injury and berberine, a chemical compound, attenuates AKI by regulating differentially methylated genes. Shi et al. indicated that variability of m6A methyltransferase METTL3 is significantly increased in clear cell renal cell carcinoma (ccRCC) which regulates translation of ABCD1, an ATP-binding cassette (ABC) transporter of fatty acids, in an m6A-dependent manner. Thus, METTLE3 promotes ccRCC progression via m6A modification-mediated translation of ABCD1. METTL3, as an m6A methyltransferase, plays an essential role in the development and progression of diseases. Nevertheless, m6A modifications by METTL3 in kidney diseases remain largely unclear. Comprehensive and systematic functions of METTL3 on post-translational modifications could be explored by conditional knockout of METTL3 from kidney in mice with kidney disease models, since METTL3 knockout mouse is embryonic lethal (Geula et al., 2015). These findings should be further verified in clinics. Specific METTL3 inhibitors may be developed for the relevant kidney diseases.

Epigenetic regulation also involves RNA interference by non-coding RNAs. Long non-coding RNAs (LncRNA) are previously reported to be regulators for multiple cellular processes and disease progresses, e.g., cell differentiation, cell proliferation, and apoptosis (Wang et al., 2017; Villa et al., 2019). Yuan et al. verified that downregulation of LncRNA H19 promotes cell proliferation, inhibits cell apoptosis, and suppresses multiple inflammatory cytokine expressions in hypoxia/reoxygenation-treated human renal proximal tubular cells by regulating the miR-130a/BCL2L11 pathway. Deng et al. also demonstrated LncRNA *MEG3* is involved in pyroptosis of renal proximal tubular cells (TECs) in lipopolysaccharide-induced AKI by regulating the miR-18a-3p/GSDMD pathway. This study showed that LncRNA might display an critical role in the pathogenesis of sepsis-related AKI through regulating pyroptosis of TECs.

In sum, epigenetic mechanisms including modification of DNA, histone proteins, or RNA interference by non-coding RNAs are designated as biochemical switches which turn on/off gene expression without affecting the DNA sequence. The manuscripts in this Research Topic provide a broad overview of the latest research investigating epigenetic regulation and relevant therapeutic potentials for diagnosis and treatments of renal diseases.

AUTHOR CONTRIBUTIONS

All authors listed have made a substantial, direct, and intellectual contribution to the work and approved it for publication.

FUNDING

This work was supported by the National Natural Science Foundation of China (Grant Nos. 81970584 and 82100727), Promotion plan of basic and clinical cooperative research in Anhui Medical University (Grant Nos. 2019xkjT014 and 2020xkjT016), the Open Fund of Inflammation and Immune Mediated Diseases Laboratory of Anhui Province (Grant No. IMMDL202002), and Provincial Natural Science Foundation (Grant No. 1908085QH377).

REFERENCES

Chen, G., Chen, H., Ren, S., Xia, M., Zhu, J., Liu, Y., et al. (2019). Aberrant DNA methylation of mTOR pathway genes promotes inflammatory activation of immune cells in diabetic kidney disease. *Kidney Int.* 96, 409–420. doi: 10.1016/j.kint.2019.02.020

Geula, S., Moshitch-Moshkovitz, S., Dominissini, D., Mansour, A. A., Kol, N., Salmon-Divon, M., et al. (2015). Stem cells. m6A mRNA methylation facilitates resolution of naive pluripotency toward differentiation. *Science* 347, 1002–1006. doi: 10.1126/science.1261417

Ginder, G. D., and Williams, D. C. Jr. (2018). Readers of DNA methylation, the MBD family as potential therapeutic targets. *Pharmacol. Ther.* 184, 98–111. doi: 10.1016/j.pharmthera.2017.11.002

Grimm, S. A., Shimbo, T., Takaku, M., Thomas, J. W., Auerbach, S., Bennett, B. D., et al. (2019). DNA methylation in mice is influenced by genetics as well as sex and life experience. *Nat. Commun.* 10:305. doi: 10.1038/s41467-018-08067-z

Guo, C., Dong, G., Liang, X., and Dong, Z. (2019). Epigenetic regulation in AKI and kidney repair: mechanisms and therapeutic implications. *Nat. Rev. Nephrol.* 15, 220–239. doi: 10.1038/s41581-018-0103-6

Kimura, H. (2013). Histone modifications for human epigenome analysis. *J. Hum. Genet.* 58, 439–445. doi: 10.1038/jhg.2013.66

Klumper, N., Ralser, D. J., Bawden, E. G., Landsberg, J., Zarbl, R., Kristiansen, G., et al. (2020). LAG3 (LAG-3, CD223.) DNA methylation correlates with LAG3 expression by tumor and immune cells, immune cell infiltration, and overall survival in clear cell renal cell carcinoma. *J. Immunother. Cancer* 8:e000552. doi: 10.1136/jitc-2020-000552

Kooistra, S. M., and Helin, K. (2012). Molecular mechanisms and potential functions of histone demethylases. *Nat. Rev. Mol. Cell Biol.* 13, 297–311. doi: 10.1038/nrm3327

Mok, A., Solomon, O., Nayak, R. R., Coit, P., Quach, H. L., Nititham, J., et al. (2016). Genome-wide profiling identifies associations between lupus nephritis and differential methylation of genes regulating tissue hypoxia and type 1 interferon responses. *Lupus Sci. Med*. 3:e000183. doi: 10.1136/lupus-2016-000183

Villa, C., Lavitrano, M., and Combi, R. (2019). Long non-coding RNAs and related molecular pathways in the pathogenesis of epilepsy. *Int. J. Mol. Sci.* 20:4898. doi: 10.3390/ijms20194898

Wang, J. Z., Xu, C. L., Wu, H., and Shen, S. J. (2017). LncRNA SNHG12 promotes cell growth and inhibits cell apoptosis in colorectal cancer cells. *Braz. J. Med. Biol. Res.* 50:e6079. doi: 10.1590/1414-431x20176079

Conflict of Interest: The authors declare that the research was conducted in the absence of any commercial or financial relationships that could be construed as a potential conflict of interest.

Publisher's Note: All claims expressed in this article are solely those of the authors and do not necessarily represent those of their affiliated organizations, or those of the publisher, the editors and the reviewers. Any product that may be evaluated in this article, or claim that may be made by its manufacturer, is not guaranteed or endorsed by the publisher.

frontiers in Physiology

ORIGINAL RESEARCH
published: 02 November 2020
doi: 10.3389/fphys.2020.579296

Extracellular Vesicles From High Glucose-Treated Podocytes Induce Apoptosis of Proximal Tubular Epithelial Cells

Ying Huang[1,2†], Ruizhao Li[2†], Li Zhang[2], Yuanhan Chen[2], Wei Dong[2], Xingchen Zhao[2], Huan Yang[2], Shu Zhang[2], Zhiyong Xie[1,2], Zhiming Ye[2], Weidong Wang[3], Chunling Li[3], Zhilian Li[2], Shuangxin Liu[2], Zheng Dong[4], Xueqing Yu[2] and Xinling Liang[1,2]**

[1]The Second School of Clinical Medicine, Southern Medical University, Guangzhou, China, [2]Division of Nephrology, Guangdong Provincial People's Hospital, Guangdong Academy of Medical Sciences, Guangzhou, China, [3]Institute of Hypertension, Zhongshan School of Medicine, Sun Yat-sen University, Guangzhou, China, [4]Department of Cellular Biology and Anatomy, Medical College of Georgia at Augusta University and Charlie Norwood Veterans Affairs Medical Center, Augusta, Georgia

OPEN ACCESS

Edited by:
Xiao-ming Meng,
Anhui Medical University, China

Reviewed by:
Lin-Li Lv,
Zhongda Hospital, Southeast University, China
Dylan Burger,
University of Ottawa, Canada

***Correspondence:**
Xueqing Yu
yuxueqing@gdph.org.cn
Xinling Liang
xinlingliang_ggh@163.com

[†]*These authors have contributed equally to this work*

Specialty section:
This article was submitted to Renal and Epithelial Physiology, a section of the journal Frontiers in Physiology

Received: *02 July 2020*
Accepted: *25 September 2020*
Published: *02 November 2020*

Citation:
Huang Y, Li R, Zhang L, Chen Y, Dong W, Zhao X, Yang H, Zhang S, Xie Z, Ye Z, Wang W, Li C, Li Z, Liu S, Dong Z, Yu X and Liang X (2020) Extracellular Vesicles From High Glucose-Treated Podocytes Induce Apoptosis of Proximal Tubular Epithelial Cells. Front. Physiol. 11:579296. doi: 10.3389/fphys.2020.579296

Diabetic kidney disease (DKD) is a serious and common complication of diabetes. Extracellular vesicles (EVs) have emerged as crucial vectors in cell-to-cell communication during the development of DKD. EVs may mediate intercellular communication between podocytes and proximal tubules. In this study, EVs were isolated from podocyte culture supernatants under high glucose (HG), normal glucose (NG), and iso-osmolality conditions, and then co-cultured with proximal tubular epithelial cells (PTECs). MicroRNAs (miRNA) sequencing was conducted to identify differentially expressed miRNAs of podocyte EVs and bioinformatics analysis was performed to explore their potential functions. The results showed that EVs secreted from HG-treated podocytes induced apoptosis of PTECs. Moreover, five differentially expressed miRNAs in response to HG condition were identified. Functional enrichment analysis revealed that these five miRNAs are likely involved in biological processes and pathways related to the pathogenesis of DKD. Overall, these findings demonstrate the pro-apoptotic effects of EVs from HG-treated podocytes on PTECs and provide new insights into the pathologic mechanisms underlying DKD.

Keywords: podocytes, proximal tubular epithelial cells, diabetic kidney disease, microRNA, extracellular vesicles

INTRODUCTION

Diabetic kidney disease (DKD) is a serious and common microvascular complication of diabetes mellitus (DM) and a primary cause of end-stage renal disease (ESRD; Tuttle et al., 2014). Although current clinical therapies and interventions can attenuate the severity of DKD, at present, there is no curative treatment as the mechanisms underlying DKD have not yet been fully described.

Podocyte injury is considered an early and crucial event in the onset and development of DKD (Li et al., 2007). Podocytes are highly differentiated cells lining the outer surface of the glomerular basement membrane that are important for the maintenance of the structure,

function, and integrity of the glomerular filtration barrier. Previous studies conducted by our team and others have shown dysfunction and depletion of podocytes under diabetic pathogenic conditions, such as hyperglycemia, increased production of glycation end-products, oxidative stress, and inflammation (Dai et al., 2017; Li et al., 2018; Zhao et al., 2018). The dysfunction and depletion of podocytes causes proteinuria (Mundel and Shankland, 2002), which is an intensive instigator of tubulointerstitial inflammation and fibrosis (Wang et al., 2000; Abbate et al., 2006; Gorriz and Martinez-Castelao, 2012). Filtered proteins induce the production of cytokines and chemokines by proximal tubular epithelial cells (PTECs), which subsequently leads to the infiltration of inflammatory cells and, ultimately, to tubulointerstitial fibrogenesis and progression to ESRD. Tubulointerstitial fibrosis is reportedly closely related to declining renal function (Nath, 1992; Taft et al., 1994). However, a number of diabetic patients progress to ESRD in the absence of proteinuria (Piscitelli et al., 2017; Viazzi et al., 2017). In addition, kidney biopsies of some DKD patients with normal albuminuria/microalbuminuria, but elevated serum creatinine, revealed severe tubular interstitial lesions with mild glomerular lesions. Therefore, apart from proteinuria, there may exist other mechanisms that mediate the crosstalk between podocytes and the proximal tubules.

Extracellular vesicles (EVs) are small membranous vesicles that released into the extracellular space by various cell types under both physiological and pathological conditions. EVs include two major categories: exosomes ranging in diameter from 30 to 150 nm and microparticles ranging in diameter from 50 to 1,000 nm (Tkach and Théry, 2016; van Niel et al., 2018). EVs have emerged as novel and crucial vectors in cell-to-cell communication *via* the delivery of bioactive molecules, which include proteins, lipids, mRNA, and MicroRNAs (miRNA), originating from parental cells (EL Andaloussi et al., 2013). Increasing evidence has revealed that EV-mediated intercellular communication plays important roles in the development of DKD. Exosomes derived from high glucose (HG)-treated glomerular endothelial cells (Wu et al., 2016, 2017), glomerular mesangial cells (Wang et al., 2018), and macrophages (Zhu et al., 2019) transfer injury information to neighboring cells, which accelerates the development of DKD. Structurally, podocytes are located on the outer surface of the glomerular capillary loops adjacent to the proximal tubules. Therefore, the proximal tubule is a likely site for the interactions of podocyte EVs (Lv et al., 2019). Also, studies have showed that EVs from podocytes can interact with PTECs and induce pro-fibrotic or apoptotic responses (Munkonda et al., 2018; Jeon et al., 2020). Thus, we proposed that under HG condition, EVs from podocytes can be internalized and exert harmful effects on PTECs.

miRNAs are small and non-coding RNAs that regulate gene expression through the repression of translation or degradation of mRNAs (Bartel, 2004). Previous evidence has demonstrated the key role of miRNA in DKD pathogenesis (Kato and Natarajan, 2015; Lu et al., 2017). EV miRNAs are emerging as critical factors involved in the pathogenesis of many diseases (Valadi et al., 2007; Zhang et al., 2015), suggesting that EV miRNAs may be novel molecular mediators of the development of DKD. The aim of the present study was to determine whether EVs derived from podocytes can be internalized and induce apoptosis of PTECs *in vitro*. Also, miRNA sequencing was performed to identify differentially expressed miRNAs in podocytes EVs in response to HG condition. In addition, bioinformatics analysis was conducted in order to explore the potential biological functions of EVs from HG-treated podocytes.

MATERIALS AND METHODS

Cell Culture and Treatment

Conditionally immortalized mouse podocytes and immortalized mouse PTECs were cultured as described previously (Li et al., 2018; Zhang et al., 2019). Podocytes were grown in Roswell Park Memorial Institute 1640 medium (Gibco BRL) supplemented with 10% fetal bovine serum (FBS; Gibco BRL) and 50 U/ml of interferon-γ (ProSpec) under an atmosphere of 5% CO_2/95% air at 33°C. Once confluence reached 70–80%, the podocytes were subcultured at 37°C in Dulbecco's modified Eagle's medium (DMEM; Gibco BRL) supplemented with 5% FBS on collagen-coated dishes for 10 days in the absence of interferon-γ to promote differentiation. Following differentiation, the podocytes were grown in serum-free DMEM for 24 h to induce quiescence. Afterward, the podocytes were cultured in DMEM supplemented with 2% exosome-depleted FBS (System Biosciences) and divided into three groups: a normal glucose group (NG-podo, 5.3 mM glucose), high-glucose group (HG-podo, 30 mM glucose), and mannitol group (MA-podo, 5.3 mM glucose + 24.7 mM mannitol; osmolality control). After 48 h of continuous treatment, the cell culture supernatants were collected for EV isolation. Mouse PTECs were cultured in DMEM/F12 (Gibco BRL) supplemented with 10% FBS under an atmosphere of 5% CO_2/95% air at 37°C and passaged every 3 days. PTECs were cultured in serum-free DMEM/F12 for 12 h to induce quiescence before being dividing into two groups: a normal glucose group (NG-PTECs) and high-glucose group (HG-PTECs). Each group was treated with podocyte EVs for 48 h.

EV Isolation

EVs from the supernatants of podocyte cultures were isolated using ExoQuick-TC Exosome Precipitation Solution (System Biosciences) in accordance with the manufacturer's recommendations. In brief, cell culture supernatants were centrifuged at 3000 × *g* for 15 min to remove cells and cellular debris. Then, the resulting supernatants were collected. Following the addition of a 20% volume of ExoQuick-TC precipitation solution, the supernatants were incubated overnight at 4°C and then centrifuged at 1500 × *g* for 30 min to pellet the EVs. The EVs were resuspended in 1× sterile phosphate-buffered saline (PBS) and stored at −80°C until use.

Transmission Electron Microscopy

Following negative staining, transmission electron microscopy (TEM) was used to reveal the morphology of the isolated EVs.

The samples were dropped onto a formvar/carbon-coated copper grid for 5 min and then stained with 4% uranyl acetate for 10 min. After drying at room temperature, EVs on the grid were imaged under a transmission electron microscope (JEM-1400 PLUS; JEOL).

Nanoparticle Tracking Analysis

Nanoparticle tracking analysis (NTA) was performed to evaluate the size distribution of the isolated EVs with the use of a NanoSight NS300 instrument (Malvern Panalytical) and the corresponding analytical software NTA version 3.3. The EVs suspension was diluted in 1 × PBS and the movement of vesicles was measured three times for a duration of 30 s each.

Western Blot Analysis

Western blot analysis was performed to detect the positive protein markers of EVs. EVs from the same cell number were used for western blotting quantification. EV samples were lysed with radioimmunoprecipitation assay buffer (Beyotime). EV proteins were separated by 9% sodium dodecyl sulfate-polyacrylamide gel electrophoresis and then transferred onto polyvinylidene fluoride membranes (EMD Millipore). After blocking with 5% non-fat milk for 1 h at room temperature, the membranes were incubated overnight at 4°C with the following primary antibodies:anti-CD63 (ab217345; dilution, 1:1,000; rabbit immunoglobulin [Ig]G; Abcam), anti-CD9 (ab92726; dilution, 1:1,000; rabbit IgG; Abcam), anti-Alix (92880; dilution, 1:1,000; rabbit IgG; Cell Signaling Technology), and anti-calnexin (ab22595; dilution, 1:1,000; rabbit IgG; Abcam). Afterward, the membranes were incubated with horseradish peroxidase-conjugated goat anti-rabbit IgG (7074; dilution, 1:3,000; Cell Signaling Technology) for 1 h at room temperature. Finally, the protein signals were detected by enhanced chemiluminescence (EMD Millipore) and visualized with an ImageQuant LAS500 instrument (GE Healthcare Bio-Sciences).

EV Uptake Experiment

EVs were labeled using the PKH67 Green Fluorescent Cell Linker Kit (Sigma-Aldrich) in accordance with the manufacturer's instructions. After incubation for 48 h with the labeled EVs, the PTECs were fixed with 4% paraformaldehyde for 30 min, then permeabilized with 0.5% Triton X-100 for 10 min, and finally stained with 4′,6-diamidino-2-phenylindole (DAPI, Sigma-Aldrich) for 10 min. The resulting fluorescent signals were observed under a confocal laser microscope (TCS-SP5; Leica Microsystems GmbH).

Flow Cytometry

Apoptotic PTECs were examined by flow cytometry using an Annexin V-FITC/propidium iodide (PI) apoptosis detection kit (Nanjing KeyGEN), as previously described (Zhang et al., 2019). Briefly, after treatment, PTECs were collected, resuspended in 500 μl of 1×binding buffer, and then stained with 5 μl of Annexin V-FITC and 5 μl of PI. Cell fluorescence was then analyzed using a BD FACSVerse™ flow cytometer (BD Biosciences).

TUNEL Staining

TUNEL staining was performed using a One-step TUNEL cell apoptosis detection kit (Nanjing KeyGEN) following the manufacturer's instructions. Cells were fixed with 4% paraformaldehyde for 30 min and permeabilized with 1% Triton X-100 for 5 min. Cell samples were then incubated with terminal deoxy-nucleotidyl transferase (TdT) enzyme reaction mixture at 37°C for 1 h, followed by incubated with streptavidin-fluorescein labeling buffer at 37°C for 30 min. Nuclei were stained with DAPI for 5 min at room temperature. The number of TUNEL-positive cells was counted under a confocal laser microscope (Nikon C2; Nikon Corporation).

miRNA Extraction and Sequencing

Total RNA of EVs from the NG-podo, MA-podo, and HG-podo groups (three replicates/group) were extracted using MagZol reagent (Magen). Library preparation, deep sequencing, and data analysis were conducted by RiboBio Co., Ltd. (Guangzhou, China). Briefly, total RNA was fractionated by gel electrophoresis and small RNAs ranging in length from approximately 18 to 40 nucleotides was used for library preparation. Sequencing was performed using an Illumina HiSeqTM 2500 instrument (Illumina). miRNA read counts were normalized using the trimmed mean of M-values normalization method and differential expression analysis was performed using edgeR package. Differentially expressed miRNAs between two groups were identified *via* $|\log_2(\text{fold change})| > 1$ and probability $p < 0.05$. Profiling of miRNA expression among samples was conducted by bidirectional hierarchical cluster analysis.

Validation of miRNAs by Quantitative Reverse Transcription-Polymerase Chain Reaction

The differentially expressed miRNAs were validated by quantitative reverse transcription-PCR (RT-qPCR). EV samples were spiked with 1 pmol cel-miR-39-3p (RiboBio Co., Ltd.) after being fully lysed by MagZol. RNA were reverse transcribed for cDNA synthesis using *Evo M-MLV* RT Kit for qPCR (Accurate Biotechnology). qPCR was performed using SYBR Green Premix *Pro Taq HS* qPCR Kit (Accurate Biotechnology) on a CFX96 Real-Time PCR System (Bio-Rad). The relative expression of miRNAs was calculated by $2^{-\Delta\Delta Ct}$ method with cel-miR-39-3p as an external reference. All the bulge-loop miRNAs RT primers and qPCR primers were purchased from RiboBio Co., Ltd. (Guangzhou, China).

Target Gene Prediction and Functional/ Pathway Enrichment Analysis

The online databases TargetScan,[1] miRDB,[2] and miRWalk[3] were used to predict differentially expressed miRNAs. To improve the accuracy of prediction, only genes that were predicted in all three databases were selected as target genes for further analysis.

[1]http://www.targetscan.org/
[2]http://www.mirdb.org/
[3]http://mirwalk.umm.uni-heidelberg.de/

The common genes were visualized using the online tool Draw Venn Diagram.[4] Then, the online database DAVID (Database for Annotation Visualization and Integrated Discovery) was used for Gene Ontology (GO) enrichment analysis and Kyoto Encyclopedia of Genes and Genomes (KEGG) pathway enrichment analysis based on predicted target genes.[5] A value of $p < 0.05$ was considered statistically significant.

Statistical Analysis

The results are presented as the mean ± standard error of the mean. Statistical analysis was performed using IBM SPSS Statistics for Windows, version 22.0 (IBM). The Student's *t*-test was used for comparisons between two groups. One-way analysis of variance and the least significant difference test were used for multiple comparisons among the groups. A value of $p < 0.05$ was considered statistically significant.

RESULTS

EV Characterization

TEM, NTA, and western blot analysis were used to confirm the presence of EVs (Théry et al., 2018). EVs were extracted from the cell culture supernatants of approximately 3.6×10^6 podocytes that treated with NG, MA, and HG stimulation. The TEM images presented in **Figure 1A** show that the membrane-bound vesicles were round with typical sizes ranging from 50 to 200 nm. As shown in **Figure 1B**, the results of NTA revealed a broad distribution of vesicle sizes with a mean diameter of approximately 150 nm. Moreover, western blot analysis confirmed the presence of the EV markers Alix, CD9, and CD63, as well as the absence of Calnexin, which is a protein marker related to the endoplasmic reticulum (**Figure 1C**). The results of western blotting indicated that podocytes secret more EVs when exposed to HG stimulation, as compared to MA and NG treatment. The above results revealed the typical morphology, size distribution, and protein markers of EVs, demonstrating that EVs were successfully extracted from the podocyte culture supernatants.

Podocytes EVs Were Taken Up by PTECs

EVs derived from the same number of podocytes were labeled with the green lipophilic fluorescent dye PKH67 and co-cultured with PTECs to determine whether PTECs could take-up EVs from podocytes. PTECs were treated with normal glucose (NG-PTECs) or high glucose (HG-PTECs). After 48 h of incubation, the cells were fixed and then observed under a confocal laser microscope. As shown in **Figure 2**, green signals in the cytoplasm of the NG-PTECs and HG-PTECs, indicated that PKH67-labeled EVs were taken up. Moreover, the PTECs internalized more fluorescent EVs when co-cultured with EVs from HG-treated podocytes.

[4]http://bioinformatics.psb.ugent.be/webtools/Venn/
[5]https://david.ncifcrf.gov/

EVs From HG-Treated Podocytes Induced Apoptosis of PTECs

To determine whether EVs from HG-treated podocytes play a pro-apoptotic role in PTECs, cultured PTECs were treated with 30 μg/ml EVs. EVs derived from NG/MA/HG-treated podocytes were added to the cultured NG-PTECs and HG-PTECs. After 48 h of continuous treatment, flow cytometry was performed to measure the proportions of apoptotic PTECs. As shown in **Figures 3A,B**, the number of apoptotic NG-PTECs (Annexin V-FITC positive) was increased by treatment with EVs from HG-treated podocytes (14.11 ± 0.71%) as compared to NG-PTECs treated with PBS (14.11 ± 0.71% vs. 7.73 ± 0.50%, respectively, $p < 0.001$) and NG-PTECs treated with EVs from NG-treated podocytes (14.11 ± 0.71% vs. 8.62 ± 0.43%, respectively, $p < 0.001$) or MA-treated podocytes (14.11 ± 0.71% vs. 8.87 ± 0.58%, respectively, $p < 0.001$). Similarly, the number of apoptotic HG-PTECs was also increased in the HG-podo-EVs group (20.92 ± 1.27%) as compared to the PBS group (20.92 ± 1.27% vs. 13.56 ± 0.96%, respectively, $p < 0.05$), NG-podo-EVs group (20.92 ± 1.27% vs. 14.08 ± 0.44%, respectively, $p < 0.05$), and MA-podo-EVs group (20.92 ± 1.27% vs. 13.19 ± 1.06%, respectively, $p < 0.05$; **Figures 3A,B**).

Apoptosis was further confirmed by TUNEL assays. Representative images showed that TUNEL positive cells (recognized as apoptotic cells) were increased after treatment with EVs from HG-treated podocytes (**Figure 3C**). The percentage of TUNEL positive PTECs were higher in HG-podo-EVs group as compared to other groups (**Figure 3D**). Taken together, these findings indicate that EVs from HG-treated podocytes exert a pro-apoptotic effect in PTECs cultured under NG or HG conditions.

Differential Expression of EV miRNA

The transfer of EV miRNA is reported to play pathogenic roles in many diseases. To explore the miRNA signature of podocytes EVs and identify differentially expressed miRNAs in response to HG condition, sequencing small RNAs of EVs was performed. The results of bidirectional hierarchical clustering of the samples are presented in **Figure 4**. A total of 1,915 known miRNAs were identified from all samples after sequencing. A comparison of the HG and NG groups showed that 11 miRNAs were differentially expressed (**Table 1**), while a comparison of the HG and MA groups showed that 18 miRNAs were differentially expressed (**Table 2**). To identify unique miRNAs that were differentially expressed in response to HG stimulation, miRNAs that exhibited differential expression in the HG group, as compared to both the MA and NG groups, were selected. The results showed that there were no differences in the expression patterns of the selected miRNAs between the MA and NG groups. Of the five miRNAs selected, the expression levels of mmu-miR-1981-3p, mmu-miR-3474, mmu-miR-7224-3p, and mmu-miR-6538 were downregulated, while that of mmu-let-7f-2-3p was upregulated (**Table 3**). In addition, to validate the findings obtained from miRNA sequencing, RT-qPCR was performed on the five miRNAs. As the results

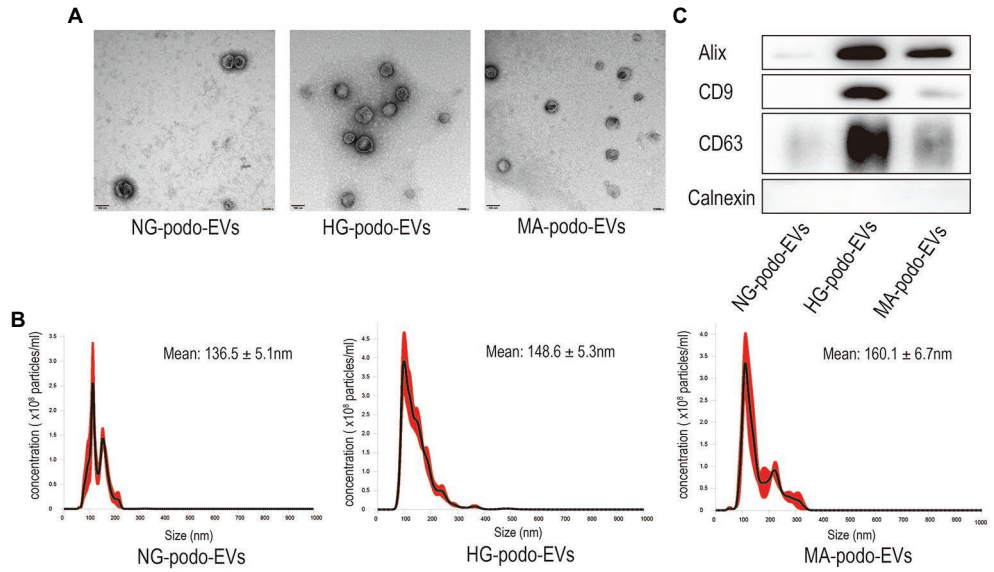

FIGURE 1 | Characterization of EVs isolated from podocytes after NG, MA, and HG treatment. **(A)** EVs were observed by TEM. Magnification, ×100,000. Scale bar, 100 nm. **(B)** The size distribution of EVs was determined by NTA. **(C)** Western blot analysis of Alix, CD9, and CD63, and the EV negative marker Calnexin. HG, high glucose; MA, mannitol; NG, normal glucose; podo, podocytes; NTA, nanoparticle tracking analysis; TEM, transmission electron microscopy.

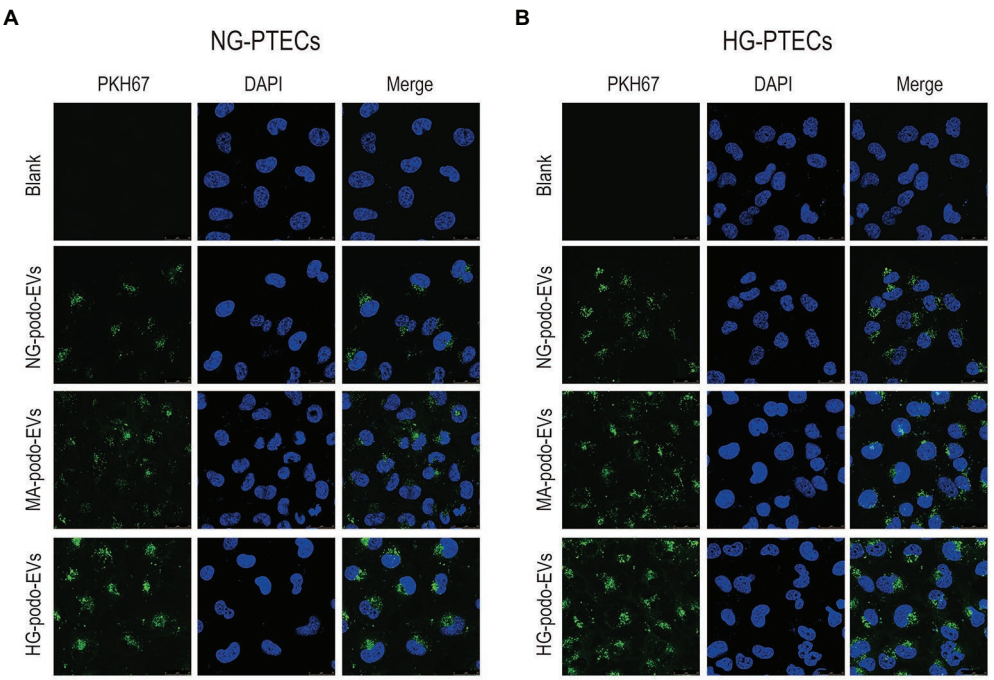

FIGURE 2 | EVs derived from NG/MA/HG-treated podocytes were internalized by cultured PTECs. EVs were labeled with PKH67. Scale bar, 25 μm. **(A)** EVs from podocytes were added to NG-treated PTECs. **(B)** EVs from podocytes were added to HG-treated PTECs. HG, high glucose; MA, mannitol; NG, normal glucose; podo, podocytes; PTECs, proximal tubular epithelial cells.

showed in **Figure 5**, the expression levels of the five miRNAs in EVs were significantly changed in HG-podo group compared to that of the NG-podo and MA-podo groups. The RT-qPCR results showed similar expression trends and therefore confirmed the sequencing data.

Target Gene Prediction

To investigate the targets of these five differentially expressed miRNAs, target gene prediction for each miRNA was conducted using the online databases TargetScan, miRDB, and miRWalk. Genes identified in all three databases were selected as potential

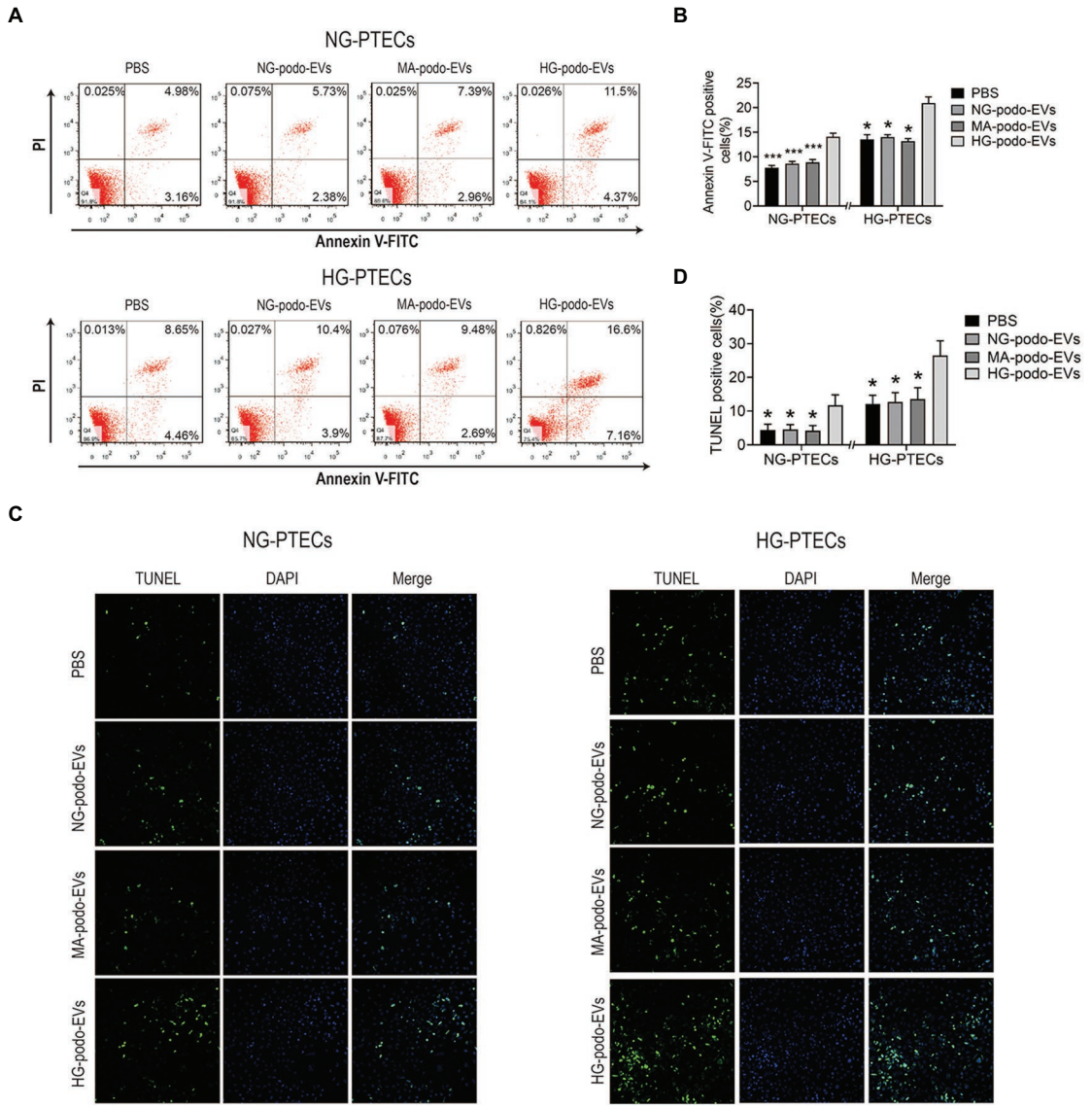

FIGURE 3 | EVs from HG-treated podocytes induced apoptosis of PTECs. Podocytes EVs were incubated with NG/HG-treated PTECs, and the proportion of apoptotic cells was determined by flow cytometry and TUNEL staining. **(A)** Apoptosis was examined using flow cytometry. **(B)** Quantification of Annexin V-FITC positive cells ($n = 4$). **(C)** Apoptosis was detected using TUNEL staining. **(D)** Quantification of TUNEL positive cells. *$p < 0.05$ vs. HG-podo-EVs group; ***$p < 0.001$ vs. HG-podo-EVs group. HG, high glucose; MA, mannitol; NG, normal glucose; podo, podocytes; PTECs, proximal tubular epithelial cells.

target genes. As shown in **Figure 6**, 152, 378, 373, 21, and 368 potential target genes of mmu-miR-1981-3p, mmu-miR-3474, mmu-miR-7224-3p, mmu-miR-6538, and mmu-let-7f-2-3p, respectively, were identified.

Functional and Pathway Enrichment Analysis

To explore the potential functions and signaling pathways of the differentially expressed miRNAs, GO enrichment analysis and KEGG pathway enrichment analyses were performed for the differentially expressed miRNAs based on the predicted target genes. GO analysis consisted of three categories: biological process, molecular function, and cellular component. The top five significant GO terms of the three categories are shown in **Figure 7**. For the downregulated miRNAs, GO analysis was most enriched in "positive regulation of transcription from RNA polymerase II promoter" in the biological process category, "protein binding" in the molecular function category, and "membrane" in the cellular component category (**Figure 7A**). For the upregulated miRNA (i.e., mmu-let-7f-2-3p), GO analysis was most enriched in "transcription, DNA-templated," "protein binding," and "nucleus" in the biological process, molecular function, and cellular component categories, respectively (**Figure 7B**). The results of KEGG pathway enrichment analysis

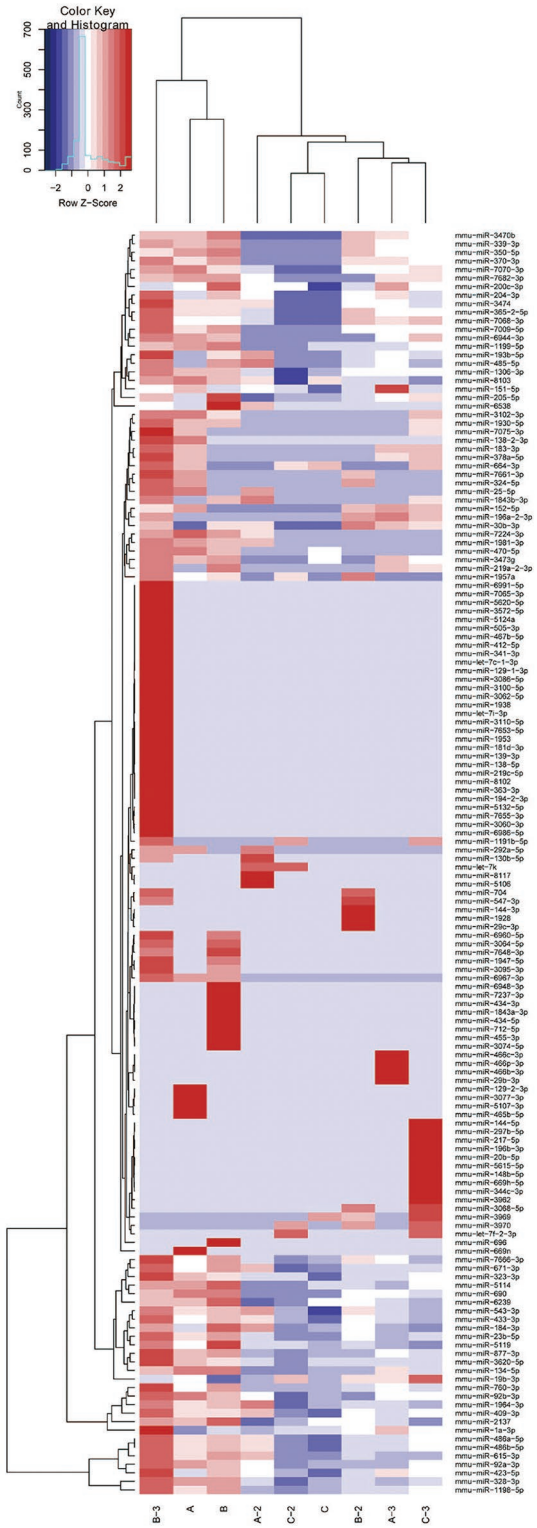

FIGURE 4 | Bidirectional hierarchical cluster result of the differentially expressed miRNAs in EVs derived from NG/MA/HG-treated podocytes ($n = 3$ per group). High expression of miRNAs is shown in red and low expression in blue. A, NG-podo-EVs; B, MA-podo-EVs; C, HG-podo-EVs; HG, high glucose; MA, mannitol; NG, normal glucose.

TABLE 1 | Differentially expressed miRNAs in EVs from HG-podo group compared to NG-podo group.

miRNA ID	Log_2(fold change)	*p*
mmu-miR-3969	5.7669	<0.01
mmu-miR-3970	5.6343	<0.01
mmu-miR-25-5p	−5.7129	<0.01
mmu-miR-7224-3p	−5.8863	<0.01
mmu-miR-1981-3p	−5.4928	<0.01
mmu-miR-292a-5p	−5.1123	<0.05
mmu-let-7f-2-3p	4.9189	<0.05
mmu-miR-1191b-5p	4.8885	<0.05
mmu-miR-669n	−6.9665	<0.05
mmu-miR-3474	−2.5186	<0.05
mmu-miR-6538	−5.7653	<0.05

TABLE 2 | Differentially expressed miRNAs in EVs from HG-podo group compared to MA-podo group.

miRNA ID	Log_2(fold change)	*p*
mmu-miR-6538	−8.9623	<0.001
mmu-miR-7224-3p	−5.9352	<0.01
mmu-let-7f-2-3p	4.9189	<0.05
mmu-miR-1981-3p	−5.7412	<0.05
mmu-miR-7661-3p	−5.7562	<0.05
mmu-miR-1947-5p	−5.5333	<0.05
mmu-miR-3095-3p	−5.5295	<0.05
mmu-miR-547-3p	−5.3122	<0.05
mmu-miR-704	−5.3136	<0.05
mmu-miR-7648-3p	−5.2449	<0.05
mmu-miR-6967-3p	−5.2361	<0.05
mmu-miR-324-5p	−5.2071	<0.05
mmu-miR-1a-3p	−3.646	<0.05
mmu-miR-6960-5p	−5.06	<0.05
mmu-miR-3064-5p	−4.934	<0.05
mmu-miR-3474	−3.341	<0.05
mmu-miR-696	−5.9605	<0.05
mmu-miR-204-3p	−3.0463	<0.05

TABLE 3 | Differentially expressed miRNAs in podocytes EVs in response to HG.

miRNA ID	Upregulated/downregulated
mmu-miR-1981-3p	Down
mmu-miR-3474	Down
mmu-miR-7224-3p	Down
mmu-miR-6538	Down
mmu-let-7f-2-3p	Up

revealed some known signaling pathways associated with DKD, which included the ErbB, MAPK, Hippo, Wnt, Ras, and PI3K-Akt signaling pathways from the analysis of downregulated miRNAs. KEGG analysis of the upregulated miRNA also identified some DKD-related pathways, including type II diabetes mellitus and the AMPK and HIF-1 signaling pathways. The DKD-related pathways are displayed in **Table 4**.

The results of the above experiments showed that EVs derived from HG-treated podocytes induced apoptosis of PTECs, indicating that EVs from HG-treated podocytes could transfer injury information to PTECs. Therefore, based on the enrichment analysis, especially the biological process category (GO analysis), the biological processes and related

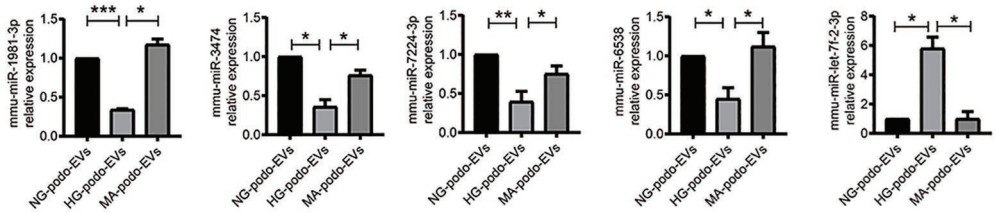

FIGURE 5 | Quantitative reverse transcription-PCR (qRT-PCR) validation of the five miRNAs in podocytes EVs ($n = 4$). $^{*}p < 0.05$; $^{**}p < 0.01$; $^{***}p < 0.001$. HG, high glucose; MA, mannitol; NG, normal glucose; podo, podocytes.

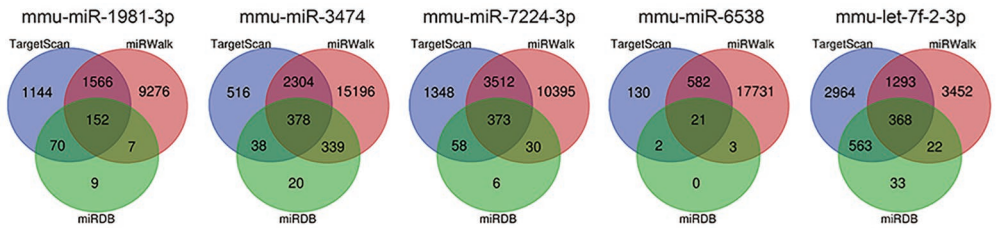

FIGURE 6 | Prediction of target genes of the five miRNAs. Target gene prediction was performed using the online databases TargetScan (blue), miRWalk (red), and miRDB (green). Genes predicted in all three databases (overlapping genes) were selected for further bioinformatics analysis.

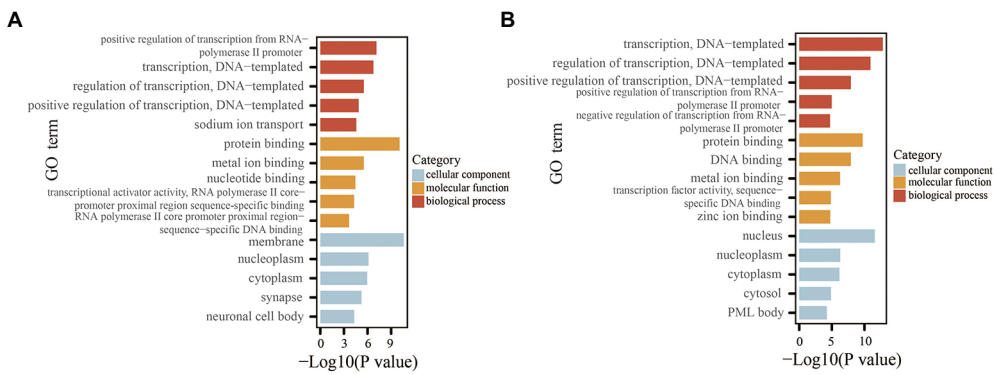

FIGURE 7 | GO analysis of the miRNAs based on the predicted target genes. **(A)** Top five significant GO terms of each category for the downregulated miRNAs. **(B)** Top five significant GO terms of each category for the upregulated miRNA. GO, Gene Ontology.

TABLE 4 | DKD-related pathways from KEGG pathway analysis.

Downregulated/upregulated miRNAs	KEGG ID	Pathway	Count	*p*
Downregulated miRNAs	mmu04012	ErbB signaling pathway	15	<0.001
	mmu04010	MAPK signaling pathway	24	<0.01
	mmu04390	Hippo signaling pathway	16	<0.01
	mmu04310	Wnt signaling pathway	15	<0.01
	mmu04014	Ras signaling pathway	20	<0.01
	mmu04151	PI3K-Akt signaling pathway	26	<0.05
Upregulated miRNA	mmu04930	Type II diabetes mellitus	7	<0.001
	mmu04152	AMPK signaling pathway	7	<0.05
	mmu04066	HIF-1 signaling pathway	6	<0.05

genes that exert pro-apoptosis effects were identified. The related terms are listed in **Table 5**. For the downregulated miRNAs (target genes were upregulated), the biological processes associated with promoting apoptosis or injury including "positive regulation of apoptotic process," "positive regulation of neuron apoptotic process," and "positive regulation of apoptotic signaling pathway." For the upregulated miRNA (i.e., mmu-let-7f-2-3p), the target genes were downregulated and the biological processes associated with promoting apoptosis included "negative regulation of extrinsic apoptotic signaling pathway," and "negative regulation of neuron apoptotic process." These biological processes and the related genes may provide informative insights for future explorations of the molecular mechanism of tubule apoptosis and injury in DKD.

DISCUSSION

DKD is a serious and common complication of DM and has become one of the most important health concerns worldwide (Tuttle et al., 2014). Glomerular sclerosis and tubulointerstitial fibrosis are major pathologic characteristics of DKD (Tervaert et al., 2010). Proteinuria is a well-known factor that links podocyte damage to tubulointerstitial injury, which triggers tubulointerstitial inflammation and fibrogenesis, and accelerates the decline of renal function (Wang et al., 2000; Abbate et al., 2006; Gorriz and Martinez-Castelao, 2012). However, EVs might be an alternative mechanism that mediate the crosstalk between podocytes and the proximal tubules. Podocytes are located adjacent to the proximal tubules, which represent a likely site for the interactions of podocytes EVs (Lv et al., 2019). Also, EVs serve as excellent carriers of bioactive molecules, since the membrane-bound structure can protect EV contents from degradation during delivery. Thus, EVs from podocytes may travel through the urinary tract and exert various biological effects on PTECs. In the present study, EVs isolated from podocytes culture supernatants were incorporated by HG- and NG-treated PTECs. Also, EVs from HG-treated podocytes induced apoptosis of PTECs.

Internephron crosstalk and interactions between the resident cells play important roles in the development of DKD (Qian et al., 2008; Maezawa et al., 2015; Lv et al., 2019). EVs have emerged as vectors for intercellular communication by transferring information between resident cells and participate in the progression of DKD (Wu et al., 2016, 2017; Wang et al., 2018; Zhu et al., 2019). EVs are membrane-bound vesicles that are continuously secreted by cells and facilitate cellular communication by transferring functional cargo consisting of proteins, lipids, DNA, and RNA (EL Andaloussi et al., 2013). The cargo of EVs also plays indispensable roles in many physiological processes, especially the immune response (Bobrie et al., 2011) and tissue regeneration (Krämer-Albers et al., 2007). However, under pathological conditions, such as hypoxia (King et al., 2012), irradiation (Pineda et al., 2019), oxidative stress (Atienzar-Aroca et al., 2016), and infection (Ståhl et al., 2015), the parental cells produce different EVs. The altered quantity and components of the secreted EVs can subsequently mediate abnormal interactions between cells and promote disease progression. In fact, the results of the present study demonstrated that HG conditions induced podocytes to release more EVs as compared to NG and iso-osmolality environments. Considering the important roles of miRNA in the pathogenesis of DKD (Kato and Natarajan, 2015; Lu et al., 2017), miRNA sequencing of podocytes EVs was performed. The results identified 11 differentially expressed miRNAs in response to HG conditions as compared to NG conditions and 18 differentially expressed miRNAs in response to HG conditions as compared to iso-osmolality conditions. In addition, five miRNAs were specifically altered in response to HG stimulation, among which, mmu-miR-1981-3p, mmu-miR-3474, mmu-miR-7224-3p, and mmu-miR-6538 were downregulated, and mmu-let-7f-2-3p was upregulated. These data indicate that podocytes can secret more EVs with altered components under HG conditions and promote apoptosis of PTECs.

TABLE 5 | Pro-apoptosis related biological processes from GO analysis.

Downregulated/ upregulated miRNAs	GO ID	Term	Count	*p*	Genes
Downregulated miRNAs	0043065	Positive regulation of apoptotic process	28	<0.01	ING5, ERBB4, WT1, TGFB2, PYCARD, IL1B, TRP53INP1, UNC5C, PHLDA1, NET1, KCNMA1, EEF1A2, STK4, ATF6, TRIM35, TNFSF10, ITGA6, RPS6KA2, RIPK1, GSK3B, CASP12, SMPD1, LRP6, MAPK8, TRP73, ABL1, BIN1, and SLC9A1
	0043525	Positive regulation of neuron apoptotic process	10	<0.01	KCNMA1, NCF2, GRIK2, GSK3B, IL1B, TFAP2A, MAPK8, ABL1, TGFB2, and ATF2
	2001235	Positive regulation of apoptotic signaling pathway	7	<0.01	ING5, TRP63, TRP53INP1, MAPK8, CAMK2B, CTSC, and TRP73
Upregulated miRNA	2001237	Negative regulation of extrinsic apoptotic signaling pathway	5	<0.01	SH3RF1, ITGA6, RB1CC1, TCF7L2, and ACVR1
	0043524	Negative regulation of neuron apoptotic process	8	<0.05	HIF1A, SET, KDM2B, FYN, GABRB2, MECP2, PPT1, and SIX4

In order to determine the biological functions of these five miRNAs, GO and KEGG pathway analyses of the downregulated and upregulated miRNAs were performed based on the predicted target genes. The results of GO and KEGG pathway analyses identified biological processes and signaling pathways that are involved in the development of DKD, including ErbB, MAPK, Hippo, Wnt, Ras, and PI3K-Akt signaling pathways, as determined by analysis of the downregulated miRNAs, and type II diabetes mellitus, and the AMPK and HIF-1 signaling pathways by analysis of the upregulated miRNA (Ni et al., 2015; Chen and Harris, 2016; Persson and Palm, 2017). The GO results also identified enriched biological processes related to apoptosis regulation for both the downregulated and upregulated miRNAs, consistent with our finding that EVs secreted from HG-treated podocytes induce apoptosis of PTECs. The results of bioinformatics analysis provide useful information for future exploration of the molecular mechanisms underlying tubule apoptosis and injury in DKD. However, whether these pro-apoptosis effects are mediated by EV miRNA was not demonstrated in this study, thus further experiments are needed to confirm these findings. Moreover, due to the diversity and complexity of EV components, other bioactive molecules, such as proteins and non-coding RNAs, should also be considered in the investigation of EV-mediated crosstalk between podocytes and PTECs.

To the best of our knowledge, this is the first study to investigate the effects of HG-treated podocytes EVs on PTECs and the first to examine miRNA profiles in EVs from HG-treated podocytes. However, there were some limitations to this study. First, the sample sizes of the groups for miRNA sequencing were relatively small. Thus, larger samples sizes are necessary to confirm the sequencing results. Second, the findings of bioinformatics analysis were based on in silico analysis. Therefore, the bioinformatics findings must be further validated. Finally, further experiments are essential to elucidate the role of EV miRNA from HG-treated podocytes in the induction of apoptosis of PTECs.

In conclusion, the results of the present study demonstrated that EVs derived from HG-treated podocytes can induce apoptosis of PTECs. Here, five differentially expressed miRNAs in EVs from HG-treated podocytes were identified. These findings provide new insights into the pathogenesis of DKD.

DATA AVAILABILITY STATEMENT

Publicly available datasets were analyzed in this study. This data can be found here: the NCBI Gene Expression Omnibus (GSE154284).

AUTHOR CONTRIBUTIONS

YH, RL, XY, and XL designed the study and wrote the manuscript. LZ, YC, WD, and XZ performed the experiments. HY, SZ, ZX, and ZY performed the bioinformatics analysis. WW, CL, ZL, and SL analyzed and interpreted the data. ZD revised the manuscript. All authors contributed to the article and approved the submitted version.

FUNDING

This research was funded by National Natural Science Foundation of China, grant number 81770667; Scientific research project of Guangdong Provincial People's Hospital-Summit plan, grant number KJ012019440; and Guangdong-Hong Kong Joint Laboratory for immune and genetic kidney disease, grant number 2019B121205005.

REFERENCES

Abbate, M., Zoja, C., and Remuzzi, G. (2006). How does proteinuria cause progressive renal damage? *J. Am. Soc. Nephrol.* 17, 2974–2984. doi: 10.1681/ASN.2006040377

Atienzar-Aroca, S., Flores-Bellver, M., Serrano-Heras, G., Martinez-Gil, N., Barcia, J. M., Aparicio, S., et al. (2016). Oxidative stress in retinal pigment epithelium cells increases exosome secretion and promotes angiogenesis in endothelial cells. *J. Cell. Mol. Med.* 20, 1457–1466. doi: 10.1111/jcmm.12834

Bartel, D. P. (2004). MicroRNAs: genomics, biogenesis, mechanism, and function. *Cell* 116, 281–297. doi: 10.1016/s0092-8674(04)00045-5

Bobrie, A., Colombo, M., Raposo, G., and Théry, C. (2011). Exosome secretion: molecular mechanisms and roles in immune responses. *Traffic* 12, 1659–1668. doi: 10.1111/j.1600-0854.2011.01225.x

Chen, J., and Harris, R. C. (2016). Interaction of the EGF receptor and the hippo pathway in the diabetic kidney. *J. Am. Soc. Nephrol.* 27, 1689–1700. doi: 10.1681/ASN.2015040415

Dai, H., Liu, Q., and Liu, B. (2017). Research progress on mechanism of podocyte depletion in diabetic nephropathy. *J. Diabetes Res.* 2017:2615286. doi: 10.1155/2017/2615286

EL Andaloussi, S., Mäger, I., Breakefield, X. O., and Wood, M. J. (2013). Extracellular vesicles: biology and emerging therapeutic opportunities. *Nat. Rev. Drug Discov.* 12, 347–357. doi: 10.1038/nrd3978

Gorriz, J. L., and Martinez-Castelao, A. (2012). Proteinuria: detection and role in native renal disease progression. *Transplant. Rev.* 26, 3–13. doi: 10.1016/j.trre.2011.10.002

Jeon, J. S., Kim, E., Bae, Y. U., Yang, W. M., Lee, H., Kim, H., et al. (2020). microRNA in extracellular vesicles released by damaged podocytes promote apoptosis of renal tubular epithelial cells. *Cells* 9:1409. doi: 10.3390/cells9061409

Kato, M., and Natarajan, R. (2015). MicroRNAs in diabetic nephropathy: functions, biomarkers, and therapeutic targets. *Ann. N. Y. Acad. Sci.* 1353, 72–88. doi: 10.1111/nyas.12758

King, H. W., Michael, M. Z., and Gleadle, J. M. (2012). Hypoxic enhancement of exosome release by breast cancer cells. *BMC Cancer* 12:421. doi: 10.1186/1471-2407-12-421

Krämer-Albers, E. M., Bretz, N., Tenzer, S., Winterstein, C., Möbius, W., Berger, H., et al. (2007). Oligodendrocytes secrete exosomes containing major myelin and stress-protective proteins: trophic support for axons? *Proteomics Clin. Appl.* 1, 1446–1461. doi: 10.1002/prca.200700522

Li, R., Dong, W., Zhang, S., Yang, H., Zhang, L., Ye, Z., et al. (2018). Septin 7 mediates high glucose-induced podocyte apoptosis. *Biochem. Biophys. Res. Commun.* 506, 522–528. doi: 10.1016/j.bbrc.2018.10.081

Li, J. J., Kwak, S. J., Jung, D. S., Kim, J. J., Yoo, T. H., Ryu, D. R., et al. (2007). Podocyte biology in diabetic nephropathy. *Kidney Int. Suppl.* 72, S36–S42. doi: 10.1038/sj.ki.5002384

Lu, Z., Liu, N., and Wang, F. (2017). Epigenetic regulations in diabetic nephropathy. *J. Diabetes Res.* 2017:7805058. doi: 10.1155/2017/7805058

Lv, L. L., Feng, Y., Tang, T. T., and Liu, B. C. (2019). New insight into the role of extracellular vesicles in kidney disease. *J. Cell. Mol. Med.* 23, 731–739. doi: 10.1111/jcmm.14101

Maezawa, Y., Takemoto, M., and Yokote, K. (2015). Cell biology of diabetic nephropathy: roles of endothelial cells, tubulointerstitial cells and podocytes. *J. Diabetes Investig.* 6, 3–15. doi: 10.1111/jdi.12255

Mundel, P., and Shankland, S. J. (2002). Podocyte biology and response to injury. *J. Am. Soc. Nephrol.* 13, 3005–3015. doi: 10.1097/01.asn.0000039661.06947.fd

Munkonda, M. N., Akbari, S., Landry, C., Sun, S., Xiao, F., Turner, M., et al. (2018). Podocyte-derived microparticles promote proximal tubule fibrotic signaling via p38 MAPK and CD36. *J. Extracell. Vesicles* 7:1432206. doi: 10.1080/20013078.2018.1432206

Nath, K. A. (1992). Tubulointerstitial changes as a major determinant in the progression of renal damage. *Am. J. Kidney Dis.* 20, 1–17. doi: 10.1016/s0272-6386(12)80312-x

Ni, W. J., Tang, L. Q., and Wei, W. (2015). Research progress in signalling pathway in diabetic nephropathy. *Diabetes Metab. Res. Rev.* 31, 221–233. doi: 10.1002/dmrr.2568

Persson, P., and Palm, F. (2017). Hypoxia-inducible factor activation in diabetic kidney disease. *Curr. Opin. Nephrol. Hypertens.* 26, 345–350. doi: 10.1097/MNH.0000000000000341

Pineda, B., Sánchez, G. F., Olascoaga, N. K., Pérez, D. L. C. V., Salazar, A., Moreno-Jiménez, S., et al. (2019). Malignant glioma therapy by vaccination with irradiated C6 cell-derived microvesicles promotes an Antitumoral immune response. *Mol. Ther.* 27, 1612–1620. doi: 10.1016/j.ymthe.2019.05.016

Piscitelli, P., Viazzi, F., Fioretto, P., Giorda, C., Ceriello, A., Genovese, S., et al. (2017). Predictors of chronic kidney disease in type 1 diabetes: a longitudinal study from the AMD Annals initiative. *Sci. Rep.* 7:3313. doi: 10.1038/s41598-017-03551-w

Qian, Y., Feldman, E., Pennathur, S., Kretzler, M., and Brosius, F. R. (2008). From fibrosis to sclerosis: mechanisms of glomerulosclerosis in diabetic nephropathy. *Diabetes* 57, 1439–1445. doi: 10.2337/db08-0061

Ståhl, A. L., Arvidsson, I., Johansson, K. E., Chromek, M., Rebetz, J., Loos, S., et al. (2015). A novel mechanism of bacterial toxin transfer within host blood cell-derived microvesicles. *PLoS Pathog.* 11:e1004619. doi: 10.1371/journal.ppat.1004619

Taft, J. L., Nolan, C. J., Yeung, S. P., Hewitson, T. D., and Martin, F. I. (1994). Clinical and histological correlations of decline in renal function in diabetic patients with proteinuria. *Diabetes* 43, 1046–1051. doi: 10.2337/diab.43.8.1046

Tervaert, T. W., Mooyaart, A. L., Amann, K., Cohen, A. H., Cook, H. T., Drachenberg, C. B., et al. (2010). Pathologic classification of diabetic nephropathy. *J. Am. Soc. Nephrol.* 21, 556–563. doi: 10.1681/ASN.2010010010

Théry, C., Witwer, K. W., Aikawa, E., Alcaraz, M. J., Anderson, J. D., Andriantsitohaina, R., et al. (2018). Minimal information for studies of extracellular vesicles 2018 (MISEV2018): a position statement of the International Society for Extracellular Vesicles and update of the MISEV2014 guidelines. *J. Extracell. Vesicles* 7:1535750. doi: 10.1080/20013078.2018.1535750

Tkach, M., and Théry, C. (2016). Communication by extracellular vesicles: where we are and where we need to go. *Cell* 164, 1226–1232. doi: 10.1016/j.cell.2016.01.043

Tuttle, K. R., Bakris, G. L., Bilous, R. W., Chiang, J. L., de Boer, I. H., Goldstein-Fuchs, J., et al. (2014). Diabetic kidney disease: a report from an ADA Consensus Conference. *Diabetes Care* 37, 2864–2883. doi: 10.2337/dc14-1296

Valadi, H., Ekström, K., Bossios, A., Sjöstrand, M., Lee, J. J., and Lötvall, J. O. (2007). Exosome-mediated transfer of mRNAs and microRNAs is a novel mechanism of genetic exchange between cells. *Nat. Cell Biol.* 9, 654–659. doi: 10.1038/ncb1596

van Niel, G., D'Angelo, G., and Raposo, G. (2018). Shedding light on the cell biology of extracellular vesicles. *Nat. Rev. Mol. Cell Biol.* 19, 213–228. doi: 10.1038/nrm.2017.125

Viazzi, F., Piscitelli, P., Giorda, C., Ceriello, A., Genovese, S., Russo, G. T., et al. (2017). Association of kidney disease measures with risk of renal function worsening in patients with hypertension and type 2 diabetes. *J. Diabetes Complicat.* 31, 419–426. doi: 10.1016/j.jdiacomp.2016.10.030

Wang, S. N., LaPage, J., and Hirschberg, R. (2000). Role of glomerular ultrafiltration of growth factors in progressive interstitial fibrosis in diabetic nephropathy. *Kidney Int.* 57, 1002–1014. doi: 10.1046/j.1523-1755.2000.00928.x

Wang, Y. Y., Tang, L. Q., and Wei, W. (2018). Berberine attenuates podocytes injury caused by exosomes derived from high glucose-induced mesangial cells through TGFβ1-PI3K/AKT pathway. *Eur. J. Pharmacol.* 824, 185–192. doi: 10.1016/j.ejphar.2018.01.034

Wu, X. M., Gao, Y. B., Cui, F. Q., and Zhang, N. (2016). Exosomes from high glucose-treated glomerular endothelial cells activate mesangial cells to promote renal fibrosis. *Biol. Open* 5, 484–491. doi: 10.1242/bio.015990

Wu, X., Gao, Y., Xu, L., Dang, W., Yan, H., Zou, D., et al. (2017). Exosomes from high glucose-treated glomerular endothelial cells trigger the epithelial-mesenchymal transition and dysfunction of podocytes. *Sci. Rep.* 7:9371. doi: 10.1038/s41598-017-09907-6

Zhang, S., Li, R., Dong, W., Yang, H., Zhang, L., Chen, Y., et al. (2019). RIPK3 mediates renal tubular epithelial cell apoptosis in endotoxin-induced acute kidney injury. *Mol. Med. Rep.* 20, 1613–1620. doi: 10.3892/mmr.2019.10416

Zhang, J., Li, S., Li, L., Li, M., Guo, C., Yao, J., et al. (2015). Exosome and exosomal microRNA: trafficking, sorting, and function. *Genomics Proteomics Bioinformatics* 13, 17–24. doi: 10.1016/j.gpb.2015.02.001

Zhao, X., Chen, Y., Tan, X., Zhang, L., Zhang, H., Li, Z., et al. (2018). Advanced glycation end-products suppress autophagic flux in podocytes by activating mammalian target of rapamycin and inhibiting nuclear translocation of transcription factor EB. *J. Pathol.* 245, 235–248. doi: 10.1002/path.5077

Zhu, Q. J., Zhu, M., Xu, X. X., Meng, X. M., and Wu, Y. G. (2019). Exosomes from high glucose-treated macrophages activate glomerular mesangial cells via TGF-β1/Smad3 pathway in vivo and in vitro. *FASEB J.* 33, 9279–9290. doi: 10.1096/fj.201802427RRR

Conflict of Interest: The authors declare that the research was conducted in the absence of any commercial or financial relationships that could be construed as a potential conflict of interest.

frontiers in Genetics

ORIGINAL RESEARCH
published: 20 November 2020
doi: 10.3389/fgene.2020.584460

Integrated Analysis of m6A Methylome in Cisplatin-Induced Acute Kidney Injury and Berberine Alleviation in Mouse

Jianxiao Shen[1†], Wanpeng Wang[2†], Xinghua Shao[1†], Jingkui Wu[1], Shu Li[1], Xiajing Che[1] and Zhaohui Ni[1*]*

[1] Department of Nephrology, Renji Hospital, Shanghai Jiao Tong University School of Medicine, Shanghai, China,
[2] Department of Nephrology, Lianshui People's Hospital, Lianshui, China

OPEN ACCESS

Edited by:
Haiyong Chen,
The University of Hong Kong,
Hong Kong

Reviewed by:
Lian Liu,
Shaanxi Normal University, China
Chen Yang,
Affiliated Hospital of Guangdong
Medical University, China

***Correspondence:**
Xiajing Che
chexj@126.com
Zhaohui Ni
profnizh@126.com

[†] These authors have contributed equally to this work

Specialty section:
This article was submitted to Epigenomics and Epigenetics, a section of the journal Frontiers in Genetics

Received: 17 July 2020
Accepted: 19 October 2020
Published: 20 November 2020

Citation:
Shen J, Wang W, Shao X, Wu J, Li S, Che X and Ni Z (2020) Integrated Analysis of m6A Methylome in Cisplatin-Induced Acute Kidney Injury and Berberine Alleviation in Mouse. Front. Genet. 11:584460. doi: 10.3389/fgene.2020.584460

Background: N6-methyladenosine (m6A) is the most abundant modification known in mRNAs. It participates in a variety of physiological and pathological processes, such as metabolism, inflammation, and apoptosis.

Aims: To explore the mechanism of m6A in cisplatin-induced acute kidney injury (AKI) and berberine alleviation in mouse.

Methods: This study investigated the N6-methyladenosine (m6A) methylome of kidneys from three mouse groups: C57 mice (controls), those with CI-AKI (injury group, IG), and those pretreated with berberine (treatment group, TG). Methylated RNA Immunoprecipitation Next Generation Sequencing (MeRIP-seq) and RNA-seq were performed to identify the differences between the injury group and the control group (IvC) and between the treatment group and the injury group (TvI). Western blotting was performed to identify the protein levels of candidate genes.

Results: In IvC, differentially methylated genes (DMGs) were enriched in metabolic processes and cell death. In TvI, DMGs were enriched in tissue development. Several genes involved in important pathways related to CI-AKI showed opposite methylation and expression trends in the IvC and TvI comparisons.

Conclusion: m6A plays an important role in cisplatin induced AKI and berberine may alleviate this process.

Keywords: M6A, cisplatin induced nephrotoxicity, berberine, FGA, SLC12A1, Havcr1

Abbreviations: m6A, N6-methyladenosine; CI-AKI, cisplatin-induced acute kidney injury; IvC, injury group vs. control group; TvI, treatment group vs. injury group; YTH, YT521-B homology; DEGs, differentially expression genes, negative control; i.p. injected intraperitoneally; Scr, serum creatinine; BUN, blood urea nitrogen; GO, Gene ontology; KEGG, Kyoto Encyclopedia of Genes and Genomes; CDS, coding sequence; MACS, Model-based Analysis of ChIP-Seq, DMMSs, differentially methylated m6A sites. H-U, hyper-methylated and upregulated, 422 hypo-methylated and downregulated (hypo-down) genes, one hyper-methylated but down-regulated (hyper-down) genes and 3 hypo-methylated but up-regulated (hypo-up).

INTRODUCTION

Cisplatin is an anticancer drug widely used for the treatment of various solid tumors, but it is also known for its nephrotoxicity. It exerts its function by interacting with and disrupting DNA and mitochondrial function. During drug metabolism, cisplatin accumulates in renal tubular cells, causing cell death and resulting in acute kidney injury (AKI) (Lebwohl and Canetta, 1998; Cummings and Schnellmann, 2002; Ozkok and Edelstein, 2014; George et al., 2018; Holditch et al., 2019; Yimit et al., 2019). Recent studies have revealed that apoptosis, necrosis, inflammation, and other mechanisms play significant roles in cisplatin-induced AKI (Sahu et al., 2015; Zuk and Bonventre, 2016; Humanes et al., 2017; Long et al., 2017).

Berberine is the principal component of many popular medical plants, such as *Coptis chinensis*, *Rhizoma coptidis*, *Hydrastis canadensis*, *Berberis aquifolium*, and *Berberis vulgaris* (Wang et al., 2017; Duan et al., 2018; Fan et al., 2019). As a promising drug, various pharmacological activities of berberine have been reported, including antimicrobial, antiemetic, antipyretic, anti-pruritic, antioxidant, anti-inflammatory, hypotensive, anti-arrhythmic, and sedative activities (Shamsa et al., 1999; Chen et al., 2012; Caliceti et al., 2016). Several reports have mentioned that berberine shows nephroprotective effects against cisplatin-induced kidney damage (Domitrović et al., 2013; Teng et al., 2015; Ojha et al., 2016; Ahmad et al., 2019). However, the mechanism of alleviating CI-AKI is still unclear.

m6A has been implicated in all aspects of posttranscriptional RNA metabolism, such as regulating reversible modifications, alternative splicing, stability, and translation. It prefers to modify sequences identified as RRACH, where R is adenine or guanine, A is the m6A site, and H is adenine, cytosine, or uracil. In addition, m6A modifications exhibit enrichment in the 3' UTR near mRNA stop codons and within long internal exons. The writing of m6A is accomplished via a complex composed of methyltransferase-like 3 (METTL3), methyltransferase-like 14 (METTL14), and Wilms tumor 1-associated protein (Ping et al., 2014; Wang et al., 2014; Spitale et al., 2015). Two m6A demethylases, fat mass and obesity-associated protein (FTO) and AlkB homolog 5, have been discovered as "erasers" (Jia et al., 2011). While proteins containing the YT521-B homology (YTH) domain, such as YTHDC1, YTHDF1, YTHDF2, and YTHDF3, directly bind m6A sites and act as readers of the m6A signal (Zheng et al., 2013).

Several studies have focused on the correlation between m6A methylation and kidney injury. Wang J. et al. (2019) reported that METTL3 overexpression plays a protective role against colistin-induced oxidative stress and apoptosis in renal tubular epithelial cells in mice. Alteration of m6A regulators was associated with pathologic stage in patients with clear cell renal cell carcinoma (Zhou J. C. et al., 2019). Another study reported that cisplatin treatment reduced FTO expression and increased m6A levels *in vivo* and *in vitro*. They also found that inhibiting FTO by meclofenamic acid aggravated renal damage and increased apoptosis in cisplatin-treated kidneys (Zhou P. et al., 2019). METTL14 is elevated in people with AKI (Xu et al., 2020). However, few studies have investigated the m6A methylome in cisplatin-induced AKI and the potential mechanism of berberine alleviation.

In this study, we found that berberine significantly alleviated cisplatin-induced AKI in a reliable mouse model. To further investigate the role of m6A in this process, MeRIP-seq was used to establish the first known transcriptome-wide m6A methylome profiles of kidneys from normal, CI-AKI, and berberine-pretreated mice. RNA-seq was performed to detect differentially expressed genes (DEGs) among the groups. Based on our results, we speculate that berberine may alleviate CI-AKI by regulating m6A methylation.

MATERIALS AND METHODS

Animals and Tissue Collection

Male C57BL/6 mice (aged 8 weeks) were randomly assigned to the control group, injury group (IG), and treatment group (TG), with four mice per group. All mice were housed under a 12 h light/dark schedule with free access to food and water. Control and IG mice were subjected to daily intraperitoneal (i.p) injections with vehicle (normal saline), while TG mice were injected daily with berberine (Sigma, St. Louis, MO, United States, 20 mg/kg) (Ruan et al., 2017). After 14 days of drug treatment, the IG and TG were injected intravenously with cisplatin (20 mg/kg), while controls were injected intravenously with a vehicle. After cisplatin injection, berberine pretreatment was stopped and all mice were housed as usual. All mice in the three groups were sacrificed at 72 h postinjection by cervical dislocation after CO_2-induced narcosis (Zhang et al., 2016; Dutta et al., 2017). Immediately afterward, the kidneys were collected.

Serum Levels of Creatinine and Blood Levels of Urea Nitrogen

Before the mice were sacrificed, blood was drawn from their tail veins. Serum samples were collected. Serum levels of creatinine (Scr) and urea nitrogen (BUN) were analyzed using a standard spectrophotometric assay (Roche Diagnostics GmbH, Mannheim, Germany).

Histopathology Analyses

Renal tissue harvested from animals was washed with 0.9% saline, fixed in 10% neutral buffered formalin, and then embedded in 10% paraffin. Sections (5 μm thick) were stained with hematoxylin eosin for further microscopic analyses. A tubular injury score was calculated (Leemans et al., 2005). The percentage of damaged tubules in the corticomedullary junction was estimated by a nephropathologist using a 5-point scale according to the following criteria: tubular dilation, cast deposition, brush border loss, and necrosis in eight randomly chosen, non-overlapping fields (×400 magnification). Lesions were graded on a scale from 0 to 5: 0 = normal; 1 = mild, involvement of less than 10% of the cortex; 2 = moderate, involvement of 10–25% of the cortex; 3 = severe, involvement of 25–50% of the cortex; 4 = very severe, involvement of 50–75%

of cortex; 5 = extensive damage, involvement of more than 75% of the cortex.

RNA MeRIP-seq and Data Analyses

In accordance with the manufacturer's instructions, TRIzol reagent (Invitrogen Corporation, CA, United States) was used to extract total RNA from kidney tissue. Ribosomal RNA was removed from total RNA with a Ribo-Zero rRNA Removal Kit (Illumina, Inc., CA, United States). Then, fragmentation buffer (Illumina, Inc.) was used to split the RNA into fragments of approximately 100 nucleotides in length. MeRIP-Seq was performed by Cloudseq Biotech Inc. (Shanghai, China). In brief, total RNA was extracted from kidney tissue using TRIzol Reagent (Life Technologies CA, United States). RNA was tested for quality via NanoDrop (Thermo Fisher Scientific, MA, United States). RNA integrity was assessed using a denaturing agarose gel. mRNA was isolated from total RNA using a Seq-Star^{TM} poly(A) mRNA Isolation Kit (Arraystar, MD, United States). The GenSeq^{TM} m6A RNA IP Kit (GenSeq Inc., China) was used to perform m6A RNA immunoprecipitation. A NEBNext® Ultra II Directional RNA Library Prep Kit (New England Biolabs, Inc., MA, United States) was used to construct both the input samples without immunoprecipitation and the m6A IP samples. All samples were subjected to 150 bp paired-end sequencing on an Illumina HiSeq instrument (Illumina, Inc.).

Paired-end reads were quality controlled by Q30. Trimming of the 3' adaptor and low-quality read removal were performed using Cutadapt software (v1.9.3) (Kechin et al., 2017). Hisat2 software (v2.0.4) (Kim et al., 2015) was used to align clean reads of all libraries to the reference genome (mm10). Then, methylated sites on RNAs (peaks) were identified using Model-based Analysis of ChIP-Seq (MACS) software (Zhang et al., 2008; Li et al., 2017; Huang et al., 2019). Identified m6A peaks were subjected to motif enrichment analyses using Hypergeometric Optimization of Motif EnRichment software (Heinz et al., 2010), and metagene m6A distribution was characterized using R package MetaPlotR (Olarerin-George and Jaffrey, 2017). Differentially methylated sites with a fold change cutoff of ≥ 2 and

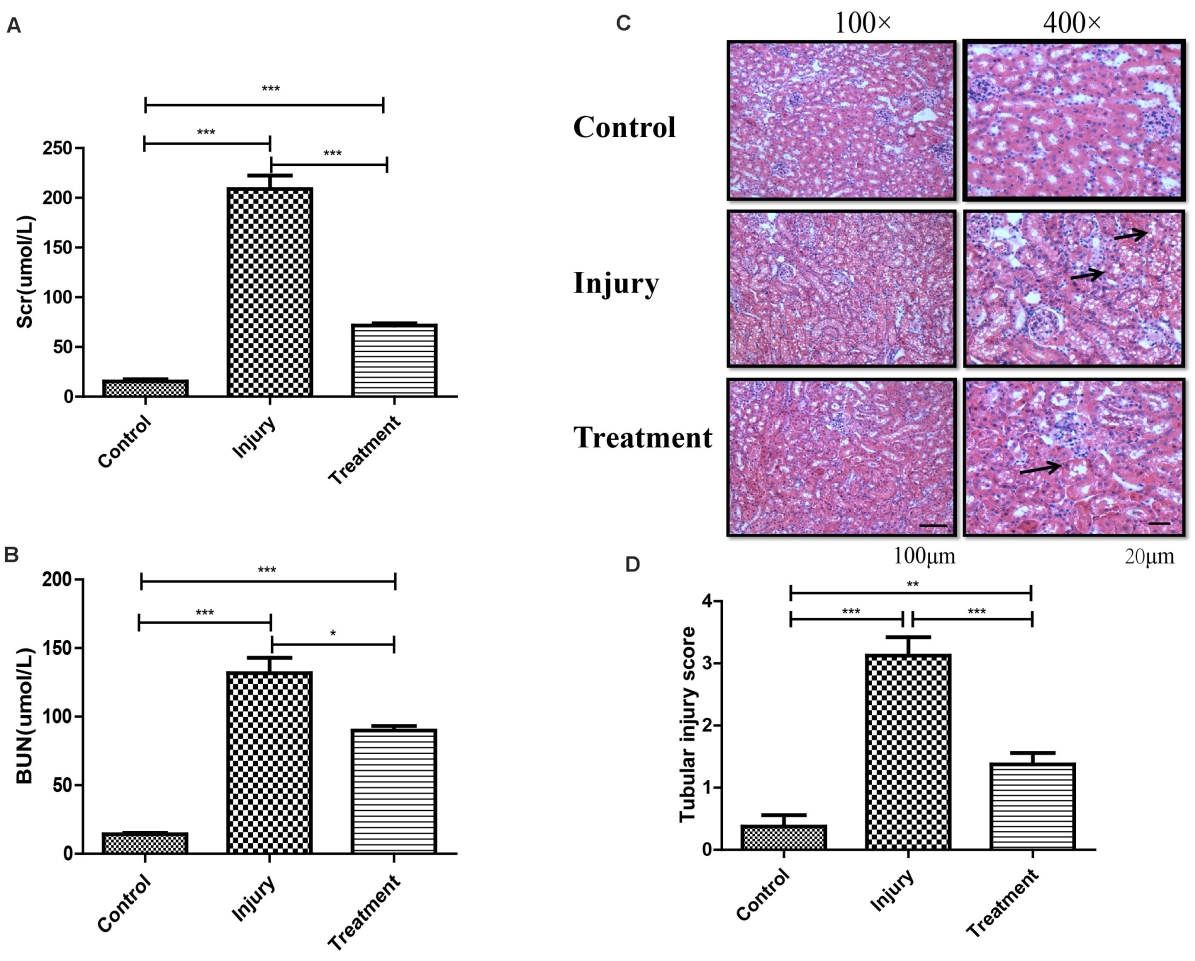

FIGURE 1 | Establishment of cisplatin-induced acute kidney injury model in C57 mouse. **(A)** Analysis of Scr level in mice following different treatments. Error bars represent the standard deviation. ***$p < 0.001$, Student's t-test. **(B)** Analysis of BUN level in mice following different treatments. Error bars represent the standard deviation. *$p < 0.05$, ***$p < 0.001$, Student's t-test. **(C)** Represents the image of hematoxylin and eosin staining in kidney (black arrows indicating the injury). **(D)** Score for characteristic histologic signs of renal injury. **$p < 0.01$, ***$p < 0.001$, Student's t-test.

$P < 0.05$ were identified using the diffReps differential analysis package (Shen et al., 2013; Wang Y. et al., 2019; Wang et al., 2020). The peaks identified by MACS and diffReps overlapping with exons of mRNA were selected for further analyses. Gene ontology (GO) and pathway enrichment analyses were performed on the differentially methylated proteins for using the GO[1] and Kyoto Encyclopedia of Genes and Genomes (KEGG)[2] databases.

RNA-Seq and Data Analyses

Total RNA was extracted from kidney samples using TRIzol reagent (Life Technologies) according to the manufacturer's protocol. Denaturing agarose gel electrophoresis was used to evaluate the integrity of total RNA. A Seq-Star TM poly(A) mRNA Isolation Kit (Arraystar, MD, United States) was utilized to purify mRNA from total RNA after measuring the quantity and quality on a NanoDrop ND-2,000. Then, a BGISEQ-500 platform was used to subject fragmented mRNA to 50 bp single-end sequencing. Adapter and low-quality reads were trimmed using SOAPnuke (Chen et al., 2018), and those trimmed reads were aligned to the reference genome using bowtie2 (Langmead and Salzberg, 2012). Finally, cuffdiff was use to analyze differential expressed genes (DEGs) (Trapnell et al., 2012).

Western Blotting

Mouse tissues were lysed using a protein lysis buffer containing 20 mM Tris (pH 7.4), 150 mM NaCl, 1 mM EDTA, 1 mM EGTA, 1% Triton X-100, 25 mM sodium pyrophosphate, and 2 mM sodium orthovanadate aprotinin. All denatured proteins were separated on an SDS-PAGE gel and then transferred to polyvinylidene difluoride membranes (Roche, Netley, NJ, United States). The membranes were blocked with 5% skimmed milk in Tris-buffered saline and then were incubated

[1]www.geneontology.org

[2]www.genome.jp/kegg

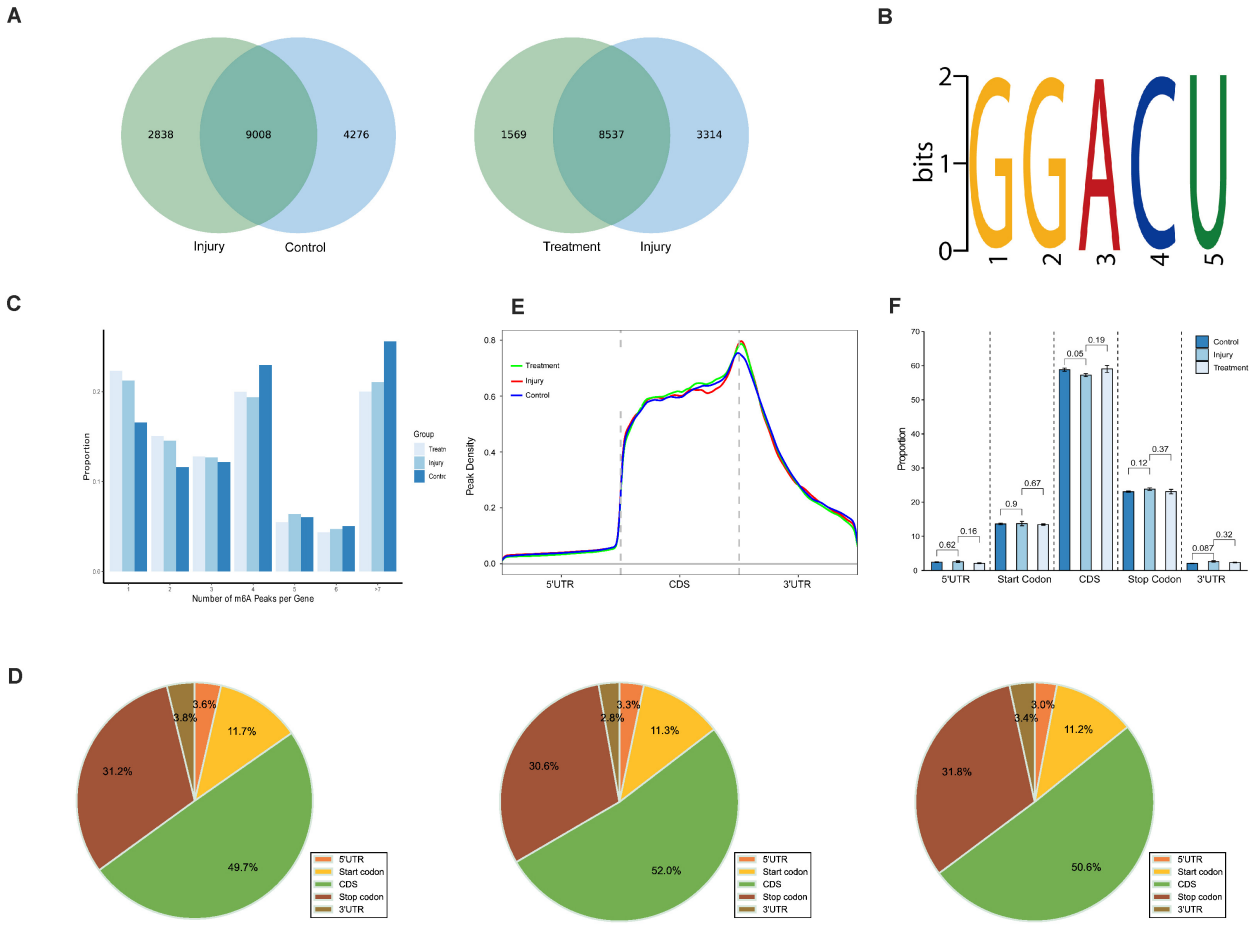

FIGURE 2 | Overview of N6-methyladenosine methylation within mRNAs in the control, injury, and treatment groups. **(A)** Venn diagram showing the overlap of m6A peaks within mRNAs between IvC (left) and Tvl (right). **(B)** The top motif enriched across m6A peaks identified from three groups. **(C)** Proportion of genes harboring different numbers of m6A peaks in three groups. The majority of genes harboring more than one m6A peak. **(D)** Pie charts showing the percentage of m6A peaks in five segments of transcripts. m6A peaks were most enriched in the coding sequence segment. **(E)** Distributions of fold enrichment of m6A peaks in five segments. The mean fold enrichment in the stop codon segments was the highest in injury group, while that value in CDS was the largest in treatment group. **(F)** Analysis of m6A peaks in different groups. Error bars represent the standard deviation. Student's *t*-test.

with 1:500 dilutions of primary antibodies as follows: anti-FGA (Abcam, Cambridge, MA, United States), anti-Slc12a1 (Abcam, Cambridge, MA, United States), and anti-Havcr1 (Abcam, Cambridge, MA, United States). Then, the samples were incubated with a horseradish peroxidase-conjugated anti-rabbit secondary antibody (Jackson ImmunoResearch, PA, United States). The bands were visualized using an ECL Western Blotting Kit (Biovision, Milpitas, CA, United States) and were quantified by Quantity One software (Bio-Rad, Hercules, CA, United States).

Statistical Analyses

Data are expressed as mean ± standard deviation (SD). Student's *t*-test was used to compare two groups. ANOVA with Tukey's post-test was used to assess the statistical significance between-group means for comparisons between multiple groups. The differences were considered statistically significant at $P < 0.05$.

RESULTS

Establishment of a Reliable CI-AKI Mouse Model

We found that 20 mg/kg cisplatin injection resulted in an approximately 18–20-fold increase in Scr and BUN relative to the control group, but significantly lower levels in TG than in IG (**Figures 1A,B**). Hematoxylin–eosin staining indicated that cisplatin induced remarkable renal structure damage in IG tissue, including extensive tubular vacuolization, tubular epithelial cell exfoliation, and thickening of glomerular basement membrane ($P < 0.001$), while these changes were notably alleviated in TG mice ($P < 0.001$) (**Figures 1C,D**). This indicated successful and reliable establishment of a CI-AKI mouse model and relief of the injury through berberine pretreatment.

General Features of m6A Methylation

MeRIP-seq analyses of mRNA derived from kidneys revealed 13,284 m6A peaks within 7,942 coding gene transcripts in controls; the values were 11,846 within 7,422 mRNAs in IG and 10,106 within 6,481 mRNAs in TG. Overall, 7,337 peaks overlapped among the three groups (**Supplementary Figure 1**). Pairwise comparisons showed that 9,008 peaks (more than 55.8% of all peaks) overlapped in IG versus control (IvC) comparisons and 8,537 peaks (more than 63.6% of all peaks) overlapped in TG versus IG (TvI) comparisons (**Figure 2A**). Approximately 40% of all peaks were non-overlapping, suggesting differences among those groups.

To determine whether the m6A peaks contained the RRACH conserved sequence motif, we detected all samples in three groups. One thousand peaks with the highest scores (−10*log10, *p*-value) were analyzed using DREME software. The results showed that the same sequence motif (RRACH) was necessary for m6A methylation in kidney mRNAs in each group (**Figure 2B**), consistent with other studies (Dominissini et al., 2012; Meyer et al., 2012; Luo et al., 2019).

Further analyses demonstrated that 16.59, 21.21, and 22.29% of the genes with m6A-methylation sites in controls, IG, and TG contained one m6A peak (**Figure 2C**). More than 75% of the genes contained two or more peaks (**Figure 2C**). This result is different from other reports on mouse liver (Luo et al., 2019) and brain (Dominissini et al., 2012), suggesting that the kidney is unique.

To understand the preferential locations of m6A peaks, all peaks were categorized into five transcript segments: the 5'

TABLE 1 | The top 20 differently methylated m6A peaks in IvC.

Gene name	Gene ID	Fold change	Regulation	Chromosome	Peak start	Peak end	Peak length	*p*-value
BC061237	385138	1489	Up	chr14	44504106	44504291	185	1.48521E-12
BC061237	385138	816.8	Up	chr14	44500121	44500197	76	3.23828E-13
Krt20	66809	498.7531381	Up	chr11	99430752	99430920	168	9.96013E-10
Krt20	66809	498.0274348	Up	chr11	99429021	99429078	57	9.08594E-10
Krt20	66809	483.5165816	Up	chr11	99432181	99432343	162	2.59398E-09
1700001F09Rik	71826	383.8	Up	chr14	43346701	43346790	89	5.98092E-15
Ccdc85b	240514	328.5877193	Up	chr19	5454141	5454580	439	3.35868E-11
Gm3543	100041849	318	Up	chr14	41982201	41982290	89	1.38739E-12
Serpina3n	20716	316.3	Up	chr12	104414261	104414329	68	7.77029E-14
Gm3543	100041849	254	Up	chr14	41982133	41982180	47	4.03611E-10
Alms1	236266	503.6	Down	chr6	85694833	85694951	118	4.2803E-10
Tas2r119	57254	385.6	Down	chr15	32177288	32177620	332	9.86777E-14
Ctnna2	12386	220.8	Down	chr6	77600041	77600380	339	1.36972E-13
Afm	280662	195.1	Down	chr5	90518931	90519060	129	1.23171E-10
Slc5a4a	64452	126.7	Down	chr10	76163688	76163769	81	7.19208E-10
Nat1	17960	123.5	Down	chr8	67490861	67491460	599	2.54765E-10
Pzp	11287	111.1290323	Down	chr6	128526621	128526720	99	8.47489E-15
Dpf3	70127	99.2	Down	chr12	83215461	83215800	339	3.4897E-12
Dgkg	110197	95.3	Down	chr16	22479365	22479426	61	1.61986E-10
Dpf3	70127	94.3	Down	chr12	83214541	83214840	299	1.03615E-10

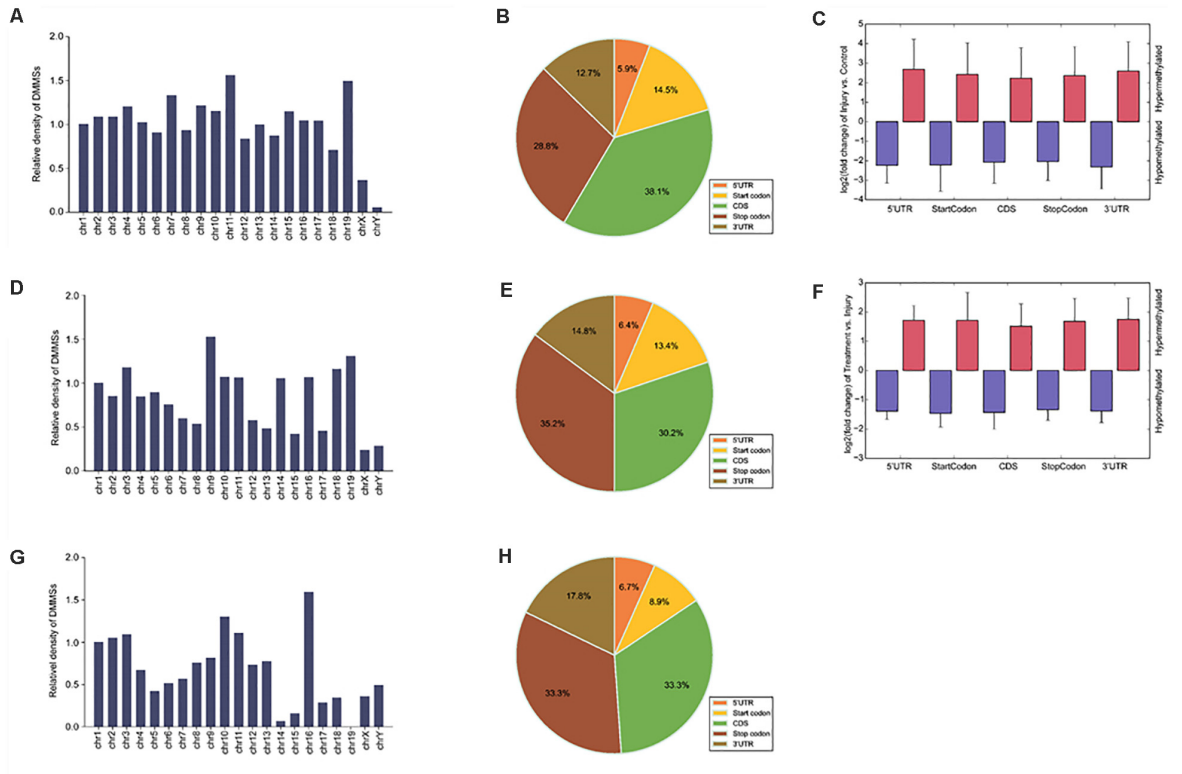

FIGURE 3 | Distribution of differentially methylated N6-methyladenosine sites. **(A)** Relative occupancy of differentially methylated m6A sites in each chromosome normalized by length in IvC. **(B)** Pie chart showing the percentage of DMM peaks in five non-overlapping segments in IvC. **(C)** Statistics of fold change of DMM peaks in five segments. The histogram shows the mean of the fold change in IvC. Error bars represent the standard error of the mean. **(D)** Relative occupancy of differentially methylated m6A sites in each chromosome normalized by length in TvI. **(E)** Pie chart showing the percentage of DMM peaks in five non-overlapping segments in TvI. **(F)** Statistics of fold change of DMM peaks in five segments. The histogram shows the mean of the fold change in TvI. Error bars represent the standard error of the mean. **(G)** Relative occupancy of differentially methylated m6A sites in each chromosome normalized by length. **(H)** Pie chart showing the percentage of DMM peaks in five non-overlapping segments.

UTR, start codon segment, coding sequence (CDS), stop codon segment, and 3' UTR. We found that m6A was mostly enriched in the CDS, and there was some enrichment near stop codons (**Figure 2D**). These results are also similar previous studies (Dominissini et al., 2012; Meyer et al., 2012).

Furthermore, m6A peaks in all groups had the highest density in stop codons (**Figure 2E**). Comparisons between different groups showed no significant difference in the volume of m6A peaks, which indicates that although many variants in m6A methylation were detected in different segments, the total proportion of m6A peaks did not significantly change (**Figure 2F**).

Distribution of Differentially Methylated m6A Sites

In IvC, we found 2,981 differentially methylated m6A sites (DMMSs) within 2,227 genes, of which 48.17% (1,436/2,981) exhibited significant increases in methylation. **Table 1** displays the top 20 differentially methylated m6A sites.

To understand the DMMS distribution profiles in those two groups, we mapped them to chromosomes. Chromosomes 4, 2, 7, and 11 were the top four chromosomes, harboring more than 200 DMMSs (**Supplementary Figure 2A**). However, when the number of DMMSs was normalized by the length of chromosomes, the top four with the highest relative densities were 11, 19, 7, and 4 (**Figure 3A**). Meanwhile, most DMMSs were within a CDS (**Figure 3B**). Further analyses showed that at sites with increased methylation, DMMSs within the 5' UTR had the highest fold change, while among the sites with decreased methylation, DMMSs within the 3' UTR had the highest fold change (**Figure 3C**), demonstrating the location preferences of methylation and demethylation within the genome.

In TvI comparisons, 526 DMMSs were identified within 420 genes, of which 66.73% (351/526) were sites with increased methylation. The top 20 m6A sites with the most increased and decreased methylation are shown in **Table 2**.

Chromosomes 3, 1, 9, and 4 were the top four chromosomes harboring the most DMMSs (**Supplementary Figure 2B**). The top four with the highest relative densities were 9, 19, 18, and 3 (**Figure 3D**). Most DMMSs were within a CDS (**Figure 3E**). DMMSs within the 3' UTR had the highest fold change among sites with increased methylation, while those near the start

TABLE 2 | The top 20 differently methylated m6A peaks in TvI.

Gene name	Gene ID	Fold change	Regulation	Chromosome	Peak start	Peak end	Peak length	*p*-value
Syt15	319508	63.6	Up	chr14	34228038	34228320	282	1.59789E-06
Celf5	319586	48.7	Up	chr10	81469443	81469523	80	1.58151E-06
Cav3	12391	46.9	Up	chr6	112459821	112459925	104	3.0379E-06
Npffr2	104443	44.1	Up	chr5	89582741	89583200	459	5.67547E-06
Kcnf1	382571	19.08571429	Up	chr12	17174961	17175260	299	3.61832E-06
Amy2a4	100043684	18.27027027	Up	chr3	113279836	113279860	24	1.19296E-06
Metap2	56307	18.03125	Up	chr10	93858488	93858660	172	2.64599E-06
Tbc1d10c	108995	17.81081081	Up	chr19	4184361	4184740	379	4.61772E-06
Cx3cr1	13051	16.29090909	Up	chr9	120051221	120051460	239	1.12074E-09
Bhlhe22	59058	16.16216216	Up	chr3	18055801	18056180	379	1.39035E-06
Fgg	99571	12.77879342	Down	chr3	83008647	83008741	94	2.1945E-09
Fgg	99571	11.67778106	Down	chr3	83010063	83010180	117	1.6791E-09
Dvl3	13544	7.87254902	Down	chr16	20522461	20522660	199	8.52622E-06
Fgb	110135	7.239726027	Down	chr3	83049701	83049803	102	2.426E-08
Slc2a5	56485	6.895348837	Down	chr4	150143641	150143960	319	9.64308E-09
Gm21994	102637277	6.525504152	Down	chr2	150254517	150255160	643	3.39444E-07
Fga	14161	5.909136445	Down	chr3	83031021	83031620	599	1.55539E-08
Fga	14161	5.251931475	Down	chr3	83026152	83026260	108	8.18498E-12
Mpped1	223726	5.03943662	Down	chr15	83856361	83856840	479	6.39334E-11
Calcb	116903	4.906439854	Down	chr7	114721974	114722161	187	6.45098E-12

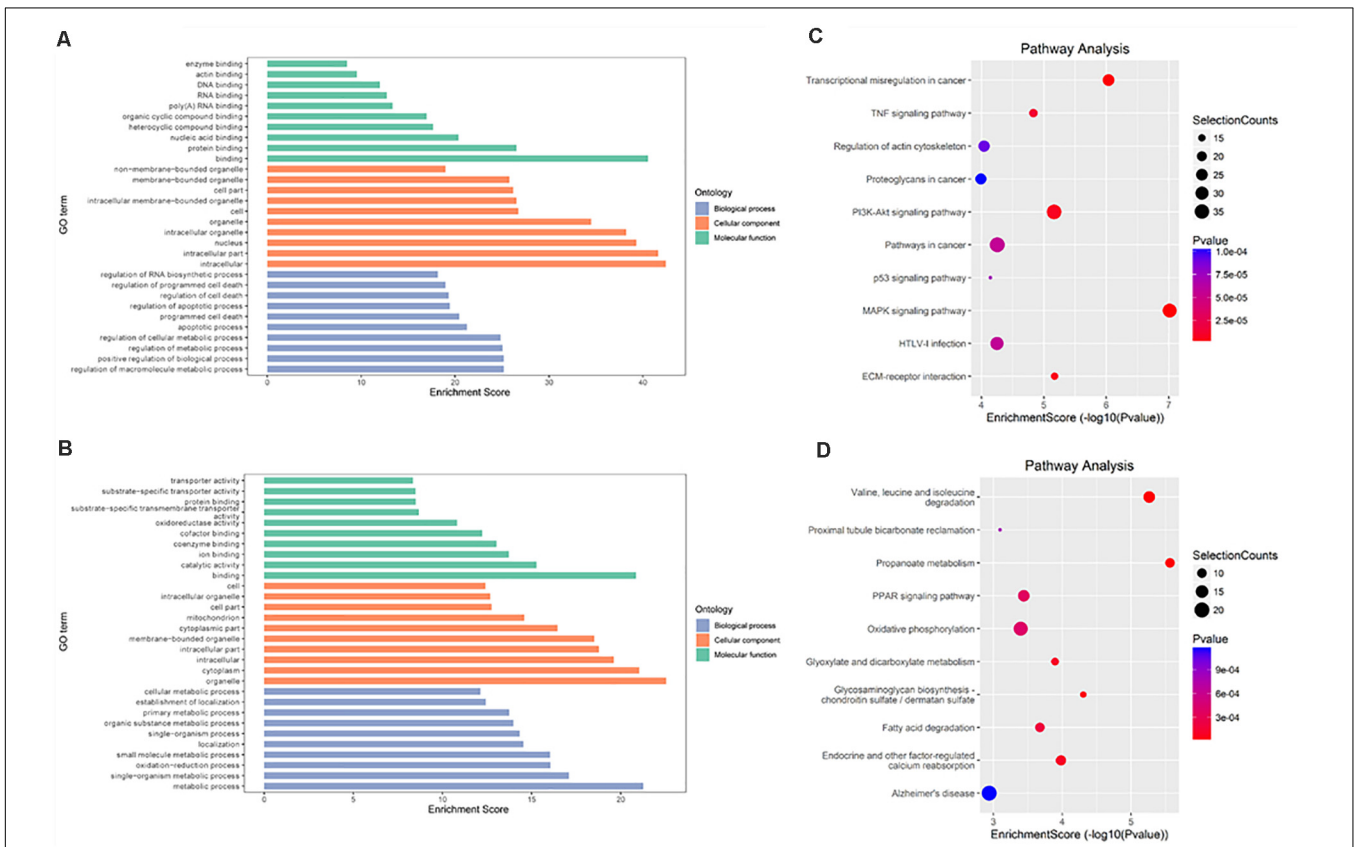

FIGURE 4 | Gene ontology and Kyoto Encyclopedia of Genes and Genomes analyses of coding genes containing DMMSs in IvC. **(A)** Major gene ontology terms were enriched for the genes containing up-regulated m6A sites in IvC. **(B)** Major gene ontology terms were enriched for the genes containing down-regulated m6A sites in IvC. **(C)** Major enriched pathways for the genes containing up-regulated m6A sites in IvC. **(D)** Major enriched pathways for the genes containing down-regulated m6A sites in IvC.

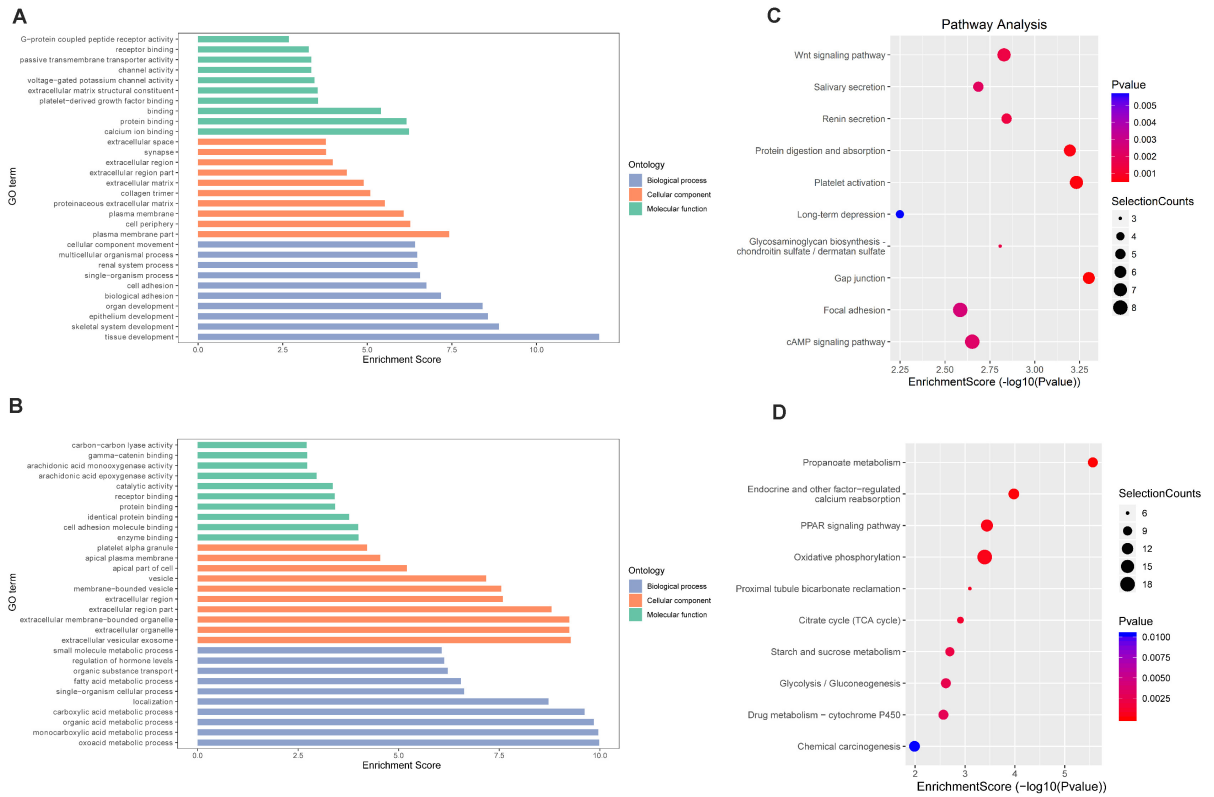

FIGURE 5 | Gene ontology and Kyoto Encyclopedia of Genes and Genomes analyses of coding genes containing DMMSs in TvI. **(A)** Major gene ontology terms were enriched for the genes containing up-regulated m6A sites in TvI. **(B)** Major gene ontology terms were enriched for the genes containing down-regulated m6A sites in TvI. **(C)** Major enriched pathways for the genes containing up-regulated m6A sites in TvI. **(D)** Major enriched pathways for the genes containing down-regulated m6A sites in TvI.

codon had the highest fold change among sites with decreased methylation (**Figure 3F**).

We further analyzed DMMSs with contrary methylation trends in IvC and TvI. In total, 94 DMMSs showed opposite trends. Of these, 42.55% (40/94) exhibited significantly increased methylation in IvC but decreased methylation in TvI.

Chromosomes 1, 2, 11, and 10 were the top four chromosomes harboring the most DMMSs (**Supplementary Figure 3**). The top four with the highest relative densities were 16, 10, 11, and 3 (**Figure 3G**). Most DMMSs were within a CDS (**Figure 3H**).

Differentially Methylated RNAs Are Involved in Important Biological Pathways

To explore the role of m6A in different groups, GO enrichment analyses and KEGG pathway analyses were used to analyze all protein coding genes containing DMMSs.

In IvC (**Figure 4**), for the BP category, genes with increased methylation of m6A sites were significantly ($p < 0.05$) enriched in the regulation of metabolic processes and cell death processes, such as macromolecule metabolic, cellular metabolic, and apoptotic processes (**Figure 4A**); genes with decreased methylation were highly enriched in metabolic processes, oxidation–reduction processes, transport, transmembrane transport, and others (**Figure 4B**). Regarding pathways, the former were significantly involved in apoptosis-associated pathways (e.g., TNF, MAPK, P53 signaling pathways) while the latter were involved in propanoate metabolism, oxidative phosphorylation, and others (**Figures 4C,D**). For the CC category, genes containing DMMSs were mainly enriched in the intracellular organelles, cytoplasm, and nucleus intracellular membrane-bound organelles. For the MF category, upregulation of m6A was notably enriched in genes involved in enzyme binding, actin binding, DNA binding, and RNA compound binding, while loss of m6A methylation was enriched in genes involved in catalytic activity, ion binding, coenzyme binding, and cofactor binding (**Figures 4A,B**). These results suggest that m6A has complicated roles in CI-AKI, with primary roles in metabolism, various pathways related to cell death, and oxidation.

In TvI (**Figure 5**), for the BP category, genes with increased methylation of m6A sites were significantly ($p < 0.05$) enriched in some development-associated processes, such as tissue, skeletal system, epithelium, and organ development (**Figure 5A**), while those with decreased methylation were highly enriched in acid metabolism processes, such as the oxoacid, organic acid, and carboxylic acid metabolic processes (**Figure 5B**). Regarding

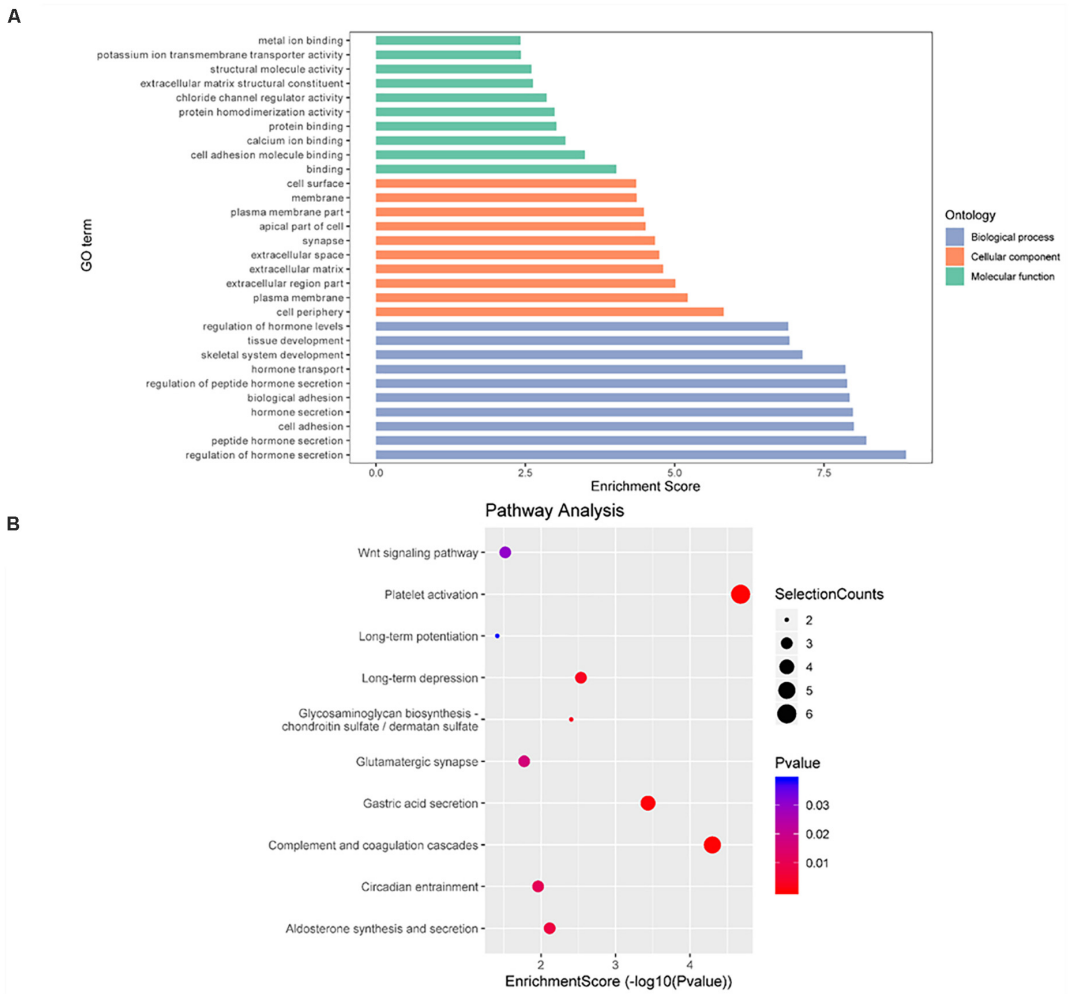

FIGURE 6 | Gene ontology and Kyoto Encyclopedia of Genes and Genomes analyses of coding genes containing DMMSs. **(A)** Major gene ontology terms were enriched for the genes containing m6A sites with reverse methylation trend between IvC and TvI. **(B)** Major enriched pathways for the genes containing m6A sites with reverse trend between IvC and TvI.

pathways, the former were significantly involved in gap junctions, protein digestion and absorption, and the Wnt pathway, while the latter were involved in metabolic processes, such as the PPAR signaling pathway (**Figures 5C,D**). For the CC category, genes containing DMMSs induced by cisplatin-induced AKI were mainly enriched in plasma membrane, cell periphery extracellular vesicular exosome, and extracellular organelles. For the MF category, increased methylation of m6A was notably enriched in calcium ion binding, protein binding, and channel activity, while decreased methylation of m6A was enriched in enzyme binding, cell adhesion molecule binding, and identical protein binding (**Figures 5A,B**). These results suggest that m6A methylation is involved in berberine alleviating CI-AKI in mouse kidneys.

Finally, GO enrichment and KEGG pathway analyses were conducted on genes containing m6A sites showing opposite methylation trends in IvC and TvI (**Figure 6**). For the BP category, genes with DMMSs were significantly ($p < 0.05$) enriched in hormone secretion processes, such as regulation of hormone secretion and peptide hormone secretion (**Figure 6A**). Pathway analyses demonstrated that genes with DMMSs were involved in platelet activation, complement and coagulation cascades, and gastric acid secretion (**Figure 6B**). For the CC category, genes containing DMMSs were mainly enriched in the cell periphery, plasma membrane, and extracellular matrix. For the MF category, genes were enriched in binding, cell adhesion molecule binding, and calcium ion binding (**Figure 6A**). These results suggest that berberine might resist the nephrotoxicity of cisplatin through different pathways.

Conjoint Analyses of m6A Modification and Gene Regulation

RNA-seq was used to detect DEGs among the groups. In IvC, 4,469 genes were differentially expressed (fold change ≥ 2 and $p < 0.05$), including 1,655 downregulated genes and 2,814 upregulated genes (**Figure 7**). Conjoint analyses of DMGs and DEGs resulted in four groups of genes: 576 hypermethylated

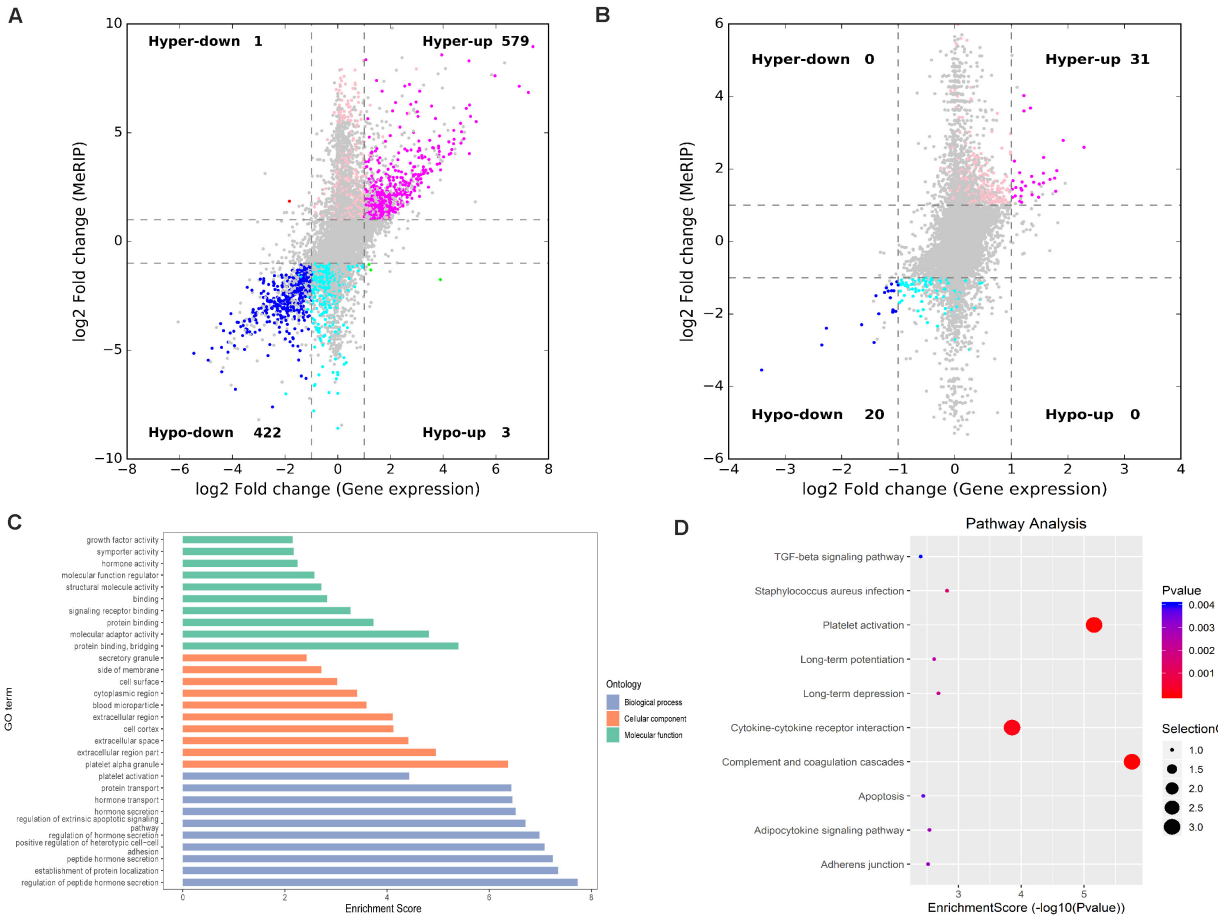

FIGURE 7 | Conjoint analysis of differentially methylated genes and differentially expressed genes. **(A)** Four-quadrant graph exhibiting the DEGs containing differentially methylated m6A peaks in IvC. **(B)** Four-quadrant graph exhibiting the DEGs containing differentially methylated m6A peaks in TvI. **(C)** Major gene ontology terms were significantly enriched for the genes containing m6A sites with reverse methylation and expression trends between IvC and TvI. **(D)** Major enriched pathways for the genes containing m6A sites with reverse methylation and expression trends between IvC and TvI.

and upregulated genes, 422 hypomethylated and downregulated genes, 1 hypermethylated but downregulated gene, and 3 hypomethylated but upregulated genes (**Figure 7A**). In TvI, 350 genes were differentially expressed, including 84 downregulated genes and 266 upregulated genes. Conjoint analyses revealed 31 hypermethylated and upregulated genes, 20 hypermethylated but downregulated genes, and no hypomethylated upregulated or hypomethylated downregulated genes (**Figure 7B**).

To further analyze the role of m6A in alleviating the action of berberine, genes with opposite methylation and expression trends in IvC and TvI were selected (**Table 3**). Overall, 9 were hypermethylated and upregulated in IvC but hypomethylated and downregulated in TvI, and 12 were hypomethylated and downregulated in IvC but hypermethylated and upregulated in TvI. GO and pathway analyses were performed to uncover the biological processes associated with these genes (**Figure 7C**). These genes were found to be highly enriched in complement and coagulation cascades, platelet activation, and cytokine–cytokine receptor interaction (**Figure 7D**). For instance, FGA/FGB/FGG genes encoding fibrinogen (Martini et al., 2019; Vilar et al., 2020) were hypermethylated and upregulated in IvC but were hypomethylated and downregulated in TvI (**Figure 8A**). Slc12a1, the key gene that mediates the electroneutral movement of Na(+) and K(+) across cell membranes (Schiessl et al., 2013; Xue et al., 2014; Hao et al., 2018; Kawaguchi et al., 2018), was hypomethylated and downregulated in IvC but hypermethylated and upregulated in TvI (**Figure 8B**). Havcr1, also known as Kim-1, is a well-known biomarker for kidney injury (Lippi et al., 2018; Seibert et al., 2018; Song et al., 2019; Zdziechowska et al., 2020). Cisplatin induced hypermethylation and upregulation of Havcr1, while berberine reversed these effects (**Figure 8C**).

Western Blotting Analyses of Protein Expression in FGA, Slc12a1, and Havcr1

Western blotting was conducted to detect the protein levels of FGA, Slc12a1, and Havcr1 in each group. Cisplatin induced an increase in Slc12a1 protein levels and a decrease in FGA and Havcr1 protein levels. However, berberine pretreatment reversed these effects (**Figure 8D**).

TABLE 3 | Genes with contrary methylation and expression trends between IvC and TvI.

Gene name	Gene ID	m6A regulation & gene regulation in IvC	m6A regulation & gene regulation in TvI	Chromosome	Peak start	Peak end	*P*-value in IvC	FDR in IvC	*P*-value in TvI	FDR in TvI
Akap12	83397	Up	Down	chr10	4353141	4353240	5.00E-05	0.00196624	5.00E-05	0.000154677
Amica1	270152	Up	Down	chr9	45107681	45108040	0.00335	0.052867	2.00E-04	0.000571614
Fga	14161	Up	Down	chr3	83031021	83031620	5.00E-05	0.00196624	5.00E-05	0.000154677
Fgb	110135	up	Down	chr3	83042246	83042340	5.00E-05	0.00196624	5.00E-05	0.000154677
Fgg	99571	Up	Down	chr3	83010063	83010180	5.00E-05	0.00196624	5.00E-05	0.000154677
Havcr1	171283	Up	Down	chr11	46756128	46756260	5.00E-05	0.00196624	5.00E-05	0.000154677
Inhbb	16324	Up	Down	chr1	119422161	119422248	5.00E-05	0.00196624	5.00E-05	0.000154677
Lep	16846	Up	Down	chr6	29073261	29073500	5.00E-05	0.00196624	5.00E-05	0.000154677
Mlph	171531	Up	Down	chr1	90950081	90950420	5.00E-05	0.00196624	5.00E-05	0.000154677
Egfl6	54156	Down	Up	chrX	166538413	166538734	5.00E-05	0.000154677	5.00E-05	0.00196624
Gbp4	17472	Down	Up	chr5	105118221	105118499	5.00E-05	0.000154677	0.00195	0.0357303
Gnaz	14687	Down	Up	chr10	75015621	75015980	2.00E-04	0.00635985	0.00045	0.00121049
Ppp1r1a	58200	Down	Up	chr15	103537841	103537992	5.00E-05	0.00196624	5.00E-05	0.000154677
Ranbp3l	223332	Down	Up	chr15	8967948	8968040	5.00E-05	0.00196624	5.00E-05	0.000154677
Slc12a1	20495	Down	Up	chr2	125152504	125152633	5.00E-05	0.00196624	5.00E-05	0.000154677
Slc16a7	20503	Down	Up	chr10	125230591	125230700	5.00E-05	0.00196624	5.00E-05	0.000154677
Snai2	20583	Down	Up	chr16	14708181	14708720	5.00E-05	0.00196624	5.00E-05	0.000154677
Tfap2b	21419	Down	Up	chr1	19212053	19212140	5.00E-05	0.00196624	5.00E-05	0.000154677
Tmem207	100043057	Down	Up	chr16	26504161	26504620	5.00E-05	0.00196624	5.00E-05	0.000154677
Tnfsf10	22035	Down	Up	chr3	27342154	27342427	5.00E-05	0.00196624	5.00E-05	0.000154677
Tril	66873	Down	Up	chr6	53818361	53819000	5.00E-05	0.00196624	5.00E-05	0.000154677

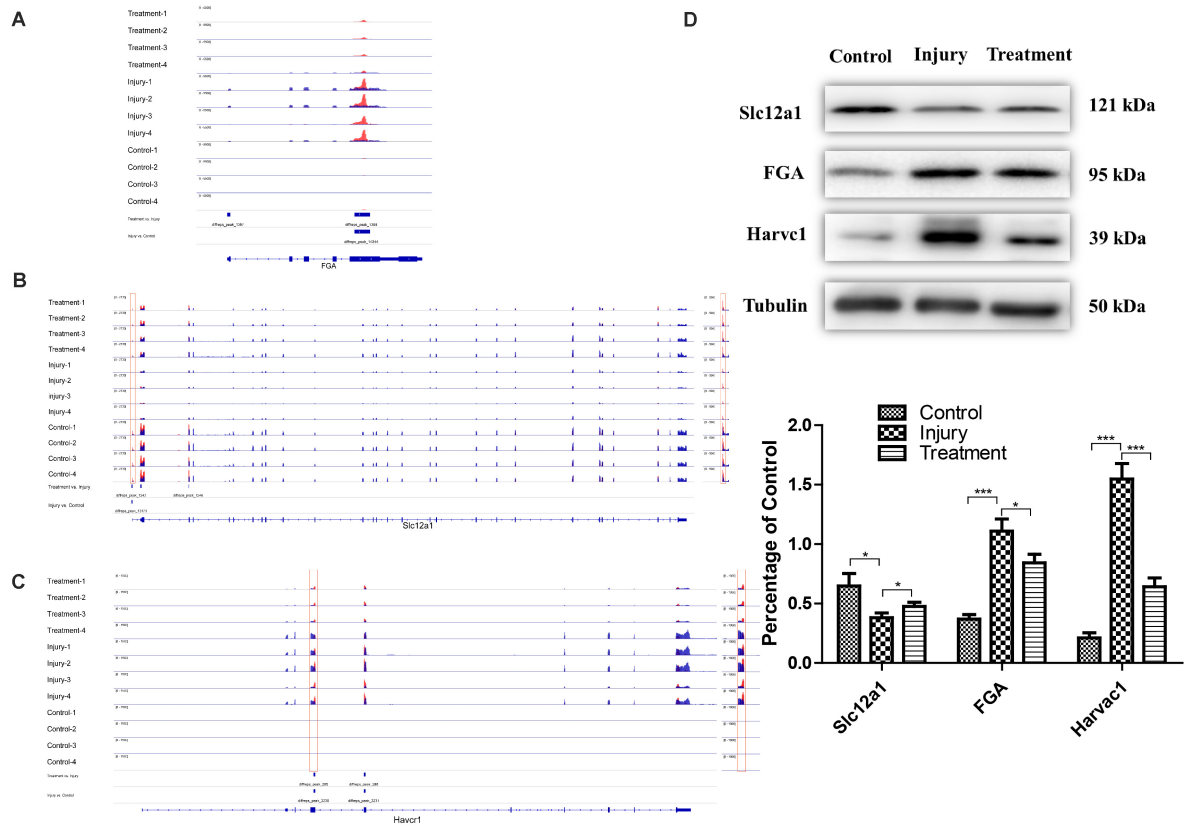

FIGURE 8 | Representative genes with opposite m6A methylation and expression trends between IvC and TvI. **(A)** Visualization of m6A-modified genes FGA in the control group, injury group, and treatment group. **(B)** Visualization of m6A modified genes Slc12a1 in the control group, injury group, and treatment group. **(C)** Visualization of m6A-modified genes Havcr1 in the control group, injury group, and treatment group. **(D)** Western blot images of FGA, Slc12a1, and Havcr1 in control group, injury group, and Havcr1 group. Error bars represent the standard deviation. $^{*}p < 0.05$, $^{***}p < 0.001$, Student's *t*-test.

DISCUSSION

m6A methylation is considered a reversible dynamic modification in many species. Previous studies have shown that m6A modification can regulate cellular responses to stimuli by affecting mRNA transcription, splicing, localization, translation, stability, and posttranscriptional regulation of gene expression at the RNA level (Zhou et al., 2015; Fry et al., 2017). Evidence (Anders et al., 2018; Wang Y. et al., 2019; Zhou P. et al., 2019; Li et al., 2020; Liu et al., 2020; Xu et al., 2020) also suggests a strong relationship between m6A modification and kidney disease, thereby revealing an important biological role for m6A in the regulation of kidney injury.

In this study, a reliable cisplatin-induced AKI model was established in mice, and the model was tested by analyzing Scr, BUN, and kidney section images. The kidney injury resulted in dynamic m6A modifications and gene expression in the kidneys. Differentially methylated mRNAs were found to be involved in many biological pathways. m6A methylation was enriched in the CDS in all groups. In IvC, GO, and KEGG analyses of coding genes harboring DMMSs demonstrated that genes with increased methylation were primarily enriched in the pathways related to metabolic processes and cell death process, such as macromolecule metabolic processes, cellular metabolic processes, the TNF signaling pathway, and the MAPK signaling pathway, while decreases in methylation were mainly enriched in metabolic processes, oxidation, and transport, indicating that cisplatin induced complicated variation in m6A methylation. Several pathways have been thoroughly studied as factors affecting CI-AKI. However, we found that variation in metabolic processes constituted the foundation of the biological and pathological changes in CI-AKI.

Different m6A methylation sites were also detected in TvI. GO, and KEGG analyses of coding genes with DMMSs revealed that the genes with increases in methylation were primarily enriched in pathways associated with tissue, the skeletal system, and epithelium development, such as gap junctions and the Wnt signaling pathway. Genes with decreases in methylation were mainly enriched in the oxoacid metabolic process and organic metabolic process. These results provide evidence of a link between m6A and berberine-mediated regulation of kidney injury, showing that berberine attenuated CI-AKI by increasing the methylation of genes associated with tissue, the skeletal system, and epithelium development. These results should prove useful for

directing future research into the underlying medical value of berberine in CI-AKI.

Furthermore, 94 DMMSs showed opposite methylation trends in IvC and TvI. The genes with those DMMSs were primarily enriched in pathways associated with hormone secretion and complement and coagulation cascades, which implies that berberine probably relieves CI-AKI by directly reversing some changes in m6A methylation.

Finally, conjoint analyses of m6A modifications and gene regulation provided a broad picture of CI-AKI and the impacts of berberine pretreatment. In total, 21 genes were found to show opposite m6A methylation and expression trends in IvC and TvI. Among these candidate genes, several drew our attention. For instance, FGA/FGB/FGG are the core genes encoding fibrinogen. Cisplatin may cause endothelial injury and inflammation, which can activate coagulation cascades (Ozkok and Edelstein, 2014). Thus, FGA/FGB/FGG were hypermethylated and upregulated in CI-AKI. However, berberine pretreatment significantly alleviated these trends. This result is consistent with one previous study (Riccioni et al., 2018). Slc12a1, also known as NKCC2, is the molecular target of loop diuretics, as it is expressed on the apical membrane of the thick ascending limb of Henle epithelial cells (Hao et al., 2018). It mediates the electroneutral movement of $Na^{(+)}$ and $K^{(+)}$, which is tightly coupled to the movement of $Cl^{(-)}$ across cell membranes (Schiessl et al., 2013; Xue et al., 2014; Kawaguchi et al., 2018). In our study, Slc12a1 was hypomethylated and downregulated by cisplatin. Berberine pretreatment maintained transmembrane ion exchange by hypermethylating and upregulating Slc12a1. Havcr1, also known as KIM-1, is a promising biomarker for predicting kidney injury (Lippi et al., 2018; Seibert et al., 2018; Song et al., 2019; Zdziechowska et al., 2020). It may reduce acute injury by mediating phagocytosis (Yang et al., 2015). In our study, it was hypermethylated and upregulated in CI-AKI. However, berberine reversed these trends. Consistently, the protein expression levels of FGA, Slc12a1, and KIM-1 were similar to the m6A methylation and gene expression levels. These results suggest that berberine has a protective effect in CI-AKI through different pathways.

CONCLUSION

We characterized the differential m6A methylome in normal, CI-AKI, and berberine-pretreated CI-AKI in mice. Our results suggest a strong association between m6A methylation and the regulation of CI-AKI. In addition, the candidate genes identified reveal the possible pathways by which berberine alleviates kidney injury. Altogether, our results provide a fundamental contribution to research into the mechanisms of and novel therapies for CI-AKI.

DATA AVAILABILITY STATEMENT

The datasets generated for this study can be found in (US National Center for Biotechnology Information Gene Expression Omnibus). The accession ID is GSE157261 (https://www.ncbi.nlm.nih.gov/geo/query/ acc. cgi?acc = GSE157261).

ETHICS STATEMENT

The animal study was reviewed and approved by The Institutional Animal Care and Use Committee of Shanghai Jiaotong University affiliated Renji Hospital.

AUTHOR CONTRIBUTIONS

ZN and XC contributed to design the research. JS, WW, and XS conducted the experiments. JS and WW analyzed and interpreted the data, and drafted the manuscript. JW and SL helped to polish the manuscript. All authors read and approved the final manuscript.

FUNDING

This work was supported in part by grants from the National Natural Science Foundation of China (No. 81700586); Key Shanghai Laboratory of Nucleic Acid Chemistry and Nanomedicine (2020ZYB009); Shanghai Municipal Planning Commission of science and Research [No. ZY(2018-2020)-FWTX-1001)]; Medical Scientific Research Project of Health and Family Planning Commission of Jiangsu Province (No. Z2018026).

ACKNOWLEDGMENTS

We are grateful to BioDataStudio (Shanghai) for the assistance of drawing figures. We are also grateful to Drs. Chaojun Qi and Wenyan Zhou for the assistance in pathobiology.

SUPPLEMENTARY MATERIAL

The Supplementary Material for this article can be found online at: https://www.frontiersin.org/articles/10.3389/fgene.2020.584460/full#supplementary-material

Supplementary Figure 1 | Venn diagram showing the overlap of m6A peaks within mRNAs in three groups.

Supplementary Figure 2 | Chromosomal distribution of all DMM sites. **(A)** Chromosomal distribution of all DMM sites in IvC. **(B)** Chromosomal distribution of all DMM sites in TvI.

Supplementary Figure 3 | Chromosomal distribution of DMM sites presenting contrary methylation trend between IvC and TvI.

REFERENCES

Ahmad, S., Hussain, A., Hussain, A., Abdullah, I., Ali, M. S., Froeyen, M., et al. (2019). Quantification of berberine in *Berberis vulgaris* L. root extract and its curative and prophylactic role in cisplatin-induced in vivo toxicity and in vitro cytotoxicity. *Antioxidants* 8:185. doi: 10.3390/antiox8060185

Anders, M., Chelysheva, I., Goebel, I., Trenkner, T., Zhou, J., Mao, Y., et al. (2018). Dynamic m(6)A methylation facilitates mRNA triaging to stress granules. *Life Sci. Alliance* 1:e201800113. doi: 10.26508/lsa.201800113

Caliceti, C., Franco, P., Spinozzi, S., Roda, A., and Cicero, A. F. (2016). Berberine: new insights from pharmacological aspects to clinical evidences in the management of metabolic disorders. *Curr. Med. Chem.* 23, 1460–1476. doi: 10.2174/0929867323666160411143314

Chen, H. Y., Ye, X. L., Cui, X. L., He, K., Jin, Y. N., Chen, Z., et al. (2012). Cytotoxicity and antihyperglycemic effect of minor constituents from Rhizoma Coptis in HepG2 cells. *Fitoterapia* 83, 67–73. doi: 10.1016/j.fitote.2011.09.014

Chen, Y., Chen, Y., Shi, C., Huang, Z., Zhang, Y., Li, S., et al. (2018). SOAPnuke: a MapReduce acceleration-supported software for integrated quality control and preprocessing of high-throughput sequencing data. *Gigascience* 7, 1–6. doi: 10.1093/gigascience/gix120

Cummings, B. S., and Schnellmann, R. G. (2002). Cisplatin-induced renal cell apoptosis: caspase 3-dependent and -independent pathways. *J. Pharmacol. Exp. Ther.* 302, 8–17. doi: 10.1124/jpet.302.1.8

Dominissini, D., Moshitch-Moshkovitz, S., Schwartz, S., Salmon-Divon, M., Ungar, L., Osenberg, S., et al. (2012). Topology of the human and mouse m6A RNA methylomes revealed by m6A-seq. *Nature* 485, 201–206. doi: 10.1038/nature11112

Domitrović, R., Jakovac, H., Marchesi, V. V., and Blažeković, B. (2013). Resolution of liver fibrosis by isoquinoline alkaloid berberine in CCl4-intoxicated mice is mediated by suppression of oxidative stress and upregulation of MMP-2 expression. *J. Med. Food* 16, 518–528. doi: 10.1089/jmf.2012.0175

Duan, Y., Liu, T., Zhou, Y., Dou, T., and Yang, Q. (2018). Glycoside hydrolase family 18 and 20 enzymes are novel targets of the traditional medicine berberine. *J. Biol. Chem.* 293, 15429–15438. doi: 10.1074/jbc.RA118.004351

Dutta, R. K., Kondeti, V. K., Sharma, I., Chandel, N. S., Quaggin, S. E., and Kanwar, Y. S. (2017). Beneficial effects of myo-inositol oxygenase deficiency in cisplatin-induced AKI. *J. Am. Soc. Nephrol.* 28, 1421–1436. doi: 10.1681/asn.2016070744

Fan, D., Liu, L., Wu, Z., and Cao, M. (2019). Combating neurodegenerative diseases with the plant alkaloid berberine: molecular mechanisms and therapeutic potential. *Curr. Neuropharmacol.* 17, 563–579. doi: 10.2174/1570159x16666180419141613

Fry, N. J., Law, B. A., Ilkayeva, O. R., Holley, C. L., and Mansfield, K. D. (2017). N(6)-methyladenosine is required for the hypoxic stabilization of specific mRNAs. *RNA* 23, 1444–1455. doi: 10.1261/rna.061044.117

George, B., Joy, M. S., and Aleksunes, L. M. (2018). Urinary protein biomarkers of kidney injury in patients receiving cisplatin chemotherapy. *Exp. Biol. Med.* 243, 272–282. doi: 10.1177/1535370217745302

Hao, S., Hao, M., and Ferreri, N. R. (2018). Renal-specific silencing of TNF (tumor necrosis factor) unmasks salt-dependent increases in blood pressure via an NKCC2A (Na(+)-K(+)-2Cl(-) cotransporter isoform A)-dependent mechanism. *Hypertension* 71, 1117–1125. doi: 10.1161/hypertensionaha.117.10764

Heinz, S., Benner, C., Spann, N., Bertolino, E., Lin, Y. C., Laslo, P., et al. (2010). Simple combinations of lineage-determining transcription factors prime cis-regulatory elements required for macrophage and B cell identities. *Mol. Cell.* 38, 576–589. doi: 10.1016/j.molcel.2010.05.004

Holditch, S. J., Brown, C. N., Lombardi, A. M., Nguyen, K. N., and Edelstein, C. L. (2019). Recent advances in models, mechanisms, biomarkers, and interventions in cisplatin-induced acute kidney injury. *Int. J. Mol. Sci.* 20:3011. doi: 10.3390/ijms20123011

Huang, H., Weng, H., Keren Zhou, K., Wu, T., Zhao, B., Sun, M., et al. (2019). Histone H3 trimethylation at lysine 36 guides m6A RNA modification co-transcriptionally. *Nature* 567, 414–419. doi: 10.1038/s41586-019-1016-7

Humanes, B., Camaño, S., Lara, J. M., Sabbisetti, V., González-Nicolás, M., Bonventre, J. V., et al. (2017). Cisplatin-induced renal inflammation is ameliorated by cilastatin nephroprotection. *Nephrol. Dial. Transplant.* 32, 1645–1655. doi: 10.1093/ndt/gfx005

Jia, G., Fu, Y., Zhao, X., Dai, Q., Zheng, G., Yang, Y., et al. (2011). N6-methyladenosine in nuclear RNA is a major substrate of the obesity-associated FTO. *Nat. Chem. Biol.* 7, 885–887. doi: 10.1038/nchembio.687

Kawaguchi, K., Hatano, R., Matsubara, M., and Asano, S. (2018). Internalization of NKCC2 is impaired in thick ascending limb of Henle in moesin knockout mice. *Pflugers Arch.* 470, 1055–1068. doi: 10.1007/s00424-018-2134-z

Kechin, A., Boyarskikh, U., Kel, A., and Filipenko, M. (2017). cutPrimers: a new tool for accurate cutting of primers from reads of targeted next generation sequencing. *J. Comput. Biol.* 24, 1138–1143. doi: 10.1089/cmb.2017.0096

Kim, D., Langmead, B., and Salzberg, S. L. (2015). HISAT: a fast spliced aligner with low memory requirements. *Nat. Methods* 12, 357–360. doi: 10.1038/nmeth.3317

Langmead, B., and Salzberg, S. L. (2012). Fast gapped-read alignment with Bowtie 2. *Nat. Methods* 9, 357–359. doi: 10.1038/nmeth.1923

Lebwohl, D., and Canetta, R. (1998). Clinical development of platinum complexes in cancer therapy: an historical perspective and an update. *Eur. J. Cancer* 34, 1522–1534. doi: 10.1016/s0959-8049(98)00224-x

Leemans, J. C., Stokman, G., Claessen, N., Rouschop, K. M., Teske, G. J., Kirschning, C. J., et al. (2005). Renal-associated TLR2 mediates ischemia/reperfusion injury in the kidney. *J. Clin. Invest.* 115, 2894–2903. doi: 10.1172/JCI22832

Li, H., Tong, J., Zhu, S., Batista, P., Duffy, E., Zhao, J., et al. (2017). m6A mRNA methylation controls T cell homeostasis by targeting the IL-7/STAT5/SOCS pathways. *Nature* 548, 338–342. doi: 10.1038/nature23450

Li, Y., Wang, J., Huang, C., Shen, M., Zhan, H., and Xu, K. (2020). RNA N6-methyladenosine: a promising molecular target in metabolic diseases. *Cell. Biosci.* 10:19. doi: 10.1186/s13578-020-00385-4

Lippi, I., Perondi, F., Meucci, V., Bruno, B., Gazzano, V., and Guidi, G. (2018). Clinical utility of urine kidney injury molecule-1 (KIM-1) and gamma-glutamyl transferase (GGT) in the diagnosis of canine acute kidney injury. *Vet. Res. Commun.* 42, 95–100. doi: 10.1007/s11259-018-9711-7

Liu, P., Zhang, B., Chen, Z., He, Y., Du, Y., Liu, Y., et al. (2020). m(6)A-induced lncRNA MALAT1 aggravates renal fibrogenesis in obstructive nephropathy through the miR-145/FAK pathway. *Aging* 12, 5280–5299. doi: 10.18632/aging.102950

Long, Y., Zhen, X., Zhu, F., Hu, Z., Lei, W., Li, S., et al. (2017). Hyperhomocysteinemia exacerbates cisplatin-induced acute kidney injury. *Int. J. Biol. Sci.* 13, 219–231. doi: 10.7150/ijbs.16725

Luo, Z., Zhang, Z., Tai, L., Zhang, L., Sun, Z., and Zhou, L. (2019). Comprehensive analysis of differences of N(6)-methyladenosine RNA methylomes between high-fat-fed and normal mouse livers. *Epigenomics* 11, 1267–1282. doi: 10.2217/epi-2019-0009

Martini, F., Cecconi, N., Paolicchi, A., Galimberti, S., Cervetti, G., Buda, G., et al. (2019). Interference of monoclonal gammopathy with fibrinogen assay producing spurious dysfibrinogenemia. *TH Open* 3, e64–e66. doi: 10.1055/s-0039-1683969

Meyer, K. D., Saletore, Y., Zumbo, P., Elemento, O., Mason, C. E., and Jaffrey, S. R. (2012). Comprehensive analysis of mRNA methylation reveals enrichment in 3' UTRs and near stop codons. *Cell* 149, 1635–1646. doi: 10.1016/j.cell.2012.05.003

Ojha, S., Venkataraman, B., Kurdi, A., Mahgoub, E., Sadek, B., and Rajesh, M. (2016). Plant-derived agents for counteracting cisplatin-induced nephrotoxicity. *Oxid. Med. Cell Longev.* 2016:4320374. doi: 10.1155/2016/4320374

Olarerin-George, A. O., and Jaffrey, S. R. (2017). MetaPlotR: a Perl/R pipeline for plotting metagenes of nucleotide modifications and other transcriptomic sites. *Bioinformatics* 33, 1563–1564. doi: 10.1093/bioinformatics/btx002

Ozkok, A., and Edelstein, C. L. (2014). Pathophysiology of cisplatin-induced acute kidney injury. *Biomed. Res. Int.* 2014:967826. doi: 10.1155/2014/967826

Ping, X. L., Sun, B. F., Wang, L., Xiao, W., Yang, X., Wang, W. J., et al. (2014). Mammalian WTAP is a regulatory subunit of the RNA N6-methyladenosine methyltransferase. *Cell Res.* 24, 177–189. doi: 10.1038/cr.2014.3

Riccioni, G., Gammone, M. A., Currenti, W., and D'Orazio, N. (2018). Effectiveness and safety of dietetic supplementation of a new nutraceutical on lipid profile and serum inflammation biomarkers in hypercholesterolemic patients. *Molecules* 23:1168. doi: 10.3390/molecules23051168

Ruan, H., Zhan, Y. Y., Hou, J., Xu, B., Chen, B., Tian, Y., et al. (2017). Berberine binds RXRα to suppress β-catenin signaling in colon cancer cells. *Oncogene* 36, 6906–6918. doi: 10.1038/onc.2017.296

Sahu, B. D., Mahesh Kumar, J., and Sistla, R. (2015). Baicalein, a bioflavonoid, prevents cisplatin-induced acute kidney injury by up-regulating antioxidant defenses and down-regulating the MAPKs and NF-κB pathways. *PLoS One* 10:e0134139. doi: 10.1371/journal.pone.0134139

Schiessl, I. M., Rosenauer, A., Kattler, V., Minuth, W. W., Oppermann, M., and Castrop, H. (2013). Dietary salt intake modulates differential splicing of the Na-K-2Cl cotransporter NKCC2. *Am. J. Physiol. Renal Physiol.* 305, F1139–F1148. doi: 10.1152/ajprenal.00259.2013

Seibert, F. S., Sitz, M., Passfall, J., Haesner, M., Laschinski, P., Buhl, M., et al. (2018). Prognostic value of urinary calprotectin, NGAL and KIM-1 in chronic kidney disease. *Kidney Blood Press. Res.* 43, 1255–1262. doi: 10.1159/000492407

Shamsa, F., Ahmadiani, A., and Khosrokhavar, R. (1999). Antihistaminic and anticholinergic activity of barberry fruit (*Berberis vulgaris*) in the guinea-pig ileum. *J. Ethnopharmacol.* 64, 161–166. doi: 10.1016/s0378-8741(98)00122-6

Shen, L., Shao, N. Y., Liu, X., Maze, I., Feng, J., and Nestler, E. J. (2013). diffReps: detecting differential chromatin modification sites from ChIP-seq data with biological replicates. *PLoS One* 8:e65598. doi: 10.1371/journal.pone.0065598

Song, J., Yu, J., Prayogo, G. W., Cao, W., Wu, Y., Jia, Z., et al. (2019). Understanding kidney injury molecule 1: a novel immune factor in kidney pathophysiology. *Am. J. Transl. Res.* 11, 1219–1229.

Spitale, R. C., Flynn, R. A., Zhang, Q. C., Crisalli, P., Lee, B., Jung, J. W., et al. (2015). Structural imprints in vivo decode RNA regulatory mechanisms. *Nature* 519, 486–490. doi: 10.1038/nature14263

Teng, Z. Y., Cheng, X. L., Cai, X. T., Yang, Y., Sun, X. Y., Xu, J. D., et al. (2015). Ancient chinese formula qiong-yu-gao protects against cisplatin-induced nephrotoxicity without reducing anti-tumor activity. *Sci. Rep.* 5:15592. doi: 10.1038/srep15592

Trapnell, C., Roberts, A., Goff, L., Pertea, G., Kim, D., Kelley, D. R., et al. (2012). Differential gene and transcript expression analysis of RNA-seq experiments with TopHat and Cufflinks. *Nat. Protoc.* 7, 562–578. doi: 10.1038/nprot.2012.016

Vilar, R., Fish, R. J., Casini, A., and Neerman-Arbez, M. (2020). Fibrin(ogen) in human disease: both friend and foe. *Haematologica* 105, 284–296. doi: 10.3324/haematol.2019.236901

Wang, J., Ishfaq, M., Xu, L., Xia, C., Chen, C., and Li, J. (2019). METTL3/m(6)A/miRNA-873-5p attenuated oxidative stress and apoptosis in colistin-induced kidney injury by modulating Keap1/Nrf2 pathway. *Front. Pharmacol.* 10:517. doi: 10.3389/fphar.2019.00517

Wang, K., Feng, X., Chai, L., Cao, S., and Qiu, F. (2017). The metabolism of berberine and its contribution to the pharmacological effects. *Drug Metab. Rev.* 49, 139–157. doi: 10.1080/03602532.2017.1306544

Wang, Y., Li, Y., Toth, J. I., Petroski, M. D., Zhang, Z., and Zhao, J. C. (2014). N6-methyladenosine modification destabilizes developmental regulators in embryonic stem cells. *Nat. Cell Biol.* 16, 191–198. doi: 10.1038/ncb2902

Wang, Y., Sun, J., Lin, Z., Zhang, W., Wang, S., Wang, W., et al. (2020). m6A mRNA methylation controls functional maturation in neonatal murine β-cells. *Diabetes Metab. Res. Rev.* 69, 1708–1722. doi: 10.2337/db19-0906

Wang, Y., Zeng, L., Liang, C., Zan, R., Ji, W., Zhang, Z., et al. (2019). Integrated analysis of transcriptome-wide m 6 A methylome of osteosarcoma stem cells enriched by chemotherapy. *Epigenomics* 11, 693–1715. doi: 10.2217/epi-2019-0262

Xu, Y., Yuan, X. D., Wu, J. J., Chen, R. Y., Xia, L., Zhang, M., et al. (2020). The N6-methyladenosine mRNA methylase METTL14 promotes renal ischemic reperfusion injury via suppressing YAP1. *J. Cell. Biochem.* 121, 524–533. doi: 10.1002/jcb.29258

Xue, H., Zhang, Z. J., Li, X. S., Sun, H. M., Kang, Q., Wu, B., et al. (2014). Localization and vasopressin regulation of the Na^+-K^+-$2Cl^-$ cotransporter in the distal colonic epithelium. *World J. Gastroenterol.* 20, 4692–4701. doi: 10.3748/wjg.v20.i16.4692

Yang, L., Brooks, C. R., Xiao, S., Sabbisetti, V., Yeung, M. Y., Hsiao, L. L., et al. (2015). KIM-1-mediated phagocytosis reduces acute injury to the kidney. *J. Clin. Invest.* 125, 1620–1636. doi: 10.1172/jci75417

Yimit, A., Adebali, O., Sancar, A., and Jiang, Y. (2019). Differential damage and repair of DNA-adducts induced by anti-cancer drug cisplatin across mouse organs. *Nat. Commun.* 10:309. doi: 10.1038/s41467-019-08290-2

Zdziechowska, M., Gluba-Brzózka, A., Franczyk, B., and Rysz, J. (2020). Biochemical markers in the prediction of contrast-induced acute kidney injury. *Curr. Med. Chem.* [Epub ahead of print]. doi: 10.2174/0929867327666200502015749

Zhang, J., Rudemiller, N. P., Patel, M. B., Wei, Q., Karlovich, N. S., Jeffs, A. D., et al. (2016). Competing actions of type 1 angiotensin II receptors expressed on T lymphocytes and kidney epithelium during cisplatin-induced AKI. *J. Am. Soc. Nephrol.* 27, 2257–2264. doi: 10.1681/asn.2015060683

Zhang, Y., Liu, T., Meyer, C. A., Eeckhoute, J., Johnson, D. S., Bernstein, B. E., et al. (2008). Model-based analysis of ChIP-Seq (MACS). *Genome Biol.* 9:R137. doi: 10.1186/gb-2008-9-9-r137

Zheng, G., Dahl, J. A., Niu, Y., Fedorcsak, P., Huang, C. M., Li, C. J., et al. (2013). ALKBH5 is a mammalian RNA demethylase that impacts RNA metabolism and mouse fertility. *Mol. Cell.* 49, 18–29. doi: 10.1016/j.molcel.2012.10.015

Zhou, J., Wan, J., Gao, X., Zhang, X., Jaffrey, S. R., and Qian, S. B. (2015). Dynamic m(6)A mRNA methylation directs translational control of heat shock response. *Nature* 526, 591–594. doi: 10.1038/nature15377

Zhou, J. C., Wang, J. Y., Hong, B. A., Ma, K. F., Xie, H. B., Li, L., et al. (2019). Gene signatures and prognostic values of m6A regulators in clear cell renal cell carcinoma - a retrospective study using TCGA database. *Aging* 11, 1633–1647. doi: 10.18632/aging.101856

Zhou, P., Wu, M., Ye, C., Xu, Q., and Wang, L. (2019). Meclofenamic acid promotes cisplatin-induced acute kidney injury by inhibiting fat mass and obesity-associated protein-mediated m(6)A abrogation in RNA. *J. Biol. Chem.* 294, 16908–16917. doi: 10.1074/jbc.RA119.011009

Zuk, A., and Bonventre, J. V. (2016). Acute kidney injury. *Annu. Rev. Med.* 67, 293–307. doi: 10.1146/annurev-med-050214-013407

Conflict of Interest: The authors declare that the research was conducted in the absence of any commercial or financial relationships that could be construed as a potential conflict of interest.

frontiers in Physiology

REVIEW
published: 18 February 2021
doi: 10.3389/fphys.2021.640700

Histone Methyltransferase EZH2: A Potential Therapeutic Target for Kidney Diseases

*Tingting Li[1], Chao Yu[1] and Shougang Zhuang[1,2]**

[1] Department of Nephrology, Shanghai East Hospital, Tongji University School of Medicine, Shanghai, China, [2] Department of Medicine, Alpert Medical School and Rhode Island Hospital, Brown University, Providence, RI, United States

Enhancer of zeste homolog 2 (EZH2) is a histone-lysine N-methyltransferase enzyme that catalyzes the addition of methyl groups to histone H3 at lysine 27, leading to gene silencing. Mutation or over-expression of EZH2 has been linked to many cancers including renal carcinoma. Recent studies have shown that EZH2 expression and activity are also increased in several animal models of kidney injury, such as acute kidney injury (AKI), renal fibrosis, diabetic nephropathy, lupus nephritis (LN), and renal transplantation rejection. The pharmacological and/or genetic inhibition of EZH2 can alleviate AKI, renal fibrosis, and LN, but potentiate podocyte injury in animal models, suggesting that the functional role of EZH2 varies with renal cell type and disease model. In this article, we summarize the role of EZH2 in the pathology of renal injury and relevant mechanisms and highlight EZH2 as a potential therapeutic target for kidney diseases.

Keywords: acute kidney injury, chronic kidney disease, diabetic nephropathy, renal cell carcinoma, epigenetic regulation, histone methyltransferase (HMT), enhancer of zeste homolog 2 (EZH2), renal fibrosis

OPEN ACCESS

Edited by:
Xiao-ming Meng,
Anhui Medical University, China

Reviewed by:
Baoxue Yang,
Peking University, China
Haiyong Chen,
The University of Hong Kong, Hong Kong

***Correspondence:**
Shougang Zhuang
szhuang@lifespan.org;
gangzhuang@hotmail.com

Specialty section:
This article was submitted to Renal and Epithelial Physiology, a section of the journal Frontiers in Physiology

Received: *11 December 2020*
Accepted: *11 January 2021*
Published: *18 February 2021*

Citation:
Li T, Yu C and Zhuang S (2021) Histone Methyltransferase EZH2: A Potential Therapeutic Target for Kidney Diseases. Front. Physiol. 12:640700. doi: 10.3389/fphys.2021.640700

INTRODUCTION

Epigenetics refers to the heritable change of gene function and phenotype without alteration in a genes DNA sequence (Berger et al., 2009). The core function of epigenetics is to control access to the DNA genetic code both spatially and temporally to ensure orderly gene expression and silencing according to external signals. Epigenetic regulation involves DNA methylation, histone modification, chromatin recombination, and non-coding RNA (Rosner and Hengstschlager, 2012; Roy and Majumdar, 2012). These modifications control the fate of cells, regulate the normal growth, and development of individuals, and are closely related to the occurrence and development of various diseases such as cancers, diabetes, heart disease, and intestinal disease (Filion et al., 2010). The importance and diversity of histone post-translational modification have been widely studied in many epigenetic regulatory mechanisms. Histone modifications include acetylation, methylation, ubiquitination, hydroxylation, phosphorylation, and ADP ribosylation (Graff and Tsai, 2013; Hyun et al., 2017; Bochyńska et al., 2018; Worden et al., 2019). Methylation can occur in histone and non-histone proteins. Histones are proteins that are abundant in lysine and arginine and are found in eukaryotic cell nuclei. Among four core histone proteins (H2A, H2B, H3, and H4), histone H3 is one of the most important epigenetic markers in transcriptional regulation. The methylation of histone H3 mainly occurs on the arginine (R) and lysine (K) residues in its tail (Wei et al., 2009). Histone arginine residues are monomethylated or dimethylated (Blanc and Richard, 2017), while histone lysine can be monomethylated (me1), dimethylated (me2), or trimethylated (me3). Different methylation sites such as H3K4, H3K9, H3K27, H3K36, and H3K79

have been identified (Wang et al., 2009). Among those sites, trimethylation of lysine 27 in histone H3 (H3K27me3) is a key marker of gene silencing, found mainly in gene promoter and enhancer regions (Duan et al., 2020).

H3K27 trimethylation is mainly carried out by Polycomb Repressor Complex (PRC2; Tie et al., 1998; Sanchez-Beato et al., 2006; Yu et al., 2007; Veneti et al., 2017). PRC2 is a histone methyltransferase that mainly trimethylates the histone H3 lysine 27 (H3K27me3; Margueron and Reinberg, 2011; Di Croce and Helin, 2013). The PRC2 complex consists of four components: enhancer of zeste homolog 1 (EZH1) or enhancer of zeste homolog 2 (EZH2), compressor of zeste12 (Suz12), embryonic ectoderm development (EED), and RbAp46/48. EZH1 and EZH2 are the core components of PRC2, while EED can interact with EZH1 or EZH2 to maintain enzyme activity (Kim et al., 2013; Eich et al., 2020). EZH2 is an essential component of PRC2 methylation activity; it can also methylate some non-histone substrates, such as actin, GATA binding protein 4 (GATA4), android receiver (AR), and estrogen receiver (ER). EZH2 can silence tumor suppressor genes and play an important role in cell aging, fate selection, and differentiation (Jacobs and van Lohuizen, 2002; Plath et al., 2003; Martinez and Cavalli, 2006; Aloia et al., 2013). In addition, EZH2-mediated methylation of non-histones such as STAT3 is an important post-translational modification involved in many life processes, such as the cell cycle, DNA repair, cell aging, differentiation, apoptosis, and tumorigenesis (Kim et al., 2013; Eich et al., 2020).

Enhancer of zeste homolog 2 was discovered in 1996 using yeast two-hybrid experiments (Hobert et al., 1996) and its gene is located on the human chromosome 7q35. EZH2 occupies nearly 40 kb in the gene structure, which contains 20 exons, and the open reading frame is distributed on 19 exons (Cardoso et al., 2000). Studies have shown that EZH2 can inhibit the expression of tumor suppressor genes in normal cells, thereby promoting the abnormal proliferation of cells, and stimulating the metastasis of tumor cells. EZH2 exhibits gene amplification and higher levels of expression in many human malignancies, such as gastric cancer, colon cancer, breast cancer, lymphoid hematopoietic tumors, liver cancer, and nephroblastoma (Su et al., 2003; Mimori et al., 2005; Raman et al., 2005; Sudo et al., 2005; Matsukawa et al., 2006; Saramaki et al., 2006; Shi et al., 2007), and is closely related to tumorigenesis and tumor progression.

Increasing evidence shows that EZH2 is associated with a variety of kidney diseases and pathology. In addition to the abnormal expression and activation of EZH2 in renal tumors, its expression levels and activity were also increased in acute kidney injury (AKI; Zhou et al., 2018b), renal fibrosis (Zhou et al., 2016), diabetic nephropathy (DN; Jia et al., 2019b), lupus nephritis (LN; Rohraff et al., 2019), hyperuricemic nephropathy (Shi et al., 2019), and transplanted and aging kidneys (Li et al., 2016; Han and Sun, 2020). Moreover, pharmacological or genetic inhibition of EZH2 can interfere with pathologic fibrosis in these animal models of kidney disease. This article reviews the role of EZH2 in the pathology of renal disease and relevant mechanisms (**Table 1**). We also highlight EZH2 as a potential target for ameliorating fibrosis in kidney disease.

EZH2 AND RENAL CELL CARCINOMA

Renal cell carcinoma (RCC), also known as renal adenocarcinoma. originates from renal tubular epithelial cells and accounts for over 90% of adult renal malignancies. The worldwide incidence RCC has increased significantly in recent years (Shah et al., 2009). At present, the cause and pathogenesis of RCC are not clear. Epidemiology speculates that the pathogenesis is related to genetics, smoking, obesity, hypertension, and antihypertensive treatment (Grossman et al., 1999). About 70% of renal cancers are associated with gene expression inactivation caused by VHL gene deletion and mutation. VHL gene encodes an E3 ubiquitin ligase complex protein, which can degrade hypoxia inducible factor (HIF). HIF is continuously activated in RCC cells, promoting the transcription of a series of downstream target genes (Mallikarjuna et al., 2018). Recently, it has been reported that epigenetic modification, in particular, EZH2 activation, participates in the occurrence and development of RCC, which provides a new direction for the treatment (Bannister and Kouzarides, 2011).

Studies have demonstrated that EZH2 can promote the development and metastasis of RCC. EZH2 is overexpressed in numerous tumor entities including renal tumor cells (Kim and Roberts, 2016; Sun et al., 2018). EZH2 overexpression leads to increases in H3K27me3, with repression of tumor-suppressor genes such as E-cadherin (Liu et al., 2016). *In vitro* and *in vivo* studies confirmed that the abnormal increase of EZH2 can inhibit the expression level of E-cadherin, induce the epithelial stromal transformation of renal cancer cells, and promote the occurrence, development and recurrence of renal cancer. Inhibition of EZH2 with 3-DZNep can reverse these pathological responses (Liu et al., 2016). EZH2 also has growth promoting activity in RCC (Wagener et al., 2010) and can enhance the proliferation and invasion of renal tubular epithelial cells (Zhang et al., 2018). Moreover, EZH2 promotes cell proliferation, migration and angiogenesis by inhibiting expression of tumor suppressor genes such as p27Kip1 and enhancing expression of proto-oncogenes (Sakurai et al., 2012). Thus, inhibition of EZH2 can reduce the survival and invasion of clear cell renal cell carcinoma (ccRCC) cells and the growth of ccRCC in xenografted mice (Sun et al., 2018). Finally, EZH2 in combination with the DNA methyltransferase DNMT can methylate the VHL promoter and inhibit its expression in RCC (Schlesinger et al., 2007).

EZH2 AND ACUTE KIDNEY INJURY

Acute kidney injury is a common pathologic process with high mortality in hospitalized patients (Raimann et al., 2018). It can be caused by ischemia/reperfusion, septicemia, or nephrotoxins (i.e., radiocontrast agents, NSAIDs, etc.) (Zuk and Bonventre, 2016; Moledina et al., 2017; Wu et al., 2017). Acute injury to the kidney usually leads to death of renal tubular epithelial cells, activation of

endothelial cells, infiltration of leukocytes, and ultimately renal dysfunction (Sato and Yanagita, 2018; Ronco et al., 2019). In mild injury, adaptive repair mechanisms can restore epithelial integrity, inhibit immune responses and reconstruct a healthy vascular system. On the contrary, severe or persistent damage can lead to inadequate repair (Sato and Yanagita, 2018; Ronco et al., 2019). Tubular cells may experience G2/M cell cycle arrest, senescence, apoptosis or necrosis, leading to release of pro-inflammatory factors (Guzzi et al., 2019). Emerging evidence has shown the role of EZH2-mediated histone modifications in AKI (Ho et al., 2017) (Bomsztyk and Denisenko, 2013).

The abnormal expression or activation of EZH2 is related to the pathogenesis of AKI Zhou et al., 2018b). Initially, it was found that EZH2 is involved in many cellular responses, such as apoptosis and inflammation (Wang Y. et al., 2018; Bamidele et al., 2019). The expression of EZH2 and H3K27me3 is up-regulated in ischemia-reperfusion and folic acid-induced AKI models (Zhou et al., 2018b). Inhibition of EZH2 with 3-DZNep can reduce renal dysfunction and tubular cell death (Zhou et al., 2018b). E-cadherin downregulation mediates disruption of cell-cell adhesion, activation of matrix metalloproteinases, and activation of ERK1/2, and it promotes activation of cell death receptor and regulation of mitochondrial damage. Inhibition of EZH2 can preserve expression of E-cadherin and tight junction protein ZO-1, inhibit expression of matrix metalloproteinase MMP-2 and MMP-9, and suppress phosphorylation of Raf-1 and ERK1/2 in renal tubular cells exposed to oxidative stress (Zhou et al., 2018b). This was confirmed by an *in vitro* study (Zhou et al., 2018b). In a murine model of cisplatin induced-AKI, inhibition of EZH2 expression by 3-DZNep could also

TABLE 1 | EZH2 inhibition on kidney diseases in various in vitro and in vivo models.

Inhibitors or Knockout mice	Models	Effects and mechanisms	References
shEZH2, 3-DZNep	RCC cell lines; Tumor xenograft in nude mice	Inhibit migration and invasion and up-regulate the expression of E-cadherin; Inhibit tumor growth and prolong survival	Liu et al., 2016
EZH2 siRNA	RCC cell lines	Prevent cell proliferation and invasion potential of 786-O cells	Zhang et al., 2018
EZH2 siRNA	RCC cell lines	Reduce the proliferation of RCC without inhibiting the tumor suppressor p27Kip1	Sakurai et al., 2012
shRNA EZH2, EPZ011989	RCC cell lines; Tumor xenograft in nude mice	Inhibit survival, invasion and growth of ccRCC cells with BAP1 mutation	Sun et al., 2018
EZH2 siRNA, 3-DZNeP	I/R induced AKI	Reduce acute kidney injury via targeting EZH2/p38 signaling pathway	Liang et al., 2019
EZH2 siRNA, 3-DZNeP	I/R or FA induced AKI	Reduce renal dysfunction and renal tubular cell death; Prevent renal tubular injury	Zhou et al., 2018b
EZH2 siRNA, 3-DZNeP	Cisplatin induced AKI	Suppress acute kidney injury via an E-cadherin-dependent mechanism	Ni et al., 2019
EZH2 siRNA, 3-DZNeP	I/R induced AKI	Alleviate I/R injury and block the activation of oxidative stress and pyroptosis	Liu et al., 2020
3-DZNeP, GSK126, EZH2 siRNA	Cultured NRK-49F cells; Mouse model of UUO	Attenuate fibrosis; Reduce the activation of renal interstitial fibroblasts	Zhou et al., 2015
3-DZNeP, EZH2 siRNA	Cultured TKPT cells; Mouse model of UUO	Attenuate renal fibrosis; Inhibit TGF-β1–induced EMT	Zhou et al., 2018a
3-DZNeP, EZH2 shRNA	Streptozotocin (STZ) -induced DN	Increase the glomerular TxnIP expression, induce podocyte injury, and increase oxidative stress and proteinuria	Siddiqi et al., 2016
EPZ-6438, EZH2 KO mice	Adriamycin nephrotoxicity; SNx	Sensitize mice to glomerular disease; Increase podocyte injury and dedifferentiation	Majumder et al., 2018
EZH2 siRNA	Rat MCs (RMC)s; Streptozotocin-induced rat model of type 1 diabetes and DN.	Destroy the low level, stable state of fibrosis and inflammatory genes in MCs. Inhibition and up-regulation of genes that cause glomerular MC and podocyte dysfunction	Jia et al., 2019a
EZH2 siRNA, 3-DZNeP, GSK126	HK-2cells; High-fat diet induced mice model of DN	Rescue SIRT1 expression and block ROS accumulation	Zeng et al., 2018
siEZH2, EPZ005687	Murine podocyte cell line; Streptozotocin-induced rat model of diabetes	Inhibit podocyte migration; reduce podocyte apoptosis	Wan et al., 2017
EZH2 siRNA, 3-DZNeP	NRK-49F and HK2 cells; Hyperuricemia-induced CKD	Decrease serum uric acid levels; Alleviate renal pathological damages	Shi et al., 2019
3-DZNeP	MRL/lpr mice	Reduce lupus associated kidney damage	Rohraff et al., 2019
3-DZNeP	T cells; mouse model of allogeneic bone marrow transplantation	Attenuate graft-versus-host disease (GVHD)	He et al., 2012
3-DZNeP	Rat model of renal transplantation	Ameliorate early acute renal allograft rejection	Li et al., 2016

reduce apoptosis of renal tubular cells and ameliorate acute renal injury by restoring expression of E-cadherin (Ni et al., 2019). Both *in vitro* and *in vivo*, cisplatin-induced renal tubular cell damage was accompanied by up-regulation of H3K27me3, while 3-DZNep treatment did not affect its expression (Ni et al., 2019). This suggests that 3-DZNeP-elicited renal protection in response to cisplatin exposure may not be through a H3K27me3-mediated mechanism. Recently, it was demonstrated that EZH2 can regulate renal injury by inducing oxidative stress as evidenced by the fact that EZH2 inhibition blocked the production of NOX4 dependent ROS through the ALK5/Smad2/3 signal pathway in an animal model of ischemia/reperfusion-induced AKI (Liu et al., 2020). In the same injury model, EZH2 inhibition also reduced renal dysfunction and tubular injury by regulating p38 signaling, apoptosis and inflammation (Liang et al., 2019). Therefore, EZH2 is an important mediator in the pathogenesis of AKI. Additional studies are needed to describe the mechanism of EZH2 in AKI in more detail.

EZH2 AND RENAL FIBROSIS

Renal fibrosis is a common pathological process in the progression of CKD to end-stage renal disease (ESRD). Renal interstitial fibrosis is considered an example of poor self-healing after injury (Iwano and Neilson, 1991; Inoue et al., 2015; Lovisa et al., 2015). It is mainly manifested by extracellular matrix (ECM) deposition, epithelial to mesenchymal transition (EMT), inflammatory response, and fibroblast activation and proliferation (Iwano and Neilson, 1991; Inoue et al., 2015; Lovisa et al., 2015). Although many studies have been conducted to elucidate its pathogenesis, there is still a lack of effective treatment for renal fibrosis (Boor et al., 2010; Nogueira et al., 2017).

Recent studies have demonstrated that EZH2 plays a critical role in the development of renal fibrosis. EZH2 expression levels are low in normal kidney tissue, but high in mice kidneys following injury and in human kidneys following disease (Zhou et al., 2015). Immunostaining showed that EZH2 was expressed both in tubular epithelial cells and renal interstitial fibroblasts (Zhou et al., 2015). Activation and proliferation of renal fibroblasts produces a large amount of ECM proteins, including fibronectin and collagen I. *In vitro*, pharmacological inhibition or siRNA mediated silencing of EZH2 reduced the activation of renal interstitial fibroblasts; *in vivo*, treatment with the EZH2 inhibitor 3-DZNep attenuated UUO-induced fibrosis in an animal model. The anti-fibrotic effect of EZH2 inhibition is related to the inhibition of expression of epidermal growth factor receptor (EGFR) and platelet-derived growth factor receptor (PDGFR) and deactivation of multiple intracellular signaling pathways, including TGFβ/Smad3, AKT and ERK1/2 (Zhou et al., 2015). EZH2 was also identified as a key regulator of epithelial-mesenchymal transition (EMT) in fibrotic kidneys (Zhou et al., 2018a). EZH2 inhibition elicits an anti-EMT effect related to preservation of E-cadherin expression, repression of transcription factors (i.e., Snail, twist), and deactivation of PTEN/Akt and β-catenin signaling pathways (Zhou et al., 2018a). Studies have also shown that EZH2 inhibition can effectively suppress the development of liver fibrosis (Zeybel et al., 2017), skin fibrosis (Tsou et al., 2019), atrial fibrosis (Song et al., 2019), pulmonary fibrosis (Xiao et al., 2016), and peritoneal fibrosis (Shi et al., 2020). These results suggest that EZH2 may serve as a promising therapeutic target for the treatment of fibrosis in many organ systems.

EZH2 AND DIABETIC NEPHROPATHY

Diabetic nephropathy is one of the most common chronic complications of diabetes (Alicic et al., 2017; Han et al., 2017; Feldman et al., 2019). The typical characteristics of DN are glomerular hypertrophy, proteinuria, progressive decrease of glomerular filtration rate, and renal fibrosis, which leads to loss of renal function. The pathological changes of diabetes are mainly composed of mesangial hyperplasia, thickening of basement membrane, occlusion of capillary lumen, disorder of podocyte structure, and decrease of podocyte number (Tung et al., 2018). However, the specific molecular mechanism of DN is not completely understood. Recent studies have shown that EZH2 activation is involved in the pathogenesis of DN. EZH2 can regulate oxidative stress in diabetic patients by inhibiting expression of Pax6, a transcription factor, and thus the expression of TxnIP, an endogenous antioxidant inhibitor (Siddiqi et al., 2016). The specific deletion of EZH2 in podocytes induced podocyte damage and dedifferentiation (Siddiqi et al., 2016) and sensitized mice to glomerular disease (Majumder et al., 2018). In human glomerular diseases such as focal segmental glomerulosclerosis and DN, H3K27me3 was decreased in podocytes. H3K27me3 and EZH2 are involved in inhibiting and maintaining the low-level and stable state of fibrosis and inflammation genes in mesangial cells, while H3K27me3 and EZH2 are inhibited by TGF-β, which increases the expression of genes that mediate glomerular mesangial dysfunction and DN, leading to renal dysfunction (Jia et al., 2019a). In contrast, the depletion or inhibition of EZH2 attenuated the increase of reactive oxygen species (ROS) in human renal tubular epithelial cells (HK-2) induced by high glucose (Zeng et al., 2018). Moreover, Wilm's tumor 1 (WT1) can improve the β-catenin mediated damage of podocytes in DN by antagonizing EZH2, which is manifested in reducing the transformation of the stroma of DN podocytes, maintaining the structural integrity of DN podocytes, reducing apoptosis and oxidative stress of DN podocytes (Wan et al., 2017). These data illustrate that EZH2 activity is necessary for protection against podocyte damage in DN. This is opposite to what has been observed in the murine model of UUO-induced renal fibrosis (Zhou et al., 2015). Currently, it remains unclear about the underlying mechanism by which EZH2 plays distinct roles in different disease models and cells. Since multiple cell types are involved in the pathogenesis of DN, and EZH2 mediated gene regulation is cell-context specific, EZH2 may play the role of a double-edged sword in different cell types in DN (Brasacchio et al., 2009). Further investigation is required to elucidate the gene and signaling pathways regulated by EZH2 during DN development.

EZH2 AND HYPERURICEMIC NEPHROPATHY

Hyperuricemia (HUA) is a purine metabolic disorder, in which the blood uric acid level is higher than the normal level due to the increase of uric acid production and/or the decrease of uric acid excretion. HUA is an independent risk factor for CKD progression (Mok et al., 2012) and has a direct correlation with renal damage (Lin et al., 2014). 10–20% of patients with primary hyperuricemia have evidence of AKI and chronic kidney disease, including chronic uric acid nephropathy, acute uric acid nephropathy and uric acid stones. Long-term HUA can cause renal damage through the urate crystal dependent pathway. Uric acid crystals are deposited in the distal collecting duct and the renal interstitium, causing chronic interstitial nephritis, which may lead to renal interstitial fibrosis (Liu et al., 2015; Yuan et al., 2017; Johnson et al., 2018). In addition, long-term HUA can cause renal damage through an independent pathway of urate crystal formation. In this regard, it has been reported that uric acid can cause renal endothelial dysfunction, renin-angiotensin system (RAS) activation, inflammation, oxidative stress (Sanchez-Lozada et al., 2008; Yu et al., 2010; Filiopoulos et al., 2012), whereas lowering serum uric acid alleviates renal damage or delays its progression (Obermayr et al., 2008; Zhou et al., 2012; Kim et al., 2014).

Although the molecular mechanism of renal damage caused by elevated uric acid levels remains obscure, uric acid has been shown to induce activation of TGF-β receptor and transcription of TGF-β1 target genes (Böttinger, 2007), leading to activation of downstream signaling pathways such as EGFR and ERK1/2 (Joo et al., 2008; Lee et al., 2010). Interestingly, blocking EZH2 by 3-DZNep inhibits TGF-β1-induced activation of renal interstitial fibroblasts *in vitro* and attenuates ECM protein deposition and α-smooth muscle actin expression in obstructed kidneys (Zhou et al., 2015). Inhibition of EZH2 by 3-DZNep also significantly reduces blood uric acid levels by reducing the activity of serum purine oxidase (XOD) and alleviates HUA-induced renal damage through various mechanisms, including inhibition of the TGF-β1/Smad3 and EGFR/ERK1/2 signaling pathways. Moreover, 3-DZNep was effective in downregulating the levels of various pro-inflammatory chemokines/cytokines and reducing the apoptosis of renal tubular cells (Shi et al., 2019). Therefore, EZH2 may be a potential therapeutic target for reducing renal damage and delaying the development of CKD caused by HUA.

EZH2 AND LUPUS NEPHRITIS

Systemic lupus erythematosus (SLE) is a chronic autoimmune inflammatory disease characterized by loss of immune tolerance to autoantigens, production of autoantibodies, formation of immune complexes and deposition in different parts of the body, causing inflammation and multiorgan damage (Marshall and Vierstra, 2018). LN is one of the most common and serious complications of SLE, affecting up to 60% of lupus patients by some estimates. LN is thus considered an important cause of chronic kidney disease (Koutsokeras and Healy, 2014; Zhu et al., 2016). The pathogenesis of SLE and LN is complex and exact mechanism(s) are largely unknown. It is generally believed that SLE is caused by genetic, endocrine, environmental factors (infection, ultraviolet radiation, etc.), and abnormal activation of the immune system. Epigenetic changes have also been reported to contribute to the pathogenesis of lupus (Ballestar et al., 2006). In particular, various abnormal patterns of DNA methylation of immune cell types isolated from lupus patients have been found to be related to clinical heterogeneity, interspecific disease variability, lupus onset and remission (Teruel and Sawalha, 2017).

Similar to DNA methylation, histone modifications can lead to abnormal gene expression and contribute to the pathogenesis of SLE (Hu et al., 2008). It has been reported that unregulated EZH2 activation in CD4+ T cells leads to T cell activation and non-Th1 immune responses, prior to transcription activity, and is related to lupus activity. In addition, levels of two microRNAs (miR-101 and miR-26a) targeting and regulating EZH2 in CD4+ T cells of lupus patients were negatively correlated with lupus disease activity (Coit et al., 2016). EZH2 can mark and control functions and survival of effector T cells through microRNAs and the Notch signaling pathway (Zhao et al., 2016). In lupus patients, overexpression of EZH2 leads to the methylation of JAM-A (junctional adhesion molecule A), which may increase the migration of T cells and lead to the invasive exosmosis of T cells. Blocking EZH2 by 3-DZNep and GSK126 can effectively inhibit the adhesion of lupus T cells to human microvascular endothelial cells. In addition, overexpression of EZH2 results in methylation changes of genes involved in gene transcription, ubiquitination and immune response, indicating that EZH2 is involved in various cellular and physiological processes crucial to the survival and function of T cells (Tsou et al., 2018). Inhibition of EZH2 by 3-DZNep significantly reduced the number of pathogenic double negative T cells and production of cytokines and chemokines in lupus prone MRL/lpr mice. Splenomegaly and lymphadenopathy in mice treated with 3-DZNep were significantly reduced. Most importantly, inhibition of EZH2 by 3-DZNep in MRL/lpr mice can reduce renal damage and increase survival rate of MRL/lpr mice. Mice with 3-DZNep treatment have relatively stable albumin:creatinine ratios, and attenuated glomerulonephritis and crescent formation. Glomerular necrosis in the prevention group of mice was significantly relieved as well. Therefore, 3-DZNep elicited inhibition of EZH2 can effectively prevent the progression of renal damage in lupus (Rohraff et al., 2019). Additional studies are necessary to examine whether other EZH2 inhibitors or gene modulators are also effective in ameliorating the pathogenesis of LN.

EZH2 AND AGING KIDNEY

Aging is an irreversible phenomenon characterized by gradual decline of cell function and gradual structural changes of many organ systems. Age-related changes in kidney function include anatomical and physiological changes (Zhou et al., 2008). The histological changes in renal aging mainly include:

renal mass reduction, glomerulosclerosis, renal tubular atrophy, renal interstitial fibrosis and arterial intimal fibrosis (Silva, 2005). The partial loss of renal function can be manifested as decreases in renal vascular elasticity, renal blood flow and glomerular filtration rate. At present, mechanisms of renal aging are incompletely studied. Increasing evidence indicates that renal aging is related to epigenetic changes (Painter et al., 2008; Au et al., 2013; Kooman et al., 2014).

Epigenetic histone modification plays a role in aging (Sen et al., 2016), especially trimethylation of 27 lysine (H3K27me3) of histone H3, which is directly related to life span and aging in different models (Jin et al., 2011; Ma et al., 2018). Previous studies have shown that EZH2 expression is related to abnormal expression of genes in aging animal models (Shumaker et al., 2006; Bracken et al., 2007; Chen et al., 2009). For example, overexpression of EZH2 can prevent stem cell failure and aging (De Haan and Gerrits, 2007) while pharmacological inhibition of EZH2 can dysregulate tissue regeneration in aged mice (Nishiguchi et al., 2018). Methylation of CpG islands related to aging may overlap with the regulatory regions of cancer genes such as c1ql3. EZH2 interacts with these regulatory regions in mice, and the occupancy of EZH2 may decrease with age at c1ql3. EZH2 is part of the protein mechanism of forming the aging epigenome (Mozhui and Pandey, 2017). A recent study found that H3K27me3 regulated the expression of Klotho in the kidney of aging mice. A decrease of Klotho levels is an important mechanism of aging. The epigenetic down-regulation of Klotho gene expression is at least partly due to the histone 3 modification of the Klotho promoter. Aging plays a role by up-regulating H3K27me3 and down-regulating hyperphosphorylation of Klotho and mTOR in renal tubules. Inhibition of EZH2 with GSK343 or EED226 was able to reduce H3K27me3 recruitment to the Klotho promoter (Han and Sun, 2020). The expression level of EZH2 decreased in older mice (Han and Sun, 2020). At present, no study has confirmed the obvious correlation between the expression of EZH2 and H3K27me3 in the kidney of aging mice or adult tissues (Margueron et al., 2008). Studies have pointed out that renal aging can up-regulate the ECM laminin genes by down-regulating 5mC and H3K27me3 in the promoter region of the ECM laminin gene. Reduction of H3K27me3 levels by 3-DZNep can inhibit expression of the laminin gene in the ECM, but administration of a more specific EZH2 inhibitor, GSK-126, did not inhibit expression of the laminin gene in ECM (Denisenko et al., 2018). Therefore, the exact mechanism(s) by which EZH2 contributes to renal aging needs further investigation.

EZH2 AND KIDNEY TRANSPLANTATION REJECTION

Currently, renal transplantation is the most effective treatment for ESRD. However, acute rejection (AR) is a common adverse reaction after kidney transplantation, usually occurring weeks to months after transplantation. Rejection after transplantation is caused by the recipient's immune system. Recognition of the graft as a foreign body stimulates secretion of various inflammatory factors to attack the graft. Eliminating the foreign body reaction and maintaining the stability of the internal environment would improve the long-term survival of the transplanted kidney. Transplantation rejection includes T-cell-mediated rejection and antibody mediated rejection (Haas et al., 2018). Acute T-cell mediated rejection is an inflammatory reaction, involving extensive T lymphocytes infiltration of the allograft and activation (Yang C. et al., 2015). T cell mediated AR of renal transplantation includes mononuclear interstitial infiltration and tubulitis with intima-intimal arteritis. Epigenetic modification is involved in T cell-mediated AR of renal transplantation (Cuddapah et al., 2010).

Enhancer of zeste homolog 2 plays an important role in maintaining T cell numbers and functions. It has been documented that EZH2 is essential for the expansion of T-effector cells (Yang X. P. et al., 2015) as well as differentiation and characteristic maintenance of regulatory T cells necessary for maintaining immune homeostasis (DuPage et al., 2015). EZH2 can also stimulate the expression of T cell multifunctional cytokines by activating the Notch pathway, and promoting T cell survival by Bcl-2 expression (Zhao et al., 2016). In addition, EZH2 can protect key T cell development regulators from DNA methylation so that they can be activated in a subsequent differentiation stage (Wang C. et al., 2018). Treatment with 3-DZNep, a EZH2 inhibitor can induce selective apoptosis of alloantigen-activated T cells and arrest persistent graft-versus-host disease (GVHD) in mice after allogeneic bone marrow transplantation (He et al., 2012). A recent study was the first to demonstrate the relationship between EZH2 and allograft rejection. EZH2 in T cells was increased after kidney transplantation in a rat model of kidney transplantation; inhibition of EZH2 by DZNep reduced AR, reduced injury and inflammatory infiltration of the transplanted kidney. The cellular mechanisms are related to the inhibition of activation and proliferation of alloreactive T cells, impairment of production of inflammatory factors, and increased apoptosis of alloreactive T cells in the transplanted kidney and peripheral blood) (Li et al., 2016). However, the specific mechanism(s) of EZH2 in AR of renal transplantation remains to be further studied.

CONCLUSION AND PERSPECTIVES

Enhancer of zeste homolog 2 is highly expressed in renal tumors and many kidney diseases. Abnormal expression or activation of EZH2 can lead to development and progression of renal tumors and several kidney diseases as indicated in this review. The molecular mechanisms of EZH2-mediated renal pathology are associated with renal tubular cell injury, podocyte dedifferentiation, renal interstitial fibroblast proliferation, production of multiple cytokines/chemokines and infiltration of inflammatory cells. Because EZH2 regulates expression of diverse genes and activation of multiple signaling pathways associated with pathogenesis of disease, its functional role may vary with cell types, tissues and disease models. In this context, EZH2 activation has been shown to contribute to renal tubular cell death, but protects against podocyte injury. Therefore, further

studies are necessary to elucidate the detailed mechanistic actions of EZH2 in the pathogenesis and progression of kidney diseases.

Given that preclinical studies have demonstrated that EZH2 inhibitors attenuate some renal diseases in animal models, EZH2 inhibitors alone, or in combination with other drugs may provide beneficial effects to ameliorate or prevent kidney diseases. This is encouraged by recent approval of tazemetostat (EPZ-6438), one of EZH2 inhibitors, for treatment of adult patients with relapsed or refractory (R/R) follicular lymphoma by the FDA (Gulati et al., 2018a). Among the 203 patients who were evaluated for efficacy, responses were seen in 24% patients who had received tazemetostat administered as a single agent in both tumor types and in EZH2 mutant and WT tumor (Gulati et al., 2018b). In addition to tazemetostat, other EZH2 inhibitors such as GSK126 and CPT-1205 are being tested in treating lymphoma and several other solid tumor types (Eich et al., 2020). Currently, there are still no clinical trials of EZH2 inhibitors for the treatment of kidney disease of any underlying cause. Based on the evidence showing the efficacy of EZH2 inhibitors in animal models of kidney disease, clinical trials assessing the effect of EZH2 inhibition may hold out the promise of treatment for some forms of progressive kidney disease in humans. However, since genetic and pharmacological inhibition of EZH2 potentiates podocyte injury in murine models of glomerular disease (Majumder et al., 2018), EZH2 inhibitors may not be suitable for treatment of renal diseases associated with podocyte injury.

AUTHOR CONTRIBUTIONS

TL and CY drafted the article. SZ edited the manuscript. All the authors reviewed the manuscript and approved for publication.

FUNDING

This work was supported by the National Natural Science Foundation of China (81670623 and 81830021 to SZ), the Branch Grant of National Key Grants of the Ministry of Science and Technology (2018YFA0108802 to SZ), and the US National Institutes of Health (1R01DK113256-01A1 to SZ).

ACKNOWLEDGMENTS

We appreciate Dr. George Bayliss for editing this manuscript.

REFERENCES

Alicic, R. Z., Rooney, M. T., and Tuttle, K. R. (2017). Diabetic kidney disease: challenges, progress, and possibilities. *Clin. J. Am. Soc. Nephrol.* 12, 2032–2045. doi: 10.2215/cjn.11491116

Aloia, L., Di Stefano, B., and Di Croce, L. (2013). Polycomb complexes in stem cells and embryonic development. *Development* 140, 2525–2534. doi: 10.1242/dev.091553

Au, C. P., Raynes-Greenow, C. H., Turner, R. M., Carberry, A. E., and Jeffery, H. (2013). Fetal and maternal factors associated with neonatal adiposity as measured by air displacement plethysmography: a large cross-sectional study. *Early Hum. Dev.* 89, 839–843. doi: 10.1016/j.earlhumdev.2013.07.028

Ballestar, E., Esteller, M., and Richardson, B. C. (2006). The epigenetic face of systemic lupus erythematosus. *J. Immunol.* 176, 7143–7147. doi: 10.4049/jimmunol.176.12.7143

Bamidele, A. O., Svingen, P. A., Sagstetter, M. R., Sarmento, O. F., Gonzalez, M., Braga Neto, M. B., et al. (2019). Disruption of FOXP3-EZH2 interaction represents a pathobiological mechanism in intestinal inflammation. *Cell Mol. Gastroenterol. Hepatol.* 7, 55–71. doi: 10.1016/j.jcmgh.2018.08.009

Bannister, A. J., and Kouzarides, T. (2011). Regulation of chromatin by histone modifications. *Cell Res.* 21, 381–395. doi: 10.1038/cr.2011.22

Berger, S. L., Kouzarides, T., Shiekhattar, R., and Shilatifard, A. (2009). An operational definition of epigenetics. *Genes Dev.* 23, 781–783. doi: 10.1101/gad.1787609

Blanc, R. S., and Richard, S. (2017). Arginine methylation: the coming of age. *Mol. Cell* 65, 8–24. doi: 10.1016/j.molcel.2016.11.003

Bochyńska, A., Lüscher-Firzlaff, J., and Lüscher, B. (2018). Modes of interaction of KMT2 histone H3 lysine 4 methyltransferase/COMPASS complexes with chromatin. *Cells* 7:17. doi: 10.3390/cells7030017

Bomsztyk, K., and Denisenko, O. (2013). Epigenetic alterations in acute kidney injury. *Semin. Nephrol.* 33, 327–340. doi: 10.1016/j.semnephrol.2013.05.005

Boor, P., Ostendorf, T., and Floege, J. (2010). Renal fibrosis: novel insights into mechanisms and therapeutic targets. *Nat. Rev. Nephrol.* 6, 643–656. doi: 10.1038/nrneph.2010.120

Böttinger, E. P. (2007). TGF-beta in renal injury and disease. *Semin.Nephrol.* 27, 309–320. doi: 10.1016/j.semnephrol.2007.02.009

Bracken, A. P., Kleine-Kohlbrecher, D., Dietrich, N., Pasini, D., Gargiulo, G., Beekman, C., et al. (2007). The Polycomb group proteins bind throughout the INK4A-ARF locus and are disassociated in senescent cells. *Genes Dev.* 21, 525–530. doi: 10.1101/gad.415507

Brasacchio, D., Okabe, J., Tikellis, C., Balcerczyk, A., George, P., Baker, E. K., et al. (2009). Hyperglycemia induces a dynamic cooperativity of histone methylase and demethylase enzymes associated with gene-activating epigenetic marks that coexist on the lysine tail. *Diabetes* 58, 1229–1236. doi: 10.2337/db08-1666

Cardoso, C., Mignon, C., Hetet, G., Grandchamps, B., Fontes, M., and Colleaux, L. (2000). The human EZH2 gene: genomic organisation and revised mapping in 7q35 within the critical region for malignant myeloid disorders. *Eur. J. Hum. Genet.* 8, 174–180. doi: 10.1038/sj.ejhg.5200439

Chen, H., Gu, X., Su, I. H., Bottino, R., Contreras, J. L., Tarakhovsky, A., et al. (2009). Polycomb protein Ezh2 regulates pancreatic beta-cell Ink4a/Arf expression and regeneration in diabetes mellitus. *Genes Dev.* 23, 975–985. doi: 10.1101/gad.1742509

Coit, P., Dozmorov, M. G., Merrill, J. T., McCune, W. J., Maksimowicz-McKinnon, K., Wren, J. D., et al. (2016). Epigenetic reprogramming in naive CD4+ T cells favoring T cell activation and Non-Th1 effector T cell immune response as an early event in lupus flares. *Arthr. Rheumatol.* 68, 2200–2209. doi: 10.1002/art.39720

Cuddapah, S., Barski, A., and Zhao, K. (2010). Epigenomics of T cell activation, differentiation, and memory. *Curr. Opin. Immunol.* 22, 341–347. doi: 10.1016/j.coi.2010.02.007

De Haan, G., and Gerrits, A. (2007). Epigenetic control of hematopoietic stem cell aging the case of Ezh2. *Ann. N. Y. Acad. Sci.* 1106, 233–239. doi: 10.1196/annals.1392.008

Denisenko, O., Mar, D., Trawczynski, M., and Bomsztyk, K. (2018). Chromatin changes trigger laminin genes dysregulation in aging kidneys. *Aging (Albany N. Y.)* 10, 1133–1145. doi: 10.18632/aging.101453

Di Croce, L., and Helin, K. (2013). Transcriptional regulation by Polycomb group proteins. *Nat.Struct. Mol. Bio.l.* 20, 1147–1155. doi: 10.1038/nsmb.2669

Duan, R., Du, W., and Guo, W. (2020). EZH2: a novel target for cancer treatment. *J. Hematol. Oncol.* 13:104. doi: 10.1186/s13045-020-00937-8

DuPage, M., Chopra, G., Quiros, J., Rosenthal, W. L., Morar, M. M., Holohan, D., et al. (2015). The chromatin-modifying enzyme Ezh2 is critical for the maintenance of regulatory T cell identity after activation. *Immunity* 42, 227–238. doi: 10.1016/j.immuni.2015.01.007

Eich, M. L., Athar, M., Ferguson, J. E. III, and Varambally, S. (2020). EZH2-targeted therapies in cancer: hype or a reality. *Cancer Res.* 80, 5449–5458. doi: 10.1158/0008-5472.CAN-20-2147

Feldman, E. L., Callaghan, B. C., Pop-Busui, R., Zochodne, D. W., Wright, D. E., Bennett, D. L., et al. (2019). Diabetic neuropathy. *Nat. Rev. Dis. Primers* 5:41. doi: 10.1038/s41572-019-0092-1

Filion, G. J., van Bemmel, J. G., Braunschweig, U., Talhout, W., Kind, J., Ward, L. D., et al. (2010). Systematic protein location mapping reveals five principal chromatin types in *Drosophila* cells. *Cell* 143, 212–224. doi: 10.1016/j.cell.2010.09.009

Filiopoulos, V., Hadjiyannakos, D., and Vlassopoulos, D. (2012). New insights into uric acid effects on the progression and prognosis of chronic kidney disease. *Ren. Fail* 34, 510–520. doi: 10.3109/0886022X.2011.653753

Graff, J., and Tsai, L. H. (2013). Histone acetylation: molecular mnemonics on the chromatin. *Nat. Rev. Neurosci.* 14, 97–111. doi: 10.1038/nrn3427

Grossman, E., Messerli, F. H., and Goldbourt, U. (1999). Does diuretic therapy increase the risk of renal cell carcinoma? *Am. J. Cardiol.* 83, 1090–1093. doi: 10.1016/s0002-9149(99)00021-1

Gulati, N., Beguelin, W., and Giulino-Roth, L. (2018a). Emerging drug profile: Enhancer of Zeste Homolog 2 (EZH2) Inhibitors. *Leuk .Lymphoma* 59, 1574–1585. doi: 10.1080/10428194.2018.1430795

Gulati, N., Beguelin, W., and Giulino-Roth, L. (2018b). Enhancer of zeste homolog 2 (EZH2) inhibitors. *Leuk. Lymphoma* 59, 1574–1585.

Guzzi, F., Cirillo, L., Roperto, R. M., Romagnani, P., and Lazzeri, E. (2019). Molecular Mechanisms of the acute kidney injury to chronic kidney disease transition: an updated view. *Int. J. Mol. Sci.* 20:941. doi: 10.3390/ijms20194941

Haas, M., Loupy, A., Lefaucheur, C., Roufosse, C., Glotz, D., Seron, D., et al. (2018). The Banff 2017 Kidney Meeting Report: Revised diagnostic criteria for chronic active T cell-mediated rejection, antibody-mediated rejection, and prospects for integrative endpoints for next-generation clinical trials. *Am. J. Transplant* 18, 293–307. doi: 10.1111/ajt.14625

Han, Q., Zhu, H., Chen, X., and Liu, Z. (2017). Non-genetic mechanisms of diabetic nephropathy. *Front. Med.* 11:319. doi: 10.1007/s11684-017-0569-9

Han, X., and Sun, Z. (2020). Epigenetic Regulation of KL (Klotho) via H3K27me3 (Histone 3 Lysine [K] 27 Trimethylation) in Renal Tubule Cells. *Hypertension* 75, 1233–1241. doi: 10.1161/HYPERTENSIONAHA.120.14642

He, S., Wang, J., Kato, K., Xie, F., Varambally, S., Mineishi, S., et al. (2012). Inhibition of histone methylation arrests ongoing graft-versus-host disease in mice by selectively inducing apoptosis of alloreactive effector T cells. *Blood* 119, 1274–1282. doi: 10.1182/blood-2011-06-364422

Ho, T. H., Kapur, P., Eckel-Passow, J. E., Christie, A., Joseph, R. W., Serie, D. J., et al. (2017). Multicenter Validation of Enhancer of Zeste Homolog 2 Expression as an Independent Prognostic Marker in Localized Clear Cell Renal Cell Carcinoma. *J. Clin. Oncol.* 35, 3706–3713. doi: 10.1200/JCO.2017.73.3238

Hobert, O., Jallal, B., and Ullrich, A. (1996). Interaction of Vav with ENX-1, a putative transcriptional regulator of homeobox gene expression. *Mol. Cell Biol.* 16, 3066–3073. doi: 10.1128/mcb.16.6.3066

Hu, N., Qiu, X., Luo, Y., Yuan, J., Li, Y., Lei, W., et al. (2008). Abnormal histone modification patterns in lupus CD4+ T cells. *J. Rheumatol.* 35, 804–810.

Hyun, K., Jeon, J., Park, K., and Kim, J. (2017). Writing, erasing and reading histone lysine methylations. *Exp. Mol. Med.* 49:e324. doi: 10.1038/emm.2017.11

Inoue, T., Umezawa, A., Takenaka, T., Suzuki, H., and Okada, H. (2015). The contribution of epithelial-mesenchymal transition to renal fibrosis differs among kidney disease models. *Kidney Int.* 87, 233–238. doi: 10.1038/ki.2014.235

Iwano, M., and Neilson, E. G. (1991). Mechanisms of tubulointerstitial fibrosis. *Kidney Int.* 39, 550–556.

Jacobs, J. J., and van Lohuizen, M. (2002). Polycomb repression: from cellular memory to cellular proliferation and cancer. *Biochim. Biophys. Acta* 1602, 151–161. doi: 10.1016/s0304-419x(02)00052-5

Jia, Y., Reddy, M. A., and Das, S. (2019a). Dysregulation of histone H3 lysine 27 trimethylation in transforming growth factor-β1-induced gene expression in mesangial cells and diabetic kidney. *J. Biol. Chem.* 294, 12695–12707.

Jia, Y., Reddy, M. A., Das, S., Oh, H. J., Abdollahi, M., Yuan, H., et al. (2019b). Dysregulation of histone H3 lysine 27 trimethylation in transforming growth factor-beta1-induced gene expression in mesangial cells and diabetic kidney. *J .Biol. Chem.* 294, 12695–12707. doi: 10.1074/jbc.RA119.007575

Jin, C., Li, J., Green, C. D., Yu, X., Tang, X., Han, D., et al. (2011). Histone demethylase UTX-1 regulates *C. elegans* life span by targeting the insulin/IGF-1 signaling pathway. *Cell Metab.* 14, 161–172. doi: 10.1016/j.cmet.2011.07.001

Johnson, R. J., Bakris, G. L., Borghi, C., Chonchol, M. B., Feldman, D., Lanaspa, M. A., et al. (2018). Hyperuricemia, acute and chronic kidney disease, hypertension, and cardiovascular disease: report of a scientific workshop organized by the national kidney foundation. *Am. J. Kidney Dis.* 71, 851–865. doi: 10.1053/j.ajkd.2017.12.009

Joo, C. K., Kim, H. S., Park, J. Y., Seomun, Y., Son, M. J., and Kim, J. T. (2008). Ligand release-independent transactivation of epidermal growth factor receptor by transforming growth factor-beta involves multiple signaling pathways. *Oncogene* 27, 614–628. doi: 10.1038/sj.onc.1210649

Kim, E., Kim, M., Woo, D. H., Shin, Y., Shin, J., Chang, N., et al. (2013). Phosphorylation of EZH2 activates STAT3 signaling via STAT3 methylation and promotes tumorigenicity of glioblastoma stem-like cells. *Cancer Cell* 23, 839–852. doi: 10.1016/j.ccr.2013.04.008

Kim, I. Y., Lee, D. W., Lee, S. B., and Kwak, I. S. (2014). The role of uric acid in kidney fibrosis: experimental evidences for the causal relationship. *Biomed. Res. Int.* 2014:638732. doi: 10.1155/2014/638732

Kim, K. H., and Roberts, C. W. (2016). Targeting EZH2 in cancer. *Nat. Med.* 22, 128–134. doi: 10.1038/nm.4036

Kooman, J. P., Kotanko, P., Schols, A. M., Shiels, P. G., and Stenvinkel, P. (2014). Chronic kidney disease and premature ageing. *Nat. Rev. Nephrol.* 10, 732–742. doi: 10.1038/nrneph.2014.185

Koutsokeras, T., and Healy, T. (2014). Systemic lupus erythematosus and lupus nephritis. *Nat. Rev. Drug Discov.* 13, 173–174. doi: 10.1038/nrd4227

Lee, E., Yi, J. Y., Chung, E., and Son, Y. (2010). Transforming growth factorbeta(1) transactivates EGFR via an H(2)O(2)-dependent mechanism in squamous carcinoma cell line. *Cancer Lett.* 290, 43–48. doi: 10.1016/j.canlet.2009.08.022

Li, L., Zhang, Y., Xu, M., Rong, R., Wang, J., and Zhu, T. (2016). Inhibition of histone methyltransferase EZH2 ameliorates early acute renal allograft rejection in rats. *BMC Immunol.* 17:41. doi: 10.1186/s12865-016-0179-3

Liang, H., Huang, Q., Liao, M. J., Xu, F., Zhang, T., He, J., et al. (2019). EZH2 plays a crucial role in ischemia/reperfusion-induced acute kidney injury by regulating p38 signaling. *Inflamm. Res.* 68, 325–336. doi: 10.1007/s00011-019-01221-3

Lin, B., Shao, L., Luo, Q., Ou-yang, L., Zhou, F., Du, B., et al. (2014). Prevalence of chronic kidney disease and its association with metabolic diseases: a cross-sectional survey in Zhejiang province, Eastern China. *BMC Nephrol.* 15:36. doi: 10.1186/1471-2369-15-36

Liu, H., Chen, Z., Weng, X., Chen, H., Du, Y., Diao, C., et al. (2020). Enhancer of zeste homolog 2 modulates oxidative stress-mediated pyroptosis in vitro and in a mouse kidney ischemia-reperfusion injury model. *Faseb J.* 34, 835–852. doi: 10.1096/fj.201901816R

Liu, L., Xu, Z., Zhong, L., Wang, H., Jiang, S., Long, Q., et al. (2016). Enhancer of zeste homolog 2 (EZH2) promotes tumour cell migration and invasion via epigenetic repression of E-cadherin in renal cell carcinoma. *BJU Int.* 117, 351–362. doi: 10.1111/bju.12702

Liu, N., Wang, L., Yang, T., Xiong, C., Xu, L., Shi, Y., et al. (2015). EGF receptor inhibition alleviates hyperuricemic nephropathy. *J. Am. Soc. Nephrol.* 26, 2716–2729. doi: 10.1681/ASN.2014080793

Lovisa, S., LeBleu, V. S., Tampe, B., Sugimoto, H., Vadnagara, K., Carstens, J. L., et al. (2015). Epithelial-to-mesenchymal transition induces cell cycle arrest and parenchymal damage in renal fibrosis. *Nat. Med.* 21, 998–1009. doi: 10.1038/nm.3902

Ma, Z., Wang, H., Cai, Y., Wang, H., Niu, K., Wu, X., et al. (2018). Epigenetic drift of H3K27me3 in aging links glycolysis to healthy longevity in Drosophila. *Elife* 7:35368. doi: 10.7554/eLife.35368

Majumder, S., Thieme, K., Batchu, S. N., Alghamdi, T. A., Bowskill, B. B., Kabir, M. G., et al. (2018). Shifts in podocyte histone H3K27me3 regulate mouse and human glomerular disease. *J. Clin. Invest.* 128, 483–499. doi: 10.1172/jci95946

Mallikarjuna, P., Sitaram, R. T., Landstrom, M., and Ljungberg, B. (2018). VHL status regulates transforming growth factor-beta signaling pathways in renal cell carcinoma. *Oncotarget* 9, 16297–16310. doi: 10.18632/oncotarget.24631

Margueron, R., Li, G., Sarma, K., Blais, A., Zavadil, J., Woodcock, C. L., et al. (2008). Ezh1 and Ezh2 maintain repressive chromatin through different mechanisms. *Mol. Cell* 32, 503–518. doi: 10.1016/j.molcel.2008.11.004

Margueron, R., and Reinberg, D. (2011). The Polycomb complex PRC2 and its mark in life. *Nature* 469, 343–349. doi: 10.1038/nature09784

Marshall, R. S., and Vierstra, R. D. (2018). To save or degrade: balancing proteasome homeostasis to maximize cell survival. *Autophagy* 14, 2029–2031. doi: 10.1080/15548627.2018.1515531

Martinez, A. M., and Cavalli, G. (2006). The role of polycomb group proteins in cell cycle regulation during development. *Cell Cycle* 5, 1189–1197. doi: 10.4161/cc.5.11.2781

Matsukawa, Y., Semba, S., Kato, H., Ito, A., Yanagihara, K., and Yokozaki, H. (2006). Expression of the enhancer of zeste homolog 2 is correlated with poor prognosis in human gastric cancer. *Cancer Sci.* 97, 484–491. doi: 10.1111/j.1349-7006.2006.00203.x

Mimori, K., Ogawa, K., Okamoto, M., Sudo, T., Inoue, H., and Mori, M. (2005). Clinical significance of enhancer of zeste homolog 2 expression in colorectal cancer cases. *Eur. J. Surg. Oncol.* 31, 376–380. doi: 10.1016/j.ejso.2004.11.001

Mok, Y., Lee, S. J., Kim, M. S., Cui, W., Moon, Y. M., and Jee, S. H. (2012). Serum uric acid and chronic kidney disease: the Severance cohort study. *Nephrol. Dial. Transplant* 27, 1831–1835. doi: 10.1093/ndt/gfr530

Moledina, D. G., Hall, I. E., Thiessen-Philbrook, H., Reese, P. P., Weng, F. L., Schroppel, B., et al. (2017). Performance of serum creatinine and kidney injury biomarkers for diagnosing histologic acute tubular injury. *Am. J. Kidney Dis.* 70, 807–816. doi: 10.1053/j.ajkd.2017.06.031

Mozhui, K., and Pandey, A. K. (2017). Conserved effect of aging on DNA methylation and association with EZH2 polycomb protein in mice and humans. *Mech. Ageing Dev.* 162, 27–37. doi: 10.1016/j.mad.2017.02.006

Ni, J., Hou, X., Wang, X., Shi, Y., Xu, L., Zheng, X., et al. (2019). 3-deazaneplanocin A protects against cisplatin-induced renal tubular cell apoptosis and acute kidney injury by restoration of E-cadherin expression. *Cell Death Dis.* 10:355. doi: 10.1038/s41419-019-1589-y

Nishiguchi, M. A., Spencer, C. A., Leung, D. H., and Leung, T. H. (2018). Aging suppresses skin-derived circulating SDF1 to promote full-thickness tissue regeneration. *Cell Rep.* 24, 3383–3392.e3385. doi: 10.1016/j.celrep.2018.08.054

Nogueira, A., Pires, M. J., and Oliveira, P. A. (2017). Pathophysiological Mechanisms of renal fibrosis: a review of animal models and therapeutic strategies. *In Vivo* 31, 1–22. doi: 10.21873/invivo.11019

Obermayr, R. P., Temml, C., Gutjahr, G., Knechtelsdorfer, M., Oberbauer, R., and Klauser-Braun, R. (2008). Elevated uric acid increases the risk for kidney disease. *J. Am. Soc. Nephrol.* 19, 2407–2413. doi: 10.1681/ASN.2008010080

Painter, R. C., Osmond, C., Gluckman, P., Hanson, M., Phillips, D. I., and Roseboom, T. J. (2008). Transgenerational effects of prenatal exposure to the Dutch famine on neonatal adiposity and health in later life. *Bjog* 115, 1243–1249. doi: 10.1111/j.1471-0528.2008.01822.x

Plath, K., Fang, J., Mlynarczyk-Evans, S. K., Cao, R., Worringer, K. A., Wang, H., et al. (2003). Role of histone H3 lysine 27 methylation in X inactivation. *Science* 300, 131–135. doi: 10.1126/science.1084274

Raimann, J. G., Riella, M. C., and Levin, N. W. (2018). International Society of Nephrology's 0by25 initiative (zero preventable deaths from acute kidney injury by 2025): focus on diagnosis of acute kidney injury in low-income countries. *Clin. Kidney J.* 11, 12–19. doi: 10.1093/ckj/sfw134

Raman, J. D., Mongan, N. P., Tickoo, S. K., Boorjian, S. A., Scherr, D. S., and Gudas, L. J. (2005). Increased expression of the polycomb group gene, EZH2, in transitional cell carcinoma of the bladder. *Clin Cancer Res.* 11(24 Pt 1), 8570–8576. doi: 10.1158/1078-0432.CCR-05-1047

Rohraff, D. M., He, Y., Farkash, E. A., Schonfeld, M., Tsou, P. S., and Sawalha, A. H. (2019). Inhibition of EZH2 ameliorates lupus-like disease in MRL/lpr mice. *Arthritis Rheumatol.* 71, 1681–1690. doi: 10.1002/art.40931

Ronco, C., Bellomo, R., and Kellum, J. A. (2019). Acute kidney injury. *Lancet* 394, 1949–1964. doi: 10.1016/S0140-6736(19)32563-2

Rosner, M., and Hengstschlager, M. (2012). Targeting epigenetic readers in cancer. *N. Engl. J. Med.* 367, 1764–1765. doi: 10.1056/NEJMc1211175

Roy, S., and Majumdar, A. P. (2012). Cancer stem cells in colorectal cancer: genetic and epigenetic changes. *J. Stem Cell Res. Ther.* 7:6. doi: 10.4172/2157-7633.S7-006

Sakurai, T., Bilim, V. N., Ugolkov, A. V., Yuuki, K., Tsukigi, M., Motoyama, T., et al. (2012). The enhancer of zeste homolog 2 (EZH2), a potential therapeutic target, is regulated by miR-101 in renal cancer cells. *Biochem. Biophys. Res. Commun.* 422, 607–614. doi: 10.1016/j.bbrc.2012.05.035

Sanchez-Beato, M., Sanchez, E., Gonzalez-Carrero, J., Morente, M., Diez, A., Sanchez-Verde, L., et al. (2006). Variability in the expression of polycomb proteins in different normal and tumoral tissues. A pilot study using tissue microarrays. *Mod. Pathol.* 19, 684–694. doi: 10.1038/modpathol.3800577

Sanchez-Lozada, L. G., Soto, V., Tapia, E., Avila-Casado, C., Sautin, Y. Y., Nakagawa, T., et al. (2008). Role of oxidative stress in the renal abnormalities induced by experimental hyperuricemia. *Am. J. Physiol. Renal Physiol.* 295, F1134–F1141. doi: 10.1152/ajprenal.00104.2008

Saramaki, O. R., Tammela, T. L., Martikainen, P. M., Vessella, R. L., and Visakorpi, T. (2006). The gene for polycomb group protein enhancer of zeste homolog 2 (EZH2) is amplified in late-stage prostate cancer. *Genes Chromosomes Cancer* 45, 639–645. doi: 10.1002/gcc.20327

Sato, Y., and Yanagita, M. (2018). Immune cells and inflammation in AKI to CKD progression. *Am. J. Physiol. Renal. Physiol.* 315, F1501–F1512. doi: 10.1152/ajprenal.00195.2018

Schlesinger, Y., Straussman, R., Keshet, I., Farkash, S., Hecht, M., Zimmerman, J., et al. (2007). Polycomb-mediated methylation on Lys27 of histone H3 pre-marks genes for de novo methylation in cancer. *Nat. Genet.* 39, 232–236. doi: 10.1038/ng1950

Sen, P., Shah, P. P., Nativio, R., and Berger, S. L. (2016). Epigenetic mechanisms of longevity and aging. *Cell* 166, 822–839. doi: 10.1016/j.cell.2016.07.050

Shah, A. R., Lazar, E. L., and Atlas, A. B. (2009). Tracheal diverticula after tracheoesophageal fistula repair: case series and review of the literature. *J. Pediatr. Surg.* 44, 2107–2111. doi: 10.1016/j.jpedsurg.2009.04.036

Shi, B., Liang, J., Yang, X., Wang, Y., Zhao, Y., Wu, H., et al. (2007). Integration of estrogen and Wnt signaling circuits by the polycomb group protein EZH2 in breast cancer cells. *Mol. Cell Biol.* 27, 5105–5119. doi: 10.1128/MCB.00162-07

Shi, Y., Tao, M., Wang, Y., Zang, X., Ma, X., Qiu, A., et al. (2020). Genetic or pharmacologic blockade of enhancer of zeste homolog 2 inhibits the progression of peritoneal fibrosis. *J. Pathol.* 250, 79–94. doi: 10.1002/path.5352

Shi, Y., Xu, L., Tao, M., Fang, L., Lu, J., Gu, H., et al. (2019). Blockade of enhancer of zeste homolog 2 alleviates renal injury associated with hyperuricemia. *Am. J. Physiol. Renal. Physiol.* 316, F488–F505. doi: 10.1152/ajprenal.00234.2018

Shumaker, D. K., Dechat, T., Kohlmaier, A., Adam, S. A., Bozovsky, M. R., Erdos, M. R., et al. (2006). Mutant nuclear lamin A leads to progressive alterations of epigenetic control in premature aging. *Proc. Natl. Acad. Sci. U.S.A.* 103, 8703–8708. doi: 10.1073/pnas.0602569103

Siddiqi, F. S., Majumder, S., Thai, K., Abdalla, M., Hu, P., Advani, S. L., et al. (2016). The histone methyltransferase enzyme enhancer of zeste homolog 2 protects against podocyte oxidative stress and renal injury in diabetes. *J. Am. Soc. Nephrol.* 27, 2021–2034. doi: 10.1681/asn.2014090898

Silva, F. G. (2005). The aging kidney: a review – part I. *Int. Urol. Nephrol.* 37, 185–205. doi: 10.1007/s11255-004-0873-6

Song, S., Zhang, R., Mo, B., Chen, L., Liu, L., Yu, Y., et al. (2019). EZH2 as a novel therapeutic target for atrial fibrosis and atrial fibrillation. *J. Mol. Cell Cardiol.* 135, 119–133. doi: 10.1016/j.yjmcc.2019.08.003

Su, I. H., Basavaraj, A., Krutchinsky, A. N., Hobert, O., Ullrich, A., Chait, B. T., et al. (2003). Ezh2 controls B cell development through histone H3 methylation and Igh rearrangement. *Nat. Immunol.* 4, 124–131. doi: 10.1038/ni876

Sudo, T., Utsunomiya, T., Mimori, K., Nagahara, H., Ogawa, K., Inoue, H., et al. (2005). Clinicopathological significance of EZH2 mRNA expression in patients with hepatocellular carcinoma. *Br. J. Cancer* 92, 1754–1758. doi: 10.1038/sj.bjc.6602531

Sun, C., Zhao, C., Li, S., Wang, J., Zhou, Q., Sun, J., et al. (2018). EZH2 Expression is increased in BAP1-mutant renal clear cell carcinoma and is related to poor prognosis. *J. Cancer* 9, 3787–3796. doi: 10.7150/jca.26275

Teruel, M., and Sawalha, A. H. (2017). Epigenetic variability in systemic lupus erythematosus: what we learned from genome-wide DNA methylation studies. *Curr. Rheumatol. Rep.* 19:32. doi: 10.1007/s11926-017-0657-5

Tie, F., Furuyama, T., and Harte, P. J. (1998). The Drosophila Polycomb Group proteins ESC and E(Z) bind directly to each other and co-localize at multiple chromosomal sites. *Development* 125, 3483–3496.

Tsou, P. S., Campbell, P., Amin, M. A., Coit, P., Miller, S., Fox, D. A., et al. (2019). Inhibition of EZH2 prevents fibrosis and restores normal angiogenesis in scleroderma. *Proc. Natl. Acad. Sci. U.S.A.* 116, 3695–3702. doi: 10.1073/pnas.1813006116

Tsou, P. S., Coit, P., Kilian, N. C., and Sawalha, A. H. (2018). EZH2 Modulates the DNA methylome and controls T Cell adhesion through junctional adhesion molecule a in lupus patients. *Arthr. Rheumatol.* 70, 98–108. doi: 10.1002/art.40338

Tung, C. W., Hsu, Y. C., Shih, Y. H., Chang, P. J., and Lin, C. L. (2018). Glomerular mesangial cell and podocyte injuries in diabetic nephropathy. *Nephrology (Carlton)* 23(Suppl. 4), 32–37. doi: 10.1111/nep.13451

Veneti, Z., Gkouskou, K. K., and Eliopoulos, A. G. (2017). Polycomb repressor complex 2 in genomic instability and cancer. *Int. J. Mol. Sci.* 18:1657. doi: 10.3390/ijms18081657

Wagener, N., Macher-Goeppinger, S., Pritsch, M., Husing, J., Hoppe-Seyler, K., Schirmacher, P., et al. (2010). Enhancer of zeste homolog 2 (EZH2) expression is an independent prognostic factor in renal cell carcinoma. *BMC Cancer* 10:524. doi: 10.1186/1471-2407-10-524

Wan, J., Hou, X., Zhou, Z., Geng, J., Tian, J., Bai, X., et al. (2017). WT1 ameliorates podocyte injury via repression of EZH2/beta-catenin pathway in diabetic nephropathy. *Free Radic. Biol. Med.* 108, 280–299. doi: 10.1016/j.freeradbiomed.2017.03.012

Wang, C., Oshima, M., Sato, D., Matsui, H., Kubota, S., Aoyama, K., et al. (2018). Ezh2 loss propagates hypermethylation at T cell differentiation-regulating genes to promote leukemic transformation. *J. Clin. Invest.* 128, 3872–3886. doi: 10.1172/JCI94645

Wang, Y., Fan, L., Cui, C., Wang, Y., and Liang, T. (2018). EZH2 inhibition promotes methyl jasmonate-induced apoptosis of human colorectal cancer through the Wnt/beta-catenin pathway. *Oncol. Lett.* 16, 1231–1236. doi: 10.3892/ol.2018.8779

Wang, Z., Schones, D. E., and Zhao, K. (2009). Characterization of human epigenomes. *Curr. Opin. Genet. Dev.* 19, 127–134. doi: 10.1016/j.gde.2009.02.001

Wei, G., Wei, L., Zhu, J., Zang, C., Hu-Li, J., Yao, Z., et al. (2009). Global mapping of H3K4me3 and H3K27me3 reveals specificity and plasticity in lineage fate determination of differentiating CD4+ T cells. *Immunity* 30, 155–167. doi: 10.1016/j.immuni.2008.12.009

Worden, E. J., Hoffmann, N. A., Hicks, C. W., and Wolberger, C. (2019). Mechanism of Cross-talk between H2B Ubiquitination and H3 Methylation by Dot1L. *Cell* 176, 1490–1501.e1412. doi: 10.1016/j.cell.2019.02.002

Wu, C. L., Su, T. C., Chang, C. C., Kor, C. T., Chang, C. H., Yang, T. H., et al. (2017). Tubular peroxiredoxin 3 as a predictor of renal recovery from acute tubular necrosis in patients with chronic kidney disease. *Sci. Rep.* 7:43589. doi: 10.1038/srep43589

Xiao, X., Senavirathna, L. K., Gou, X., Huang, C., Liang, Y., and Liu, L. (2016). EZH2 enhances the differentiation of fibroblasts into myofibroblasts in idiopathic pulmonary fibrosis. *Physiol. Rep.* 4:12915. doi: 10.14814/phy2.12915

Yang, C., Zhang, Y., Wang, J., Li, L., Wang, L., Hu, M., et al. (2015). A novel cyclic helix B peptide inhibits dendritic cell maturation during amelioration of acute kidney graft rejection through Jak-2/STAT3/SOCS1. *Cell Death Dis.* 6:e1993. doi: 10.1038/cddis.2015.338

Yang, X. P., Jiang, K., Hirahara, K., Vahedi, G., Afzali, B., Sciume, G., et al. (2015). EZH2 is crucial for both differentiation of regulatory T cells and T effector cell expansion. *Sci. Rep.* 5:10643. doi: 10.1038/srep10643

Yu, J., Yu, J., Rhodes, D. R., Tomlins, S. A., Cao, X., Chen, G., et al. (2007). A polycomb repression signature in metastatic prostate cancer predicts cancer outcome. *Cancer Res.* 67, 10657–10663. doi: 10.1158/0008-5472.CAN-07-2498

Yu, M. A., Sanchez-Lozada, L. G., Johnson, R. J., and Kang, D. H. (2010). Oxidative stress with an activation of the renin-angiotensin system in human vascular endothelial cells as a novel mechanism of uric acid-induced endothelial dysfunction. *J. Hypertens* 28, 1234–1242.

Yuan, J., Shen, Y., Yang, X., Xie, Y., Lin, X., Zeng, W., et al. (2017). Thymosin beta4 alleviates renal fibrosis and tubular cell apoptosis through TGF-beta pathway inhibition in UUO rat models. *BMC Nephrol.* 18:314. doi: 10.1186/s12882-017-0708-1

Zeng, S., Wu, X., Chen, X., Xu, H., Zhang, T., and Xu, Y. (2018). Hypermethylated in cancer 1 (HIC1) mediates high glucose induced ROS accumulation in renal tubular epithelial cells by epigenetically repressing SIRT1 transcription. *Biochim. Biophys. Acta Gene Regul. Mech.* 1861, 917–927. doi: 10.1016/j.bbagrm.2018.08.002

Zeybel, M., Luli, S., Sabater, L., Hardy, T., Oakley, F., Leslie, J., et al. (2017). A Proof-of-concept for epigenetic therapy of tissue fibrosis: inhibition of liver fibrosis progression by 3-deazaneplanocin A. *Mol. Ther.* 25, 218–231. doi: 10.1016/j.ymthe.2016.10.004

Zhang, D., Yang, X. J., Luo, Q. D., Fu, D. L., Li, H. L., Li, H. C., et al. (2018). EZH2 enhances the invasive capability of renal cell carcinoma cells via activation of STAT3. *Mol. Med. Rep.* 17, 3621–3626. doi: 10.3892/mmr.2017.8363

Zhao, E., Maj, T., Kryczek, I., Li, W., Wu, K., Zhao, L., et al. (2016). Cancer mediates effector T cell dysfunction by targeting microRNAs and EZH2 via glycolysis restriction. *Nat. Immunol.* 17, 95–103. doi: 10.1038/ni.3313

Zhou, X., Xiong, C., Tolbert, E., Zhao, T. C., Bayliss, G., and Zhuang, S. (2018a). Targeting histone methyltransferase enhancer of zeste homolog-2 inhibits renal epithelial-mesenchymal transition and attenuates renal fibrosis. *Faseb J.* 32:fj201800237R. doi: 10.1096/fj.201800237R

Zhou, X., Zang, X., Guan, Y., Tolbert, T., Zhao, T. C., Bayliss, G., et al. (2018b). Targeting enhancer of zeste homolog 2 protects against acute kidney injury. *Cell Death Dis.* 9:1067. doi: 10.1038/s41419-018-1012-0

Zhou, X., Zang, X., Ponnusamy, M., Masucci, M. V., Tolbert, E., Gong, R., et al. (2016). Enhancer of zeste homolog 2 inhibition attenuates renal fibrosis by maintaining Smad7 and phosphatase and tensin homolog expression. *J. Am. Soc. Nephrol.* 27, 2092–2108. doi: 10.1681/ASN.2015040457

Zhou, X., Zang, X., Ponnusamy, M., Masucci, M. V., and Zhuang, S. (2015). Enhancer of zeste homolog 2 inhibition attenuates renal fibrosis by maintaining smad7 and phosphatase and tensin homolog expression. *J. Am. Soc. Nephrol.* 27:2092.

Zhou, X. J., Saxena, R., Liu, Z., Vaziri, N. D., and Silva, F. G. (2008). Renal senescence in 2008: progress and challenges. *Int. Urol. Nephrol.* 40, 823–839. doi: 10.1007/s11255-008-9405-0

Zhou, Y., Fang, L., Jiang, L., Wen, P., Cao, H., He, W., et al. (2012). Uric acid induces renal inflammation via activating tubular NF-kappaB signaling pathway. *PLoS One* 7:e39738. doi: 10.1371/journal.pone.0039738

Zhu, H., Mi, W., Luo, H., Chen, T., Liu, S., Raman, I., et al. (2016). Whole-genome transcription and DNA methylation analysis of peripheral blood mononuclear cells identified aberrant gene regulation pathways in systemic lupus erythematosus. *Arthritis Res. Ther.* 18:162. doi: 10.1186/s13075-016-1050-x

Zuk, A., and Bonventre, J. V. (2016). Acute kidney injury. *Annu. Rev. Med.* 67, 293–307. doi: 10.1146/annurev-med-050214-013407

Conflict of Interest: The authors declare that the research was conducted in the absence of any commercial or financial relationships that could be construed as a potential conflict of interest.

frontiers in Genetics

PERSPECTIVE
published: 25 February 2021
doi: 10.3389/fgene.2021.637148

Epigenetic Regulation of the N-Terminal Truncated Isoform of Matrix Metalloproteinase-2 (NTT-MMP-2) and Its Presence in Renal and Cardiac Diseases

Juliana de Oliveira Cruz[1,2], Alessandra O. Silva[3], Jessyca M. Ribeiro[3], Marcelo R. Luizon[1,2] and Carla S. Ceron[4]**

[1] Graduate Program in Genetics, Institute of Biological Sciences, Federal University of Minas Gerais, Belo Horizonte, Brazil, [2] Department of Genetics, Ecology and Evolution, Institute of Biological Sciences, Federal University of Minas Gerais, Belo Horizonte, Brazil, [3] Department of Food and Drugs, Faculty of Pharmaceutical Sciences, Federal University of Alfenas, Alfenas, Brazil, [4] Department of Biological Sciences, Institute of Exact and Biological Sciences, Federal University of Ouro Preto, Ouro Preto, Brazil

OPEN ACCESS

Edited by:
Haiyong Chen,
The University of Hong Kong,
Hong Kong

Reviewed by:
Richard Schulz,
University of Alberta, Canada
Robert Raffai,
University of California,
San Francisco, United States

***Correspondence:**
Marcelo R. Luizon
luizonmr@gmail.com
Carla S. Ceron
carlasceron@gmail.com

Specialty section:
This article was submitted to Epigenomics and Epigenetics, a section of the journal Frontiers in Genetics

Received: 02 December 2020
Accepted: 26 January 2021
Published: 25 February 2021

Citation:
Cruz JdeO, Silva AO, Ribeiro JM, Luizon MR and Ceron CS (2021) Epigenetic Regulation of the N-Terminal Truncated Isoform of Matrix Metalloproteinase-2 (NTT-MMP-2) and Its Presence in Renal and Cardiac Diseases. Front. Genet. 12:637148. doi: 10.3389/fgene.2021.637148

Several clinical and experimental studies have documented a compelling and critical role for the full-length matrix metalloproteinase-2 (FL-MMP-2) in ischemic renal injury, progressive renal fibrosis, and diabetic nephropathy. A novel N-terminal truncated isoform of MMP-2 (NTT-MMP-2) was recently discovered, which is induced by hypoxia and oxidative stress by the activation of a latent promoter located in the first intron of the *MMP2* gene. This NTT-MMP-2 isoform is enzymatically active but remains intracellular in or near the mitochondria. In this perspective article, we first present the findings about the discovery of the NTT-MMP-2 isoform, and its functional and structural differences as compared with the FL-MMP-2 isoform. Based on publicly available epigenomics data from the Encyclopedia of DNA Elements (ENCODE) project, we provide insights into the epigenetic regulation of the latent promoter located in the first intron of the *MMP2* gene, which support the activation of the NTT-MMP-2 isoform. We then focus on its functional assessment by covering the alterations found in the kidney of transgenic mice expressing the NTT-MMP-2 isoform. Next, we highlight recent findings regarding the presence of the NTT-MMP-2 isoform in renal dysfunction, in kidney and cardiac diseases, including damage observed in aging, acute ischemia-reperfusion injury (IRI), chronic kidney disease, diabetic nephropathy, and human renal transplants with delayed graft function. Finally, we briefly discuss how our insights may guide further experimental and clinical studies that are needed to elucidate the underlying mechanisms and the role of the NTT-MMP-2 isoform in renal dysfunction, which may help to establish it as a potential therapeutic target in kidney diseases.

Keywords: acute kidney injury, alternative promoter, chronic kidney disease, histone modifications, matrix metalloproteinase-2, mitochondria, epigenetics (DNA methylation), epigenomics

INTRODUCTION

Matrix metalloproteinases (MMPs) are a large family of zinc-containing endopeptidases that participate in multiple cellular processes beyond extracellular matrix (ECM) remodeling and in kidney diseases (Tan and Liu, 2012; Parrish, 2017). Regarding the MMPs known as gelatinases, the full-length MMP-2 (FL-MMP-2) is synthesized and was originally thought to be only secreted, but later it was found to be only inefficiently targeted to the secretory pathway (Ali et al., 2012). The FL-MMP-2 can be activated by extracellular proteolysis and intracellularly by direct chemical modification by peroxynitrite/oxidative stress (Viappiani et al., 2009; Kandasamy et al., 2010; Sariahmetoglu et al., 2012).

In the renal ECM, FL-MMP-2 has a role in the regulated turnover of the tubular epithelial basement membrane (Cheng et al., 2006). However, enhanced FL-MMP-2 synthesis distorts the basement membrane architecture and results in progressive renal injury (Cheng et al., 2006), cardiac remodeling and contractile dysfunction (Jacob-Ferreira and Schulz, 2013). The regulation and role of FL-MMP-2 have been extensively studied in both kidney (Tan and Liu, 2012; Dimas et al., 2017; Mansour et al., 2017; Narula et al., 2018) and cardiac injuries (Coker et al., 1999; Wang et al., 2002; Sawicki et al., 2005; Sung et al., 2007; Ali et al., 2010). Besides ECM proteins, FL-MMP-2 also cleaves vasoactive peptides, chemokines, and intracellular sarcomere and nuclear proteins (Fernandez-Patron et al., 1999, 2000; Martinez et al., 2004; Denney et al., 2009; Jacob-Ferreira and Schulz, 2013; DeCoux et al., 2014).

A novel N-terminal truncated isoform of MMP-2 (NTT-MMP-2) was recently discovered, which is induced by hypoxia and oxidative stress by the activation of a latent promoter in the first intron of the *MMP2* gene, thereby generating a 5′-truncated mRNA transcript (Lovett et al., 2012). This NTT-MMP-2 isoform is enzymatically active but lacks the secretory sequence and the inhibitory propeptide, remains intracellular in the mitochondria, triggers mitochondrial-nuclear stress signaling *via* nuclear factor-κβ (NF-κβ) and nuclear factor of activated T cells (NFAT), and induces innate immune response genes (Lovett et al., 2012).

This perspective presents the findings about the discovery of the NTT-MMP-2 isoform, its functional and structural differences as compared with the FL-MMP-2 isoform, the alterations in the kidney of transgenic mice expressing the NTT-MMP-2 isoform, insights into the epigenetic regulation of the latent promoter located in the first intron of *MMP2* gene that support the activation of the NTT-MMP-2 isoform, and highlights the role of the NTT-MMP-2 isoform in renal and cardiac diseases.

THE FL-MMP-2 AND THE NOVEL NTT-MMP-2 ISOFORM

The structure of the 68 kDa FL-MMP-2 is a short N-terminal signal sequence for secretory vesicle processing, a propeptide domain responsible for the enzyme latency, a highly conserved zinc-binding catalytic domain and hemopexin and fibronectin domains, which binds to ECM substrates (Turck et al., 1996; Morgunova et al., 1999). The FL-MMP-2 latency is maintained by the presence of a cysteine residue of the prodomain extended along the catalytic site, the "cysteine-switch" mechanism. The mRNA transcript of FL-MMP-2 is translated, and a portion of enzymatically inactive full-length protein is secreted by vesicles to the extracellular space, where occurs the proteolytic activation of the latent MMP-2 protein by other MMPs, ending in an active 62 kDa MMP-2 after cleavage of the inhibitory prodomain. In the ECM, the active enzyme degrades ECM components, such as collagen IV, laminin, and elastin (Turck et al., 1996; Morgunova et al., 1999).

The intracellular MMP-2 was first observed distributed in a pattern consistent with sarcomeric and sarcolemmal in cardiomyocytes (Coker et al., 1999), and the cleavage of sarcomeric troponin I by the 68 kDa FL-MMP-2 following acute ischemia-reperfusion injury (IRI) of the heart was later reported (Wang et al., 2002). Next, myosin light chain-1 (Sawicki et al., 2005), α-actinin (Sung et al., 2007), and titin (Ali et al., 2010) were reported as intracellular targets of the FL-MMP-2 in cardiomyocytes, leading to impaired heart contractility. This intracellular 68 kDa FL-MMP-2 is able to escape the secretory pathway (Ali et al., 2012), and is activated by the cysteine-switch opening by reactive oxygen species and peroxynitrite (Viappiani et al., 2009), and its activity was shown to be further modulated by its phosphorylation in cardiomyocytes (Sariahmetoglu et al., 2007, 2012).

Regarding kidney diseases, most of the studies focused on the extracellular or intracellular roles of the FL-MMP-2, mainly its deleterious action in the tubular basement membrane (Cheng et al., 2006). A novel intracellular MMP-2 isoform with 65 kDa (NTT-MMP-2) was recently discovered, which is generated by the activation of an alternate promoter in the first intron of the *MMP2* gene (Lovett et al., 2012). This novel isoform was first observed in the hearts of both FL-MMP-2 transgenic mice and aging wild-type mice (Lovett et al., 2012). Cardiomyoblasts submitted to mitochondrial stress generated with transient inhibition of oxidative phosphorylation induced the NTT-MMP-2 isoform expression on mitochondria-enriched cell fractions (Lovett et al., 2012). The NTT-MMP-2 is functionally and structurally distinct from the FL-MMP-2 (**Figure 1**).

While the FL-MMP-2 is present in the cytoplasm or ECM, and in cells of control conditions, the NTT-MMP-2 is intracellular, predominantly located at or near the mitochondria, and its transcription is induced only in conditions of tissue damage (Lovett et al., 2012). Transfection of the NTT-MMP-2 cDNA in cardiomyoblasts resulted in increased luciferase reporter activity for NF-kβ, NFAT, and response elements for interferon regulatory factors (IRFs) and induced innate immune response transcription factors and chemokines/cytokines, thereby activating a proinflammatory, pro-apoptotic innate immune response (Lovett et al., 2012).

EPIGENETIC REGULATION OF THE NTT-MMP-2 ISOFORM EXPRESSION

The transcriptional start site for the FL-MMP-2 isoform is located in the 5′ flanking region of *MMP2*, and transcription from this site encodes the FL-MMP-2 beginning at M1 amino

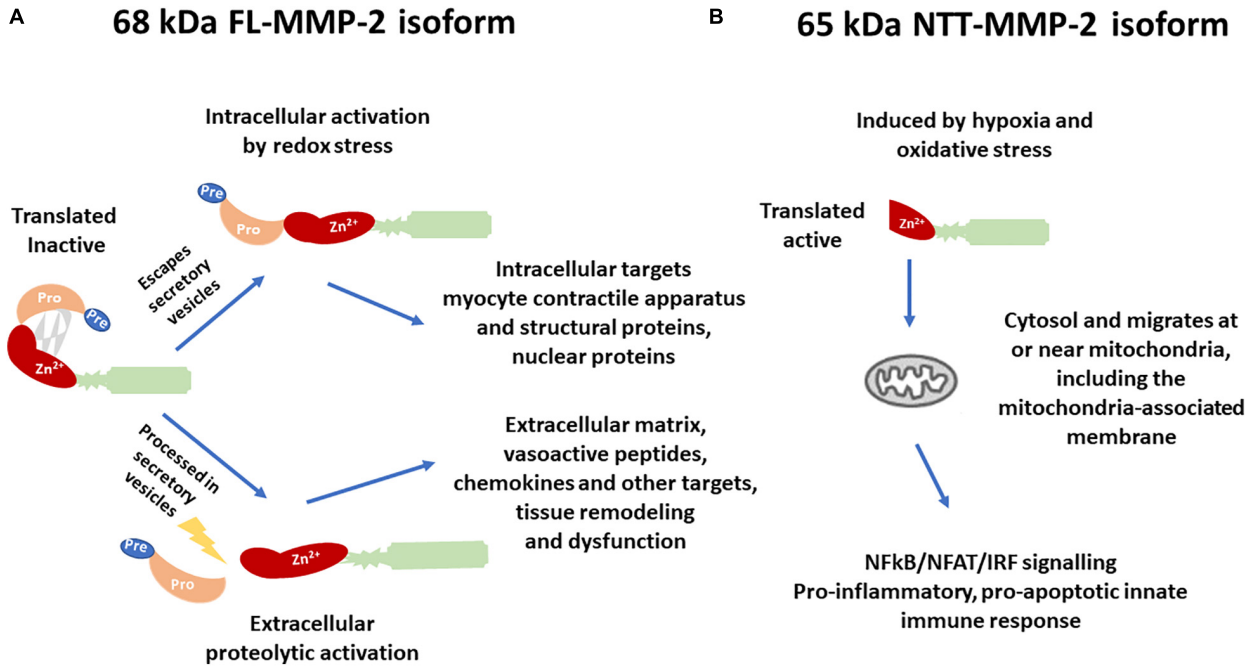

FIGURE 1 | Differences in the structure, activation, and biological targets/outcomes between **(A)** the 68 kDa full-length isoform of MMP-2 (FL-MMP-2) and **(B)** the 65 kDa N-terminal truncated isoform of MMP-2 (NTT-MMP-2).

acid in the first exon of the *MMP2* gene (Lovett et al., 2012). Transcription of NTT-MMP-2 starts with activation of a latent promoter induced by hypoxia and oxidative stress, in an alternate transcriptional start site located at the 3′ end of the first intron of the *MMP2*, which encodes the NTT-MMP-2 isoform beginning at M77 amino acid located within the second exon of *MMP2* (Lovett et al., 2012).

Figure 2 shows the promoter region of the *MMP2* with the transcriptional start site as indicated by the Eukaryotic Promoter Database (Dreos et al., 2013) and highlights the overlap of the first intron with several epigenomics data from the Encyclopedia of DNA Elements (ENCODE) (Consortium, 2012) and GENCODE consortium (Frankish et al., 2019), including ENCODE registry of candidate *cis*-regulatory elements (cCREs), DNase I hypersensitivity clusters (Thurman et al., 2012), chromatin immunoprecipitation-sequencing (ChIP-seq) data for histone marks, and transcription factor ChIP-seq clusters (Consortium, 2012). This approach using epigenomics data to identify gene regulatory regions was recently performed elsewhere (Linhares et al., 2020).

HISTONE MODIFICATIONS AND THE NTT-MMP-2 ISOFORM EXPRESSION

The trimethylation of histone H3 on lysine 4 (H3K4me3) is associated with promoters (Rosenbloom et al., 2012). The acetylation of histone H3 on lysine 27 (H3K27ac) is often found near active regulatory elements such as enhancers and distinguishes active from poised enhancers containing the monomethylation of histone H3 on lysine 4 (H3K4me1) alone (Creyghton et al., 2010).

H3K4me1 is commonly associated with distal enhancers, but it is also present at promoter regions proximal to transcriptional start site (Cheng et al., 2014; Bae and Lesch, 2020). Noteworthy, H3K4me1 peak density was recently examined around promoters in human and mouse germ cells (Bae and Lesch, 2020). H3K4me1 was found to exhibit either a bimodal pattern at active promoters, where it flanks H3K4me3, or a unimodal pattern at poised promoters, where it coincides with both H3K4me3 and trimethylation at lysine 27 of histone H3 (H3K27me3). H3K4me1 distribution was proposed as a key feature of the poised epigenetic state and poising at promoters (Bae and Lesch, 2020).

Interestingly, a region with enhancer-like signature (E1817412/enhP) identified by the ENCODE cCREs in the first intron of the *MMP2* gene overlaps with a DNase I hypersensitivity cluster, and with ENCODE ChIP-seq data for the histone modification H3K4me1, for the histone acetyltransferase EP300, and for the transcription factors FOS, JUND, and MAFK, which are known to cooperate in hypoxia-induced gene transcription (**Figure 2**). Hypoxic conditions were shown to induce the transcriptional activation of c-fos in HeLa cells (Muller et al., 1997). Notably, c-Jun was shown to functionally cooperate with hypoxia-inducible factor 1 (HIF-1) transcriptional activity in different cell types (Alfranca et al., 2002). In this context, the small Maf protein, MafG, possess a basic leucine zipper domain that is required for homodimer or heterodimer complex formation with other transcription factors. MafG was shown to interact with HIF-1α, a key factor in hypoxic response, and it was suggested to regulate the hypoxic

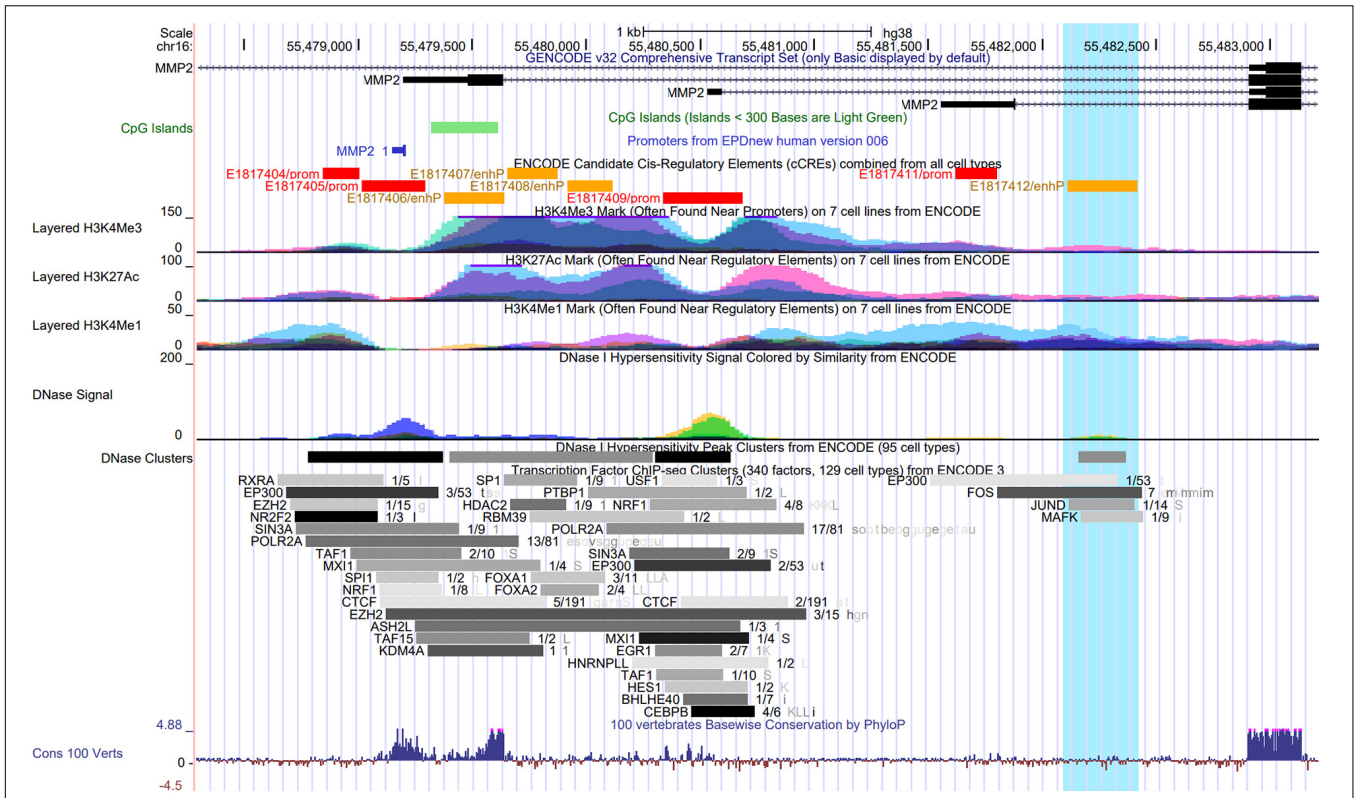

FIGURE 2 | UCSC Genome Browser view of the promoter and the first intron of the *MMP2* gene showing the overlap with several epigenomics data from the ENCODE Project, including the ENCODE registry of candidate cis-regulatory elements (cCREs), DNase I hypersensitivity clusters, ChIP-seq data for three histone marks on seven cell lines, and Transcription Factor ChIP-seq clusters. The transcriptional start site in the promoter region of *MMP2* gene is indicated by the Eukaryotic Promoter Database (EPDnew). Highlighted (in light blue) is a region with an enhancer-like signature (E1817412/enhP) identified by the ENCODE cCREs in the first intron of *MMP2*, which overlaps with a DNase I hypersensitivity cluster, and with ENCODE ChIP-seq data for the histone modification H3K4me1, for the histone acetyltransferase EP300, and for the hypoxia-induced transcription factors FOS, JUND, and MAFK.

response by detaining HIF-1α in the nucleus (Ueda et al., 2008). These data further support the presence of the poised promoter located in the first intron of the *MMP2* gene and suggest that it may be affected by a putative enhancer element activated by the binding of well-known hypoxia-induced transcription factors in the activation of the NTT-MMP-2 expression. However, this hypothesis remains to be tested.

DNA METHYLATION AND THE NTT-MMP-2 ISOFORM EXPRESSION

DNA methylation consists of the addition of the methyl group in cytosines followed by guanines, named CpG dinucleotides. CpG islands are regions enriched in CpG dinucleotides that are normally located in gene promoters and that are implicated in the regulation of gene expression (Gardiner-Garden and Frommer, 1987; Jones, 2012). ENCODE data show a CpG island located in the promoter/exon 1 of the *MMP2* gene (**Figure 2**), which are not methylated in most of the ENCODE cell lines. However, there is no CpG methylation data by Methyl 450K Bead Arrays from ENCODE, which overlap with the latent promoter region in the intron 1 of the *MMP2* gene (**Supplementary Figure 1**).

DNA methylation represses gene transcription when located in promoter regions and activates transcription when located in gene body (Jones, 2012). Methylation pattern is known to differ between promoters and alternative promoters in the same gene and among different tissues, indicating a dynamic physiological change in DNA methylation. Thus, DNA methylation may have a significant role in the differential use of alternative promoters, which may be related to the functional differentiation of promoters with or without CpG islands (Cheong et al., 2006). Moreover, intragenic DNA methylation has a major role in regulating alternative promoters in gene bodies (Maunakea et al., 2010). While there are no DNA methylation data from ENCODE for the intron 1 of the *MMP2* gene, there are other CpG islands in this region (**Supplementary Figure 1**). However, it is unknown whether the overlap of the intron 1 region with DNA methylation may affect the NTT-MMP-2 expression.

The NTT-MMP-2 isoform is induced by hypoxia (Lovett et al., 2012), which is present in cancer and other diseases (Ivan and Kaelin, 2017). The cells sense and adapt to hypoxia by activating hypoxia-inducible transcription factors, but the cells differ in their transcriptional response to hypoxia (Ivan and Kaelin, 2017). A probable explanation is that the hypoxia-inducible transcription factors do not bind to CpG dinucleotides that are

methylated. Therefore, the specific DNA methylation patterns of a cell established under normoxic conditions determine the hypoxia-inducible binding profiles for the transcription factors, and define how cell types response to hypoxia (D'Anna et al., 2020). Taken together, these processes could explain the mechanism for regulating the latent promoter located in the intron of the *MMP2* gene in the condition of hypoxia by DNA methylation. However, these hypotheses remain to be proved.

FUNCTIONAL ASSESSMENT OF THE NTT-MMP-2 ISOFORM

Cardiac-specific transgenic mice expressing the NTT-MMP-2 isoform were generated to determine its functional significance (Lovett et al., 2013). These mice developed progressive cardiomyocyte and ventricular hypertrophy associated with systolic heart failure. The NTT-MMP-2 transgenic hearts also showed more severe injury following *ex vivo* IRI. Therefore, this NTT-MMP-2 isoform induced by oxidative stress directly contributed, in the absence of superimposed injury, to cardiomyocyte hypertrophy, inflammation, systolic heart failure, and enhanced susceptibility to IRI (Lovett et al., 2013).

Further studies evaluated the effects of the presence of the NTT-MMP-2 isoform (Lovett et al., 2014). At 4 to 5-month-old transgenic mice, the NTT-MMP-2 expression was located in the mitochondria and in the Z-line of the sarcomere. When compared with wild-type mice, transgenic mice expressing the NTT-MMP-2 isoform presented impaired myocardial contraction, without decreasing myofilament force, but affecting calcium transients. However, the FL-MMP-2 impaired cardiomyocyte contractility by decreasing myofilament force. Thus, the FL-MMP-2 and NTT-MMP-2 have distinctive pathophysiological mechanisms in the cardiomyocyte by impairing different intracellular processes (Lovett et al., 2014).

Transgenic mice expressing the NTT-MMP-2 isoform specifically in the renal proximal tubule cells were generated to evaluate the effects of this isoform (Ceron et al., 2017). At 4 months of age, the NTT-MMP-2 transgenic mouse kidneys presented tubular epithelial cell necrosis, mitochondrial loss of organized cristae, and mitochondrial permeability transition, mitophagy observed at ultrastructural analysis. At 8 months old, transgenic mice expressing the NTT-MMP-2 isoform presented severe structural kidney abnormalities, as tubular atrophy, necrosis of tubular epithelial cells, and mononuclear cell infiltration and evidence of mitochondrial reactive oxygen species production. Glomerular changes were not present. At this time point, transgenic mice expressing the NTT-MMP-2 isoform also had a decrease in renal function compared with wild-type mice (Ceron et al., 2017).

NTT-MMP-2 AND RENAL DYSFUNCTION AND KIDNEY DISEASES

Delayed graft function, a clinical example of renal acute IRI, is a complication of renal transplantation, which results from tubular epithelial cell injury and has consequences as post-transplantation dialysis, increased incidence of acute rejection, and poorer long-term outcomes (Moeckli et al., 2019; Nieuwenhuijs-Moeke et al., 2020). The extent of tubular epithelial injury and the expression of both FL-MMP-2 and NTT-MMP-2 were analyzed in renal biopsies of controls and patients diagnosed with delayed graft function, and these expressions were correlated with the amount of tubular damage in patients (Wanga et al., 2015). While FL-MMP-2 expression was diffusely found in control kidney biopsies, NTT-MMP-2 was found located in a pattern characteristic of mitochondria only in biopsies of patients with delayed graft function (Wanga et al., 2015).

The mitochondrial NTT-MMP-2 isoform was also evaluated in *acute kidney injury*, a frequent complication in severely ill patients that may progress to *chronic kidney disease*. Mitochondria dysfunction increases oxidative stress and cause tubular inflammation, one of the major fibrotic processes in renal diseases (Maekawa and Inagi, 2019; Husain-Syed et al., 2020). Wild-type mice and transgenic NTT-MMP-2 mice were submitted to 40 min of unilateral renal IRI, and the contralateral non-clamped kidney was evaluated for systemic inflammatory responses (Ceron et al., 2017). At 96 h following IRI, the contralateral kidney of wild-type mice presented normal morphology, while the kidney subjected to IRI presented a mild degree of tubular dilatation, inflammation, and cast formation. However, the contralateral kidney of NTT-MMP-2 transgenic mice showed mild to moderate degrees of injury, and the kidneys subjected to IRI showed more extensive injury, with massive cast formation, tubular dilatation, and cellular inflammation than the wild-type kidneys subjected to IRI (Ceron et al., 2017).

Three weeks after IRI, the differences between wild-type and NTT-MMP-2 transgenic mice were more prominent. While IRI and contralateral of wild-type mice showed moderate injury, the kidney of NTT-MMP-2 mice subjected to IRI showed extensive mononuclear cell infiltration, fibrosis, and tubular epithelial cell dropout (Ceron et al., 2017). Moreover, the contralateral kidneys showed cellular inflammation, fibrosis, tubular dilatation, and tubular epithelial cell dropout, indicating a sustained systemic inflammatory response. These findings suggest that the NTT-MMP-2 sensitizes the kidneys to more severe IRI (Ceron et al., 2017).

The NTT-MMP-2 was also showed to induce sustained systemic inflammatory response after IRI, which was not observed in the wild-type kidneys. The kidney of the NTT-MMP-2 transgenic mice present enhanced expression of *OAS-1*, *IRF-7*, and *CXCL-10* at 96 h following IRI when compared with IRI kidneys of the wild-type mice and the contralateral kidneys, suggesting the induction of a systemic inflammatory response by NTT-MMP-2. This enhanced expression of innate immunity genes and a sustained release of danger-associated molecular patterns were persistent 3 weeks following the IRI in the kidney subjected to the injury and the contralateral kidney of NTT-MMP-2 transgenic mice (Ceron et al., 2017).

The NTT-MMP-2 also participates in chronic kidney disease. The HypoE/SR-B1 Mx1-Cre mice is a mice model of accelerated atherogenesis, which develops a diffuse atherosclerosis, chronic kidney disease and ischemic cardiomyopathy were given a

high-fat diet (Wang et al., 2014; Luk et al., 2016). After 22 days of high-fat diet, an increased expression of both FL-MMP-2 and NTT-MMP-2 was associated with tubular epithelial cell necrosis, kidney inflammation, and elevated plasma blood urea nitrogen levels when compared with normal diet-fed mice (Ceron et al., 2017).

Normal *aging* also leads to a decline in the kidney function. While the mechanisms are not fully known, oxidative stress and inflammation may participate in the aging changes in organ functions (Panickar and Jewell, 2018). NTT-MMP-2 was increased in the renal proximal tubules in aged mouse (14 months old wild-type mice), but it was absent at 4 months old wild-type mice. No differences were observed in FL-MMP-2 expression as a function of increasing age. The NTT-MMP-2 was suggested to be a link between the inflammatory state and the declined renal function that occurs on the aging process (Ceron et al., 2017).

Diabetic nephropathy is a complication of diabetes mellitus and a frequent cause of chronic kidney disease. The participation of both MMP-2 isoforms was also examined in diabetic nephropathy (Kim et al., 2017). The increased expression of the FL-MMP-2 and NTT-MMP-2 was observed in HK2 cells cultured in high glucose or 4-hydroxy-2-hexenal (an oxidative stress inductor). However, the pretreatment of HK2 cells with the antioxidant/NF-κB inhibitor pyrrolidine dithiocarbamate inhibited only the NTT-MMP-2 expression. In the murine model of type 1 diabetes mellitus induced by streptozotocin, NTT-MMP-2 was intensely expressed in the diabetic kidneys, while FL-MMP-2 was present in control and diabetic kidneys. Finally, an increase in both MMP-2 isoforms was found in renal biopsies of patients with diabetic nephropathy (Kim et al., 2017).

To explore the possible mechanisms of aging in renal function, the FL-MMP-2 and NTT-MMP-2 were examined in two mouse models of chronic kidney disease, the streptozotocin-induced model of type 1 diabetes mellitus, and the 5/6 nephrectomy model of chronic kidney disease in mice aged 8 weeks (young mice) or 14 months (old mice). The expression of both isoforms was increased independently of mice age in both mouse models. However, only the NTT-MMP-2 expression was increased in mice aged 14 months, which was associated with the tubulointerstitial fibrosis development in chronic kidney disease (Rhee et al., 2018).

The temporal and spatial locations of both MMP-2 isoforms were examined in a mouse model of type 1 diabetes mellitus induced by streptozotocin and in the db/db mouse model of type 2 diabetes mellitus. Both the FL-MMP-2 and NTT-MMP-2 were increased earlier in the kidney of streptozotocin mice than in db/db mice. However, while FL-MMP-2 was located in the cortices and outer medullae, NTT-MMP-2 was located only in the cortices. Moreover, the levels of nitrotyrosine, a marker of nitrosative stress, were increased similarly to the NTT-MMP-2 isoform (Kim et al., 2018).

NTT-MMP-2 AND HEART INJURY

Diabetic cardiomyopathy is a condition associated with enhanced reactive oxygen species production and mitochondrial dysfunction (Cieluch et al., 2020). The expression of FL-MMP-2 and NTT-MMP-2 was increased both in H9C2 cells exposed to high glucose media and in the heart of streptozotocin-induced diabetes mouse model. The FL-MMP-2 was located in the cardiomyocyte sarcomeres, and the NTT-MMP-2 mainly in the subsarcolemmal space, where mitochondria are abundant. The degree of mitochondrial damage was positively correlated to NTT-MMP-2 expression, and the decreased left ventricular systolic function observed in diabetic mice was associated with the increased expression of both MMP-2 isoforms (Lee H. W. et al., 2019).

Increased cardiac MMP-2 activity was found in hearts of mice treated with doxorubicin, in part, by upregulating NTT-MMP-2. Cardiotoxicity was attenuated by MMP inhibitors (Chan et al., 2021). Regarding MMPs inhibitors, they are shown to be protective in different models of renal and cardiac diseases, including type 1 diabetes (Yaras et al., 2008), *in vivo* renal injury (Labossiere et al., 2015; Lee T. F. et al., 2019), and other models of cardiac injury and cardiovascular dysfunction (Kandasamy et al., 2010; Rizzi et al., 2010; Guimaraes et al., 2011; Castro et al., 2012). In this context, FL-MMP-2 and NTT-MMP-2 are relevant targets of pharmacological intervention.

CONCLUSION AND PERSPECTIVES

We provide insights into the epigenetic regulation of the latent promoter located in the first intron of *MMP-2*, which support the activation of the NTT-MMP-2 isoform. Moreover, we reviewed recent evidence for the presence of NTT-MMP-2 in renal dysfunction and in kidney and cardiac diseases. Noteworthy, both the FL-MMP-2 and NTT-MMP-2 isoforms can be activated in tissue injury/oxidative stress models. However, FL-MMP-2 is directly activated by oxidative stress whereas there is transcriptional activation and expression of NTT-MMP-2. Further studies should consider that these isoforms would act in different time frames, subcellular locales, and protein targets in the development of tissue injuries and diseases. Taken together, these findings may help to understand how hypoxia and oxidative stress trigger NTT-MMP-2 expression, which are relevant pathophysiological mechanisms to several diseases. Our insights may guide further experimental and clinical studies that are needed to elucidate the underlying mechanisms and the role of NTT-MMP-2 in renal dysfunction. We expect that these future efforts may help to establish the NTT-MMP-2 as a potential therapeutic target in kidney diseases.

DATA AVAILABILITY STATEMENT

Publicly available datasets were analyzed in this study. This data can be found here: UCSC Genome Browser Gateway, available at: https://genome.ucsc.edu/cgi-bin/hgTracks?db=hg38&lastVirtModeType=default&lastVirtModeExtraState=&virtModeType=default&virtMode=0&non-VirtPosition=&position=chr16%3A55478079%2D55483623&hgsid=963348143_Mp3s46YxzZ1zGnQs8Ct0oWoyZOKp.

AUTHOR CONTRIBUTIONS

JC, ML, and CC drafted the manuscript and prepared figures. JC, AS, ML, and CC edited and revised the manuscript. All authors have read and approved the final version of manuscript for submission.

FUNDING

This work was supported by the National Council for Scientific and Technological Development (CNPq/Brazil) (Grants #406177/2016-3 and #312599/2019-6), the Minas Gerais Research Foundation (FAPEMIG/Brazil) (Grants PPM-00383-18, APQ-01239-16, and APQ-01960-18), and the Coordination for the Improvement of Higher Education Personnel (CAPES/Brazil) (Finance Code 001).

SUPPLEMENTARY MATERIAL

The Supplementary Material for this article can be found online at: https://www.frontiersin.org/articles/10.3389/fgene.2021.637148/full#supplementary-material

Supplementary Figure 1 | UCSC Genome Browser on Human Feb. 2009 (GRCh37/hg19) Assembly. Characterization of the genomic position chr16:55,512,747-55,517,056 showing the location of CpG dinucleotides and CpG islands located in the *MMP2* gene. **(A)** The CpG methylation by Methyl 450K Bead Array ENCODE/HAIB showing the CpG dinucleotides and CpG islands in the promoter region/exon 1 and intron 1 that are not methylated in most of the ENCODE cell lines, except in the HeLa-S3 line, and the DNA methylation by reduced representation bisulfite Seq from ENCODE/HudsonAlpha showing the same pattern of methylation in this region. **(B)** The output of MethPrimer showed other CpG dinucleotides and CpG islands in the *MMP2* gene, which are not covered by the ENCODE techniques publicly available at the UCSC Genome Browser.

REFERENCES

Alfranca, A., Gutierrez, M. D., Vara, A., Aragones, J., Vidal, F., and Landazuri, M. O. (2002). c-Jun and hypoxia-inducible factor 1 functionally cooperate in hypoxia-induced gene transcription. *Mol. Cell Biol.* 22, 12–22. doi: 10.1128/mcb.22.1.12-22.2002

Ali, M. A., Cho, W. J., Hudson, B., Kassiri, Z., Granzier, H., and Schulz, R. (2010). Titin is a target of matrix metalloproteinase-2: implications in myocardial ischemia/reperfusion injury. *Circulation* 122, 2039–2047. doi: 10.1161/circulationaha.109.930222

Ali, M. A., Chow, A. K., Kandasamy, A. D., Fan, X., West, L. J., Crawford, B. D., et al. (2012). Mechanisms of cytosolic targeting of matrix metalloproteinase-2. *J. Cell Physiol.* 227, 3397–3404. doi: 10.1002/jcp.24040

Bae, S., and Lesch, B. J. (2020). H3K4me1 distribution predicts transcription state and poising at promoters. *Front. Cell Dev. Biol.* 8:289. doi: 10.3389/fcell.2020.00289

Castro, M. M., Rizzi, E., Ceron, C. S., Guimaraes, D. A., Rodrigues, G. J., Bendhack, L. M., et al. (2012). Doxycycline ameliorates 2K-1C hypertension-induced vascular dysfunction in rats by attenuating oxidative stress and improving nitric oxide bioavailability. *Nitric Oxide* 26, 162–168. doi: 10.1016/j.niox.2012.01.009

Ceron, C. S., Baligand, C., Joshi, S., Wanga, S., Cowley, P. M., Walker, J. P., et al. (2017). An intracellular matrix metalloproteinase-2 isoform induces tubular regulated necrosis: implications for acute kidney injury. *Am. J. Physiol. Renal. Physiol.* 312, F1166–F1183.

Chan, B. Y. H., Roczkowsky, A., Cho, W. J., Poirier, M., Sergi, C., Keschrumrus, V., et al. (2021). MMP inhibitors attenuate doxorubicin cardiotoxicity by preventing intracellular and extracellular matrix remodelling. *Cardiovasc. Res.* 117, 188–200. doi: 10.1093/cvr/cvaa017

Cheng, J., Blum, R., Bowman, C., Hu, D., Shilatifard, A., Shen, S., et al. (2014). A role for H3K4 monomethylation in gene repression and partitioning of chromatin readers. *Mol. Cell.* 53, 979–992. doi: 10.1016/j.molcel.2014.02.032

Cheng, S., Pollock, A. S., Mahimkar, R., Olson, J. L., and Lovett, D. H. (2006). Matrix metalloproteinase 2 and basement membrane integrity: a unifying mechanism for progressive renal injury. *FASEB J* 20, 1898–1900. doi: 10.1096/fj.06-5898fje

Cheong, J., Yamada, Y., Yamashita, R., Irie, T., Kanai, A., Wakaguri, H., et al. (2006). Diverse DNA methylation statuses at alternative promoters of human genes in various tissues. *DNA Res.* 13, 155–167. doi: 10.1093/dnares/dsl008

Cieluch, A., Uruska, A., and Zozulinska-Ziolkiewicz, D. (2020). Can we prevent mitochondrial dysfunction and diabetic cardiomyopathy in Type 1 diabetes mellitus? pathophysiology and treatment options. *Int. J. Mol. Sci.* 21:2852, doi: 10.3390/ijms21082852

Coker, M. L., Doscher, M. A., Thomas, C. V., Galis, Z. S., and Spinale, F. G. (1999). Matrix metalloproteinase synthesis and expression in isolated LV myocyte preparations. *Am. J. Physiol.* 277, H777–H787.

Consortium, T. E. P. (2012). An integrated encyclopedia of DNA elements in the human genome. *Nature* 489, 57–74. doi: 10.1038/nature11247

Creyghton, M. P., Cheng, A. W., Welstead, G. G., Kooistra, T., Carey, B. W., Steine, E. J., et al. (2010). Histone H3K27ac separates active from poised enhancers and predicts developmental state. *Proc. Natl. Acad. Sci. U. S. A.* 107, 21931–21936. doi: 10.1073/pnas.1016071107

D'Anna, F., Van Dyck, L., Xiong, J., Zhao, H., Berrens, R. V., Qian, J., et al. (2020). DNA methylation repels binding of hypoxia-inducible transcription factors to maintain tumor immunotolerance. *Genome Biol.* 21:182.

DeCoux, A., Lindsey, M. L., Villarreal, F., Garcia, R. A., and Schulz, R. (2014). Myocardial matrix metalloproteinase-2: inside out and upside down. *J. Mol. Cell. Cardiol.* 77, 64–72. doi: 10.1016/j.yjmcc.2014.09.016

Denney, H., Clench, M. R., and Woodroofe, M. N. (2009). Cleavage of chemokines CCL2 and CXCL10 by matrix metalloproteinases-2 and -9: implications for chemotaxis. *Biochem. Biophys. Res. Commun.* 382, 341–347. doi: 10.1016/j.bbrc.2009.02.164

Dimas, G. G., Didangelos, T. P., and Grekas, D. M. (2017). Matrix gelatinases in atherosclerosis and diabetic nephropathy: progress and challenges. *Curr. Vasc. Pharmacol.* 15, 557–565.

Dreos, R., Ambrosini, G., Cavin Perier, R., and Bucher, P. (2013). EPD and EPDnew, high-quality promoter resources in the next-generation sequencing era. *Nucleic Acids Res.* 41, D157–D164.

Fernandez-Patron, C., Radomski, M. W., and Davidge, S. T. (1999). Vascular matrix metalloproteinase-2 cleaves big endothelin-1 yielding a novel vasoconstrictor. *Circ. Res.* 85, 906–911. doi: 10.1161/01.res.85.10.906

Fernandez-Patron, C., Stewart, K. G., Zhang, Y., Koivunen, E., Radomski, M. W., and Davidge, S. T. (2000). Vascular matrix metalloproteinase-2-dependent cleavage of calcitonin gene-related peptide promotes vasoconstriction. *Circ. Res.* 87, 670–676. doi: 10.1161/01.res.87.8.670

Frankish, A., Diekhans, M., Ferreira, A. M., Johnson, R., Jungreis, I., Loveland, J., et al. (2019). GENCODE reference annotation for the human and mouse genomes. *Nucleic Acids Res.* 47, D766–D773.

Gardiner-Garden, M., and Frommer, M. (1987). CpG islands in vertebrate genomes. *J. Mol. Biol.* 196, 261–282. doi: 10.1016/0022-2836(87)90689-9

Guimaraes, D. A., Rizzi, E., Ceron, C. S., Oliveira, A. M., Oliveira, D. M., Castro, M. M., et al. (2011). Doxycycline dose-dependently inhibits MMP-2-mediated vascular changes in 2K1C hypertension. *Basic Clin. Pharmacol. Toxicol.* 108, 318–325. doi: 10.1111/j.1742-7843.2010.00656.x

Husain-Syed, F., Rosner, M. H., and Ronco, C. (2020). Distant organ dysfunction in acute kidney injury. *Acta Physiol. (Oxf.)* 228:e13357.

Ivan, M., and Kaelin, W. G. Jr. (2017). The EGLN-HIF O2-sensing system: multiple inputs and feedbacks. *Mol. Cell.* 66, 772–779. doi: 10.1016/j.molcel.2017.06.002

Jacob-Ferreira, A. L., and Schulz, R. (2013). Activation of intracellular matrix metalloproteinase-2 by reactive oxygen-nitrogen species: consequences and

therapeutic strategies in the heart. *Arch. Biochem. Biophys.* 540, 82–93. doi: 10.1016/j.abb.2013.09.019

Jones, P. A. (2012). Functions of DNA methylation: islands, start sites, gene bodies and beyond. *Nat. Rev. Genet.* 13, 484–492. doi: 10.1038/nrg3230

Kandasamy, A. D., Chow, A. K., Ali, M. A., and Schulz, R. (2010). Matrix metalloproteinase-2 and myocardial oxidative stress injury: beyond the matrix. *Cardiovasc. Res.* 85, 413–423. doi: 10.1093/cvr/cvp268

Kim, I. Y., Kim, S. S., Lee, H. W., Bae, S. S., Ha, H. K., Jung, E. S., et al. (2018). The two isoforms of matrix metalloproteinase- 2 have distinct renal spatial and temporal distributions in murine models of types 1 and 2 diabetes mellitus. *BMC Nephrol.* 19:248. doi: 10.1186/s12882-018-1029-8

Kim, S. S., Shin, N., Bae, S. S., Lee, M. Y., Rhee, H., Kim, I. Y., et al. (2017). Enhanced expression of two discrete isoforms of matrix metalloproteinase-2 in experimental and human diabetic nephropathy. *PLoS One* 12:e0171625. doi: 10.1371/journal.pone.0171625

Labossiere, J. R., Pelletier, J. S., Thiesen, A., Schulz, R., Bigam, D. L., and Cheung, P. Y. (2015). Doxycycline attenuates renal injury in a swine model of neonatal hypoxia-reoxygenation. *Shock* 43, 99–105. doi: 10.1097/shk.0000000000000257

Lee, H. W., Lee, S. J., Lee, M. Y., Park, M. W., Kim, S. S., Shin, N., et al. (2019). Enhanced cardiac expression of two isoforms of matrix metalloproteinase-2 in experimental diabetes mellitus. *PLoS One* 14:e0221798. doi: 10.1371/journal.pone.0221798

Lee, T. F., Lu, M., Pasquin, M. P., Schmolzer, G. M., and Cheung, P. Y. (2019). Attenuation of acute renal injury after the post-resuscitation administration of doxycycline in surviving newborn piglets with severe hypoxia-reoxygenation. *Front. Pediatr.* 7:75. doi: 10.3389/fped.2019.00075

Linhares, N. D., Pereira, D. A., Conceicao, I. M., Franco, G. R., Eckalbar, W. L., Ahituv, N., et al. (2020). Noncoding SNPs associated with increased GDF15 levels located in a metformin-activated enhancer region upstream of GDF15. *Pharmacogenomics* 21, 509–520. doi: 10.2217/pgs-2020-0010

Lovett, D. H., Chu, C., Wang, G., Ratcliffe, M. B., and Baker, A. J. (2014). A N-terminal truncated intracellular isoform of matrix metalloproteinase-2 impairs contractility of mouse myocardium. *Front. Physiol.* 5:363. doi: 10.3389/fphys.2014.00363

Lovett, D. H., Mahimkar, R., Raffai, R. L., Cape, L., Maklashina, E., Cecchini, G., et al. (2012). A novel intracellular isoform of matrix metalloproteinase-2 induced by oxidative stress activates innate immunity. *PLoS One* 7:e34177. doi: 10.1371/journal.pone.0034177

Lovett, D. H., Mahimkar, R., Raffai, R. L., Cape, L., Zhu, B. Q., Jin, Z. Q., et al. (2013). N-terminal truncated intracellular matrix metalloproteinase-2 induces cardiomyocyte hypertrophy, inflammation and systolic heart failure. *PLoS One* 8:e68154. doi: 10.1371/journal.pone.0068154

Luk, F. S., Kim, R. Y., Li, K., Ching, D., Wong, D. K., Joshi, S. K., et al. (2016). Immunosuppression With FTY720 reverses cardiac dysfunction in hypomorphic apoe mice deficient in SR-BI expression that survive myocardial infarction caused by coronary atherosclerosis. *J. Cardiovasc. Pharmacol.* 67, 47–56. doi: 10.1097/fjc.0000000000000312

Maekawa, H., and Inagi, R. (2019). Pathophysiological role of organelle stress/crosstalk in AKI-to-CKD transition. *Semin. Nephrol.* 39, 581–588. doi: 10.1016/j.semnephrol.2019.10.007

Mansour, S. G., Puthumana, J., Coca, S. G., Gentry, M., and Parikh, C. R. (2017). Biomarkers for the detection of renal fibrosis and prediction of renal outcomes: a systematic review. *BMC Nephrol.* 18:72. doi: 10.1186/s12882-017-0490-0

Martinez, A., Oh, H. R., Unsworth, E. J., Bregonzio, C., Saavedra, J. M., Stetler-Stevenson, W. G., et al. (2004). Matrix metalloproteinase-2 cleavage of adrenomedullin produces a vasoconstrictor out of a vasodilator. *Biochem. J.* 383, 413–418. doi: 10.1042/bj20040920

Maunakea, A. K., Nagarajan, R. P., Bilenky, M., Ballinger, T. J., D'souza, C., Fouse, S. D., et al. (2010). Conserved role of intragenic DNA methylation in regulating alternative promoters. *Nature* 466, 253–257. doi: 10.1038/nature09165

Moeckli, B., Sun, P., Lazeyras, F., Morel, P., Moll, S., Pascual, M., et al. (2019). Evaluation of donor kidneys prior to transplantation: an update of current and emerging methods. *Transpl. Int.* 32, 459–469. doi: 10.1111/tri.13430

Morgunova, E., Tuuttila, A., Bergmann, U., Isupov, M., Lindqvist, Y., Schneider, G., et al. (1999). Structure of human pro-matrix metalloproteinase-2: activation mechanism revealed. *Science* 284, 1667–1670. doi: 10.1126/science.284.5420.1667

Muller, J. M., Krauss, B., Kaltschmidt, C., Baeuerle, P. A., and Rupec, R. A. (1997). Hypoxia induces c-fos transcription via a mitogen-activated protein kinase-dependent pathway. *J. Biol. Chem.* 272, 23435–23439. doi: 10.1074/jbc.272.37.23435

Narula, S., Tandon, C., and Tandon, S. (2018). Role of matrix metalloproteinases in degenerative kidney disorders. *Curr. Med. Chem.* 25, 1805–1816. doi: 10.2174/0929867325666171205143441

Nieuwenhuijs-Moeke, G. J., Pischke, S. E., Berger, S. P., Sanders, J. S. F., Pol, R. A., Struys, M., et al. (2020). Ischemia and reperfusion injury in kidney transplantation: relevant mechanisms in injury and repair. *J. Clin. Med.* 9:253, doi: 10.3390/jcm9010253

Panickar, K. S., and Jewell, D. E. (2018). The benefit of anti-inflammatory and renal-protective dietary ingredients on the biological processes of aging in the kidney. *Biology (Basel)* 7:45. doi: 10.3390/biology7040045

Parrish, A. R. (2017). Matrix metalloproteinases in kidney disease: role in pathogenesis and potential as a therapeutic target. *Prog. Mol. Biol. Transl. Sci.* 148, 31–65. doi: 10.1016/bs.pmbts.2017.03.001

Rhee, H., Han, M., Kim, S. S., Kim, I. Y., Lee, H. W., Bae, S. S., et al. (2018). The expression of two isoforms of matrix metalloproteinase-2 in aged mouse models of diabetes mellitus and chronic kidney disease. *Kidney Res. Clin. Pract.* 37, 222–229. doi: 10.23876/j.krcp.2018.37.3.222

Rizzi, E., Castro, M. M., Prado, C. M., Silva, C. A., Fazan, R. Jr., Rossi, M. A., et al. (2010). Matrix metalloproteinase inhibition improves cardiac dysfunction and remodeling in 2-kidney, 1-clip hypertension. *J. Card. Fail.* 16, 599–608. doi: 10.1016/j.cardfail.2010.02.005

Rosenbloom, K. R., Dreszer, T. R., Long, J. C., Malladi, V. S., Sloan, C. A., Raney, B. J., et al. (2012). ENCODE whole-genome data in the UCSC genome browser: update 2012. *Nucleic Acids Res.* 40, D912–D917.

Sariahmetoglu, M., Crawford, B. D., Leon, H., Sawicka, J., Li, L., Ballermann, B. J., et al. (2007). Regulation of matrix metalloproteinase-2 (MMP-2) activity by phosphorylation. *FASEB J* 21, 2486–2495.

Sariahmetoglu, M., Skrzypiec-Spring, M., Youssef, N., Jacob-Ferreira, A. L., Sawicka, J., Holmes, C., et al. (2012). Phosphorylation status of matrix metalloproteinase 2 in myocardial ischaemia-reperfusion injury. *Heart* 98, 656–662. doi: 10.1136/heartjnl-2011-301250

Sawicki, G., Leon, H., Sawicka, J., Sariahmetoglu, M., Schulze, C. J., Scott, P. G., et al. (2005). Degradation of myosin light chain in isolated rat hearts subjected to ischemia-reperfusion injury: a new intracellular target for matrix metalloproteinase-2. *Circulation* 112, 544–552. doi: 10.1161/circulationaha.104.531616

Sung, M. M., Schulz, C. G., Wang, W., Sawicki, G., Bautista-Lopez, N. L., and Schulz, R. (2007). Matrix metalloproteinase-2 degrades the cytoskeletal protein alpha-actinin in peroxynitrite mediated myocardial injury. *J. Mol. Cell. Cardiol.* 43, 429–436. doi: 10.1016/j.yjmcc.2007.07.055

Tan, R. J., and Liu, Y. (2012). Matrix metalloproteinases in kidney homeostasis and diseases. *Am. J. Physiol. Renal. Physiol.* 302, F1351–F1361.

Thurman, R. E., Rynes, E., Humbert, R., Vierstra, J., Maurano, M. T., Haugen, E., et al. (2012). The accessible chromatin landscape of the human genome. *Nature* 489, 75–82.

Turck, J., Pollock, A. S., Lee, L. K., Marti, H. P., and Lovett, D. H. (1996). Matrix metalloproteinase 2 (gelatinase A) regulates glomerular mesangial cell proliferation and differentiation. *J. Biol. Chem.* 271, 15074–15083. doi: 10.1074/jbc.271.25.15074

Ueda, K., Xu, J., Morimoto, H., Kawabe, A., and Imaoka, S. (2008). MafG controls the hypoxic response of cells by accumulating HIF-1alpha in the nuclei. *FEBS Lett.* 582, 2357–2364. doi: 10.1016/j.febslet.2008.05.040

Viappiani, S., Nicolescu, A. C., Holt, A., Sawicki, G., Crawford, B. D., Leon, H., et al. (2009). Activation and modulation of 72kDa matrix metalloproteinase-2 by peroxynitrite and glutathione. *Biochem. Pharmacol.* 77, 826–834. doi: 10.1016/j.bcp.2008.11.004

Wang, G., Kim, R. Y., Imhof, I., Honbo, N., Luk, F. S., Li, K., et al. (2014). The immunosuppressant FTY720 prolongs survival in a mouse model of diet-induced coronary atherosclerosis and myocardial infarction. *J. Cardiovasc. Pharmacol.* 63, 132–143. doi: 10.1097/fjc.0000000000000031

Wang, W., Schulze, C. J., Suarez-Pinzon, W. L., Dyck, J. R., Sawicki, G., and Schulz, R. (2002). Intracellular action of matrix metalloproteinase-2 accounts for acute

myocardial ischemia and reperfusion injury. *Circulation* 106, 1543–1549. doi: 10.1161/01.cir.0000028818.33488.7b

Wanga, S., Ceron, C. S., Delgado, C., Joshi, S. K., Spaulding, K., Walker, J. P., et al. (2015). Two distinct isoforms of matrix metalloproteinase-2 are associated with human delayed kidney graft function. *PLoS One* 10:e0136276. doi: 10.1371/journal.pone.0136276

Yaras, N., Sariahmetoglu, M., Bilginoglu, A., Aydemir-Koksoy, A., Onay-Besikci, A., Turan, B., et al. (2008). Protective action of doxycycline against diabetic cardiomyopathy in rats. *Br. J. Pharmacol.* 155, 1174–1184. doi: 10.1038/bjp.2008.373

Conflict of Interest: The authors declare that the research was conducted in the absence of any commercial or financial relationships that could be construed as a potential conflict of interest.

frontiers in Physiology

ORIGINAL RESEARCH
published: 26 February 2021
doi: 10.3389/fphys.2021.632398

Long Non-coding RNA H19 Augments Hypoxia/Reoxygenation-Induced Renal Tubular Epithelial Cell Apoptosis and Injury by the miR-130a/BCL2L11 Pathway

*Yuan Yuan[1], Xiaoling Li[2], Yudong Chu[1], Gongjie Ye[1], Lei Yang[1] and Zhouzhou Dong[1]**

[1] Ningbo Medical Center Li Huili Hospital, Ningbo University, Ningbo, China, [2] Guilin People's Hospital, Guilin, China

Acute kidney injury (AKI) is a severe kidney disease defined by partial or abrupt loss of renal function. Emerging evidence indicates that non-coding RNAs (ncRNAs), particularly long non-coding RNAs (lncRNAs), function as essential regulators in AKI development. Here we aimed to explore the underlying molecular mechanism of the lncRNA H19/miR-130a axis for the regulation of inflammation, proliferation, and apoptosis in kidney epithelial cells. Human renal proximal tubular cells (HK-2) were induced by hypoxia/reoxygenation to replicate the AKI model *in vitro*. After treatment, the effects of LncRNA H19 and miR-130a on proliferation and apoptosis of HK-2 cells were investigated by CCK-8 and flow cytometry. Meanwhile, the expressions of LncRNA H19, miR-130a, and inflammatory cytokines were detected by qRT-PCR, western blot, and ELISA assays. The results showed that downregulation of LncRNA H19 could promote cell proliferation, inhibit cell apoptosis, and suppress multiple inflammatory cytokine expressions in HK-2 cells by modulating the miR-130a/BCL2L11 pathway. Taken together, our findings indicated that LncRNA H19 and miR-130a might represent novel therapeutic targets and early diagnostic biomarkers for the treatment of AKI.

Keywords: acute kidney injury (AKI), lncRNA H19, miR-130a, BCL2L11, renal tubular epithelial cells

OPEN ACCESS

Edited by:
Xiao-ming Meng,
Anhui Medical University, China

Reviewed by:
Pei-Hui Lin,
The Ohio State University, United States
Michelle L. Gumz,
University of Florida, United States

***Correspondence:**
Zhouzhou Dong
zhouzhou662255d@163.com

Specialty section:
This article was submitted to Renal and Epithelial Physiology, a section of the journal Frontiers in Physiology

Received: *23 November 2020*
Accepted: *25 January 2021*
Published: *26 February 2021*

Citation:
Yuan Y, Li X, Chu Y, Ye G, Yang L and Dong Z (2021) Long Non-coding RNA H19 Augments Hypoxia/Reoxygenation-Induced Renal Tubular Epithelial Cell Apoptosis and Injury by the miR-130a/BCL2L11 Pathway. Front. Physiol. 12:632398. doi: 10.3389/fphys.2021.632398

INTRODUCTION

Acute kidney injury (AKI), characterized by persistent oliguria and elevated serum creatinine, is a frequent complication accompanied by high mortality, long-term hospitalization, and decreased kidney filtration function ability (Zafrani et al., 2016). Sepsis is a common cause of AKI, and previous studies found that severe sepsis could result in 60% AKI incidence clinically (Gómez and Kellum, 2016). The pathogenesis of sepsis-induced AKI includes inflammation, oxidative stress, and tubular epithelial response (Zhao et al., 2016). Hypoxia, a common cause of AKI, may contribute to tubular epithelial cell necrosis and immune responses (Potteti et al., 2016). Therefore, elucidating the underlying mechanisms of AKI and exploring novel therapeutic targets or early diagnostic biomarkers are important for the treatment of AKI.

Long non-coding RNAs (LncRNAs) are a class of non-protein-coding RNAs > 200 bp in length (Ye et al., 2020). LncRNAs are previously reported to be regulators involved in multiple cellular and disease progresses, including cell differentiation, cell proliferation, and apoptosis (Jiang et al., 2015; Wang et al., 2017; Villa et al., 2019). The abnormal expressions of certain lncRNAs are found to be indicators of immune system diseases (Atianand and Fitzgerald, 2014; Stachurska et al., 2014). Moreover, LncRNAs are also reported to play a crucial regulatory role in AKI (Yu et al., 2016; Ignarski et al., 2019). LncRNA H19, first described in 1991, was found to be predominantly located in extra embryonic tissues and the embryo proper (Poirier et al., 1991; Zhou et al., 2019). Previous studies also indicated that lncRNA H19 regulated tumor carcinogenesis, angiogenesis, and metastasis. For example, Cao proved the functions of LncRNA H19 in inflammation and endothelial cell injury (Cao et al., 2019). Interestingly, dysregulation of LncRNA H19 was also found in the embryonic renals of mice with maternal hyperglycemia which may lead to kidney diseases (Lorenzen and Thum, 2016). Moreover, Xie showed that lncRNA-H19 expression was significantly upregulated in TGF-β2-induced HK-2 cell fibrosis and unilateral ureteral obstruction (UUO)-induced renal fibrosis *in vivo*, indicating that H19 upregulation contributes to renal fibrosis (Xie et al., 2016).

MicroRNAs (miRNAs) are approximately 22-nt endogenous RNAs which play important regulatory roles in animals and plants by targeting mRNAs for cleavage or translational repression (Bartel, 2004). Emerging evidence shows that in addition to LncRNAs, miRNAs also exert crucial functions by regulating a lot of signaling pathways in various cell processes. miR-130a, a member of the miR-130 family, has been reported to regulate cell proliferation, apoptosis, and inflammation and is related to renal diseases (Muralidharan et al., 2017; Li et al., 2020). However, few studies have focused on LncRNA H19 and miR-130a expressions and their functions in modulating AKI development.

Therefore, in the present study, we systematically investigated the expressions and functions of LncRNA H19 and miR-130a *in vitro* via the hypoxia-induced human renal proximal tubular cell (HK-2) model. The results showed that downregulation of LncRNA H19 could promote cell proliferation, inhibit cell apoptosis, and suppress multiple inflammatory cytokine expressions in HK-2 cells by modulating the miR-130a/BCL2L11 pathway. Our findings indicated that LncRNA H19 and miR-130a might represent novel therapeutic targets and early diagnostic biomarkers for the treatment of AKI.

MATERIALS AND METHODS

Cell Culture and Hypoxia/Reoxygenation Treatment

The cells used in this study including human kidney epithelial cell line HK-2 and human kidney cell line HEK-293 were purchased from ATCC (American Type Culture Collection, United States). Cells were cultured in RPMI 1640 Medium supplemented with 10% heat-inactivated fetal bovine serum (FBS) and 1% penicillin–streptomycin (Sigma-Aldrich Inc., St. Louis, MO, United States). The incubation conditions were at 37°C, 5% CO_2, and humidified atmosphere. For hypoxia/reoxygenation (H/R) treatment, HK-2 cells were cultured in a low glucose concentration medium for 48 h, removed, washed with PBS two times and inhaled pure oxygen (100% oxygen) for 15 min, and placed in an airtight container with 95% N_2 and 5% CO_2 for 3 h, then reoxygenated (95% air and 5% CO_2) with the addition of fresh low glucose DMEM with 10% FBS at 37°C, for a total 3 h of reoxygenation. The H/R model was used for the functional experiments.

Plasmid Construction and Cell Transfection

For downregulation of H19, the small interfering RNA (siRNA) against H19 (si-H19) and its negative control (si-nc) were designed and cloned into the pAdTrack-CMV vector by GenePharma (Shanghai, China). The resulting plasmids were transfected into K-293T cells for viral packaging. At 72 h post transfection, virus-containing supernatants were collected and then used for infection of HK-2 cells via Polybrene. To yield the BCL2L11 overexpression plasmid pcDNA3.1-BCL2L11, the cDNA sequence of human BCL2L11 (Gene ID: 10018) was amplified by PCR, followed by digestion and subsequent insertion into the pcDNA3.1 vector (Invitrogen, Carlsbad, CA, United States). The miR-130a mimics, miR-130a inhibitor, and their negative controls (nc) were designed and synthesized by GenePharma (Shanghai, China). The cell transfection experiments were performed using Lipofectamine 2000 reagent according to the manufacturer's instructions (Invitrogen, Carlsbad, CA, United States).

Quantitative Real-Time PCR (qRT-PCR)

RNA extraction was isolated from cells using TRIzol reagent (Thermo Fisher Scientific, Inc., Waltham, MA, United States) followed by treatment with RNase-free DNase I. Approximately 1 μg amount of total RNA was transcribed into cDNA using a High-Capacity cDNA Reverse Transcription Kit (Applied Biosystems, Carlsbad, CA, United States) according to the manufacturer's instructions. The glyceraldehyde-3-phosphate dehydrogenase (GAPDH) and U6 small nuclear RNA (U6 snRNA) were used as two internal references for normalization of mRNA and miRNA, respectively. The primers used in this study are listed in **Supplementary Table 1**. PCR was performed in a 20-μl reaction volume containing 10 μl of 2 × AceQ Universal SYBR qPCR Master Mix (Vazyme, Shanghai, China), 2 μl of cDNA, 1 μl of each primer (10 μM), and 6 μl of ddH2O. The PCR reactions were detected by an ABI 7500 System (Applied Biosystems, Carlsbad, CA, United States) using the following program: 95°C for 3 min, followed by 40 cycles of 95°C for 10 s, 60°C for 30 s, and 72°C for 10 s. All experiments were performed in biological triplicates (n = 6), and data were representative of three independent experiments. Data were calculated with the ($2^{-\Delta\Delta Ct}$) method and compared with the corresponding internal reference. The statistically

significant differences were determined by Student's *t*-test for unpaired comparisons between different groups using GraphPad Prism software (version 7.0). The $P < 0.05$ was considered as statistically significant.

Western Blot

Ice-cold Triton X-100 lysis buffer supplemented with a protease inhibitor cocktail (Sigma-Aldrich, Shanghai, China) was used to lyse cells and extract total protein. The protein concentration was determined by the BCA assay according to the supplier's instructions (Pierce, Appleton, WI, United States). The protein samples were loaded and separated by 10% SDS-polyacrylamide gel electrophoresis (SDS-PAGE; Solarbio Life Sciences, Beijing, China), then transferred to PVDF membranes (PVDF; Solarbio Life Sciences, Beijing, China). The non-specific sites were blocked with 5% skimmed milk diluted in Tris-buffered saline with 0.05% Tween (TBST) for 1 h at RT. Then, membranes were incubated with diluted first antibody (1:1000; Abcam Inc., Cambridge, MA, United States) at 4°C overnight. The primary antibodies used were listed as the following: anti-BCL2L11 (1:1000, MA5-14848, Sigma, United States); anti-Bax (1:1000, ab182733, Abcam, United Kingdom); anti-Cyto-c (1:1000, ab133504, Abcam, United Kingdom); anti-Bcl-2 (1:1000, MA5-11757, Sigma, United States); anti-Caspase 3 (1:1000, 31A1067, Santa Cruz Biotechnology, United States); and anti-GAPDH (1:1000, ab181602, Abcam, United Kingdom). The next day, after washing three times with TBST, membranes were incubated with a second antibody (horseradish peroxidase-conjugated anti-rabbit IgG; 1:5,000; Abcam Inc., Cambridge, MA, United States), followed by reaction with chemiluminescent substrate. Finally, the immunoblots were visualized using an ImageQuant LAS 4000 mini (GE Healthcare, Piscataway, NJ, United States). All experiments were performed in biological triplicates ($n = 6$), and data were representative of three independent experiments.

ELISA Assay

The expression levels of inflammatory factors IL-1β, IL-6, IL-10, and tumor necrosis factor-alpha (TNF-α) were quantitatively detected by ELISA assay. Briefly, culture supernatants were collected at different times post-transfection and later determined by standard ELISA kits (Thermo Fisher Scientific, Inc., Waltham, MA, United States) according to the manufacturer's instructions. The optical density (OD) values at 450 nm were read using a microplate reader (Bio-Tek Instruments, Winooski, VT, United States). The concentrations were obtained according to the linear standard curve established by standard solutions. All experiments were performed in biological triplicates ($n = 6$), and data were representative of three independent experiments.

CCK-8 Assay

Briefly, after transfection and H/R administration treatment, HK-2 cells were seeded at 1×10^3 cells/well in 96-well plates. Cell viabilities were determined using the Cell Counting Kit-8 (CCK-8; Beyotime, Shanghai, China), at different time points. At each time point, 100 μl CCK-8 (Beyotime Biotechnology, Shanghai, China) was added to each well of a 96-well plate, which was then placed in a 37°C, 5% CO_2 incubator for a further 2 h. The absorbance value at 450-nm wavelength was read on a microplate reader (Bio-Tek Instruments, Winooski, VT, United States). All experiments were performed in biological triplicates ($n = 6$), and data were representative of three independent experiments.

Cell Apoptosis Analysis

Cell apoptosis was determined using the Annexin V-FITC apoptosis detection kit (Beyotime Biotechnology, Shanghai, China). Data analysis was conducted using BD FACSDiva Software version 6.1.3 (BD Biosciences, San Jose, CA, United States). Briefly, after transfection and H/R treatment, HK-2 cells were seeded at 1×10^5 cells into 6-well plates and incubated at 37°C under 5% CO_2 in a humidified atmosphere for 48 h. Cells were then washed twice with ice-cold PBS and incubated with Annexin V-FITC/PI staining solution according to the manufacturer's protocol. All experiments were performed in biological triplicates ($n = 6$), and data were representative of three independent experiments.

Dual-Luciferase Reporter Assay

The dual-luciferase reporter plasmids including H19-mutant and BCL2L11-mutant were constructed by Genscript (Nanjing, China). The lncRNA H19 and 3′-UTR of BCL2L11 cDNA fragments containing the potential binding sequences of miR-130a sites were amplified from PCR and inverted into the pGL3 vector (Promega, Madison, WI, United States). For dual luciferase assay, HEK-293T cells were cultured in 24-well plates transiently co-transfected with luciferase vectors, miR-130a mimics, or miR-nc. Lipofectamine 2000 reagent (Invitrogen, Carlsbad, CA, United States) was used for plasmid and siRNA transfection. Luciferase activity assays were performed using the Dual-Luciferase Reporter Assay System (Promega, Madison, WI, United States) in line with the manufacturer's protocol. All experiments were performed in biological triplicates ($n = 6$), and data were representative of three independent experiments.

Biotin-Labeled miR-130a Pull-Down Assay

The RNA pull-down assay was performed as described (Teng et al., 2016). Briefly, biotin-labeled miR-130a (biotin-miR-130a) and biotin-labeled negative control (biotin-nc) were purchased from GenePharma (Shanghai, China) and transfected into HEK-293 cells, respectively. 48 h after transfection, cells were harvested and lysed. Samples (50 μl) were aliquoted for input and then thoroughly mixed with Dynabeads M-280 Streptavidin (Invitrogen, Carlsbad, CA, United States) by incubating overnight rotating at 4°C following the manufacturer's protocol. Beads were washed and treated in RNase-free solutions, then incubated with equal volumes of biotinylated miR-130a for 15 min at room temperature using gentle rotation. Lastly, the bead-bound target mRNAs were extracted and purified for next qRT-PCR analysis. Simultaneously, total fragmented chromatin (Input) was extracted and purified as a control. All experiments

were performed in biological triplicates (n = 6), and data were representative of three independent experiments.

Mitochondrial Membrane Potential Analysis

The mitochondrial membrane potential analysis was carried out as described (Chen et al., 2020). Briefly, after treatment, the transfected cells were incubated with 10 mM 5,5′,6,6′-tetrachloro-1,1′,3,3′-tetraethylbenzimidazolylcarbocyanine iodide (JC-1) (Beyotime, Shanghai, China) for 30 min at 37°C. Then, the fluorescence-labeled cells were washed with PBS and fluorescence was measured at 530 nm excitation and 590 nm emission. Mitochondrial membrane potential was represented by the ratio of fluorescence (530/590 nm). All experiments were performed in biological triplicates (n = 6), and data were representative of three independent experiments.

Statistical Analysis

Statistical analyses for biological data were carried out using the SPSS statistical software (SPSS, Chicago, IL, United States) and GraphPad Prism software 7.0 (GraphPad Software, San Diego, CA, United States). All results were expressed as mean ± standard deviation (SD). Statistical comparisons between two groups were evaluated with Student s t-test (unpaired t-test, two-tailed). Significance between multiple groups was determined by one-way analysis of variance followed by either Dunnett's or Tukey's multiple-comparison test. Statistical significance was defined as a P-value less than 0.05.

RESULTS

LncRNA H19 Regulates Cell Proliferation, Apoptosis, and Inflammatory Cytokine Expressions in HK-2 Cells Under H/R Conditions

As shown in **Figure 1A**, H/R treatment could significantly suppress HK-2 cell proliferation *in vitro*, and cell viability was inhibited to a minimum level 8 h post reoxygenation treatment ($^*P < 0.05$). Meanwhile, the HK-2 cell apoptosis rate was significantly promoted, reaching the highest level at 8 h ($^*P < 0.05$; **Figure 1B**). At the same time windows, the LncRNA H19 expressions were detected by qRT-PCR. The results showed that the relative expressions of LncRNA H19 in HK-2 cells gradually increased after H/R treatment, reaching the highest level 8 h post reoxygenation treatment ($^*P < 0.05$; **Figure 1C**). The expressions of inflammatory cytokines (IL-1β, IL-6, IL-10, and TNF-α) regulated by LncRNA H19 in HK-2 cell under H/R conditions were also monitored by qRT-PCR and ELISA assays, respectively. The results showed that the mRNA/protein expression levels of IL-1β, IL-6, and TNF-α were significantly increased, while the expressions of IL-10 were significantly reduced in HK-2 cells under H/R conditions, compared with those from the untreated control groups ($^*P < 0.05$; **Figures 1D,E**).

Downregulation of LncRNA H19 Promotes Cell Proliferation, Inhibits Apoptosis, and Modulates Inflammatory Cytokines Expressions in HK-2 Cells Under H/R Treatment

In a pilot experiment, transient transfection efficiency was assessed by transfections with Ad-nc and Ad-siH19 vectors and subsequent measurement of LncRNA H19 gene expressions by qRT-PCR. As demonstrated in **Figure 2A**, the relative gene expression levels of LncRNA H19 in the Ad-siH19 group were significantly lower than those detected from Ad-nc and control groups ($^*P < 0.05$). After H/R administration, the CCK-8 assay results indicated a significant decline in proliferating HK-2 cells in H/R-treated groups, although it was partially reversed by transfection of the Ad-siH19 vector ($^*P < 0.05$; $\#P < 0.05$; **Figure 2B**). Meanwhile, HK-2 cell apoptosis was significantly induced after H/R treatment, although the variations could be partially reversed by Ad-siH19 transfection ($^*P < 0.05$; $\#P < 0.05$; **Figure 2C**). At the same time windows, the inflammatory cytokine expressions were also monitored. As demonstrated in **Figures 2D,E**, the mRNA/protein expression levels of IL-1β, IL-6, and TNF-α were significantly increased, while IL-10 expressions were decreased in the H/R or H/R+Ad-nc groups, compared with those from untreated groups ($^*P < 0.05$). However, transfection with Ad-siH19 could reverse H/R-induced variations in inflammatory cytokine expressions ($^*P < 0.05$; $\#P < 0.05$). These observations indicated that LncRNA H19 plays an anti-proliferative and apoptotic role in HK-2 cells under H/R conditions.

Negative Regulation Between lncRNA H19 and miR-130a Expression in HEK-293 Cells

A biological prediction website Starbase was used to predict the target binding site of lncRNA H19 (Li et al., 2014). The bioinformatics analysis results revealed promising binding sites of miR-130a within LncRNA H19 sequences, indicating a potential link between lncRNA H19 and miR-130a (**Figure 3A**). Afterward, the dual-luciferase reporter assay confirmed that the co-transfection of HEK-293 cells with wild-type LncRNA H19 and the miR-130a mimics resulted in significantly decreased luciferase activity as compared with the miR-nc group ($^*P < 0.05$; **Figure 3B**). Meanwhile, the relative expression of LncRNA H19 was significantly lower in the miR-130a mimics group than those in the miR-nc group ($^*P < 0.05$; **Figure 3C**). However, LncRNA H19 expression was remarkably increased after transfection with the miR-130a inhibitor ($\#P < 0.05$; **Figure 3C**). Then, RNA pull-down assay was performed to detect the interplay between lncRNA H19 and miR-130a. Interestingly, almost little of lncRNA H19 in the miR-130a-WT pulled-down pellet was observed when compared with negative control (biotin-nc), but more enrichment of LncRNA H19 was detected in the miR-130a pulled-down pellet ($^*P < 0.05$; **Figure 3D**). The Pearson correlation analysis results also reflected that the expression of miR-130a was negatively correlated with LncRNA H19

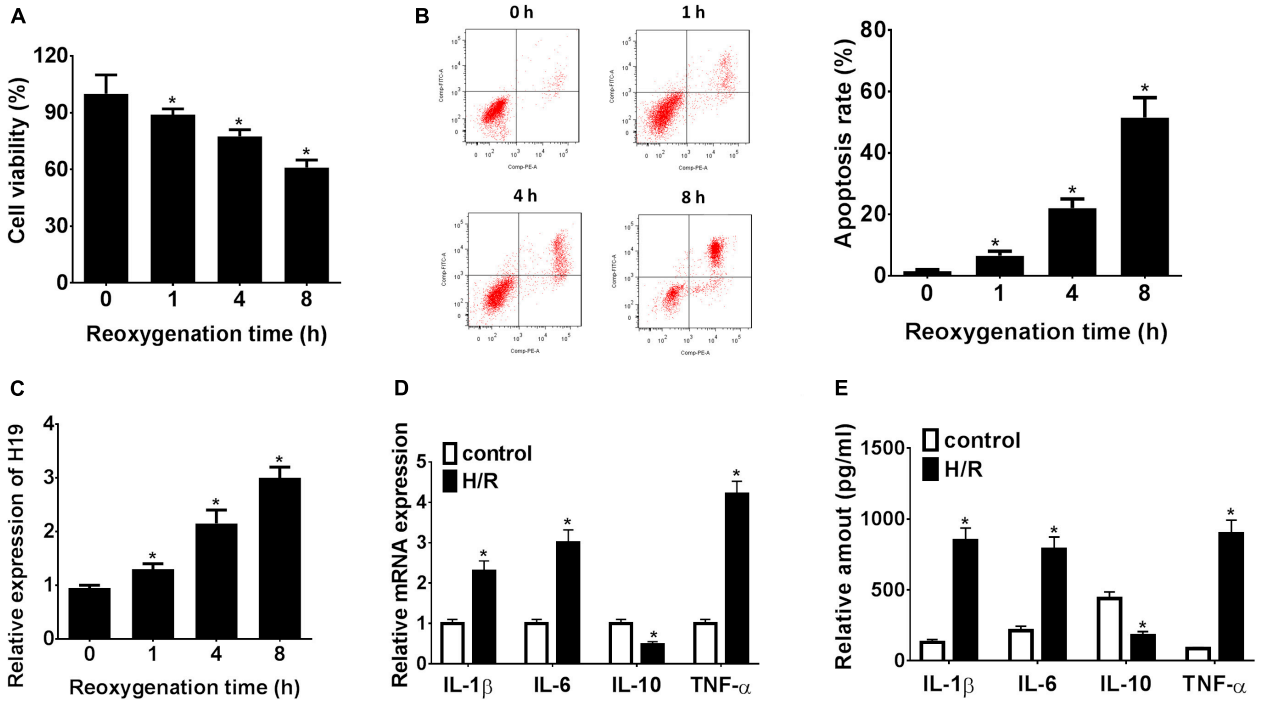

FIGURE 1 | LncRNA H19 regulates cell proliferation, apoptosis, and inflammatory cytokine expressions in HK-2 cells under H/R conditions. **(A)** HK-2 cell viability analysis after H/R treatment. **(B)** HK-2 cell apoptosis assay after H/R treatment. **(C)** Relative expressions of LncRNA H19 after H/R treatment. **(D,E)** mRNA/protein expression levels of inflammatory cytokines in HK-2 cells after H/R treatment. H/R, hypoxia/reoxygenation treatment; Control, untreated cells; IL-1β, interleukin-1β; IL-6, interleukin-6; IL-10, interleukin-10; TNF-α, tumor necrosis factor α. All experiments were performed in biological triplicates ($n = 6$), and data were representative of three independent experiments. The results were expressed as mean ± standard deviation (SD). Statistical comparisons between two groups were evaluated with Student's *t*-test. $^{*}P < 0.05$, compared with the control groups.

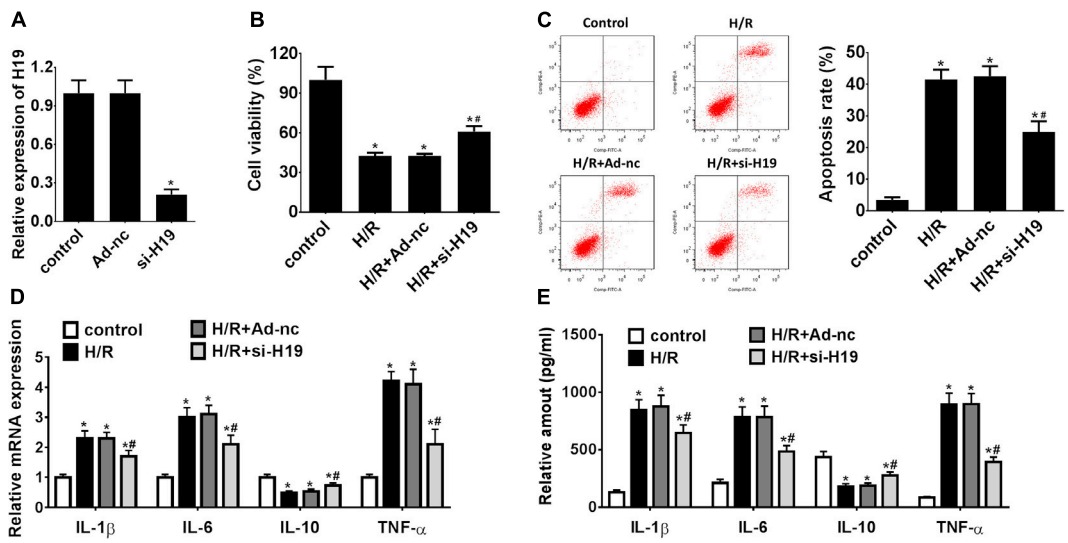

FIGURE 2 | Downregulation of LncRNA H19 promotes cell proliferation, inhibits apoptosis, and modulates inflammatory cytokine expressions in HK-2 cells under H/R treatment. **(A)** Relative expressions of LncRNA H19 after recombinant adenovirus vector transfection. **(B)** HK-2 cell viability analysis after H/R treatment. **(C)** HK-2 cell apoptosis assay after H/R treatment. **(D,E)** mRNA/protein expression levels of inflammatory cytokines in HK-2 cells after H/R treatment. H/R, hypoxia/reoxygenation treatment; Control, untreated cells; Ad-nc, Ad-siRNA-NC; Ad-siH19, Ad-siRNA-H19; IL-1β, interleukin-1β; IL-6, interleukin-6; IL-10, interleukin-10; TNF-α, tumor necrosis factor α. All experiments were performed in biological triplicates ($n = 6$), and data were representative of three independent experiments. The results were expressed as mean ± standard deviation (SD). Statistical comparisons between two groups were evaluated with Student's *t*-test. $^{*}P < 0.05$, compared with the control groups; $^{\#}P < 0.05$, compared with the H/R groups.

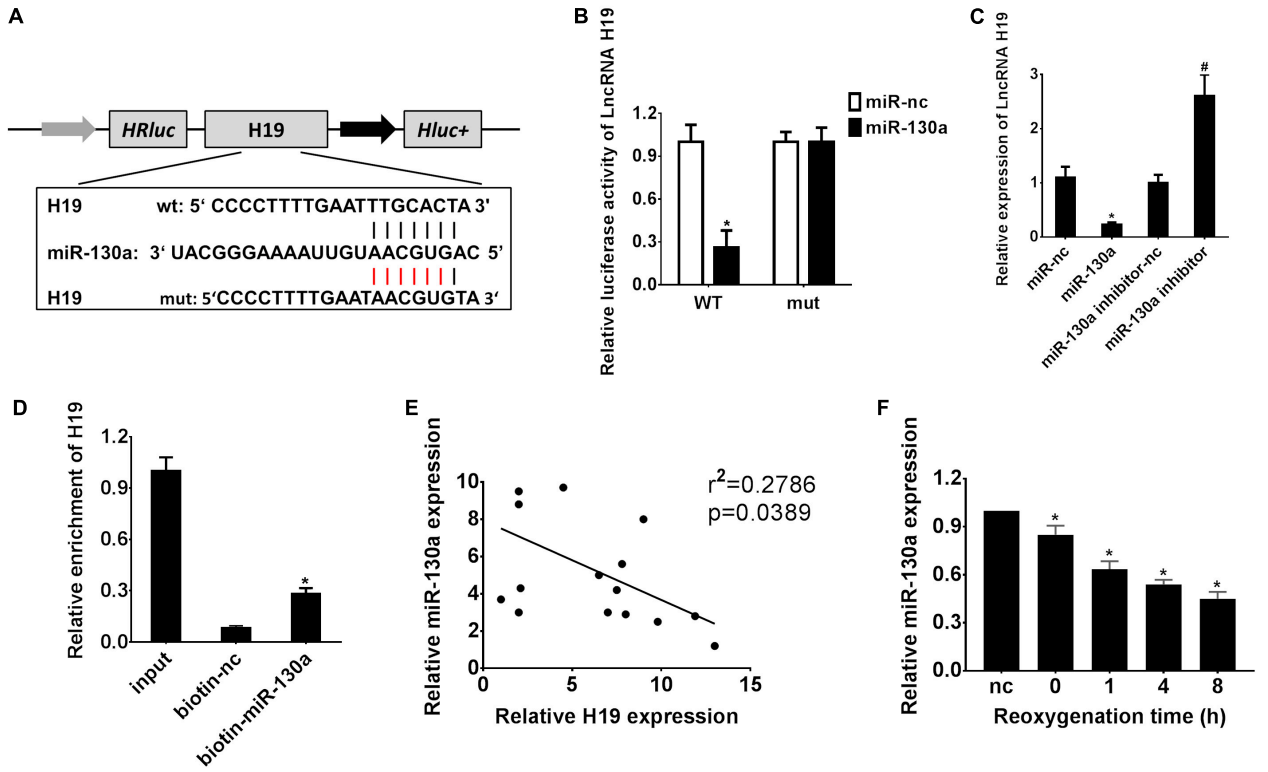

FIGURE 3 | Reciprocal inhibition between LncRNA H19 and miR-130a in HEK-293 cells. **(A)** Putative binding sites of miR-30a within LncRNA H19 mRNA, and the sequences of wild-type and mutant-type vectors. **(B)** The relative luciferase activities of luciferase reporters containing WT or mutant LncRNA H19 were assayed 48 h after co-transfection with miR-30a mimics or miR-nc. **(C)** The relative expressions of LncRNA H19 after transfection with miR-130a mimics or inhibitor. **(D)** The expression level of LncRNA H19 mRNA was measured by RT-qPCR in the sample pulled down by biotinylated miR-130a. **(E)** The correlation analysis between LncRNA H19 and miR-130a. **(F)** The relative expressions of miR-130a after H/R treatment. All experiments were performed in biological triplicates (n = 6), and data were representative of three independent experiments. The results were expressed as mean ± standard deviation (SD). Statistical comparisons between two groups were evaluated with Student's t-test. $^{*}P < 0.05$, compared with the control groups; $^{\#}P < 0.05$, compared with the other control groups.

(r^2 = 0.2786, P = 0.0389; **Figure 3E**). In addition, the relative expression of miR-130a was observed to be gradually decreased in HK-2 cells after H/R treatment, reaching the highest level 8 h post reoxygenation ($^{*}P < 0.05$; **Figure 3F**). Taken together, these results suggest that lncRNA H19 may modulate the expression of miR-130a, indicating miR-130a as a direct target of LncRNA H19.

Upregulation of miR-130a Partially Counteracted LncRNA H19-Induced Cell Proliferation, Apoptosis, and Inflammatory Cytokines Expression in HK-2 Cells After H/R Treatment

As demonstrated in **Figure 4A**, transfection with Ad-siH19 remarkably increased the expression level of miR-130a after H/R administration, whereas this change could be offset by co-transfection of the miR-130a inhibitor ($^{*}P < 0.05$; $\#P < 0.05$). After H/R administration, the CCK-8 assay results showed significant inhibition in HK-2 cell proliferation ($^{*}P < 0.05$; **Figures 2B**, **4B**). However, after transfection with Ad-siH19, a much less significant decrease in cell viability was observed, which was partially rescued by co-transfection with the miR-130a inhibitor ($^{*}P < 0.05$; $\#P < 0.05$; $\&P < 0.05$; **Figure 4B**). As shown in **Figures 2C**, **4C,D**, H/R administration could induce significant cell apoptosis in HK-2 cells. However, a significant decrease of cell apoptosis in HK-2 cells was observed when transfected with Ad-siH19, which was partially reversed by co-transfection with the miR-130a inhibitor ($^{*}P < 0.05$; $\#P < 0.05$; $\&P < 0.05$). In addition, as demonstrated in **Figures 4E,F**, a significant enhanced mRNA/protein expression levels of IL-1β, IL-6, and TNF-α and meanwhile a decrease expression levels of IL-10 were observed in the H/R group, compared to those detected from untreated groups ($^{*}P < 0.05$). Moreover, co-transfection with Ad-siH19 and miR-nc inhibited the expression levels of IL-1β, IL-6, and TNF-α while it increased the expression levels of IL-10. The variations in inflammatory factors induced by Ad-siH19 could be counteracted through transfection with Ad-siH19 and miR-130a inhibitor ($^{*}P < 0.05$; #P < 0.05).

miR-130a Targets BCL2L11 Gene in HEK-293 Cells

The bioinformatics website TargetScan was used to predict the potential targets for miR-130a (Agarwal et al., 2015). As indicated in **Figure 5A**, the binding sites of BCL2L11 were

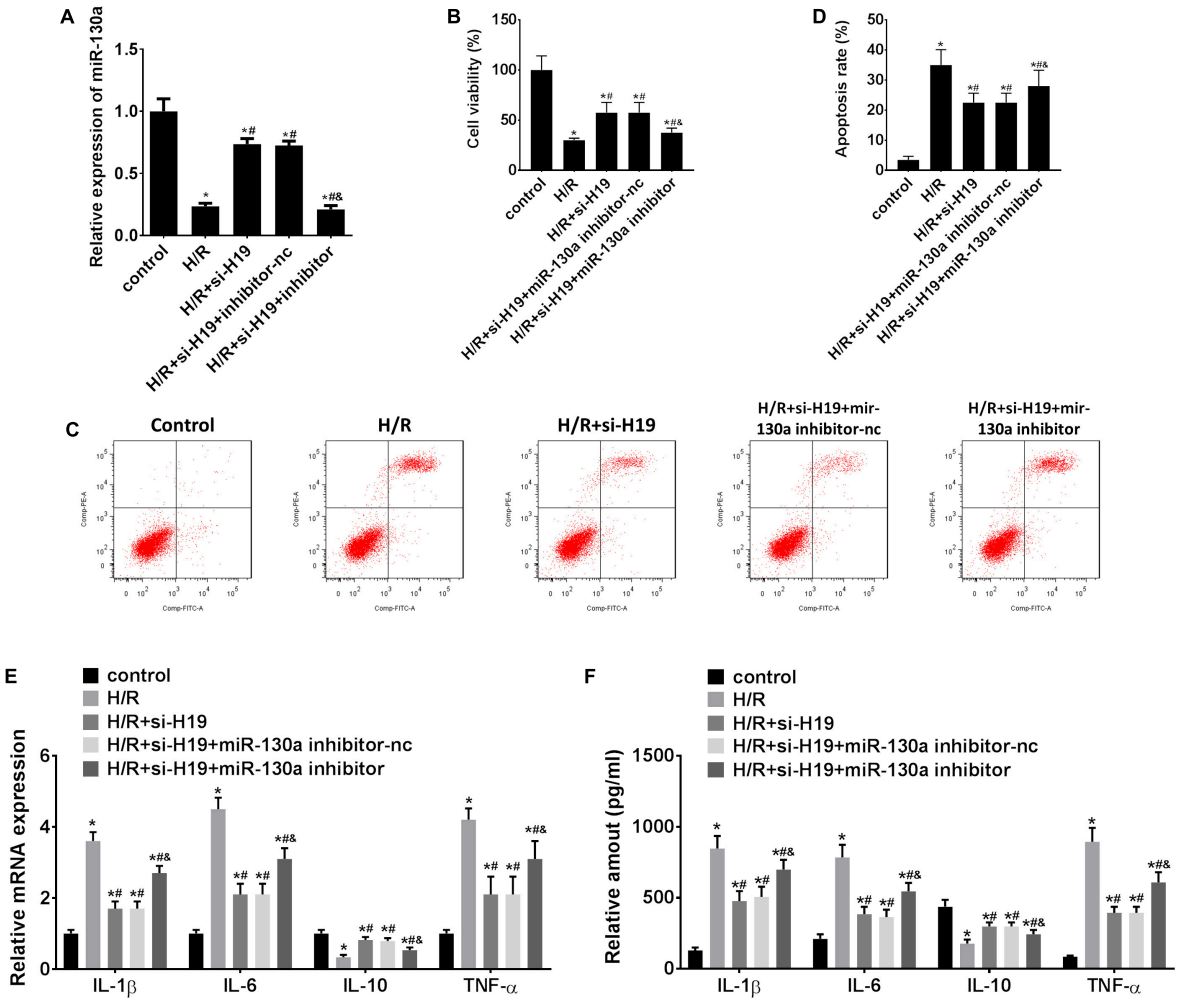

FIGURE 4 | Upregulation of miR-130a partially counteracts LncRNA H19-induced cell proliferation, apoptosis, and inflammatory cytokine expression in HK-2 cells after H/R treatment. **(A)** The relative expressions of miR-130a after transfection with Ad-siH19 and miR-130a mimics. **(B)** HK-2 cell viability analysis after H/R treatment. **(C,D)** HK-2 cell apoptosis analysis after H/R treatment. **(E,F)** mRNA/protein expression levels of inflammatory cytokines in HK-2 cells after H/R treatment. H/R, hypoxia/reoxygenation treatment; Control, untreated cells; IL-1β, interleukin-1β; IL-6, interleukin-6; IL-10, interleukin-10; TNF-α, tumor necrosis factor α. All experiments were performed in biological triplicates ($n = 6$), and data were representative of three independent experiments. The results were expressed as mean ± standard deviation (SD). Statistical comparisons between two groups were evaluated with Student's *t*-test. $^{*}P < 0.05$, compared with the control groups; $^{\#}P < 0.05$, compared with the H/R groups; $^{\&}P < 0.05$, compared with the H/R+si-H19 groups.

found within miR-130a miRNA. The dual-luciferase reporter analysis results also demonstrated that co-transfection of HEK-293 cells with wild-type BCL2L11 3'-UTR and miR-130a mimics resulted in significantly inhibited luciferase activity, as compared to the miR-nc group ($^{*}P < 0.05$; **Figure 5B**). Meanwhile, both mRNA/protein expression levels of BCL2L11 were significantly reduced in the miR-130a mimic group compared with the miR-nc group ($^{*}P < 0.05$; **Figures 5D,E**). However, the inhibitory effect was remarkably reversed by transfection with the miR-130a inhibitor ($\#P < 0.05$; **Figures 5D,E**). The RNA pull-down assay further verified that BCL2L11 could be pulled down and enriched by the biotinylated miR-130a, which confirmed the interaction between miR-130a and BCL2L11 ($^{*}P < 0.05$; **Figure 5C**). The correlation results in **Figure 5F** showed an inverse relationship between BCL2L11 expression and miR-130a ($r^2 = 0.3335$; $P = 0.0242$). Altogether, these results identified BCL2L11 as a direct target of miR-130a.

Upregulation of BCL2L11 Partially Reverse the Inhibition Effect on Cell Apoptosis Induced by Downregulation of LncRNA H19 After H/R Treatment

The protein expression changes of BCL2L11, Bax, Cyto-c, Bcl-2, and Caspase-3 were detected by western blot analysis. As indicated in **Figure 6A**, the protein expressions of BCL2L11, Bax, Cyto-c, and Caspase-3 significantly increased while Bcl-2 decreased after H/R treatment, compared with those detected from the untreated group. After transfection of Ad-siH19,

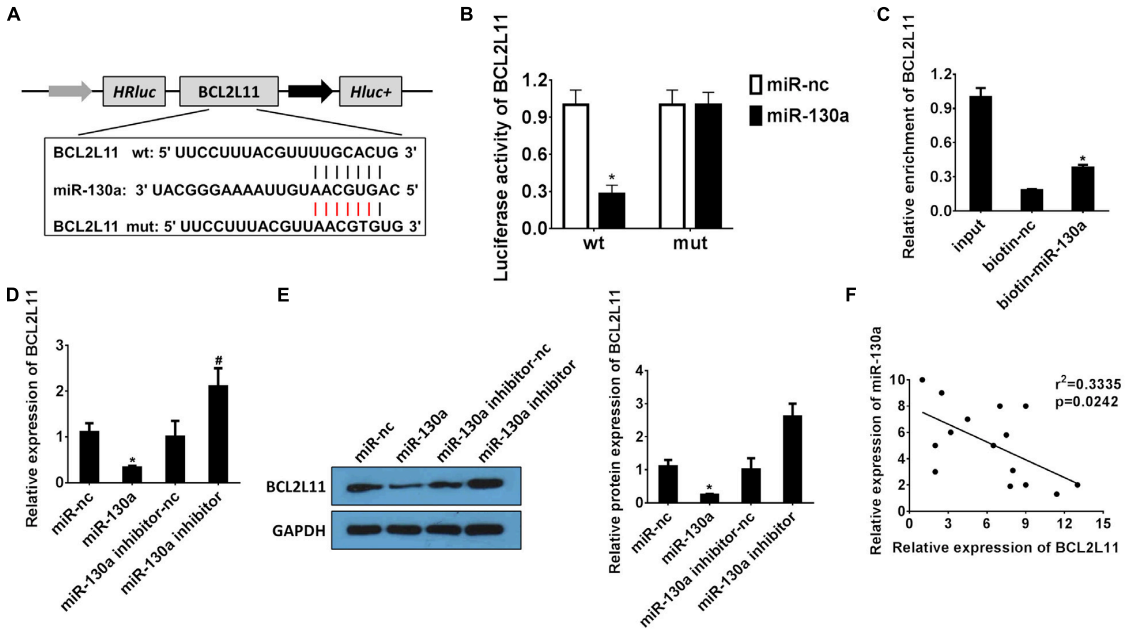

FIGURE 5 | miR-130a targets the BCL2L11 gene in HEK-293 cells. **(A)** Putative binding sites of BCL2L11 within miR-130a mRNA, and the sequences of wild-type and mutant-type vectors. **(B)** The relative luciferase activities of luciferase reporters containing WT or mutant BCL2L11 were assayed 48 h after co-transfection with miR-30a mimics or miR-nc. **(C)** The expression level of BCL2L11 mRNA was measured by RT-qPCR in the sample pulled down by biotinylated miR-130a. **(D,E)** The relative mRNA/protein expressions of BCL2L11 after transfection with miR-130a mimics or inhibitor. **(F)** The correlation analysis between miR-130a and BCL2L11. All experiments were performed in biological triplicates (n = 6), and data were representative of three independent experiments. The results were expressed as mean ± standard deviation (SD). Statistical comparisons between two groups were evaluated with Student's t-test. $^{*}P < 0.05$, compared with the control groups; $^{\#}P < 0.05$, compared with the other control groups.

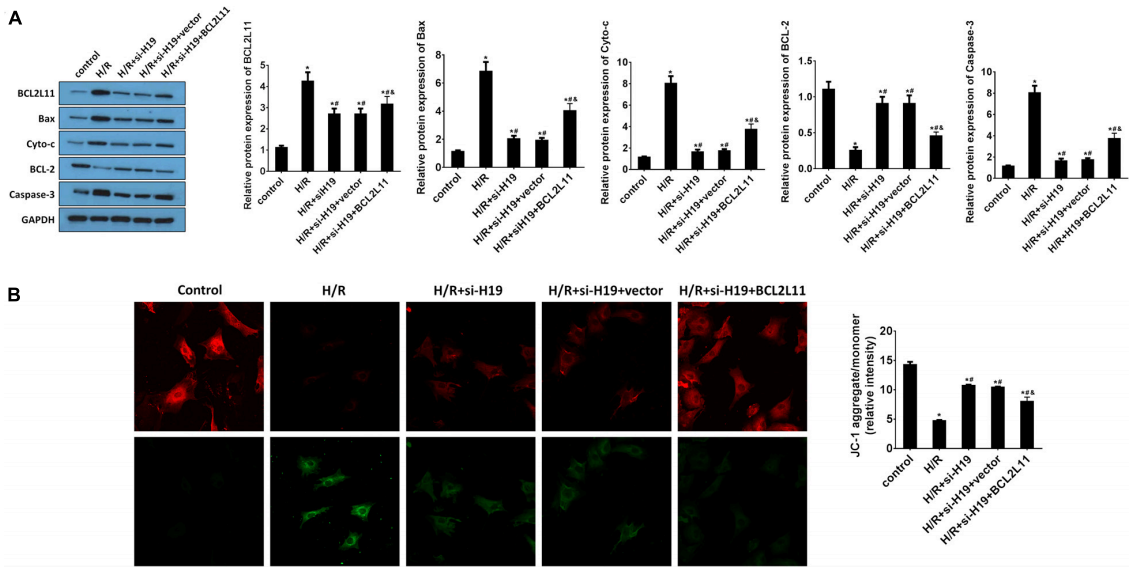

FIGURE 6 | Upregulation of BCL2L11 partially reverses the inhibition effect on cell apoptosis induced by downregulation of LncRNA H19 after H/R treatment. **(A)** The protein expression analysis of BCL2L11, Bax, Cyto-c, Bcl-2, and Caspase-3 by western blot assay. HK-2 cells were co-transfected with Ad-siH19 and pcDNA3.1-BCL2L11 after H/R treatment. **(B)** Mitochondrial membrane potential analyzed by JC-1 fluorescent probe in HK-2 cells after H/R treatment. H/R, hypoxia/reoxygenation treatment; Control, untreated cells; Ad-siH19 (siH19), Ad-siRNA-H19; vector, pcDNA3.1 vector; BCL2L11, Bcl-2 like protein 11; GAPDH, glyceraldehyde-3-phosphate dehydrogenase. All experiments were performed in biological triplicates (n = 6), and data were representative of three independent experiments. The results were expressed as mean ± standard deviation (SD). Statistical comparisons between two groups were evaluated with Student's t-test. $^{*}P < 0.05$, compared with the control groups; $^{\#}P < 0.05$, compared with the H/R groups; $^{\&}P < 0.05$, compared with the H/R+si-H19 groups.

BCL2L11, Bax, Cyto-c, and Caspase-3 were reduced while Bcl-2 was increased. However, the variations induced by Ad-siH19 could be counteracted through co-transfection with the BCL2L11 vector ($^*P < 0.05$; $\#P < 0.05$; $\&P < 0.05$). Subsequently, the mitochondrial membrane potential analysis was carried out. The mitochondria-mediated apoptosis was restrained by co-transfection with Ad-siH19 and BCL2L11, as evidenced by enhanced mitochondrial membrane potential ($^*P < 0.05$; $\#P < 0.05$; $\&P < 0.05$; **Figure 6B**).

DISCUSSION

Acute kidney injury is a frequent complication accompanied by high mortality, long-term hospitalization, and decreased kidney filtration function ability (Zafrani et al., 2016). The pathogenesis of sepsis-induced AKI includes inflammation, oxidative stress, and tubular epithelial response (Zhao et al., 2016). LncRNAs are previously reported to be regulators involved in multiple cellular and disease progresses, including cell differentiation, cell proliferation, and apoptosis (Jiang et al., 2015; Wang et al., 2017; Villa et al., 2019). However, there were still few studies on lncRNA in AKI. In the present study, we systematically investigated the expressions and functions of LncRNA H19 and miR-130a *in vitro* via a hypoxia-induced human renal proximal tubular cell (HK-2) model. The results showed that downregulation of LncRNA H19 could promote cell proliferation, inhibit cell apoptosis, and suppress multiple inflammatory cytokine expressions in HK-2 cells by modulating the miR-130a/BCL2L11 pathway.

Recently, accumulating reports suggested that certain LncRNAs and miRNAs were associated with pathogenesis and development of AKI (Brandenburger et al., 2018; Brandenburger and Lorenzen, 2020; Yan et al., 2020). Our results showed that lncRNA H19 was significantly increased while miR-130a was decreased in HK-2 cells under H/R treatment. Moreover, downregulation of LncRNA H19 could promote hypoxia-induced HK-2 cell proliferation but inhibit apoptosis; however, the variation could be reversed by co-transfection with the miR-130a inhibitor. Some studies showed that LncRNA H19 could participate in the regulation of various biological processes such as cell proliferation, apoptosis, and metabolism (Zhang et al., 2018, 2019; Wang et al., 2019; Zhou et al., 2020); others also indicated that lncRNA H19 regulated tumor carcinogenesis, angiogenesis, and metastasis (Lorenzen and Thum, 2016; Xie et al., 2016; Cao et al., 2019). For example, Cao proved the functions of LncRNA H19 in inflammation and endothelial cell injury (Cao et al., 2019). Interestingly, dysregulation of LncRNA H19 was also found in the embryonic renals of mice with maternal hyperglycemia which may lead to kidney diseases (Lorenzen and Thum, 2016). Moreover, Xie showed that lncRNA-H19 expression was significantly upregulated in TGF-β2-induced HK-2 cell fibrosis and UUO-induced renal fibrosis *in vivo*, indicating that H19 upregulation contributes to renal fibrosis (Xie et al., 2016). However, the underlying molecular mechanism of LncRNA H19 in AKI is still unclear. In the present study, LncRNA H19 was observed to be upregulated in hypoxia-induced HK-2 cellular model and knockdown LncRNA H19 promotes cell proliferation, inhibits apoptosis, and modulates inflammatory cytokine expressions in HK-2 cells under H/R treatment (**Figures 1**, **2**), indicating that LncRNA H19 plays regulatory roles in AKI progression.

Emerging evidence showed that LncRNAs function as miRNA sponges to modulate the depression of miRNA targets (Thomson and Dinger, 2016). Recently, miR-130a, a well-documented miRNA, has been reported to regulate cell proliferation, apoptosis, and inflammation and is related to renal diseases (Muralidharan et al., 2017; Li et al., 2020). However, the relationship between LncRNA H19 and miR-130a in AKI development and progress has not been reported yet. In our present study, based on the results of bioinformatics analysis (**Figures 3A**, **5A**), dual-luciferase reporter assay (**Figures 3B**, **5B**), RNA pull-down assay (**Figures 3D**, **5C**), and Pearson correlation analysis (**Figures 3E**, **5F**), we demonstrated that miR-130a was a direct target of LncRNA H19 and negatively regulates its downstream target protein BCL2L11, which has been well documented as a pro-apoptosis protein (Luo and Rubinsztein, 2013; Dai and Grant, 2015; Zhang et al., 2016).

Inflammation is related to the pathogenesis or development of AKI (Sato and Yanagita, 2018). AKI was also considered to be associated with intra-renal and systematic inflammation (Rabb et al., 2016). Clinical data suggested that AKI often results in an abnormal repair process as a result of hypoxia treatment and leads to aberrant inflammatory cytokine expressions and chronic renal dysfunction (Kurts et al., 2013; Anders and Schaefer, 2014). Interestingly, our results demonstrated that the *in vitro* expression levels of pro-inflammatory cytokines IL-1β, IL-6, and TNF-α were increased while anti-inflammatory cytokine IL-10 level was decreased in HK-2 cells after H/R treatment (**Figures 1D,E**, **2D,E**). Consistent with previous studies, *in vivo* expression levels of IL-1β, IL-6, and TNF-α were increased in the AKI mouse model while IL-10 was decreased (Shi et al., 2017; Sakai et al., 2019). Moreover, knockdown of LncRNA H19 increased IL-10 expression while it inhibited IL-1β, IL-6, and TNF-α expressions. The variation of cytokine expressions induced by LncRNA H19 could be partially reversed by co-transfection with the miR-130a inhibitor (**Figures 4E,F**).

Recent studies have also provided more and more evidenced proofs on the important functions of ncRNAs in renal disease or kidney cancers. For example, Shi demonstrated a high expression of lncRNA H19 in the diabetic kidney and in TGF-β2-induced fibrosis in HMVECs, and inhibition of H19 attenuated kidney fibrosis and restored the normal kidney structure (Shi et al., 2020); Zhu suggested that lncRNAHIF1A-AS2 promotes renal carcinoma cell proliferation and migration via the miR-130a-5p/ERBB2 pathway (Zhu et al., 2020); Ai verified that miR-130a-3p facilitates the TGF-β1/Smad pathway in renal tubular epithelial cells and may participate in renal fibrosis by targeting SnoN, which could be a possible strategy for renal fibrosis treatment (Ai et al., 2020). However, the precise mechanism by which LncRNA H19 and miR-130a regulate the AKI process remains unknown, and *in vivo* studies and clinical data revealing the role of LncRNA H19 and miR-130a in AKI pathogenesis are

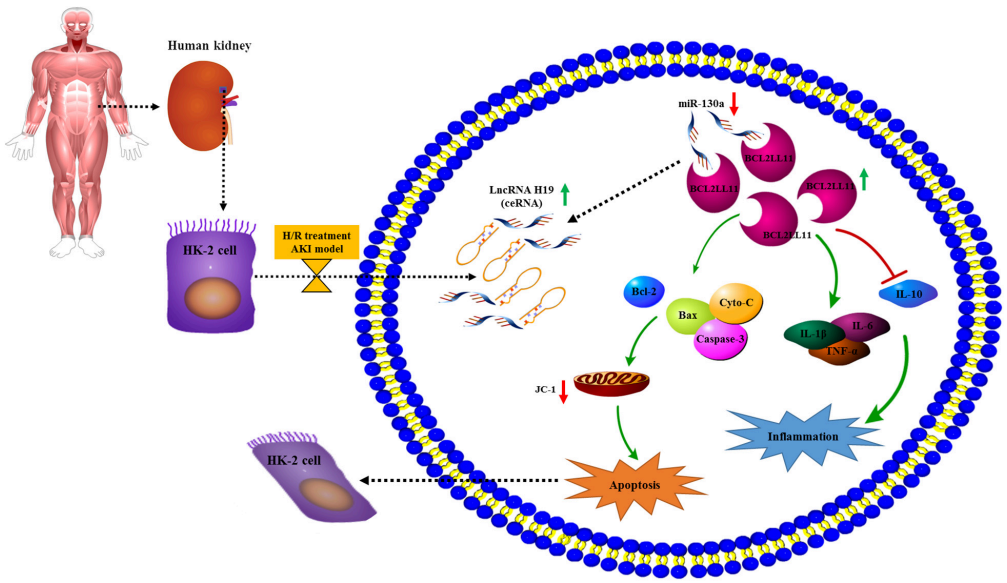

FIGURE 7 | Potential mechanism elucidating the relationship and interplay of the LncRNA H19/miR-130a/BCL2L11 regulation axis in the human renal proximal tubular cell (HK-2) cellular process under H/R conditions. The expressions of LncRNA H19 were increased in HK-2 cells after H/R treatment. Further, the LncRNA H19 might function as miRNA sponges to modulate the depression of miR-130a targets, which negatively regulates its downstream target pro-apoptosis protein BCL2L11. Moreover, the upregulation of LncRNA H19 also affects multiple inflammatory cytokine expressions in HK-2 cells by modulating the miR-130a/BCL2L11 pathway.

still limited and much needed. Therefore, we intend to address these deficiencies in the future research.

CONCLUSION

In conclusion, here we for the first time explored the relationship and interplay of the LncRNA H19/miR-130a/BCL2L11 regulation axis in the human renal proximal tubular cell (HK-2) cellular process under H/R conditions. As indicated in **Figure 7**, the expressions of LncRNA H19 were gradually increased in HK-2 cells after H/R treatment. By systematically investigating the expressions and functions of LncRNA H19 and miR-130a via the hypoxia-induced HK-2 model, we speculated that LncRNAs H19 might function as miRNA sponges to modulate the depression of miR-130a targets. The results of bioinformatics analysis (**Figures 3A**, **5A**), dual-luciferase reporter assay (**Figures 3B**, **5B**), RNA pull-down assay (**Figures 3D**, **5C**), and Pearson correlation analysis (**Figures 3E**, **5F**) further demonstrated that miR-30a was a direct target of LncRNA H19 and negatively regulates its downstream target, a pro-apoptosis protein BCL2L11. The upregulation of LncRNA H19 could also regulate multiple inflammatory cytokine expressions in HK-2 cells by modulating the miR-130a/BCL2L11 pathway. All these results have demonstrated that LncRNA H19 presented pro-apoptotic and anti-proliferative effects in HK-2 cells via a miR-130a/BCL2L11-dependent mechanism during H/R treatment (**Figure 7**). Our findings indicated that LncRNA H19 and miR-130a might represent novel therapeutic targets and early diagnostic biomarkers for the treatment of AKI.

DATA AVAILABILITY STATEMENT

The raw data supporting the conclusions of this article will be made available by the authors, without undue reservation.

AUTHOR CONTRIBUTIONS

ZD and YY: conceptualization. XL and GY: formal analysis. YC and LY: methodology. YY: writing–original draft. ZD: writing–review and editing. All authors have read and agreed to the published version of the manuscript.

FUNDING

This research was funded by the Clinical Foundation of Zhejiang Province (No. ZYC-A61).

ACKNOWLEDGMENTS

We appreciate support from Ningbo Medical Center of Ningbo University.

SUPPLEMENTARY MATERIAL

The Supplementary Material for this article can be found online at: https://www.frontiersin.org/articles/10.3389/fphys.2021.632398/full#supplementary-material

REFERENCES

Agarwal, V., Bell, G. W., Nam, J. W., and Bartel, D. P. (2015). Predicting effective microRNA target sites in mammalian mRNAs. *eLife* 4:e05005.

Ai, K., Zhu, X., Kang, Y., Li, H., and Zhang, L. (2020). miR-130a-3p inhibition protects against renal fibrosis in vitro via the TGF-beta1/Smad pathway by targeting SnoN. *Exp. Mol. Pathol.* 112:104358. doi: 10.1016/j.yexmp.2019.104358

Anders, H. J., and Schaefer, L. (2014). Beyond tissue injury-damage-associated molecular patterns, toll-like receptors, and inflammasomes also drive regeneration and fibrosis. *J. Am. Soc. Nephrol.* 25, 1387–1400. doi: 10.1681/asn.2014010117

Atianand, M. K., and Fitzgerald, K. A. (2014). Long non-coding RNAs and control of gene expression in the immune system. *Trends Mol. Med.* 20, 623–631. doi: 10.1016/j.molmed.2014.09.002

Bartel, D. P. (2004). MicroRNAs: genomics, biogenesis, mechanism, and function. *Cell* 116, 281–297.

Brandenburger, T., and Lorenzen, J. M. (2020). Diagnostic and therapeutic potential of microRNAs in acute kidney injury. *Front. Pharmacol.* 11:657. doi: 10.3389/fphar.2020.00657

Brandenburger, T., Salgado Somoza, A., Devaux, Y., and Lorenzen, J. M. (2018). Noncoding RNAs in acute kidney injury. *Kidney Int.* 94, 870–881. doi: 10.1016/j.kint.2018.06.033

Cao, L., Zhang, Z., Li, Y., Zhao, P., and Chen, Y. (2019). LncRNA H19/miR-let-7 axis participates in the regulation of ox-LDL-induced endothelial cell injury via targeting periostin. *Int. Immunopharmacol.* 72, 496–503. doi: 10.1016/j.intimp.2019.04.042

Chen, L., Wei, L., Yu, Q., Shi, H., and Liu, G. (2020). Tanshinone IIA alleviates hypoxia/reoxygenation induced cardiomyocyte injury via lncRNA AK003290/miR-124-5p signaling. *BMC Mol. Cell Biol.* 21:20. doi: 10.1186/s12860-020-00264-3

Dai, Y., and Grant, S. (2015). BCL2L11/Bim as a dual-agent regulating autophagy and apoptosis in drug resistance. *Autophagy* 11, 416–418. doi: 10.1080/15548627.2014.998892

Gómez, H., and Kellum, J. A. (2016). Sepsis-induced acute kidney injury. *Curr. Opin. Crit. Care* 22, 546–553.

Ignarski, M., Islam, R., and Müller, R. U. (2019). Long non-coding RNAs in kidney disease. *Int. J. Mol. Sci.* 20:3276. doi: 10.3390/ijms20133276

Jiang, W., Liu, Y., Liu, R., Zhang, K., and Zhang, Y. (2015). The lncRNA DEANR1 facilitates human endoderm differentiation by activating FOXA2 expression. *Cell Rep.* 11, 137–148. doi: 10.1016/j.celrep.2015.03.008

Kurts, C., Panzer, U., Anders, H. J., and Rees, A. J. (2013). The immune system and kidney disease: basic concepts and clinical implications. *Nat. Rev. Immunol.* 13, 738–753. doi: 10.1038/nri3523

Li, J. H., Liu, S., Zhou, H., Qu, L. H., and Yang, J. H. (2014). starBase v2.0: decoding miRNA-ceRNA, miRNA-ncRNA and protein-RNA interaction networks from large-scale CLIP-Seq data. *Nucleic Acids Res.* 42, D92–D97.

Li, R., Luo, S., and Zhang, D. (2020). Circular RNA hsa_circ_0054537 sponges miR-130a-3p to promote the progression of renal cell carcinoma through regulating cMet pathway. *Gene* 754:144811. doi: 10.1016/j.gene.2020.144811

Lorenzen, J. M., and Thum, T. (2016). Long noncoding RNAs in kidney and cardiovascular diseases. *Nat. Rev. Nephrol.* 12, 360–373. doi: 10.1038/nrneph.2016.51

Luo, S., and Rubinsztein, D. C. (2013). BCL2L11/BIM: a novel molecular link between autophagy and apoptosis. *Autophagy* 9, 104–105. doi: 10.4161/auto.22399

Muralidharan, J., Ramezani, A., Hubal, M., Knoblach, S., Shrivastav, S., Karandish, S., et al. (2017). Extracellular microRNA signature in chronic kidney disease. *Am. J. Physiol. Renal Physiol.* 312, F982–F991.

Poirier, F., Chan, C. T., Timmons, P. M., Robertson, E. J., Evans, M. J., and Rigby, P. W. (1991). The murine H19 gene is activated during embryonic stem cell differentiation in vitro and at the time of implantation in the developing embryo. *Development* 113, 1105–1114.

Potteti, H. R., Tamatam, C. R., Marreddy, R., Reddy, N. M., Noel, S., Rabb, H., et al. (2016). Nrf2-AKT interactions regulate heme oxygenase 1 expression in kidney epithelia during hypoxia and hypoxia-reoxygenation. *Am. J. Physiol. Renal Physiol.* 311, F1025–F1034.

Rabb, H., Griffin, M. D., Mckay, D. B., Swaminathan, S., Pickkers, P., Rosner, M. H., et al. (2016). Inflammation in AKI: current understanding, key questions, and knowledge gaps. *J. Am. Soc. Nephrol.* 27, 371–379. doi: 10.1681/asn.2015030261

Sakai, K., Nozaki, Y., Murao, Y., Yano, T., Ri, J., Niki, K., et al. (2019). Protective effect and mechanism of IL-10 on renal ischemia-reperfusion injury. *Lab. Invest.* 99, 671–683. doi: 10.1038/s41374-018-0162-0

Sato, Y., and Yanagita, M. (2018). Immune cells and inflammation in AKI to CKD progression. *Am. J. Physiol. Renal Physiol.* 315, F1501–F1512.

Shi, M., Zeng, X., Guo, F., Huang, R., Feng, Y., Ma, L., et al. (2017). Anti-inflammatory pyranochalcone derivative attenuates LPS-induced acute kidney injury via inhibiting TLR4/NF-κB pathway. *Molecules* 22:1683. doi: 10.3390/molecules22101683

Shi, S., Song, L., Yu, H., Feng, S., He, J., Liu, Y., et al. (2020). Knockdown of LncRNA-H19 ameliorates kidney fibrosis in diabetic mice by suppressing miR-29a-mediated EndMT. *Front. Pharmacol.* 11:586895. doi: 10.3389/fphar.2020.586895

Stachurska, A., Zorro, M. M., Van Der Sijde, M. R., and Withoff, S. (2014). Small and long regulatory RNAs in the immune system and immune diseases. *Front. Immunol.* 5:513. doi: 10.3389/fimmu.2014.00513

Teng, H., Wang, P., Xue, Y., Liu, X., Ma, J., Cai, H., et al. (2016). Role of HCP5-miR-139-RUNX1 feedback loop in regulating malignant behavior of glioma cells. *Mol. Ther.* 24, 1806–1822. doi: 10.1038/mt.2016.103

Thomson, D. W., and Dinger, M. E. (2016). Endogenous microRNA sponges: evidence and controversy. *Nat. Rev. Genet.* 17, 272–283. doi: 10.1038/nrg.2016.20

Villa, C., Lavitrano, M., and Combi, R. (2019). Long non-coding RNAs and related molecular pathways in the pathogenesis of epilepsy. *Int. J. Mol. Sci.* 20:4898. doi: 10.3390/ijms20194898

Wang, F., Liang, R., Tandon, N., Matthews, E. R., Shrestha, S., Yang, J., et al. (2019). H19X-encoded miR-424(322)/-503 cluster: emerging roles in cell differentiation, proliferation, plasticity and metabolism. *Cell Mol. Life Sci.* 76, 903–920. doi: 10.1007/s00018-018-2971-0

Wang, J. Z., Xu, C. L., Wu, H., and Shen, S. J. (2017). LncRNA SNHG12 promotes cell growth and inhibits cell apoptosis in colorectal cancer cells. *Braz. J. Med. Biol. Res.* 50:e6079.

Xie, H., Xue, J. D., Chao, F., Jin, Y. F., and Fu, Q. (2016). Long non-coding RNA-H19 antagonism protects against renal fibrosis. *Oncotarget* 7, 51473–51481. doi: 10.18632/oncotarget.10444

Yan, Z., Zang, B., Gong, X., Ren, J., and Wang, R. (2020). MiR-214-3p exacerbates kidney damages and inflammation induced by hyperlipidemic pancreatitis complicated with acute renal injury. *Life Sci.* 241:117118. doi: 10.1016/j.lfs.2019.117118

Ye, Y., Gu, J., Liu, P., Wang, H., Jiang, L., Lei, T., et al. (2020). Long non-coding RNA SPRY4-IT1 reverses cisplatin resistance by downregulating MPZL-1 via Suppressing EMT in NSCLC. *Onco Targets Ther.* 13, 2783–2793. doi: 10.2147/ott.s232769

Yu, T. M., Palanisamy, K., Sun, K. T., Day, Y. J., Shu, K. H., Wang, I. K., et al. (2016). RANTES mediates kidney ischemia reperfusion injury through a possible role of HIF-1α and LncRNA PRINS. *Sci. Rep.* 6:18424.

Zafrani, L., Ergin, B., Kapucu, A., and Ince, C. (2016). Blood transfusion improves renal oxygenation and renal function in sepsis-induced acute kidney injury in rats. *Crit. Care* 20:406.

Zhang, H., Duan, J., Qu, Y., Deng, T., Liu, R., Zhang, L., et al. (2016). Onco-miR-24 regulates cell growth and apoptosis by targeting BCL2L11 in gastric cancer. *Protein Cell* 7, 141–151. doi: 10.1007/s13238-015-0234-5

Zhang, L., Cheng, H., Yue, Y., Li, S., Zhang, D., and He, R. (2018). H19 knockdown suppresses proliferation and induces apoptosis by regulating miR-148b/WNT/beta-catenin in ox-LDL -stimulated vascular smooth muscle cells. *J. Biomed. Sci.* 25:11.

Zhang, L., Deng, X., Shi, X., and Dong, X. (2019). Silencing H19 regulated proliferation, invasion, and autophagy in the placenta by targeting miR-18a-5p. *J. Cell Biochem.* 120, 9006–9015. doi: 10.1002/jcb.28172

Zhao, W. Y., Zhang, L., Sui, M. X., Zhu, Y. H., and Zeng, L. (2016). Protective effects of sirtuin 3 in a murine model of sepsis-induced acute kidney injury. *Sci. Rep.* 6:33201.

Zhou, J., Xu, J., Zhang, L., Liu, S., Ma, Y., Wen, X., et al. (2019). Combined single-cell profiling of lncRNAs and functional screening reveals that H19 is pivotal for embryonic hematopoietic stem cell development. *Cell Stem Cell* 24, 285–298.e5.

Zhou, Q., Liu, Z. Z., Wu, H., and Kuang, W. L. (2020). LncRNA H19 promotes cell proliferation, migration, and angiogenesis of glioma by regulating Wnt5a/beta-catenin pathway via targeting miR-342. *Cell Mol. Neurobiol.* doi: 10.1007/s10571-020-00995-z [Epub ahead of print].

Zhu, Y., Yang, Z., Chen, H., Pan, Y., Gong, L., Chen, F., et al. (2020). lncRNAHIF1A-AS2 promotes renal carcinoma cell proliferation and migration via miR-130a-5p/ERBB2 pathway. *Onco Targets Ther.* 13, 9807–9820. doi: 10.2147/ott.s260191

Conflict of Interest: The authors declare that the research was conducted in the absence of any commercial or financial relationships that could be construed as a potential conflict of interest.

frontiers in Physiology

REVIEW
published: 02 March 2021
doi: 10.3389/fphys.2021.637480

DNA Methylation Sustains "Inflamed" Memory of Peripheral Immune Cells Aggravating Kidney Inflammatory Response in Chronic Kidney Disease

Xiao-Jun Chen[1,2†], Hong Zhang[3†], Fei Yang[1,2], Yu Liu[1,2] and Guochun Chen[1,2]*

[1]*Department of Nephrology, The Second Xiangya Hospital, Central South University, Changsha, China,* [2]*Hunan Key Laboratory of Kidney Disease and Blood Purification, Changsha, China,* [3]*Department of Cardiovascular Surgery, The Second Xiangya Hospital of Central South University, Changsha, China*

The incidence of chronic kidney disease (CKD) has rapidly increased in the past decades. A progressive loss of kidney function characterizes a part of CKD even with intensive supportive treatment. Irrespective of its etiology, CKD progression is generally accompanied with the development of chronic kidney inflammation that is pathologically featured by the low-grade but chronic activation of recruited immune cells. Cumulative evidence support that aberrant DNA methylation pattern of diverse peripheral immune cells, including T cells and monocytes, is closely associated with CKD development in many chronic disease settings. The change of DNA methylation profile can sustain for a long time and affect the future genes expression in the circulating immune cells even after they migrate from the circulation into the involved kidney. It is of clinical interest to reveal the underlying mechanism of how altered DNA methylation regulates the intensity and the time length of the inflammatory response in the recruited effector cells. We and others recently demonstrated that altered DNA methylation occurs in peripheral immune cells and profoundly contributes to CKD development in systemic chronic diseases, such as diabetes and hypertension. This review will summarize the current findings about the influence of aberrant DNA methylation on circulating immune cells and how it potentially determines the outcome of CKD.

Keywords: chronic kidney disease, DNA methylation, inflammation, peripheral immune cells, epigenetic memory

OPEN ACCESS

Edited by:
Xiao-ming Meng,
Anhui Medical University, China

Reviewed by:
Yanggang Yuan,
Nanjing Medical University, China
Rui Zeng,
Huazhong University of Science and Technology, China

***Correspondence:**
Guochun Chen
chenguochun@hotmail.com;
guochunchen@csu.edu.cn

†These authors have contributed equally to this work

Specialty section:
This article was submitted to Renal and Epithelial Physiology, a section of the journal Frontiers in Physiology

Received: *03 December 2020*
Accepted: *04 February 2021*
Published: *02 March 2021*

Citation:
Chen X-J, Zhang H, Yang F, Liu Y and Chen GC (2021) DNA Methylation Sustains "Inflamed" Memory of Peripheral Immune Cells Aggravating Kidney Inflammatory Response in Chronic Kidney Disease. Front. Physiol. 12:637480. doi: 10.3389/fphys.2021.637480

INTRODUCTION

Over the past decades, the incidence of chronic kidney disease (CKD) has rapidly increased worldwide (GBD Chronic Kidney Disease Collaboration, 2020), likely due to the huge changes in human living habits and the environment. A subset of CKD is characterized by a gradual loss of kidney function over time even with intensive supportive treatment and thereby irreversibly progresses to end-stage renal disease (ESRD). Epidemiological studies have revealed that all stages of CKD are correlated with greater risks of cardiovascular morbidity, premature death rates, declined quality of life, and tremendous economic burden (Cockwell and Fisher, 2020). In 2017, the number of deaths caused by CKD reached 1.2 million, known as the 12th leading

causes of global death (DALYs GBD and Collaborators H, 2018). Undoubtedly, CKD is one of the biggest threats to global health as well as one of the top challenges to limited medical resources in most countries. Because multiple factors contribute to the disease progression, current therapeutic strategies to manage CKD mostly rely on the control of the detectable abnormalities, like proteinuria, hyperglycemia, hypertension, and so on. However, a proportion of CKD still progresses to ESRD even when these mentioned disadvantages are fully under control. For example, compelling evidence from multiple large-scale clinical trials remains insufficient to definitively conclude a relative risk reduction by intensive glycemic control for long-term diabetic kidney disease (DKD) exposures, which are generally accompanied by chronic hyperglycemia (Hemmingsen et al., 2011). A more in-depth understanding of the underlying molecular mechanisms implicated in the pathogenesis of CKD remains necessary for the development of novel therapeutic strategies.

Chronic kidney inflammation in the process of CKD is featured by the diffusive interstitial infiltration of various immunocytes, including T lymphocytes, B lymphocytes, neutrophils, and monocytes. In general, the function of leukocytes trafficking to the kidney is to eliminate pathogens, remove necrotic cells and tissue debris from the original insult, and finally facilitate kidney tissue repair. The infiltrated leukocytes produce abundant cytokines and growth factors to establish an inflammatory milieu. Meanwhile, they also secrete anti-inflammatory and pro-regenerative cytokines to promote inflammation resolution as well as tissue repair (Peiseler and Kubes, 2019). Usually, transient activation of kidney recruited immune cells is beneficial for tissue repair and functional recovery because they are helpful in removing the pathogenic factors of kidney injury. However, the accumulation of recruited leukocytes in the renal interstitial compartment promotes chronic inflammation and ultimately leads to renal fibrosis (Gieseck et al., 2018). Emerging evidence has identified altered the trafficking of pathogenic immune cells as crucial drivers of tubulointerstitial inflammation and tissue destruction in the progression of CKD (Schnaper, 2017; Tang and Yiu, 2020). Therefore, the recruited leukocytes might facilitate or undermine the kidney repair process under different conditions. An intriguing issue is which underlying mechanism determines the role of recruited immune cells in the kidney.

CKD IS AN INFLAMMATORY DISEASE

Chronic inflammation is generally characterized by persistent production of pro-inflammatory cytokines from both circulating and resident effector cells (Anderton et al., 2020). Emerging evidence has demonstrated that systemic chronic inflammation (SCI) is a major pathological event implicated in the development of most chronic diseases or pathological conditions (e.g., chronic heart disease, diabetes mellitus, and CKD; Furman et al., 2017, 2019; Bennett et al., 2018). Under SCI, the low-grade but persistent activation of effector immune cells consistently compromise the normal tissue at the cellular level by direct contact or paracrine of pro-inflammatory cytokines (Kotas and Medzhitov, 2015). Of note, a gradual loss of renal function per se can initiate SCI in disease progression, which is commonly mixed with some other inflammatory conditions, including diabetes mellitus, hypertension, and obesity. For example, DKD is the leading cause of CKD, which has also been considered as an inflammatory disease (Tuttle, 2005). In the condition of DKD, hyperglycemia-induced oxidative stress pathologically activates circulating immune cells, which infiltrate into the involved kidney and aggravate tissue inflammation by abundant production of pro-inflammatory cytokines and chemokines (Donate-Correa et al., 2020). The accumulation of macrophages in the kidney has been correlated to a decline of renal function in DKD patients (Klessens et al., 2017). Furthermore, these infiltrated cells account for the huge release of cytokines, growth factors, reactive oxygen species (ROS), and metalloproteinases, which initiate and amplify the irreversible process of renal fibrogenesis (Matoba et al., 2019). Another common cause of CKD is hypertension that is likewise featured by progressive SCI (Harrison et al., 2011; Chen et al., 2019b). In the progression of hypertension-associated kidney involvements, predominant accumulation of different immune cells, including antigen-presenting cells and T cells, can be detected at the early stage of kidney inflammatory response (Loperena et al., 2018; Norlander et al., 2018). In the pathogenesis, hypertension-associated influence initially activates dendritic cells (DCs) in the kidney largely by promoting the exuberant formation of isoketals. The activated DCs produce abundant cytokines, including interleukin (IL)-6, IL-1β, and IL-23, to recruit T cells from secondary lymphoid organs to the kidney (Kirabo et al., 2014). Meanwhile, hypertension per se can promote T cell infiltration into the kidney by increasing glomerular perfusion pressure (Evans et al., 2017). As a vicious cycle, infiltrated T cells enhance the production of angiotensin (ANG) II and further aggravate hypertension-associated kidney involvements (De Miguel et al., 2010). Collectively, regardless of its pathogenesis, SCI plays a detrimental role in the progression of CKD by promoting renal infiltration of circulating immune cell and aggravating chronic kidney inflammation. It is of clinical significance to further understand the regulatory mechanism of immune cells recruitment in the context of CKD progression.

ABERRANT DNA METHYLATION PARTICIPATES IN CKD DEVELOPMENT

DNA methylation is a common type of epigenetic modification that reversibly affects gene expression without changes in the sequence of nucleotides (Berger et al., 2009; Chen and Riggs, 2011). This process of adding a methyl group to the cytosine is catalyzed by DNA methyltransferases (DNMT), including DNMT1, DNMT3A, and DNMT3B. Generally, DNMT3A and DNMT3B are the major *de novo* DNA methyltransferases, whereas DNMT1 acts as a maintenance enzyme, restoring hemi-methylated DNA to full methylation after replication

(Jones and Liang, 2009; Jones, 2012). In the course of cell division, DNA demethylation occurs in the absence of DNMT1 activation. On the other hand, active DNA demethylation can be induced by the mammalian ten-eleven translocation (TET) family, which catalyzes the stepwise oxidation of 5-methylcytosine in DNA to 5-hydroxymethylcytosine (5hmC; Ambrosi et al., 2017). In somatic cells, functional DNA methylation mostly occurs in clusters of CpG dinucleotides (termed CpG islands), and approximately 60–70% of human gene promoters contain a CpG island (Saxonov et al., 2006; Illingworth et al., 2010). DNA methylation is generally believed to induce transcriptional downregulation, either by impairing the interaction between transcription factors and their targets or by recruiting transcriptional repressors with specific affinity for the methylated DNA. At present, known transcriptional repressors can be classified into three families: the methyl-CpG binding domain (MBD) proteins (Hendrich and Bird, 1998; Defossez and Stancheva, 2011), the UHRF proteins (Hashimoto et al., 2008), and the zinc finger proteins (Hudson and Buck-Koehntop, 2018). In brief, DNA methylation, by altering DNA accessibility to gene promoters, induces transcriptional suppression while demethylation is associated with transcriptional activation.

In recent decades, a surge in epigenome-wide association studies (EWAS) has highlighted that DNA methylation can be markedly influenced by environmental exposures, like CKD and SCI (Ligthart et al., 2016; Heintze, 2018). A Renal Insufficiency Cohort (CRIC) identifies enhanced DNA methylation in genes of IQ motif and Sec7 domain 1 (*IQSEC1*), nephronophthisis 4 (*NPHP4*), and transcription factor 3 (*TCF3*) in participants with stable renal function while compared to those with rapid loss of eGFR (Wing et al., 2014). Meanwhile, differential DNA methylation profiles between the two groups can also be detected in the genes associated with oxidative stress and inflammation. Using whole blood DNA, recent EWAS on a large CKD cohort demonstrated that abnormal DNA methylation of 19 CpG sites is significantly associated with CKD development. Importantly, five of these differential methylated sites are also associated with fibrosis in renal biopsies of CKD patients (Chu et al., 2017). The concordant DNA methylation changes can be further identified in the kidney cortex. In animal studies, targeting DNA methylation, either global or gene-specific, can effectively attenuate renal inflammation and fibrosis in progressive CKD (Tampe et al., 2014, 2015; Yin et al., 2017). For example, low-dose hydralazine induces promoter demethylation in the gene of RAS protein activator like 1 (RASAL1), and subsequently attenuates renal fibrosis in the context of AKI to CKD (Tampe et al., 2017). Although hydralazine is an anti-hypertensive medication, the optimum demethylating activity seems to be independent of its blood pressure-lowering effect. Consistently, altered DNA methylation patterns in the renal outer medulla have been shown to induce differential gene expression regulating metabolism and inflammation in the hypertension animal model (Liu et al., 2018), further supporting that DNA methylation is involved in chronic kidney inflammation and a subsequent loss of kidney function. A number of studies have also highlighted the importance of DNA methylation in the pathogenesis of polycystic kidney disease (PKD; Li, 2020). For instance, downregulation of *PKD1* in kidney tissue by hypermethylation may contribute to cyst formation and progression (Woo et al., 2014). Given its relevance to environmental influences, DNA methylation has been intensively explored in DKD. Cumulative evidence suggests that progressive loss of renal function is closely correlated to abnormal DNA methylation in DKD subjects (Swan et al., 2015; Qiu et al., 2018; Gluck et al., 2019; Gu, 2019; Kim and Park, 2019; Park et al., 2019). A recent genome-wide analysis of DNA methylation on 500 DKD subjects reveals that DNA methylation-mediated gene expression likely determines the disease phenotypes, including glycemic control, albuminuria, and kidney function decline. Importantly, further functional annotation analysis indicates that distinct DNA methylation patterns are involved in the pathogenesis of DKD-associated inflammation (Sheng et al., 2020). Collectively, DNA methylation participates in the development of CKD and chronic kidney inflammation in particular.

DNA METHYLATION IN PERIPHERAL IMMUNE CELLS

Chronic kidney inflammation occurs in the process of CKD development regardless of its pathogenesis. Pathologically, it is featured in the cumulative infiltration of diverse immune cells from the circulation into the tubulointerstitial compartment. The recruited immune cells are major participants in the progression of chronic kidney inflammation. Upon infiltration, these cells produce abundant chemokines to establish a pro-inflammatory milieu; meanwhile, they also secrete anti-inflammatory cytokines and pro-regenerative growth factors to promote inflammation resolution as well as tissue fibrosis (Gieseck et al., 2018; Tang and Yiu, 2020). It is of clinical interest to understand the underlying mechanism that regulates the intensity and the time length of the inflammatory response in these circulating immune cells. The current status of epigenetic research acknowledges that altered DNA methylation induces permissive or negative expressions of target genes, which result in pathogenic activation of effector immune cells and the consequential loss of inflammatory homeostasis (Stylianou, 2019). Compelling evidence has revealed that circulating immune cells experience dynamic epigenetic changes in their response to the challenge of either acute insult or chronic pathogenic factors (Keating et al., 2016). The epigenetic "memory" of the previous stimuli can sustain for a long time and affect the future gene expression profile even after their migration from the circulation into the involved kidney. Recent emerging findings support the fact that an aberrant DNA methylation pattern of diverse peripheral immune cells is closely associated with CKD development in multiple disease settings (summarized in **Table 1**).

Firstly, we have recently reported that chronic hyperglycemia induces over-expression of DNMT1 and subsequent aberrant DNA methylation of multiple regulator genes of the mechanistic target of rapamycin (mTOR) in peripheral blood mononuclear cells (PBMCs). These effector cells in turn activate and migrate into the involved kidney with the abundant secretion of

TABLE 1 | Summary of main changes in DNA methylation in CKD development with immune cells.

Disease	Subjects (References)	Immune cells	Mechanism	Gene(s) modified
DKD	20 Chinese patients with DKD (Chen et al., 2019a)	Peripheral blood mononuclear cell	DNMT1↑	Upstream regulators of mTOR pathway
	181 Pima Indians with diabetes (Qiu et al., 2018)	Blood leukocytes	–	CDGAP, FKBPL, and ATF6B
LN	30 patients with lupus (Zhu et al., 2016)	Peripheral blood mononuclear cell	–	MX1, GPR84, E2F2
	322 women of European descent with lupus, 80 of whom had LN (Mok et al., 2016)	Peripheral blood mononuclear cell, $CD4^+$ T cells	–	HIF3A, IFI44, PRR4
	56 patients with lupus (Coit et al., 2015a)	Naïve $CD4^+$ T cells	–	IRF7
	SJL mice (Strickland et al., 2015)	$CD4^+$T-cells	DNMT1↓	CD70, CD40L, KirL1
	51 patients with lupus (Wardowska et al., 2019)	Dendritic cells	DNMT1↓, MBD2↓	IRFs
	54 female lupus patients (32 patients of European American ancestry and 22 patients of African American ancestry; Coit et al., 2020)	Neutrophils	–	GALNT18
IgAN	30 patients with IgAN (Xia et al., 2020)	Peripheral blood mononuclear cell	DNMT3B↓	C1GALT1
	24 patients with IgAN (Sallustio et al., 2016)	$CD4^+$ T cells	–	TRIM27, DUSP3, VTRNA2-1
Hypertensive injury	SS/MCW (JrHsdMcwi) rats, SS/CRL (JrHsdMcwiCrl) rats (Dasinger et al., 2020)	T cells	–	–
CKD/CVD	27 patients with CVD/CKD (Yang et al., 2016)	Monocytes	DNMT1↓	CD40

CKD, chronic kidney disease; LN, lupus nephrites; IgAN, IgA nephropathy; DKD, diabetic kidney disease; CVD, cardiovascular disease; DNMT, DNA methyltransferase; mTOR, mammalian target of rapamycin; CDGAP, Cdc42 GTPase-activating protein; FKBPL, FK506-binding protein-like; ATF6B, activating Transcription Factor 6 Beta; MX1, myxovirus resistant 1; GPR84, G protein-coupled receptor 84; E2F2, E2F transcription factor 2; HIF3A, hypoxia-inducible factor 3α gene; IFI44, interferon induced protein 44; PRR4, proline-rich protein 4; IRF, interferon regulatory factor; KirL; GALNT18 polypeptide nacetylgalactosaminyltransferase 18; C1GALT1, core 1 synthase, glycoprotein-N-acetylgalactosamine 3-beta-galactosyltransferase 1; TRIM27, tripartite motif-containing 27; DUSP3, dual-specificity phosphatase 3; VTRNA2-1, vault RNA 2-1.

inflammatory cytokines, resulting in persistent kidney inflammatory injuries and progressive fibrosis (Chen et al., 2019a). By adoptive transfer, we confirm that circulating PBMCs with "inflammatory memory" can aggravate DKD progression in the recipient animals. Of clinical importance, we demonstrate that the inhibition of DNA methylation by targeting DNMT1 promotes the regulatory phenotype of circulating immune cells and improves the diabetic inflammatory state and the long-term outcome of DKD. Aberrant DNA methylation is also observed in PBMCs from lupus nephritis (LN) patients. Hypomethylated CpG sites can be detected in the promoter region of interferon (IFN)- and toll-like receptor (TLR)-related genes, which are highly associated with the pathogenic inflammatory condition of LN progression (Mok et al., 2016; Zhu et al., 2016). These findings highly support the fact that the differential methylation of genes regulating the inflammatory activity of PBMCs has a causal role in the pathogenesis of LN. In addition, we have observed that mRNA expression of *DNMT3B* is notably increased in PBMCs isolated from immunoglobulin A nephropathy (IgAN) patients (Xia et al., 2020).

Based on these findings, we propose that SCI occurs and progresses in the condition of CKD derived from multiple primary and secondary diseases, such as hyperglycemia, hypertension, autoimmune disorder, and chronic infection. These chronic stimuli substantially alter the DNA methylation profile of circulating immune cells, leading to enhanced activities of pro-inflammatory genes and a cell-type switch toward inflammatory effectors. The altered DNA methylation might act as "epigenetic memory" and sustain in circulating immune cells for a long time. It thereby pathologically and persistently activates the inflammatory response of immune cells, which continue to participate in chronic tissue injury after their kidney recruitments. It might partly explain why a subset of CKD is characterized by ongoing kidney inflammation and irreversibly progresses to ESRD even when treatment targets have been achieved, like glycemic recovery and blood pressure control (**Figure 1**). Of note, leukocytes are composed of a variety of circulating immune cells and DNA methylation affects genes transcription activity by a cell type-specific manner. Although emerging evidence has revealed abnormal DNA methylation in both B cells (Absher et al., 2013; Fali et al., 2014; Scharer et al., 2019; Breitbach et al., 2020; Wardowska, 2020) and neutrophils (Lande et al., 2011; Coit et al., 2015b, 2020) in the condition of SLE, there is a lack of data derived from studies with kidney involvements by far. Therefore, we next discuss the potential role of DNA methylation in CKD development with a focus on T cell and monocyte lineages.

DNA METHYLATION IN T CELL LINEAGES

Upon antigen stimulation, naïve T cells differentiate into several lineages, including T helper (Th)1, Th2, Th17, and regulatory

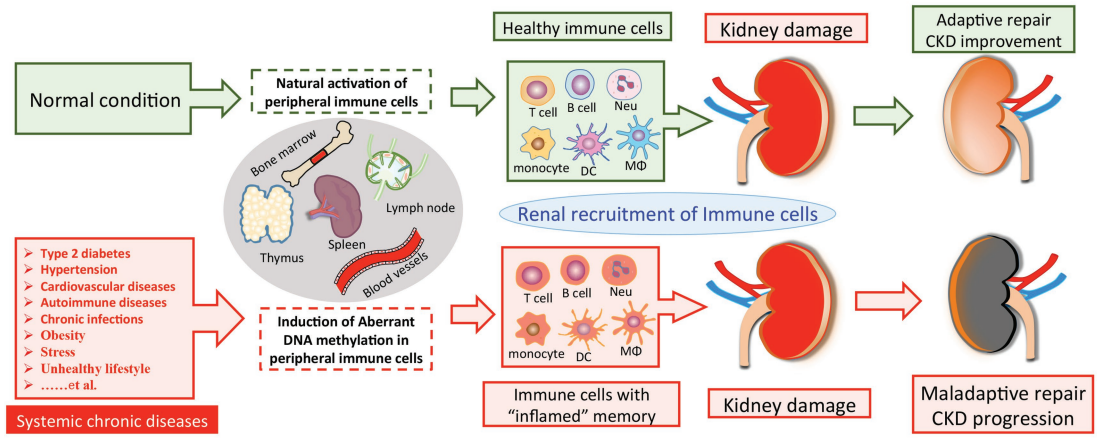

FIGURE 1 | A model of DNA methylation in peripheral immune cells in the pathogenesis of CKD development. Chronic pathogenic conditions induce aberrant DNA methylation in peripheral immune cells, leading to enhanced activities of pro-inflammatory genes and a cell-type switch toward "inflamed" effectors. Normally, renal recruitment of circulating immune cells can facilitate adaptive repair and improve the outcome of kidney damage. On the other hand, peripheral immune cells with "inflamed" DNA methylation profile may constantly migrate into the diseased kidney and overact tissue inflammation, which consequentially results in maladaptive repair and CKD progression. CKD, chronic kidney disease; Neu, neutrophil; DC, dendritic cell; Mϕ, macrophage.

T (Treg) cells. Th1 cells control intracellular bacterial infection, while Th2 cells initiate antibody response against the extracellular pathogens. During the polarization of $CD4^+$ T cells toward Th1, DNA hypomethylation occurs in Th1 cytokine genes (such as interferon gamma, IFNγ) whereas Th2 cytokine genes achieve DNA methylation, and vice versa in the polarization of Th2 cells. Evidence showed that the imbalance of Th1/Th2 cytokine profiles play a crucial role in the pathogenesis of IgAN (Suzuki and Suzuki, 2018). In the early stage of IgAN studied in ddY mice, strong polarization toward Th1 can be observed (Suzuki et al., 2007). A genome-wide screening for DNA methylation shows that the ratio of IL-2 to IL-5 is significantly elevated, indicating a Th1 shift of $CD4^+$ T cells in IgAN (Sallustio et al., 2016). In brief, this Th1/Th2 polarization is associated with three specific aberrantly methylated DNA regions in peripheral $CD4^+$T cells from IgAN patients. Low methylation levels are observed in genes involved in T cell receptor (TCR) signaling, including tripartite motif-containing 27 (*TRIM27*) and dual-specificity phosphatase 3 (*DUSP3*). Meanwhile, a hypermethylated region can be detected in the miR-886 precursor and is associated with decreased $CD4^+$ T cell proliferation following TCR stimulation. Therefore, aberrant DNA methylation causes reduced TCR signal strength and the low activation of $CD4^+$ T cells in the pathogenesis of IgAN.

Th17 cells are characterized by the signature production of cytokines such as IL-17A and IL-17F and the expression of the key transcription factor retinoic orphan receptor γt (RORγt; Cua et al., 2003). Due to their pro-inflammatory phenotype, Th17 cells are capable of protecting against infections on mucosal surfaces (Park et al., 2005) but contribute to the development of renal inflammatory diseases (Turner et al., 2010). On the other hand, Treg cells are characterized by the expression of forkhead box P3 (*Foxp3*) and the production of anti-inflammatory cytokines (e.g., IL-10 and transforming growth factor-β; Lu et al., 2017) and usually have a pivotal role in dampening chronic kidney inflammation (Chen et al., 2016; Sharma and Kinsey, 2018). Changes in epigenetic status at the *Foxp3* and *IL17* gene loci are essential for the polarization of $CD4^+$ T cells toward the Treg or Th17 cells (Yang et al., 2015; Lu et al., 2016). Peripheral $CD4^+$ T cells from SLE patients were presented with decreased expression of regulatory factor X 1 (*RFX1*), which causes DNA demethylation in the IL17A locus of $CD4^+$ T cells and thereby promotes Th17 cell differentiation (Zhao et al., 2018). On the other hand, abnormal epigenetic regulation of *Foxp3* in Treg cells has been documented in SLE patients, which suggests that hypermethylation of the $Foxp3^+$ promoter region is associated with a decreased proportion of Treg cells and increased disease activity (Zhao et al., 2012). Of clinical significance, DNA methylation levels of the *Foxp3* promoter region can be markedly suppressed by effective treatment, which consequently downregulates Foxp3 expression and promotes $CD4^+CD25^+$ Treg cells.

In addition, recent EWAS has revealed that unique DNA methylation patterns in $CD4^+$ T cells are closely related to disease activity. In SLE, the DNA methylation state in peripheral naïve $CD4^+$ T cells is significantly different between patients with and without renal involvement (Coit et al., 2015a). Increased DNA methylation in multiple IFN-regulated genes is closely associated with the onset of LN. Moreover, a lupus susceptibility gene, the type-I interferon master regulator gene (*IRF7*), is specifically demethylated as shown in patients with LN. Consistently, the modification of DNA methylation, by targeting DNMT1 expression in $CD4^+$ T cells, contributes to the development of LN-like glomerulonephritis in animals (Strickland et al., 2015).

As described above, abnormal epigenetics is implicated in the pathogenesis of hypertensive renal injury due to its influence on immune homeostasis. It is known that high salt intake is the major cause of hypertension and intriguingly associated with obesity, independent of energy intake (Ma et al., 2015).

An intriguing question is whether and how environmental influences, like unhealthy diet, might induce aberrant epigenetic changes in immune cells that subsequently participate in hypertension-associated kidney inflammatory involvement. The Dahl salt-sensitive (SS) rat is a genetic model of hypertension and renal disease that is accompanied with immune cell activation in response to a high-salt diet (Mattson et al., 2006). In SS rats, a high-salt diet induced increasing global methylation rate in circulating and kidney T cells, of which differentially methylated regions (DMRs) are more prominent in animals with a pronounced hypertensive phenotype. Importantly, the application of decitabine, a hypomethylating agent, significantly attenuates hypertension and renal inflammatory injury in SS rats (Dasinger et al., 2020). In-depth RNA-seq analysis on kidney T cells has revealed the upregulation of multiple inflammatory and oxidative genes in response to a high-salt diet, which are inversely correlated with DNA methylation levels. These genes are known to play an important role in the development of salt sensitivity in the SS rat (Zheleznova et al., 2016). Collectively, these findings thereby highlight the important role of DNA methylation in linking the influence of abnormal environment/diet to the clinical manifestations of hypertension-associated involvements, which might be at least partly mediated by pathologically activated T cells.

DNA METHYLATION IN MONOCYTE LINEAGES

Monocytes, representing the mononuclear phagocyte system, are the largest type of circulating immune cells and can differentiate into macrophages (Mϕ) and myeloid lineage dendritic cells (DCs). Multiple lines of evidence have confirmed the fundamental roles of monocyte lineage in the inflammatory progression of CKD (Heine et al., 2012; Kinsey, 2014; Bowe et al., 2017). Generally, Mϕ can be divided into two subsets, classically activated Mϕ (M1) and alternatively activated Mϕ (M2), depending on their activation paradigm and cellular functions. The classic M1 macrophages commonly produce pro-inflammatory cytokines and cytotoxic mediators contributing to acute and chronic tissue inflammation. On the other hand, M2 macrophages are mostly implicated in inflammation resolution, tissue remodeling, and fibrogenesis by secreting various anti-inflammatory cytokines, growth factors, and proangiogenic cytokines (Wang et al., 2014; Tian and Chen, 2015). In the context of DKD, Mϕ constitutes a major part of infiltrated leucocytes and their accumulation is associated with the progression of diabetic status and renal pathological changes (Chow et al., 2004; Tesch, 2010). Importantly, M1/M2 ratio is positively associated with the progression of chronic inflammation into pathogenic fibrosis during CKD development (Tang et al., 2019; Zhang et al., 2019). Recent studies have revealed an essential role of epigenetic regulation in the phenotype switch of M1 and M2. For example, DNMT3B plays an important role in regulating macrophage polarization and is expressed relatively less in M2 compared to M1 (Yang et al., 2014). Deletion/inhibition of DNMT1, either pharmacologically or genetically, contributes to M2 alternative activation in obesity (Wang et al., 2016), which is known as a typical type of SCI. Under the pathological conditions of hyperlipidemia and type 2 diabetes mellitus, DNA methylation alterations steer the Mϕ phenotype toward pro-inflammatory M1 as opposed to the tissue repairing M2 phenotype by differentially methylating gene promoters of M1 and M2 (Babu et al., 2015).

Besides differentiation into Mϕ, monocytes can be classified into various subsets with diverse inflammatory phenotypes based on their cell surface markers expression (Zawada et al., 2012), which similarly can be interfered with in the stage of CKD. Accumulation of uremic toxins during CKD progression induces aberrant DNA methylation that affects some transcription regulators that are important for monocyte differentiation (Zawada et al., 2016). Similar to other chronic diseases, CKD can promote a pro-inflammatory phenotype of monocytes *via* the DNA hypomethylation of CD40, which activates and contributes to inflammatory involvements and disease progression (Yang et al., 2016). DCs can be generally divided into two groups, myeloid dendritic cells (mDCs) and plasmacytoid dendritic cells (pDCs; Kitching and Ooi, 2018). Although the majority of DCs within the kidney are cDCs, active pDCs can migrate and contribute to tissue inflammation in nephritic kidneys (Fiore et al., 2008; Tucci et al., 2008). Myeloid DCs (mDCs, $BDCA1^+$ or $BDCA3^+$ DCs) are also shown to increase in the renal tubulointerstitium of patients with LN (Fiore et al., 2008). DNA methylome of peripheral DCs reveals that global DNA hypermethylation in LN patients is associated with severe kidney involvement (Wardowska et al., 2019). Taken together, current evidence supports the fact that aberrant DNA methylation induces an inflammatory switch of monocyte lineage, which contributes to the development of chronic kidney inflammation in multiple chronic disease settings, like obesity, hypertension, diabetes, lupus, and CKD.

SUMMARY AND PERSPECTIVES

In summary, a variety of pathological conditions induce an aberrant DNA methylation profile in circulating immune cells with a cell-type specific manner, leading to a phenotype switch toward the inflammatory side (**Figure 2**). These "inflamed" immune cells sustain enhanced inflammatory activity upon the recruitment into diseased kidneys and consequentially participate in chronic kidney inflammation and CKD progression. DNA methylation-targeted treatment by either inhibiting methylation (e.g., 5-azacytidine) or activating demethylation (e.g., hydralazine) have been explored to ameliorate kidney injury in several preclinical studies (**Table 2**), though some of the interventions have nephrotoxic potential in the clinical setting. A series of novel therapeutic methods, such as modified oligonucleotide inhibitors and small RNA molecules targeting DNMTs, have yet to be tested in the setting of kidney disease (Xu et al., 2016). Meanwhile, there is a lack of intervention strategies specifically targeting immune cells. Given its complex roles in cell biology, clinicians should

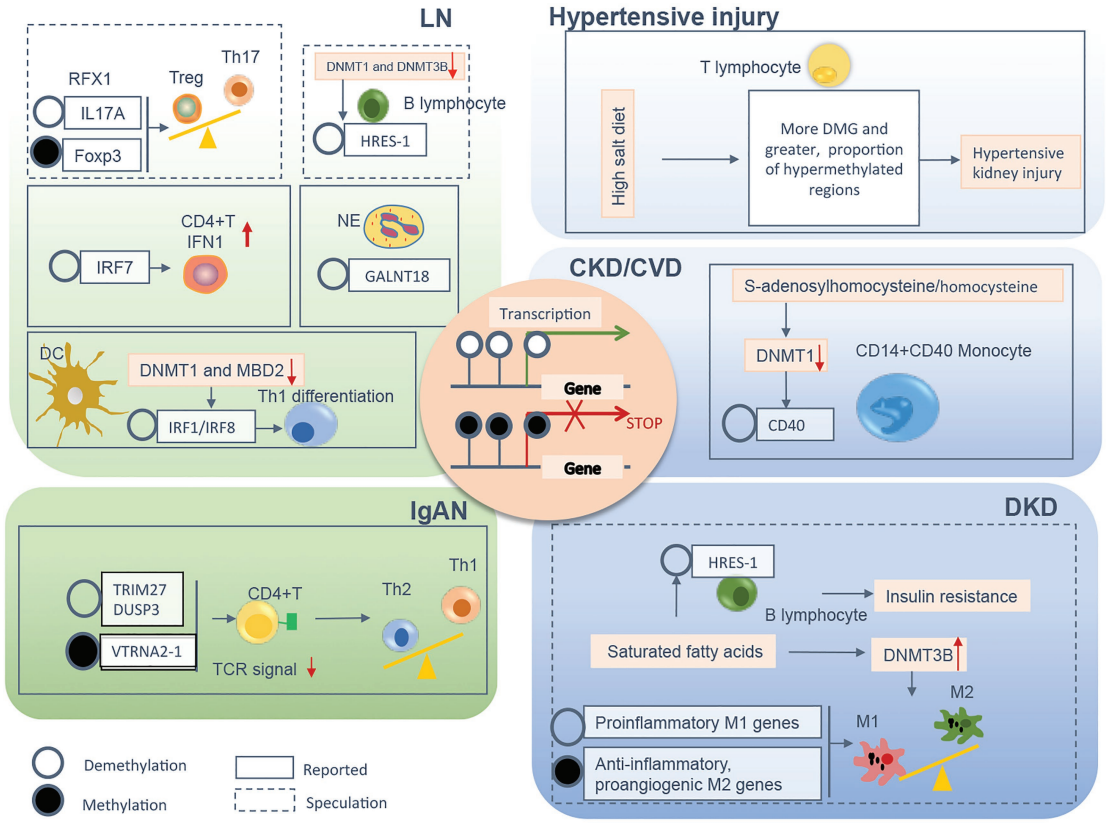

FIGURE 2 | The relevant DNA methylation profiles in immune cells from CKD patients are summarized by different chronic pathogenic conditions, including LN, IgAN, hypertensive kidney injury, DKD, and uremia. Demethylation or methylation of certain genes regulates immune cell phenotype shift/differentiation, or pro/anti-inflammation signal, therefore contributes to uncontrolled kidney inflammation and CKD progression. The mechanism boxed off with solid lines is documented in CKD with different etiology, whereas the one with dashed lines is speculated to relate to the development of kidney diseases founded on circumstantial evidence. CKD, chronic kidney disease; LN, lupus nephrites; IgAN, IgA nephropathy; DKD, diabetic kidney disease; CVD, cardiovascular disease; Treg, regulatory T; Th, T helper; NE, neutrophil; DC, dendritic cell; TCR, T cell receptor; M1, classically activated macrophage; M2, alternatively activated macrophage; IFN, interferon; Foxp3, forkhead box P3; DNMT, DNA methyltransferase; MBD, methyl-CpG binding domain; RFX, regulatory factor X; HRES-1, human T cell lymphotropic virus-related endogenous sequence-1; IRF, interferon regulatory factor; GALNT18, polypeptide nacetylgalactosaminyltransferase 18; TRIM27, tripartite motif-containing 27; DUSP3, dual-specificity phosphatase 3; VTRNA2-1, vault RNA 2-1.

TABLE 2 | Summary of existing potential treatment of CKD targeting on DNA methylation.

Drugs	Target	Model	Effect	References
5-azacytidine	DNMT inhibitor	Mouse folic-acid-induced AKI Mouse db/db DKD	Fibrosis↓ Renal function↑, proteinuria↓, Renal injury↓	Bechtel et al., 2010 Zhang et al., 2017
Hydralazin	Demethylating activity: induction of TET3	Mouse UUO	Fibrosis↓	Tampe et al., 2015
		Mouse IRI, Mouse hRASAL1-pTreTight transgenic	*RASAL1* promoter demethylation↑, Fibrosis↓, Renal function↑	Tampe et al., 2017
BMP7	Normalization of aberrant Rasal1 methylation, which is dependent on Tet3-mediated hydroxymethylation	Mouse streptozotocin -induced DKD, mouse UUO, *COL4A3*-deficient Alport mice, mouse 5/6 nephrectomy-induced CKD	Fibrosis↓	Tampe et al., 2014
Decitabine	DNMT inhibitor	Mouse UUO	Fibrosis↓	Bechtel et al., 2010
5'-deoxy-5'-methylthioadenosine	Indirect inhibitor of methyltransferases	Mouse MRL/lpr lupus	IgG deposition and cellular infiltration in the kidney↓	Yang et al., 2013

DNMT, DNA methyltransferase; AKI, acute kidney injury; DKD, diabetic kidney disease; TET, ten-eleven translocation; UUO, unilateral ureteral obstruction; IRI, ischemia-reperfusion injury; RASAL1, RAS protein activator like 1; BMP7, bone morphogenetic protein 7.

comprehensively assess the therapeutic value, as well as the potential risk of targeting DNA methylation in immune cells. An in-depth understanding of DNMTs functions in different scenarios might help to develop effective strategies to restore immune homeostasis with consideration of the timing, the signaling intensity, and the disease settings. In future mechanistic research, it remains necessary to clarify the causal relationship between DNA methylation and CKD development, since it is technically hard to separate "driver" events from "passenger" events in the setting of SCI. A combined application of current cutting-edge technologies, like single-cell epigenomic methods of ATAC-seq (Mezger et al., 2018) and single-cell RNA-seq (Kolodziejczyk et al., 2015), may be able to provide a solution to this problem.

AUTHOR CONTRIBUTIONS

GC conceived the review. X-JC and HZ collected literature data, interpreted literature, and wrote the manuscript. FY and YL created and revised the figures and tables. GC oversaw the work and revised the manuscript. All authors contributed to the article and approved the submitted version.

FUNDING

This work was supported by grants from the National Natural Science Foundation of China to Dr. Guochun Chen (81770691, 81300566).

REFERENCES

Absher, D. M., Li, X., Waite, L. L., Gibson, A., Roberts, K., Edberg, J., et al. (2013). Genome-wide DNA methylation analysis of systemic lupus erythematosus reveals persistent hypomethylation of interferon genes and compositional changes to $CD4^+$ T-cell populations. *PLoS Genet.* 9:e1003678. doi: 10.1371/journal.pgen.1003678

Ambrosi, C., Manzo, M., and Baubec, T. (2017). Dynamics and context-dependent roles of DNA methylation. *J. Mol. Biol.* 429, 1459–1475. doi: 10.1016/j.jmb.2017.02.008

Anderton, H., Wicks, I. P., and Silke, J. (2020). Cell death in chronic inflammation: breaking the cycle to treat rheumatic disease. *Nat. Rev. Rheumatol.* 16, 496–513. doi: 10.1038/s41584-020-0455-8

Babu, M., Durga Devi, T., Makinen, P., Kaikkonen, M., Lesch, H. P., Junttila, S., et al. (2015). Differential promoter methylation of macrophage genes is associated with impaired vascular growth in ischemic muscles of hyperlipidemic and Type 2 diabetic mice: genome-wide promoter methylation study. *Circ. Res.* 117, 289–299. doi: 10.1161/CIRCRESAHA.115.306424

Bechtel, W., McGoohan, S., Zeisberg, E. M., Muller, G. A., Kalbacher, H., Salant, D. J., et al. (2010). Methylation determines fibroblast activation and fibrogenesis in the kidney. *Nat. Med.* 16, 544–550. doi: 10.1038/nm.2135

Bennett, J. M., Reeves, G., Billman, G. E., and Sturmberg, J. P. (2018). Inflammation-nature's way to efficiently respond to all types of challenges: implications for understanding and managing "the epidemic" of chronic diseases. *Front. Med.* 5:316. doi: 10.3389/fmed.2018.00316

Berger, S. L., Kouzarides, T., Shiekhattar, R., and Shilatifard, A. (2009). An operational definition of epigenetics. *Genes Dev.* 23, 781–783. doi: 10.1101/gad.1787609

Bowe, B., Xie, Y., Xian, H., Li, T., and Al-Aly, Z. (2017). Association between monocyte count and risk of incident CKD and progression to ESRD. *Clin. J. Am. Soc. Nephrol.* 12, 603–613. doi: 10.2215/CJN.09710916

Breitbach, M. E., Ramaker, R. C., Roberts, K., Kimberly, R. P., and Absher, D. (2020). Population-specific patterns of epigenetic defects in the B cell lineage in patients with systemic lupus erythematosus. *Arthritis Rheum.* 72, 282–291. doi: 10.1002/art.41083

Chen, J., Bundy, J. D., Hamm, L. L., Hsu, C. Y., Lash, J., Miller, E. R. 3rd, et al. (2019b). Inflammation and apparent treatment-resistant hypertension in patients with chronic kidney disease. *Hypertension* 73, 785–793. doi: 10.1161/HYPERTENSIONAHA.118.12358

Chen, G., Chen, H., Ren, S., Xia, M., Zhu, J., Liu, Y., et al. (2019a). Aberrant DNA methylation of mTOR pathway genes promotes inflammatory activation of immune cells in diabetic kidney disease. *Kidney Int.* 96, 409–420. doi: 10.1016/j.kint.2019.02.020

Chen, G., Dong, Z., Liu, H., Liu, Y., Duan, S., Liu, Y., et al. (2016). mTOR signaling regulates protective activity of transferred $CD4^+Foxp3^+$ T cells in repair of acute kidney injury. *J. Immunol.* 197, 3917–3926. doi: 10.4049/jimmunol.1601251

Chen, Z. X., and Riggs, A. D. (2011). DNA methylation and demethylation in mammals. *J. Biol. Chem.* 286, 18347–18353. doi: 10.1074/jbc.R110.205286

Chow, F., Ozols, E., Nikolic-Paterson, D. J., Atkins, R. C., and Tesch, G. H. (2004). Macrophages in mouse type 2 diabetic nephropathy: correlation with diabetic state and progressive renal injury. *Kidney Int.* 65, 116–128. doi: 10.1111/j.1523-1755.2004.00367.x

Chu, A. Y., Tin, A., Schlosser, P., Ko, Y. A., Qiu, C., Yao, C., et al. (2017). Epigenome-wide association studies identify DNA methylation associated with kidney function. *Nat. Commun.* 8:1286. doi: 10.1038/s41467-017-01297-7

Cockwell, P., and Fisher, L. A. (2020). The global burden of chronic kidney disease. *Lancet* 395, 662–664. doi: 10.1016/S0140-6736(19)32977-0

Coit, P., Ortiz-Fernandez, L., Lewis, E. E., McCune, W. J., Maksimowicz-McKinnon, K., and Sawalha, A. H. (2020). A longitudinal and transancestral analysis of DNA methylation patterns and disease activity in lupus patients. *JCI Insight* 5:e143654. doi: 10.1172/jci.insight.143654

Coit, P., Renauer, P., Jeffries, M. A., Merrill, J. T., McCune, W. J., Maksimowicz-McKinnon, K., et al. (2015a). Renal involvement in lupus is characterized by unique DNA methylation changes in naive $CD4^+$ T cells. *J. Autoimmun.* 61, 29–35. doi: 10.1016/j.jaut.2015.05.003

Coit, P., Yalavarthi, S., Ognenovski, M., Zhao, W., Hasni, S., Wren, J. D., et al. (2015b). Epigenome profiling reveals significant DNA demethylation of interferon signature genes in lupus neutrophils. *J. Autoimmun.* 58, 59–66. doi: 10.1016/j.jaut.2015.01.004

Cua, D. J., Sherlock, J., Chen, Y., Murphy, C. A., Joyce, B., Seymour, B., et al. (2003). Interleukin-23 rather than interleukin-12 is the critical cytokine for autoimmune inflammation of the brain. *Nature* 421, 744–748. doi: 10.1038/nature01355

DALYs GBD and Collaborators H (2018). Global, regional, and national disability-adjusted life-years (DALYs) for 359 diseases and injuries and healthy life expectancy (HALE) for 195 countries and territories, 1990–2017: a systematic analysis for the Global Burden of Disease Study 2017. *Lancet* 392, 1859–1922. doi: 10.1016/S0140-6736(18)32335-3

Dasinger, J. H., Alsheikh, A. J., Abais-Battad, J. M., Pan, X., Fehrenbach, D. J., Lund, H., et al. (2020). Epigenetic modifications in T cells: the role of DNA methylation in salt-sensitive hypertension. *Hypertension* 75, 372–382. doi: 10.1161/HYPERTENSIONAHA.119.13716

De Miguel, C., Das, S., Lund, H., and Mattson, D. L. (2010). T lymphocytes mediate hypertension and kidney damage in Dahl salt-sensitive rats. *Am. J. Phys. Regul. Integr. Comp. Phys.* 298, R1136–R1142. doi: 10.1152/ajpregu.00298.2009

Defossez, P. A., and Stancheva, I. (2011). Biological functions of methyl-CpG-binding proteins. *Prog. Mol. Biol. Transl. Sci.* 101, 377–398. doi: 10.1016/B978-0-12-387685-0.00012-3

Donate-Correa, J., Luis-Rodriguez, D., Martin-Nunez, E., Tagua, V. G., Hernandez-Carballo, C., Ferri, C., et al. (2020). Inflammatory targets in diabetic nephropathy. *J. Clin. Med.* 9:458. doi: 10.3390/jcm9020458

Evans, L. C., Petrova, G., Kurth, T., Yang, C., Bukowy, J. D., Mattson, D. L., et al. (2017). Increased perfusion pressure drives renal T-cell infiltration in the Dahl salt-sensitive rat. *Hypertension* 70, 543–551. doi: 10.1161/HYPERTENSIONAHA.117.09208

Fali, T., Le Dantec, C., Thabet, Y., Jousse, S., Hanrotel, C., Youinou, P., et al. (2014). DNA methylation modulates HRES1/p28 expression in B cells from patients with lupus. *Autoimmunity* 47, 265–271. doi: 10.3109/08916934.2013.826207

Fiore, N., Castellano, G., Blasi, A., Capobianco, C., Loverre, A., Montinaro, V., et al. (2008). Immature myeloid and plasmacytoid dendritic cells infiltrate renal tubulointerstitium in patients with lupus nephritis. *Mol. Immunol.* 45, 259–265. doi: 10.1016/j.molimm.2007.04.029

Furman, D., Campisi, J., Verdin, E., Carrera-Bastos, P., Targ, S., Franceschi, C., et al. (2019). Chronic inflammation in the etiology of disease across the life span. *Nat. Med.* 25, 1822–1832. doi: 10.1038/s41591-019-0675-0

Furman, D., Chang, J., Lartigue, L., Bolen, C. R., Haddad, F., Gaudilliere, B., et al. (2017). Expression of specific inflammasome gene modules stratifies older individuals into two extreme clinical and immunological states. *Nat. Med.* 23, 174–184. doi: 10.1038/nm.4267

GBD Chronic Kidney Disease Collaboration (2020). Global, regional, and national burden of chronic kidney disease, 1990–2017: a systematic analysis for the Global Burden of Disease Study 2017. *Lancet* 395, 709–733. doi: 10.1016/S0140-6736(20)30045-3

Gieseck, R. L. 3rd., Wilson, M. S., and Wynn, T. A. (2018). Type 2 immunity in tissue repair and fibrosis. *Nat. Rev. Immunol.* 18, 62–76. doi: 10.1038/nri.2017.90

Gluck, C., Qiu, C., Han, S. Y., Palmer, M., Park, J., Ko, Y. A., et al. (2019). Kidney cytosine methylation changes improve renal function decline estimation in patients with diabetic kidney disease. *Nat. Commun.* 10:2461. doi: 10.1038/s41467-019-10378-8

Gu, H. F. (2019). Genetic and epigenetic studies in diabetic kidney disease. *Front. Genet.* 10:507. doi: 10.3389/fgene.2019.00507

Harrison, D. G., Guzik, T. J., Lob, H. E., Madhur, M. S., Marvar, P. J., Thabet, S. R., et al. (2011). Inflammation, immunity, and hypertension. *Hypertension* 57, 132–140. doi: 10.1161/HYPERTENSIONAHA.110.163576

Hashimoto, H., Horton, J. R., Zhang, X., Bostick, M., Jacobsen, S. E., and Cheng, X. (2008). The SRA domain of UHRF1 flips 5-methylcytosine out of the DNA helix. *Nature* 455, 826–829. doi: 10.1038/nature07280

Heine, G. H., Ortiz, A., Massy, Z. A., Lindholm, B., Wiecek, A., Martinez-Castelao, A., et al. (2012). Monocyte subpopulations and cardiovascular risk in chronic kidney disease. *Nat. Rev. Nephrol.* 8, 362–369. doi: 10.1038/nrneph.2012.41

Heintze, J. M. (2018). Epigenetics: EWAS of kidney function. *Nat. Rev. Nephrol.* 14:3. doi: 10.1038/nrneph.2017.164

Hemmingsen, B., Lund, S. S., Gluud, C., Vaag, A., Almdal, T., Hemmingsen, C., et al. (2011). Intensive glycaemic control for patients with type 2 diabetes: systematic review with meta-analysis and trial sequential analysis of randomised clinical trials. *BMJ* 343:d6898. doi: 10.1136/bmj.d6898.

Hendrich, B., and Bird, A. (1998). Identification and characterization of a family of mammalian methyl-CpG binding proteins. *Mol. Cell. Biol.* 18, 6538–6547. doi: 10.1128/MCB.18.11.6538

Hudson, N. O., and Buck-Koehntop, B. A. (2018). Zinc finger readers of methylated DNA. *Molecules* 23:2555. doi: 10.3390/molecules23102555

Illingworth, R. S., Gruenewald-Schneider, U., Webb, S., Kerr, A. R., James, K. D., Turner, D. J., et al. (2010). Orphan CpG islands identify numerous conserved promoters in the mammalian genome. *PLoS Genet.* 6:e1001134. doi: 10.1371/journal.pgen.1001134

Jones, P. A. (2012). Functions of DNA methylation: islands, start sites, gene bodies and beyond. *Nat. Rev. Genet.* 13, 484–492. doi: 10.1038/nrg3230

Jones, P. A., and Liang, G. (2009). Rethinking how DNA methylation patterns are maintained. *Nat. Rev. Genet.* 10, 805–811. doi: 10.1038/nrg2651

Keating, S. T., Plutzky, J., and El-Osta, A. (2016). Epigenetic changes in diabetes and cardiovascular risk. *Circ. Res.* 118, 1706–1722. doi: 10.1161/CIRCRESAHA.116.306819

Kim, Y., and Park, C. W. (2019). Mechanisms of Adiponectin action: implication of Adiponectin receptor agonism in diabetic kidney disease. *Int. J. Mol. Sci.* 20:1782. doi: 10.3390/ijms20071782

Kinsey, G. R. (2014). Macrophage dynamics in AKI to CKD progression. *J. Am. Soc. Nephrol.* 25, 209–211. doi: 10.1681/ASN.2013101110

Kirabo, A., Fontana, V., de Faria, A. P., Loperena, R., Galindo, C. L., Wu, J., et al. (2014). DC isoketal-modified proteins activate T cells and promote hypertension. *J. Clin. Invest.* 124, 4642–4656. doi: 10.1172/JCI74084

Kitching, A. R., and Ooi, J. D. (2018). Renal dendritic cells: the long and winding road. *J. Am. Soc. Nephrol.* 29, 4–7. doi: 10.1681/ASN.2017101145

Klessens, C. Q. F., Zandbergen, M., Wolterbeek, R., Bruijn, J. A., Rabelink, T. J., Bajema, I. M., et al. (2017). Macrophages in diabetic nephropathy in patients with type 2 diabetes. *Nephrol. Dial. Transplant.* 32, 1322–1329. doi: 10.1093/ndt/gfw260

Kolodziejczyk, A. A., Kim, J. K., Svensson, V., Marioni, J. C., and Teichmann, S. A. (2015). The technology and biology of single-cell RNA sequencing. *Mol. Cell* 58, 610–620. doi: 10.1016/j.molcel.2015.04.005

Kotas, M. E., and Medzhitov, R. (2015). Homeostasis, inflammation, and disease susceptibility. *Cell* 160, 816–827. doi: 10.1016/j.cell.2015.02.010

Lande, R., Ganguly, D., Facchinetti, V., Frasca, L., Conrad, C., Gregorio, J., et al. (2011). Neutrophils activate plasmacytoid dendritic cells by releasing self-DNA-peptide complexes in systemic lupus erythematosus. *Sci. Transl. Med.* 3:73ra19. doi: 10.1126/scitranslmed.3001180

Li, X. (2020). Epigenetics and cell cycle regulation in cystogenesis. *Cell. Signal.* 68:109509. doi: 10.1016/j.cellsig.2019.109509

Ligthart, S., Marzi, C., Aslibekyan, S., Mendelson, M. M., Conneely, K. N., Tanaka, T., et al. (2016). DNA methylation signatures of chronic low-grade inflammation are associated with complex diseases. *Genome Biol.* 17:255. doi: 10.1186/s13059-016-1119-5

Liu, P., Liu, Y., Liu, H., Pan, X., Li, Y., Usa, K., et al. (2018). Role of DNA De novo (De)methylation in the kidney in salt-induced hypertension. *Hypertension* 72, 1160–1171. doi: 10.1161/HYPERTENSIONAHA.118.11650

Loperena, R., Van Beusecum, J. P., Itani, H. A., Engel, N., Laroumanie, F., Xiao, L., et al. (2018). Hypertension and increased endothelial mechanical stretch promote monocyte differentiation and activation: roles of STAT3, interleukin 6 and hydrogen peroxide. *Cardiovasc. Res.* 114, 1547–1563. doi: 10.1093/cvr/cvy112

Lu, L., Barbi, J., and Pan, F. (2017). The regulation of immune tolerance by FOXP3. *Nat. Rev. Immunol.* 17, 703–717. doi: 10.1038/nri.2017.75

Lu, C. H., Wu, C. J., Chan, C. C., Nguyen, D. T., Lin, K. R., Lin, S. J., et al. (2016). DNA methyltransferase inhibitor promotes human $CD4^{+}CD25^{h}FOXP3^{+}$ regulatory T lymphocyte induction under suboptimal TCR stimulation. *Front. Immunol.* 7:488. doi: 10.3389/fimmu.2016.00488

Ma, Y., He, F. J., and MacGregor, G. A. (2015). High salt intake: independent risk factor for obesity? *Hypertension* 66, 843–849. doi: 10.1161/HYPERTENSIONAHA.115.05948

Matoba, K., Takeda, Y., Nagai, Y., Kawanami, D., Utsunomiya, K., and Nishimura, R. (2019). Unraveling the role of inflammation in the pathogenesis of diabetic kidney disease. *Int. J. Mol. Sci.* 20:3393. doi: 10.3390/ijms20143393

Mattson, D. L., James, L., Berdan, E. A., and Meister, C. J. (2006). Immune suppression attenuates hypertension and renal disease in the Dahl salt-sensitive rat. *Hypertension* 48, 149–156. doi: 10.1161/01.HYP.0000228320.23697.29

Mezger, A., Klemm, S., Mann, I., Brower, K., Mir, A., Bostick, M., et al. (2018). High-throughput chromatin accessibility profiling at single-cell resolution. *Nat. Commun.* 9:3647. doi: 10.1038/s41467-018-05887-x

Mok, A., Solomon, O., Nayak, R. R., Coit, P., Quach, H. L., Nititham, J., et al. (2016). Genome-wide profiling identifies associations between lupus nephritis and differential methylation of genes regulating tissue hypoxia and type 1 interferon responses. *Lupus Sci. Med.* 3:e000183. doi: 10.1136/lupus-2016-000183

Norlander, A. E., Madhur, M. S., and Harrison, D. G. (2018). The immunology of hypertension. *J. Exp. Med.* 215, 21–33. doi: 10.1084/jem.20171773

Park, J., Guan, Y., Sheng, X., Gluck, C., Seasock, M. J., Hakimi, A. A., et al. (2019). Functional methylome analysis of human diabetic kidney disease. *JCI Insight* 4:e128886. doi: 10.1172/jci.insight.128886

Park, H., Li, Z., Yang, X. O., Chang, S. H., Nurieva, R., Wang, Y. H., et al. (2005). A distinct lineage of CD4 T cells regulates tissue inflammation by producing interleukin 17. *Nat. Immunol.* 6, 1133–1141. doi: 10.1038/ni1261.

Peiseler, M., and Kubes, P. (2019). More friend than foe: the emerging role of neutrophils in tissue repair. *J. Clin. Invest.* 129, 2629–2639. doi: 10.1172/JCI124616

Qiu, C., Hanson, R. L., Fufaa, G., Kobes, S., Gluck, C., Huang, J., et al. (2018). Cytosine methylation predicts renal function decline in American Indians. *Kidney Int.* 93, 1417–1431. doi: 10.1016/j.kint.2018.01.036

Sallustio, F., Serino, G., Cox, S. N., Dalla Gassa, A., Curci, C., De Palma, G., et al. (2016). Aberrantly methylated DNA regions lead to low activation of $CD4^{+}$ T-cells in IgA nephropathy. *Clin. Sci.* 130, 733–746. doi: 10.1042/CS20150711

Saxonov, S., Berg, P., and Brutlag, D. L. (2006). A genome-wide analysis of CpG dinucleotides in the human genome distinguishes two distinct classes of promoters. *Proc. Natl. Acad. Sci. U. S. A.* 103, 1412–1417. doi: 10.1073/pnas.0510310103

Scharer, C. D., Blalock, E. L., Mi, T., Barwick, B. G., Jenks, S. A., Deguchi, T., et al. (2019). Epigenetic programming underpins B cell dysfunction in human SLE. *Nat. Immunol.* 20, 1071–1082. doi: 10.1038/s41590-019-0419-9

Schnaper, H. W. (2017). The tubulointerstitial pathophysiology of progressive kidney disease. *Adv. Chronic Kidney Dis.* 24, 107–116. doi: 10.1053/j.ackd.2016.11.011

Sharma, R., and Kinsey, G. R. (2018). Regulatory T cells in acute and chronic kidney diseases. *Am. J. Physiol. Ren. Physiol.* 314, F679–F698. doi: 10.1152/ajprenal.00236.2017

Sheng, X., Qiu, C., Liu, H., Gluck, C., Hsu, J. Y., He, J., et al. (2020). Systematic integrated analysis of genetic and epigenetic variation in diabetic kidney disease. *Proc. Natl. Acad. Sci. U. S. A.* 117, 29013–29024. doi: 10.1073/pnas.2005905117

Strickland, F. M., Li, Y., Johnson, K., Sun, Z., and Richardson, B. C. (2015). $CD4^+$ T cells epigenetically modified by oxidative stress cause lupus-like autoimmunity in mice. *J. Autoimmun.* 62, 75–80. doi: 10.1016/j.jaut.2015.06.004

Stylianou, E. (2019). Epigenetics of chronic inflammatory diseases. *J. Inflamm. Res.* 12, 1–14. doi: 10.2147/JIR.S129027

Suzuki, H., and Suzuki, Y. (2018). Murine models of human IgA nephropathy. *Semin. Nephrol.* 38, 513–520. doi: 10.1016/j.semnephrol.2018.05.021

Suzuki, H., Suzuki, Y., Aizawa, M., Yamanaka, T., Kihara, M., Pang, H., et al. (2007). Th1 polarization in murine IgA nephropathy directed by bone marrow-derived cells. *Kidney Int.* 72, 319–327. doi: 10.1038/sj.ki.5002300

Swan, E. J., Maxwell, A. P., and McKnight, A. J. (2015). Distinct methylation patterns in genes that affect mitochondrial function are associated with kidney disease in blood-derived DNA from individuals with Type 1 diabetes. *Diabet. Med.* 32, 1110–1115. doi: 10.1111/dme.12775

Tampe, B., Steinle, U., Tampe, D., Carstens, J. L., Korsten, P., Zeisberg, E. M., et al. (2017). Low-dose hydralazine prevents fibrosis in a murine model of acute kidney injury-to-chronic kidney disease progression. *Kidney Int.* 91, 157–176. doi: 10.1016/j.kint.2016.07.042

Tampe, B., Tampe, D., Muller, C. A., Sugimoto, H., LeBleu, V., Xu, X., et al. (2014). Tet3-mediated hydroxymethylation of epigenetically silenced genes contributes to bone morphogenic protein 7-induced reversal of kidney fibrosis. *J. Am. Soc. Nephrol.* 25, 905–912. doi: 10.1681/ASN.2013070723

Tampe, B., Tampe, D., Zeisberg, E. M., Muller, G. A., Bechtel-Walz, W., Koziolek, M., et al. (2015). Induction of Tet3-dependent epigenetic remodeling by low-dose hydralazine attenuates progression of chronic kidney disease. *EBioMedicine* 2, 19–36. doi: 10.1016/j.ebiom.2014.11.005

Tang, P. M., Nikolic-Paterson, D. J., and Lan, H. Y. (2019). Macrophages: versatile players in renal inflammation and fibrosis. *Nat. Rev. Nephrol.* 15, 144–158. doi: 10.1038/s41581-019-0110-2

Tang, S. C. W., and Yiu, W. H. (2020). Innate immunity in diabetic kidney disease. *Nat. Rev. Nephrol.* 16, 206–222. doi: 10.1038/s41581-019-0234-4

Tesch, G. H. (2010). Macrophages and diabetic nephropathy. *Semin. Nephrol.* 30, 290–301. doi: 10.1016/j.semnephrol.2010.03.007

Tian, S., and Chen, S. Y. (2015). Macrophage polarization in kidney diseases. *Macrophage* 2:e679. doi: 10.14800/macrophage.679

Tucci, M., Quatraro, C., Lombardi, L., Pellegrino, C., Dammacco, F., and Silvestris, F. (2008). Glomerular accumulation of plasmacytoid dendritic cells in active lupus nephritis: role of interleukin-18. *Arthritis Rheum.* 58, 251–262. doi: 10.1002/art.23186

Turner, J. E., Paust, H. J., Steinmetz, O. M., and Panzer, U. (2010). The Th17 immune response in renal inflammation. *Kidney Int.* 77, 1070–1075. doi: 10.1038/ki.2010.102

Tuttle, K. R. (2005). Linking metabolism and immunology: diabetic nephropathy is an inflammatory disease. *J. Am. Soc. Nephrol.* 16, 1537–1538. doi: 10.1681/ASN.2005040393

Wang, X., Cao, Q., Yu, L., Shi, H., Xue, B., and Shi, H. (2016). Epigenetic regulation of macrophage polarization and inflammation by DNA methylation in obesity. *JCI Insight* 1:e87748. doi: 10.1172/jci.insight.87748

Wang, N., Liang, H., and Zen, K. (2014). Molecular mechanisms that influence the macrophage m1-m2 polarization balance. *Front. Immunol.* 5:614. doi: 10.3389/fimmu.2014.00614

Wardowska, A. (2020). The epigenetic face of lupus: focus on antigen-presenting cells. *Int. Immunopharmacol.* 81:106262. doi: 10.1016/j.intimp.2020.106262

Wardowska, A., Komorniczak, M., Bullo-Piontecka, B., Debska-Slizien, M. A., and Pikula, M. (2019). Transcriptomic and epigenetic alterations in dendritic cells correspond with chronic kidney disease in lupus nephritis. *Front. Immunol.* 10:2026. doi: 10.3389/fimmu.2019.02026

Wing, M. R., Devaney, J. M., Joffe, M. M., Xie, D., Feldman, H. I., Dominic, E. A., et al. (2014). DNA methylation profile associated with rapid decline in kidney function: findings from the CRIC study. *Nephrol. Dial. Transplant.* 29, 864–872. doi: 10.1093/ndt/gft537

Woo, Y. M., Bae, J. B., Oh, Y. H., Lee, Y. G., Lee, M. J., Park, E. Y., et al. (2014). Genome-wide methylation profiling of ADPKD identified epigenetically regulated genes associated with renal cyst development. *Hum. Genet.* 133, 281–297. doi: 10.1007/s00439-013-1378-0

Xia, M., Chen, G., Liu, D., Tang, X., Liu, Y., Wu, L., et al. (2020). Association analysis of DNA methyltransferases in IgA nephropathy. *Int. Immunopharmacol.* 80:106147. doi: 10.1016/j.intimp.2019.106147

Xu, P., Hu, G., Luo, C., and Liang, Z. (2016). DNA methyltransferase inhibitors: an updated patent review (2012–2015). *Expert Opin. Ther. Pat.* 26, 1017–1030. doi: 10.1080/13543776.2016.1209488

Yang, J., Fang, P., Yu, D., Zhang, L., Zhang, D., Jiang, X., et al. (2016). Chronic kidney disease induces inflammatory $CD40^+$ monocyte differentiation via homocysteine elevation and DNA hypomethylation. *Circ. Res.* 119, 1226–1241. doi: 10.1161/CIRCRESAHA.116.308750.

Yang, B. H., Floess, S., Hagemann, S., Deyneko, I. V., Groebe, L., Pezoldt, J., et al. (2015). Development of a unique epigenetic signature during in vivo Th17 differentiation. *Nucleic Acids Res.* 43, 1537–1548. doi: 10.1093/nar/gkv014

Yang, M. L., Gee, A. J., Gee, R. J., Zurita-Lopez, C. I., Khare, S., Clarke, S. G., et al. (2013). Lupus autoimmunity altered by cellular methylation metabolism. *Autoimmunity* 46, 21–31. doi: 10.3109/08916934.2012.732133

Yang, X., Wang, X., Liu, D., Yu, L., Xue, B., and Shi, H. (2014). Epigenetic regulation of macrophage polarization by DNA methyltransferase 3b. *Mol. Endocrinol.* 28, 565–574. doi: 10.1210/me.2013-1293

Yin, S., Zhang, Q., Yang, J., Lin, W., Li, Y., Chen, F., et al. (2017). TGFbeta-incurred epigenetic aberrations of miRNA and DNA methyltransferase suppress Klotho and potentiate renal fibrosis. *Biochim. Biophys. Acta Mol. Cell Res.* 1864, 1207–1216. doi: 10.1016/j.bbamcr.2017.03.002

Zawada, A. M., Rogacev, K. S., Schirmer, S. H., Sester, M., Bohm, M., Fliser, D., et al. (2012). Monocyte heterogeneity in human cardiovascular disease. *Immunobiology* 217, 1273–1284. doi: 10.1016/j.imbio.2012.07.001

Zawada, A. M., Schneider, J. S., Michel, A. I., Rogacev, K. S., Hummel, B., Krezdorn, N., et al. (2016). DNA methylation profiling reveals differences in the 3 human monocyte subsets and identifies uremia to induce DNA methylation changes during differentiation. *Epigenetics* 11, 259–272. doi: 10.1080/15592294.2016.1158363

Zhang, X., Yang, Y., and Zhao, Y. (2019). Macrophage phenotype and its relationship with renal function in human diabetic nephropathy. *PLoS One* 14:e0221991. doi: 10.1371/journal.pone.0221991

Zhang, L., Zhang, Q., Liu, S., Chen, Y., Li, R., Lin, T., et al. (2017). DNA methyltransferase 1 may be a therapy target for attenuating diabetic nephropathy and podocyte injury. *Kidney Int.* 92, 140–153. doi: 10.1016/j.kint.2017.01.010

Zhao, M., Liang, G. P., Tang, M. N., Luo, S. Y., Zhang, J., Cheng, W. J., et al. (2012). Total glucosides of paeony induces regulatory $CD4^+$ $CD25^+$ T cells by increasing Foxp3 demethylation in lupus $CD4^+$ T cells. *Clin. Immunol.* 143, 180–187. doi: 10.1016/j.clim.2012.02.002

Zhao, M., Tan, Y., Peng, Q., Huang, C., Guo, Y., Liang, G., et al. (2018). IL-6/STAT3 pathway induced deficiency of RFX1 contributes to Th17-dependent autoimmune diseases via epigenetic regulation. *Nat. Commun.* 9:583. doi: 10.1038/s41467-018-02890-0

Zheleznova, N. N., Yang, C., and Cowley, A. W. Jr. (2016). Role of Nox4 and p67phox subunit of Nox2 in ROS production in response to increased tubular flow in the mTAL of Dahl salt-sensitive rats. *Am. J. Physiol. Ren. Physiol.* 311, F450–F458. doi: 10.1152/ajprenal.00187.2016

Zhu, H., Mi, W., Luo, H., Chen, T., Liu, S., Raman, I., et al. (2016). Whole-genome transcription and DNA methylation analysis of peripheral blood mononuclear cells identified aberrant gene regulation pathways in systemic lupus erythematosus. *Arthritis Res. Ther.* 18:162. doi: 10.1186/s13075-016-1050-x

Conflict of Interest: The authors declare that the research was conducted in the absence of any commercial or financial relationships that could be construed as a potential conflict of interest.

frontiers in Physiology

ORIGINAL RESEARCH
published: 29 April 2021
doi: 10.3389/fphys.2021.663216

Long Non-coding RNA *MEG3* Promotes Renal Tubular Epithelial Cell Pyroptosis by Regulating the miR-18a-3p/GSDMD Pathway in Lipopolysaccharide-Induced Acute Kidney Injury

*Junhui Deng, Wei Tan, Qinglin Luo, Lirong Lin, Luquan Zheng and Jurong Yang**

The Third Affiliated Hospital of Chongqing Medical University, Chongqing, China

OPEN ACCESS

Edited by:
Xiao-ming Meng,
Anhui Medical University, China

Reviewed by:
Rui Zeng,
Huazhong University of Science and Technology, China
Jia Fu,
Icahn School of Medicine at Mount Sinai, United States

***Correspondence:**
Jurong Yang
650230@hospital.cqmu.edu.cn;
yjr923@163.com

Specialty section:
This article was submitted to Renal and Epithelial Physiology, a section of the journal Frontiers in Physiology

Received: *02 February 2021*
Accepted: *31 March 2021*
Published: *29 April 2021*

Citation:
Deng J, Tan W, Luo Q, Lin L, Zheng L and Yang J (2021) Long Non-coding RNA MEG3 Promotes Renal Tubular Epithelial Cell Pyroptosis by Regulating the miR-18a-3p/GSDMD Pathway in Lipopolysaccharide-Induced Acute Kidney Injury. Front. Physiol. 12:663216. doi: 10.3389/fphys.2021.663216

Background and Objective: Acute kidney injury (AKI) is a complication of sepsis. Pyroptosis of gasdermin D (GSDMD)-mediated tubular epithelial cells (TECs) play important roles in pathogenesis of sepsis-associated AKI. Long non-coding RNA (lncRNA) maternally expressed gene 3 (*MEG3*), an imprinted gene involved in tumorigenesis, is implicated in pyroptosis occurring in multiple organs. Herein, we investigated the role and mechanisms of *MEG3* in regulation of TEC pyroptosis in lipopolysaccharide (LPS)-induced AKI.

Materials and Methods: Male C57BL/6 mice and primary human TECs were treated with LPS for 24 h to establish the animal and cell models, respectively, of sepsis-induced AKI. Renal function was assessed by evaluation of serum creatinine and urea levels. Renal tubule injury score was assessed by Periodic acid-Schiff staining. Renal pyroptosis was assessed by evaluating expression of caspase-1, GSDMD, and inflammatory factors IL-1β and IL-18. Cellular pyroptosis was assessed by analyzing the release rate of LDH, expression of IL-1β, IL-18, caspase-1, and GSDMD, and using EtBr and EthD2 staining. *MEG3* expression in renal tissues and cells was detected using RT-qPCR. The molecular mechanisms of *MEG3* in LPS-induced AKI were assessed through bioinformatics analysis, RNA-binding protein immunoprecipitation, dual luciferase reporter gene assays, and a rescue experiment.

Results: Pyroptosis was detected in both LPS-induced animal and cell models, and the expression of *MEG3* in these models was significantly up-regulated. *MEG3*-knockdown TECs treated with LPS showed a decreased number of pyroptotic cells, down-regulated secretion of LDH, IL-1β, and IL-18, and decreased expression of GSDMD, compared with those of controls; however, there was no difference in the expression of caspase-1 between *MEG3* knockdown cells and controls. Bioinformatics analysis screened

out miR-18a-3P, and further experiments demonstrated that *MEG3* controls GSDMD expression by acting as a ceRNA for miR-18a-3P to promote TECs pyroptosis.

Conclusion: Our study demonstrates that lncRNA *MEG3* promoted renal tubular epithelial pyroptosis by regulating the miR-18a-3p/GSDMD pathway in LPS-induced AKI.

Keywords: acute kidney injury, renal tubular epithelial cells, pyroptosis, *MEG3*, GSDMD, sepsis, miR-18a-3p

INTRODUCTION

Sepsis, a syndrome characterized by systemic inflammation caused by infection, has become a global health problem (Singer et al., 2016; Rhodes et al., 2017). Acute kidney injury (AKI) is one of the most common complications in patients with sepsis (Bouchard et al., 2015). Septic patients with AKI show a 6-day longer hospital stay and 3.4-fold increased risk of mortality compared with those of septic patients without AKI (Søvik et al., 2019). The mechanism of sepsis-related AKI is complicated and poorly understood at the clinical and research levels (Gyawali et al., 2019). Therefore, more studies are needed to help diagnose and prevent sepsis-related AKI.

Renal tubular epithelial cells (TECs) are the main cell type in kidney tissue; therefore, programmed death of these cells is the main pathophysiological process of AKI (Krautwald and Linkermann, 2014). Studies have shown that pyroptosis of TECs plays an important role in the pathogenesis of sepsis-related AKI (Ye et al., 2019; Zhou et al., 2020). The classic pathway of pyroptosis involves inflammasome-mediated activation of caspase-1, which leads to the cleavage of gasdermin D (GSDMD) into the active *N*-terminal and formation of a cell membrane pore; these events promote the production and release of pro-inflammatory mediators, such as IL-1β and IL-18, thereby producing a waterfall-level inflammatory response (Shi et al., 2015; Broz and Dixit, 2016). The active *N*-terminal of GSDMD is an indispensable "molecular switch" required to open membrane pores and release inflammatory factors. Indeed, stimulation with lipopolysaccharide (LPS) cannot effectively promote the release of IL-1β, IL-18, and other pro-inflammatory mediators after a GSDMD knockout (Sborgi et al., 2016). Moreover, a genetic knockout of GSDMD can significantly improve renal function and alleviate renal tissue inflammation in AKI mice (Miao et al., 2019). Therefore, it is particularly important to explore the regulatory mechanisms of GSDMD in TEC pyroptosis during sepsis-related AKI.

Long non-coding RNAs (lncRNAs), which are RNAs having a length of more than 200 nucleotides, are involved in the regulation of various biological processes such as the cell cycle, apoptosis, and pyroptosis (Mahmoud et al., 2019; He et al., 2020; Simion et al., 2020). LncRNA maternally expressed gene 3 (*MEG3*), an imprinted gene related to tumorigenesis (Braconi et al., 2011; He et al., 2017), is involved in pyroptosis occurring in multiple organs, such as that occurring during hyperbaric oxygen lung injury (Zou et al., 2020), atherosclerotic endothelial injury (Zhang Y. et al., 2018), or cerebral ischemia/reperfusion injury (Liang et al., 2020). *MEG3* shows up-regulated expression in renal tissue and renal TECs of patients with AKI (Yang et al., 2018). However, the role of *MEG3* in TEC pyroptosis occurring during sepsis-related AKI is unknown. In this study, we used *in vivo* and *in vitro* models to examine the role and mechanisms of *MEG3* in pyroptosis occurring during LPS-induced AKI. The findings obtained in our present study will provide new targets for the clinical diagnosis and prevention of septic AKI.

MATERIALS AND METHODS

Mouse Model

Adult male C57 mice, weighing about 22–28 *g*, were purchased from the Animal Experimental Center at the Chongqing Medical University. Mice were randomly divided into four groups and injected intraperitoneally with normal saline or LPS (Sigma-Aldrich, United States) that was diluted with saline to the concentrations of 10, 20, and 40 mg/kg. Blood and renal tissues were collected at 24 h after the injection. For specimen collection, the mice were anesthetized by intraperitoneal injection with sodium pentobarbital; then, 1.5 ml blood was collected from the eye orbit, and the thoracic cavity was opened for cardiac perfusion. Renal-tissue specimens were obtained from both kidneys, the kidney capsule was removed, and part of the kidney was fixed in 4% paraformaldehyde for renal pathological tissue staining; the remaining part was stored at −80°C for subsequent analyses.

Cell Model

Human primary renal TECs and epithelial cell medium were purchased from Sciencell, United States. Epithelial cells were cultured in a constant-temperature incubator maintained at 37°C and 5% CO_2, in an epithelial cell medium containing 2% fetal bovine serum, 1% epithelial cell growth factor, and 1% penicillin/streptomycin; cells within four generations were used for experiments. When the cells were at 90% confluence, PBS (used as vehicle control) or LPS (diluted in PBS to the concentrations of 15, 30, or 60 μg/ml) was added into the culture medium. Cells and cellular supernatants were collected after continuous culture for 24 h.

Assessment of Renal Function

Collected blood was stored in a refrigerator at 4°C for 1 h, then centrifuged at 4°C in a low-temperature centrifuge (at 3,000 rpm for 10 min); supernatants were then collected and used for the detection of serum creatinine and urea nitrogen levels using a Beckman 5800 automatic analyzer (Beckman, Germany).

PAS Staining

Renal tissues were fixed overnight in 4% paraformaldehyde, then washed in distilled water, dehydrated, embedded in paraffin, and sectioned at 4 μm, and then soaked in anhydrous ethanol, 95% ethanol, and 70% ethanol, for 5 min in each. To observe the degree of renal pathological injury, Periodic acid-Schiff (PAS) staining was performed as follows. The sections were immersed in periodate oxidation solution for 10 to 20 min, then washed twice with distilled water, stained with Schiff solution for 10 to 30 min at 37°C, and washed again with distilled water for 5 min. Nuclei were stained with hematoxylin for 3 to 5 min, differentiated in hydrochloric-acid alcohol, and washed with tap water until the nuclei turned blue. The sections were then dehydrated, and sealed with Permount™ Mounting Medium. Two nephrologists, under double-blinded conditions, observed, and scored each specimen using a light microscope at 200×, and each specimen was randomly observed using at least 10 non-repetitive fields. The extent of tubular injury was assessed by estimating the percentage of renal tubular epithelial tissue necrosis as follows: 0 points for no injury; 1 point (0–10%) and 2 points (11–20%) for mild injury; 3 points (21–40%) and 4 points (41–60%) for moderate injury; and 5 points (61–75%) and 6 points (>75%) for severe injury.

Western Blotting

After protein was extracted from renal tissues and cells, protein concentration was determined using the BCA method. After denaturation, 30–80 μg protein was separated using 12% SDS-PAGE. Proteins were transferred to PVDF membranes using wet transfer. The membranes were blocked in 5% skim milk at room temperature for 1.5 h, and then incubated overnight at 4°C with the following primary antibodies specific for: IL-1β (1:1000, #12242, Cell Signaling, Shanghai, China); IL-18 (1:1000, ab71495, Abcam, Shanghai, China); caspase-1 (1:500, GTX14367, GeneTex, United States); GSDMD (1:500, orb390052, Biorbyt, Cambridge, United Kingdom); and β-actin (1:5000, AC004, ABclonal, Wuhai, China). The membranes were then washed and incubated at room temperature in the dark for 2 h with the following secondary antibodies: anti-mouse IgG (H + L, DyLight™ 800 Conjugate, 1:15000, #5257, Cell Signaling, Shanghai, China) and anti-rabbit IgG (H + L, DyLight™ 680 Conjugate, 1:15000, #5366, Cell Signaling, Shanghai, China). A two-color infrared fluorescence imaging system was used to visualize protein bands. Protein concentration in the bands was quantified using ImageJ and normalized against that of β-actin, used as loading control.

RT-qPCR

Total RNA was extracted from kidney tissues and cells using Trizol, and RNA was quantified using OD 260 nm. cDNA reverse transcription and amplification were performed using the Hairpin-it™ microRNA and U6 snRNA Normalization RT-PCR Quantitation Kit, or Custom gene qRT-PCR Quantitation Kit (GenePharma, Suzhou, China). Relative gene expression was assessed using the $2^{-\Delta\Delta Ct}$ formula, with U6 or GAPDH used as housekeeping genes. The primer sequences were as follows:

Primer name	Base sequence
mmu-MEG3 (F)	5′ -CGCGAGGACTTCACGCACAA-3′
mmu-MEG3 (R)	5′ -TCTGTGTCCGTGTGTCCAGG-3′
hsa-MEG3 (F)	5′ -CTGCCCATCTACACCTCACG-3′
hsa-MEG3 (R)	5′ -ATCCTTTGCCATCCTGGTCC-3′
mmu-miR-18a-3P (F)	5′ -TCCAGACTGCCCTAAGTGC-3′
mmu-miR-18a-3P (R)	5′ -CAGTGCGTGTCGTGGAGT-3′
mmu-miR-541-3P (F)	5′ -ATCAGACTATGGCGAACACAGAA-3′
mmu-miR-541-3P (R)	5′ -TATCCTTGTTCACGACTCCTTCAC-3′
mmu-miR-654-5P (F)	5′ -TGGTAAGCTGCAGAACATGTGT-3′
mmu-miR-654-5P (R)	5′ -ATCCAGTGCAGGGTCCGAGG-3′
hsa-miR-18a-3P (F)	5′ -TGATACTGCCCTAAGTGCTCC-3′
hsa-miR-18a-3P (R)	5′ -CAGTGCCGTGTCGTGGAGT-3′
hsa-GSDMD (F)	5′ -TGATACTGCCCTAAGTGCTCC-3′
hsa-GSDMD (R)	5′ -GGCTCAGTCCTGATAGCAGTG-3′
mmu-GAPDH (F)	5′ -GAGAAACCTGCCAAGTATGATGAC-3′
mmu-GAPDH (R)	5′ -AGAGTGGGAAGTTGCTGTTGAAG-3′
hsa-GAPDH (F)	5′ -CATGAGAAGTATGACAACAGCCT-3′
hsa-GAPDH (R)	5′ -AGTCCTTCCACGATACCAAAGT-3′
mmu-U6 (F)	5′ -CAGCACATATACTAAAATTGGAACG-3′
mmu-U6 (R)	5′ -ACGAATTTGCGTGTCATCC-3′
hsa-U6 (F)	5′ -CAGCACATATACTAAAATTGGAACG-3′
hsa-U6 (R)	5′ -ACGAATTTGCGTGTCATCC-3′

Lactate Dehydrogenase Release Rate (LDH%)

Cells were seeded in 96-well plates, and the wells were designated into the following groups: control wells, treatment wells, maximum-release wells, and spontaneous release wells. In the maximum-release group, 1 μl Triton X-100 was added to each well. The spontaneous release wells contained only cell-free media. After 30 min of continuous culture, supernatants were collected from all the wells and centrifuged at 4°C for 15 min. Then, 20 μl supernatant obtained from each well was added into the corresponding well of a new 96-well plate; 25 μl matrix solution and 5 μl coenzyme I application solution were then added to each well, and the plate was agitated in a water bath at 37°C for 15 min. Consequently, 25 μl 2, 4-dinitrophenylhydrazine was added to each well, and the plate was incubated in a water bath at 37°C for an additional 15 min. NaOH solution was diluted to 0.4 mol/l, and 250 μl of this diluted solution was added to each well and mixed by shaking. The plate was allowed to incubate at room temperature for 3 min, and LDH release rate was analyzed using a multifunctional enzyme label analyzer at 450 nm and calculated as follows: LDH release rate = (measured well OD value-spontaneous well OD value)/(maximum release well OD value-spontaneous well OD value) × 100%.

ELISA

Cells were inoculated into 24-well plates, and cell-culture supernatants were collected after treatment. ELISA kits (Human IL-18 and IL-1β ELISA Kits from RayBiotech, United States) were used for detection. The standard-curve formula was determined

using the OD value of the gradient concentration standard, and the final concentration of each well was calculated according to this formula.

EtBr and EthD2 Staining

Two different red nucleic-acid dyes, EtBr (molecular weight of 394 Da) and EthD2 (molecular weight of 1293 Da), were used to detect membrane pores. TECs were seeded into the wells of a 24-well plate. After the TECs were treated, they were washed three times with PBS, fixed using 4% paraformaldehyde at room temperature for 15 min, and then washed again with PBS. The positive-control group was treated with PBST (PBS solution containing 1% Triton) and drilled at room temperature for 20 min. The cells were stained with DAPI nuclear stain in the dark for 5 min, and then treated with EtBr (25 μg/ml, Sigma, United States) or EthD2 (25 μg/ml, Thermo Fisher, United States). Images were acquired using a fluorescence microscope (Nikon, Japan) at 200×.

Transfection of siRNA, Inhibitor and Mimic

siRNA, inhibitor and mimic were designed and synthesized by Shanghai Jima, China. Human renal TECs were transfected using Lipofectamine TM 3000 transfection reagent. Cells were used at 70% confluence. For transfection, siRNA, inhibitor, mimic, or transfection reagent was mixed with Opti-MEM^{TM} medium. The mixture containing siRNA, inhibitor or mimic was added to the mixture containing transfection reagent. After standing at room temperature for 15 min, each mixture was added to the cell medium. Subsequent treatments were administered at 48 h after transfection.

Double Luciferase Reporter Assay

LncMEG3 wild-type and mutant plasmids, and GSDMD wild-type and mutant plasmids were constructed using a pMIRGLO vector. pMIRGLO-lncMEG3-WT and miR-18a-3p mimic, pMIRGLO-lncMEG3-WT and NC mimic, pMIRGLO-lncMEG3-Mut and miR-18a-3p mimic, pMIRGLO-lncMEG3-Mut and NC mimic, pMIRGLO-GSDMD-WT and miR-18a-3p mimic, pMIRGLO-GSDMD-WT and NC mimic, pMIRGLO-GSDMD-Mut and miR-18a-3p mimic, and pMIRGLO-GSDMD- Mut and NC mimic were co-transfected into human embryonic kidney cells (HEK293) using LipofectamineTM 3000. After 24 h, the cells were collected and lysed. Fluorescence activity was detected according to the instructions of the Dual-Luciferase® Reporter Assay System (Promega, United States).

RIP Assay

RNA immunoprecipitation (RIP) kit (BersinBiotech, Guangzhou, China) was used for RIP analysis. First, cultured primary human renal TECs were collected and lysed with a complete RIP lysis buffer. The cell lysate was then incubated overnight with magnetic beads (Abcam, Shanghai, China) containing either Ago2 antibody or negative control IgG antibody at 4°. The next day, the magnetic beads were washed with washing solution for 3 times, and then protease K buffer was used to remove the proteins. Finally, RNA was extracted for qRT-PCR.

Statistical Analyses

IBM SPSS 23 statistical software was for data analysis; measurement data were expressed as mean ± standard deviation. One-way ANOVA was used after homogeneity of variance test for multiple-group comparison, and unpaired *t* test was used after normal distribution test for comparison between two groups. $P < 0.05$ indicated statistically significant difference.

RESULTS

MEG3 Is Up-regulated in the Kidneys of LPS-AKI Mice

First, we established our LPS-AKI mouse model to assess the expression levels of *MEG3* in the kidney. Compared with those in saline-treated mice, serum creatine and urea levels in LPS-treated mice had increased significantly (**Figures 1A,B**). Concurrently, PAS staining of renal tissue demonstrated that renal epithelial cells obtained from mice in the saline-treated group showed a close and orderly arrangement, with normal cell morphology, complete brush border, and clear lumen; in the LPS-treated group, we observed degeneration of the tubular epithelial vacuoloid, swelling, disappearance of the brush margin, tubular deposition, and infiltration of inflammatory cells. The renal-tubule injury score, obtained by scoring the degree of renal-tubule injury, was significantly increased in LPS mice compared with that of saline-treated mice (**Figures 1C,D**). These results show that renal function was impaired in mice after treatment with LPS. Next, we used western blotting to assess the expression levels of caspase-1, GSDMD, and inflammatory cytokines IL-1β and IL-18, in renal tissues during renal pyroptosis in mice. The expression levels of caspase-1, cleaved caspase-1, GSDMD, GSDMD-N, IL-1β, and IL-18 in the renal tissues of LPS-treated mice were significantly increased compared with those of the saline-treated mice (**Figures 1E–H**), indicating that renal pyroptosis occurred in mice after treatment with LPS. Using RT-qPCR, we also found that the level of *MEG3* in the LPS-treated group had increased in a concentration-dependent manner, consistent with the degree of renal damage and pyroptosis (**Figure 1I**). These results suggest that *MEG3* played a role in renal pyroptosis during septic AKI.

MEG3 Expression Is Up-Regulated in LPS-Induced Primary Human TECs

In order to delineate the relationship between MEG3 expression and TEC pyroptosis after LPS-induced injury, we established the model of LPS-induced injury in primary human TECs. Our results indicate that the levels of LDH in the supernatants of LPS-treated cells were significantly increased compared with those in PBS-treated controls (**Figure 2A**). The results of ELISA showed that the levels of inflammatory cytokines IL-1β and IL-18 in the supernatants of LPS-treated cells were also significantly increased compared with those in PBS-treated controls (**Figures 2B,C**). The

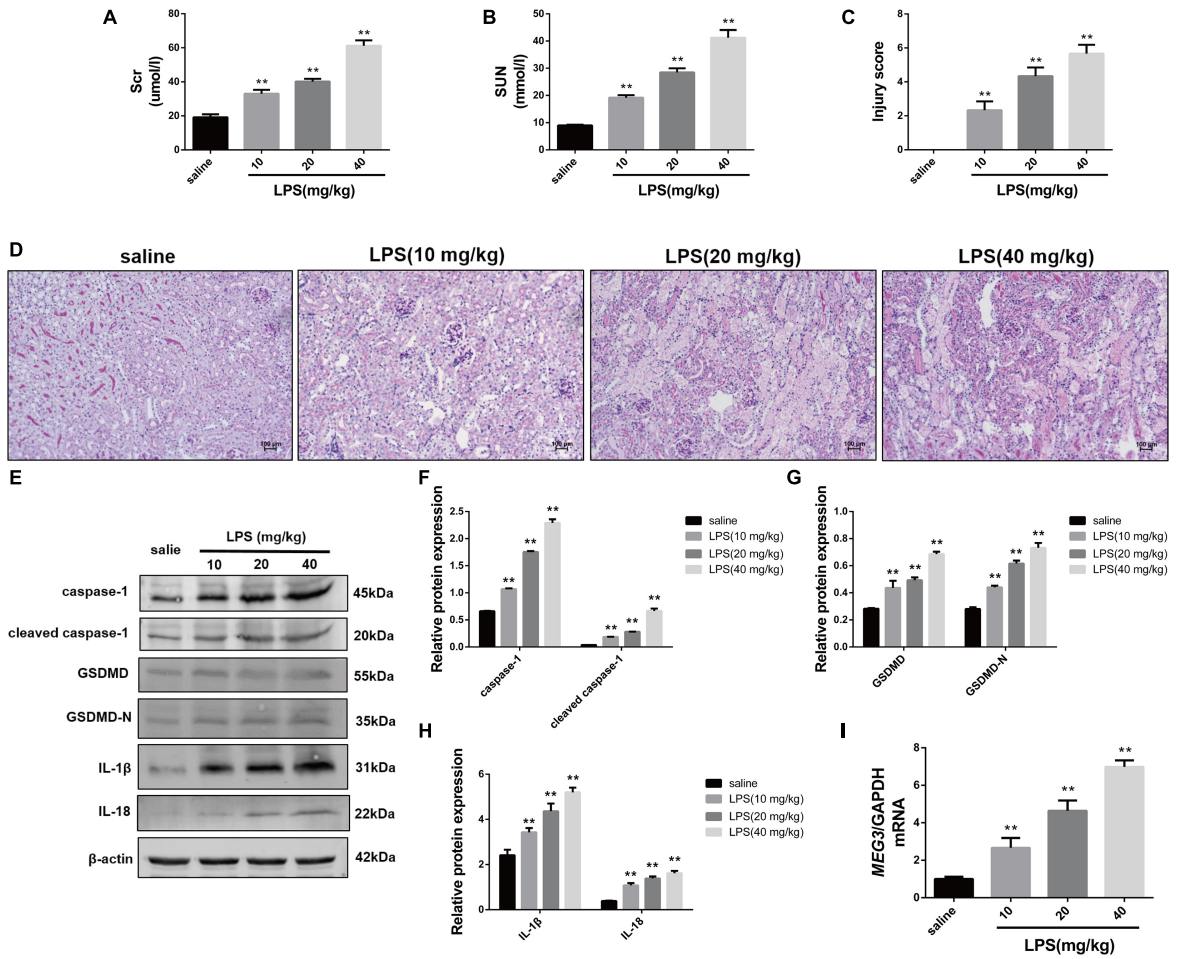

FIGURE 1 | Increased expression of pyroptosis-associated proteins and *MEG3* in kidneys of mice with LPS-induced AKI (n = 6). **(A)** Serum creatinine level in mice with LPS-induced AKI and control saline-treated mice. **(B)** Serum urea nitrogen levels in mice with LPS-induced AKI and control saline-treated mice. **(C)** PAS staining of mouse kidneys (200×). **(D)** Score of renal tubular injury in mice. **(E–H)** Expression of caspase-1, cleaved caspase-1, GSDMD, GSDMD-N, IL-1β, and IL-18 in renal tissues of mice. **(I)** Expression level of *MEG3* mRNA in mouse kidney tissue. $^{**}P < 0.01$, compared with normal saline-treated group; all values are expressed as mean ± standard deviation (SD).

results of our western blotting analysis showed that the levels of caspase-1, cleaved caspase-1, GSDMD, and GSDMD-N in LPS-treated cells were significantly increased compared with those of PBS-treated controls (**Figures 2D–F**). These findings indicate that pyroptosis occurred in primary human TECs after treatment with LPS. Similarly, RT-qPCR analysis showed that the levels of *MEG3* in the LPS-treated cells had increased in a concentration-dependent manner (**Figure 2G**). These results further suggest that *MEG3* may have a potential function in TEC pyroptosis after LPS-induced injury.

Knockdown of *MEG3* Inhibits LPS-Induced Pyroptosis in Primary Human TECs

To verify the effect of *MEG3* on LPS-induced primary human TEC pyroptosis, we transfected *MEG3* siRNA into primary human TECs. Our results indicate that the relative mRNA level of *MEG3* in TECs transfected with si*MEG3* was reduced by approximately 73% compared with that in TECs transfected with NC siRNA (**Figure 3A**). Next, we detected pyroptosis using nucleic-acid dyes EtBr and EthD2 in in TECs transfected with si*MEG3* and in NC siRNA-transfected controls. During the process of pyroptosis, cells form a membrane pore having a diameter of approximately 20 nm. The nucleic-acid dye EtBr, which possesses small molecular weight, can pass through the membrane pore, but the large-molecular—weight EthD2 cannot. Therefore, cells positive for EtBr and negative for EthD2 staining are considered to be undergoing pyroptosis (Wang et al., 2017; Feng et al., 2018). Our results show that the number of pyroptotic TECs was significantly increased after treatment with LPS (60 μg/ml; the same concentration was used in subsequent experiments), but reduced after transfection with si*MEG3*, compared with that in the NC siRNA-transfected group (**Figure 3B**). The levels of LDH, IL-1β, and IL-18 were significantly reduced in the supernatants of siMEG3-transfected

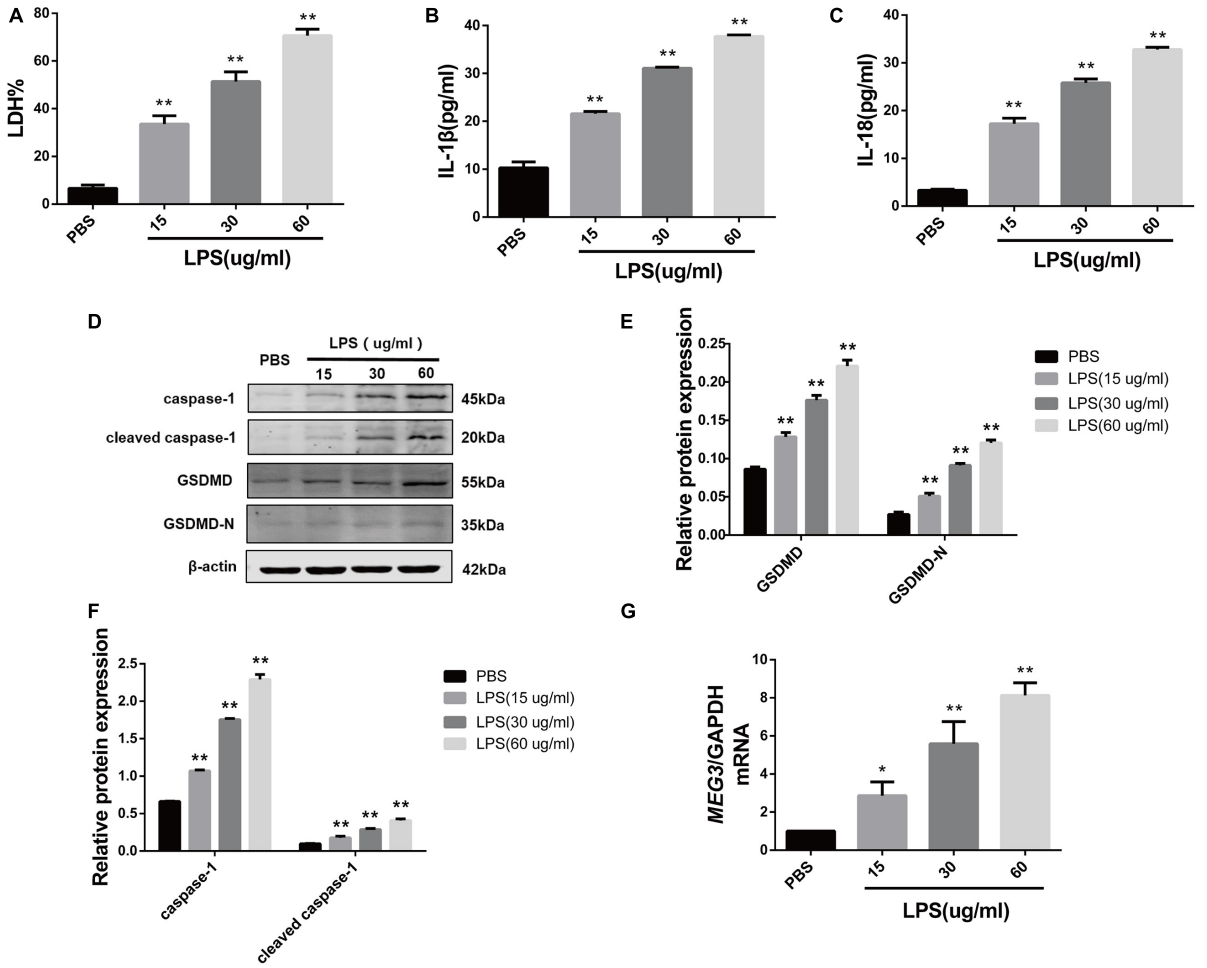

FIGURE 2 | Increased expression of *MEG3* in primary human renal tubular epithelial cells treated with LPS. **(A)** LDH% in TECs supernatants. **(B,C)** Release of IL-1β and IL-18 in TECs supernatants. **(D–F)** Protein expression of caspase-1, cleaved caspase-1, GSDMD, and GSDMD-N in TECs. **(G)** Expression level of *MEG3* mRNA in TECs. $^{*}P < 0.05$, $^{**}P < 0.01$, and compared with the PBS group.

cells compared with those of NC siRNA-transfected group (**Figures 3C–E**). These results suggest that knockdown of *MEG3* in TECs could reduce LPS-induced pyroptosis. In si*MEG3*-transfected TECs, LPS induced a significant decrease in the expression of GSDMD precursor and active form, but no difference was observed in the expression of caspase-1 precursor and active form (**Figures 3F–H**). Based on these results, we speculate that the mechanism of *MEG3*-mediated promotion of pyroptosis may occur through regulation of GSDMD expression rather than regulation of its activation.

miR-18a-3P Is Decreased in LPS-AKI

Long non-coding RNAs are a newly discovered type of regulatory RNAs that competitively regulate the expression of target genes by interfering with miRNAs. To explore the mechanism of *MEG3*-mediated regulation of *GSDMD* expression, we used http://www.targetscan.org/vert_72/and http://carolina.imis.athena-innovation.gr/diana_tools/web/index.php?r=lncbasev2%2Findex to predict miRNAs regulated by *MEG3* and targeting *GSDMD* expression. Three miRNAs related to inflammation (miR-18a-3P, miR-541-3P, and miR-654-5P) were screened out using our functional review. We then assessed the expression of each miRNA in the renal tissues of our LPS-AKI mice. Our results indicate that only miR-18a-3P expression was significantly decreased (**Figure 4A**). We also found that miR-18a-3P expression was down-regulated in LPS-induced primary human TECs, but increased after transfection with si*MEG3* compared with that after transfection with siNC (**Figure 4B**). This result indicates that *MEG3* may regulate GSDMD through miR-18a-3P.

Overexpression of miR-18a-3P Inhibits LPS-Induced Pyroptosis in Primary Human TECs

In order to verify the effect of miR-18a-3P on LPS-induced primary human TEC pyroptosis, we transfected an miR-18a-3P mimic into primary human TECs. Compared with

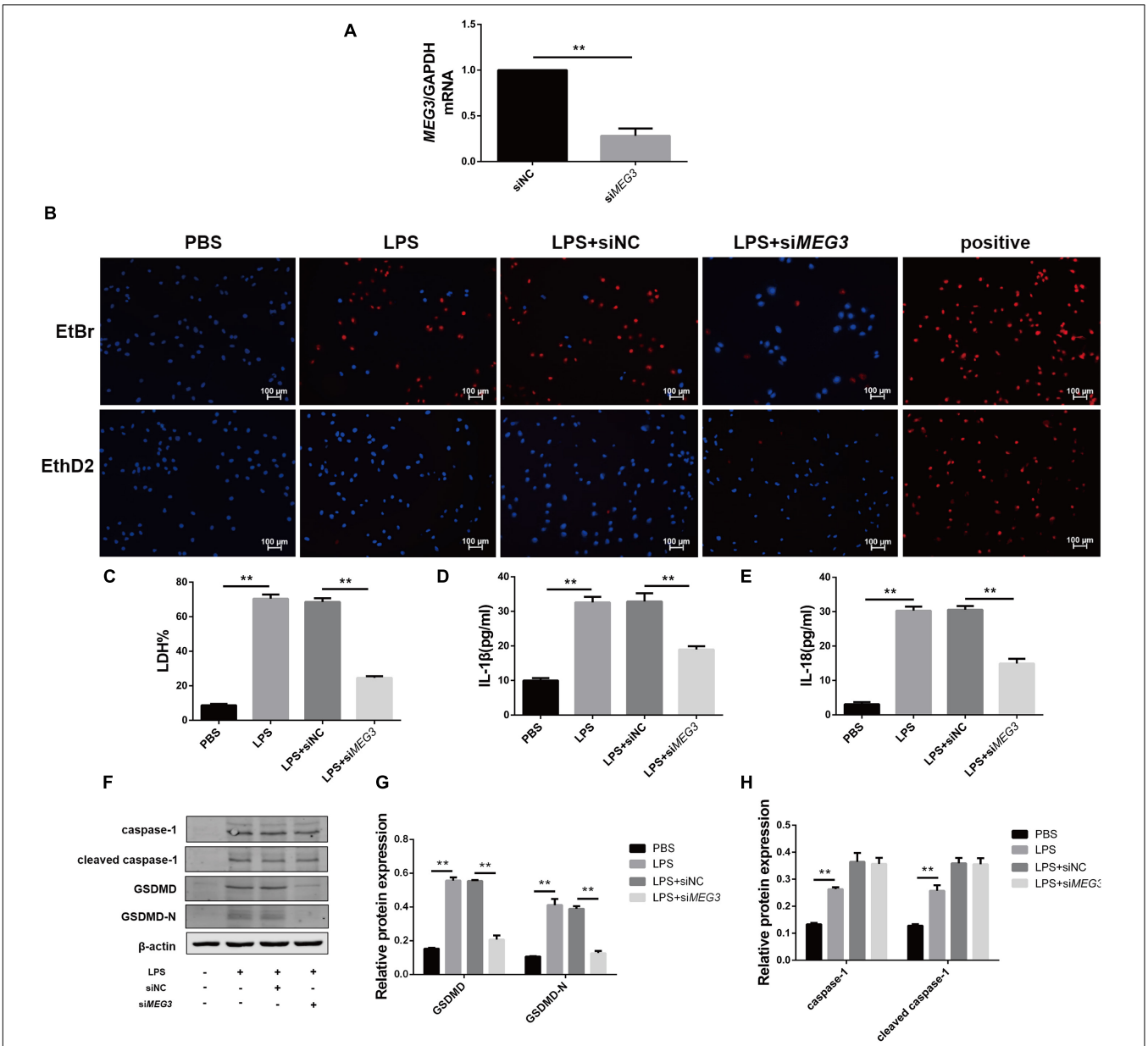

FIGURE 3 | Knockdown of *MEG3* in TECs inhibited LPS-induced pyroptosis. **(A)** *MEG3* mRNA levels transfected with siRNA. **(B)** siRNA-transfected TECs stained with EtBr and EthD2. **(C)** LDH% in supernatants obtained from siRNA-transfected TECs. **(D–G)** Release of IL-1β and IL-18 in supernatants obtained from siRNA-transfected TECs. **(F–H)** Protein expression of caspase-1, cleaved caspase-1, GSDMD, and GSDMD-N in siRNA-transfected TECs. $^{**}P < 0.01$, compared with the respective control group.

NC mimic, the relative mRNA expression level of miR-18a-3P increased by approximately 20-fold after transfection with a miR-18a-3P mimic (**Figure 5A**). We also found that the expression level of GSDMD in primary human TECs was significantly decreased in the miR-18a-3P mimic group after treatment with LPS compared with that of the NC mimic group (**Figures 5B–D**). At the same time, the levels of LDH, IL-1β, and IL-18 were significantly reduced in the cell supernatant after LPS treatment was also significantly reduced after transfection ofmiR-18a-3P mimic (**Figures 5E–G**). These results suggest that overexpression of miR-18a-3P inhibits LPS-induced pyroptosis in primary human TECs.

Knocking Down miR-18a-3p Reversed the Inhibitory Effect of si*MEG3* on Pyroptosis in Primary Human TECs

To verify whether knockdown of miR-18a-3p could reversed the inhibitory effect of si*MEG3* on pyroptosis in primary human TECs, we transfected si*MEG3* and miR-18a-3p inhibitor

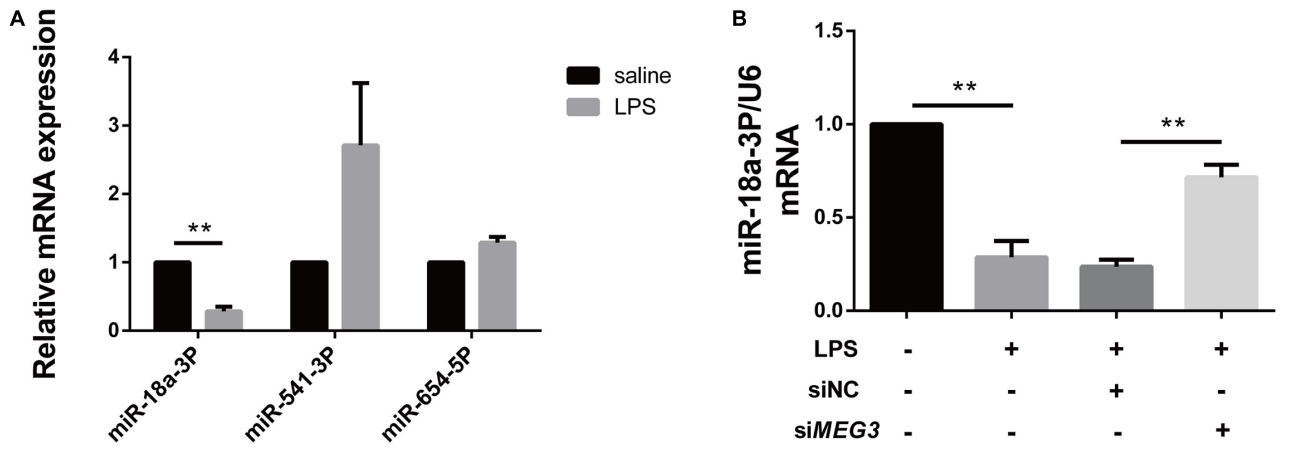

FIGURE 4 | miR-18a-3P is decreased in LPS-AKI. **(A)** Expression levels of miRNA in renal tissues of LPS-AKI mice (40 mg/kg). **(B)** Expression levels of miR-18a-3p in siRNA-transfected TECs. $^{**}P < 0.01$, compared with the respective control group.

separately or simultaneously. First, we detected that the inhibitory efficiency of miR-18a-3P inhibitor reached 66% (**Figure 6A**). Then, we continued to detect that, miR-18a-3P inhibitor transfection significantly offset the decrease in GSDMD mRNA and protein levels caused by si*MEG3* transfection in LPS-induced primary human TECs (**Figures 6B–D**). Consistently, we also found that knocking down miR-18a-3P also significantly offset the reduction in LDH% and IL-1β and IL-18 release caused by si*MEG3* transfection (**Figures 6E–G**). These results indicate that *MEG3* regulates LPS-induced primary human TEC pyroptosis through miR-18a-3P.

MEG3 Binds to miR-18a-3P, and miR-18a-3P Binds to *GSDMD*

In order to detect the targeted binding relationships between *MEG3* and miR-18a-3P, and between miR-18a-3P and GSDMD, we constructed the pMIRGLO-lnc*MEG3*-WT, pMIRGLO-lnc*MEG3*-Mut, pMIRGLO-GSDMD-WT, and pMIRGLO-GSDMD-Mut plasmids, and used bioinformatics analysis to predict the base binding sites between *MEG3* and miR-18a-3P, and between miR-18a-3P and GSDMD (**Figures 7A,B**). Firstly, double-luciferase activity indicated that, miR-18a-3p mimic significantly inhibited the luciferase activity of *MEG3* and GSDMD wild-type carriers, but had no inhibitory effect on mutant carriers (**Figures 7C,D**). In addition, through RIP assay, it was found that *MEG3*, miR-18a-3P and GSDMD were all significantly up-regulated in Ago2-RIP compared with the negative control IgG-RIP (**Figures 7E–G**). These results indicate that *MEG3* can directly bind to miR-18a-3p and miR-18a-3p can directly bind to GSDMD.

DISCUSSION

In this study, we verified that pyroptosis occurred in both the *in vivo* and *in vitro* models of LPS-induced septic AKI. Our findings indicate that *MEG3* expression was up-regulated during pyroptosis. Our results, obtained using the *in vitro* model, show that *MEG3* played an important role in LPS-induced TEC pyroptosis, and that direct targeting of miR-18a-3p in regulation of GSDMD expression was involved in this pyroptotic mechanism.

Multiple mechanisms are involved in the development of septic AKI including renal hemodynamic abnormalities, inflammatory responses, and oxidative stress (Prowle and Bellomo, 2015; Shum et al., 2016; Khajevand-Khazaei et al., 2019). The inflammatory response is a major factor leading to impairment of renal function (Peerapornratana et al., 2019; Poston and Koyner, 2019). Studies on immune inflammatory cells have shown that pyroptosis, the most important cell-death pathway in septic AKI, produces pro-inflammatory mediators and triggers an inflammatory response (Doitsh et al., 2014). The activity of the inflammatory factor caspase-1 cleaves GSDMD, which exposes the GSDMD active *N*-terminal domain that inserts into the phospholipid structure of cellular intima, forming micropores of approximately 20 nm. This allows water to enter the cell, causing cell swelling and membrane rupture, and leading to the release of numerous pro-inflammatory mediators. This phenomenon is known as the classical pyroptotic pathway (Fink and Cookson, 2019). In previous studies, we examined indicators of pyroptosis in a rat model of ischemia/reperfusion AKI. Our results confirmed that pyroptosis occurs in renal TECs during AKI, which was closely related to AKI severity (Yang et al., 2014). Subsequent studies using mouse models of LPS-, cisplatin-, ischemia/reperfusion, and contrast-agent—induced AKI have reported that renal function and cell damage are considerably reduced by disruption of pyroptosis (Zhang Z. et al., 2018; Miao et al., 2019; Ye et al., 2019). In this study, we detected increased expression of caspase-1 precursor and its active form, GSDMD and its *N*-terminal, and inflammatory cytokines IL-1β and IL-18, in LPS-induced mouse kidneys and primary human TECs. Based on these findings, we conclude that pyroptosis is likely the main mechanism involved in pathogenesis of AKI.

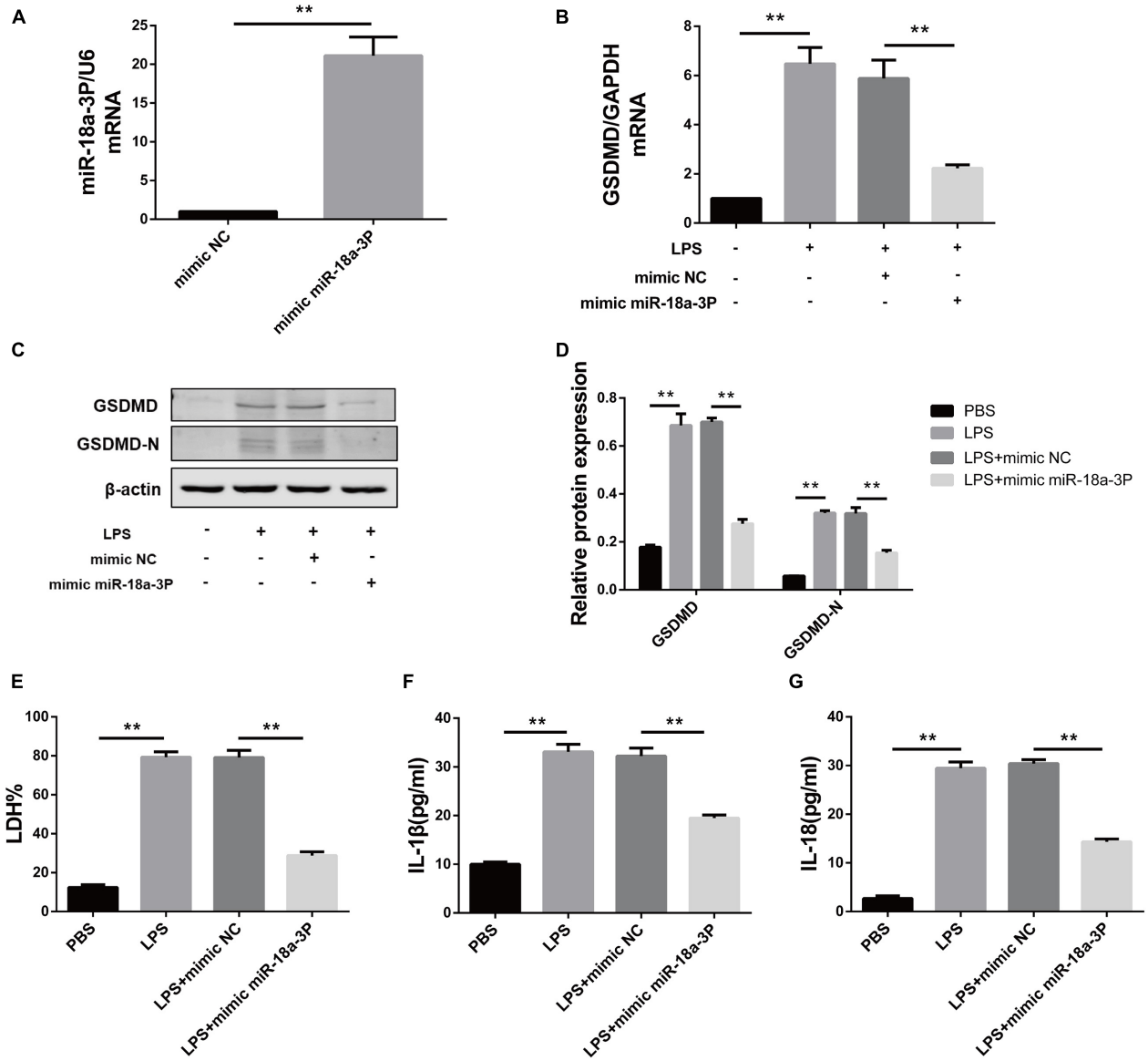

FIGURE 5 | Overexpression of miR-18a-3P inhibits LPS-induced pyroptosis in primary human TECs. **(A)** Expression level of miR-18a-3p mRNA in TECs transfected with mimic. **(B)** GSDMD mRNA expression level in TECs transfected with mimic. **(C,D)** Protein expression levels of GSDMD and GSDMD-N in TECs transfected with mimic. **(E)** LDH% in supernatants obtained from TECs transfected with mimic. **(F,G)** Release of IL-1β and IL-18 in supernatants obtained from TECs transfected with mimic. $^{**}P < 0.01$, compared with the respective control group.

Long non-coding RNAs, which are non-protein-coding RNAs, are involved in the regulatory mechanisms of various diseases (Zhang et al., 2017), including the injury and repair mechanisms of AKI (Liu Z. et al., 2019). The lncRNA *MEG3* was initially found to be a tumor suppressor that can inhibit the proliferation of tumor cells (Benetatos et al., 2011), but has also been found recently to regulate pyroptosis (Zhang Y. et al., 2018; Liang et al., 2020; Zou et al., 2020). Multiple studies have shown that *MEG3* is involved in regulating inflammatory-response mechanisms in various diseases such as acute pancreatitis (Xue et al., 2020), chronic obstructive pulmonary disease (Lei et al., 2021), and ultraviolet skin injury (Zhang et al., 2019). Disrupting the expression of *MEG3* can reduce the production of inflammatory factors via various pathways. In addition, *MEG3* also plays a key regulatory role in kidney diseases such as ischemic reperfusion-induced AKI (Yang et al., 2018), diabetic nephropathy (Zha et al., 2019), and transplanted kidney injury (Pang et al., 2019). In addition, one study has found that *MEG3* expression is increased in the blood of septic patients (Na et al., 2020). In this study, we detected significant upregulation of *MEG3* expression in both *in vivo* and *in vitro* models of septic AKI; this upregulation of *MEG3* expression occurred in a concentration-dependent manner and was consistent with pyroptosis. We detected LPS-induced TEC pyroptosis after transfection of si*MEG3*, and found

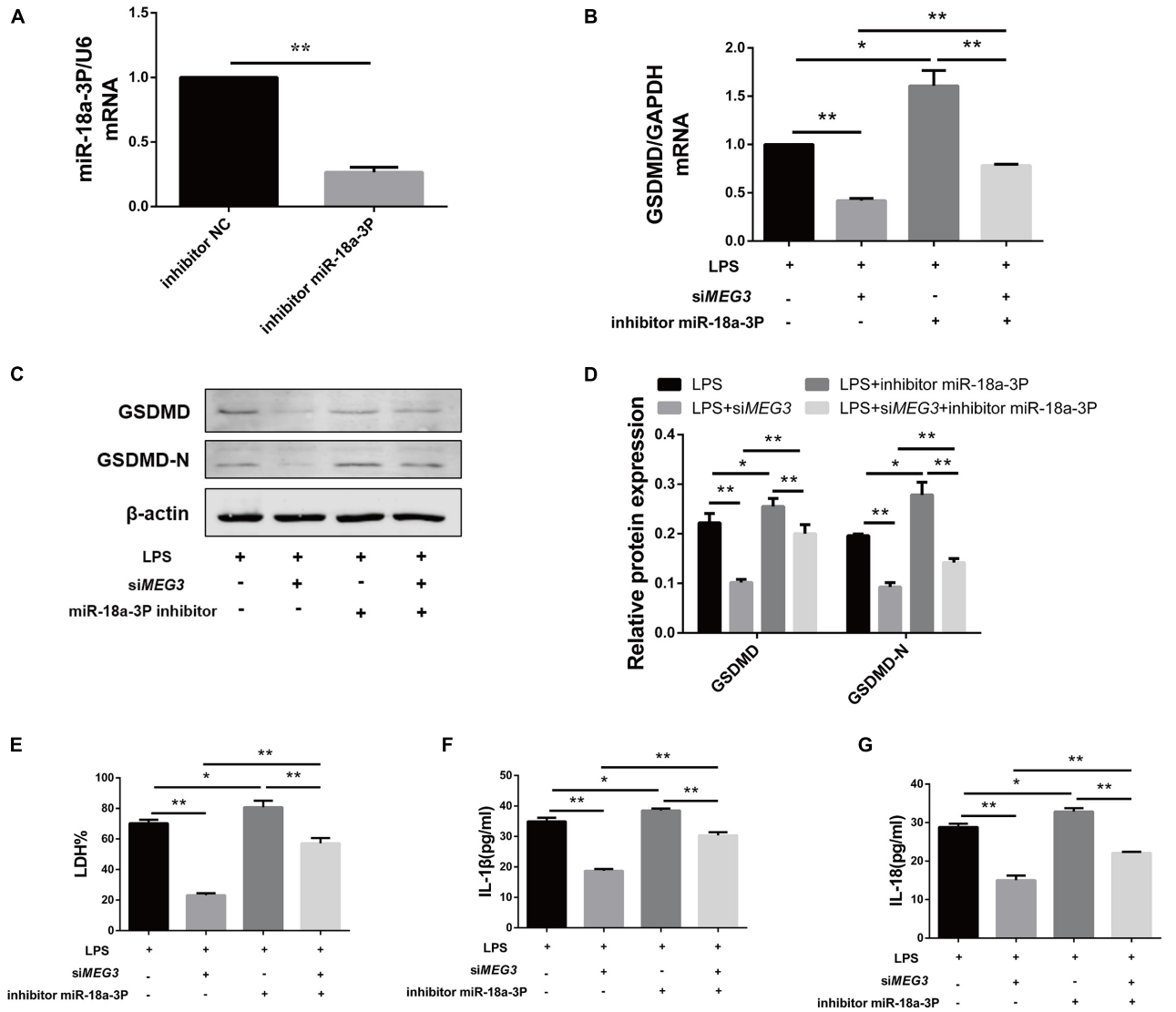

FIGURE 6 | Knocking down miR-18a-3p reversed the inhibitory effect of siMEG3 on pyroptosis in primary human TECs. **(A)** Expression level of miR-18a-3p mRNA in TECs transfected with inhibitor. **(B)** GSDMD mRNA expression level in TECs transfected with siMEG3 and miR-18a-3P inhibitor separately or together. **(C,D)** Protein expression levels of GSDMD and GSDMD-N in TECs transfected with siMEG3 and miR-18a-3P inhibitor separately or together. **(E)** LDH% in supernatants obtained from TECs transfected with siMEG3 and miR-18a-3P inhibitor separately or together. **(F,G)** Release of IL-1β and IL-18 in supernatants obtained from TECs transfected with siMEG3 and miR-18a-3P inhibitor separately or together. $^{*}P < 0.05$, $^{**}P < 0.01$, and compared with the respective control group.

that knockdown of *MEG3* reduced pyroptosis. Knockdown of *MEG3* also affected the expression of GSDMD precursor and *N*-terminal, but did not change the expression of caspase-1 precursor and active form. These findings indicate that regulation of *MEG3* in TEC pyroptosis occurred via regulation of GSDMD expression.

Long non-coding RNAs also function as ceRNAs and regulate other mRNA transcripts by competing for miRNAs, which can degrade target mRNAs and are, thereby, involved in regulation of gene expression (Song et al., 2016; Liu Y. et al., 2019). We used bioinformatics analysis to explore the specific miRNAs targeted by *MEG3* in regulation of GSDMD expression. Our results indicate that three miRNAs could be paired with both *MEG3* and GSDMD bases, and were functionally related to inflammation. We evaluated the expression of these miRNAs in the kidneys of our LPS mice, and found that only the expression of miR-18a-3p was negatively correlated with that of *MEG3*. Previous studies have reported that miR-18a-3p is down-regulated in the cruciate ligament of patients with osteoarthritis (Li et al., 2017). *In vitro* studies have shown that miR-18a-3p is involved in the regulation of pathological mechanisms of osteoarthritis (Ding et al., 2020). These studies suggest that miR-18a-3p plays a role in regulating inflammation. Therefore, we evaluated the role of miR-18a-3p in LPS-induced TEC pyroptosis. Our results show that knockdown of *MEG3* significantly increased miR-18a-3p expression in LPS-induced TECs, and that a miR-18a-3p mimic reduced the expression of GSDMD and the release of inflammatory factors. Moreover, our results also show that knocking down miR-18a-3P

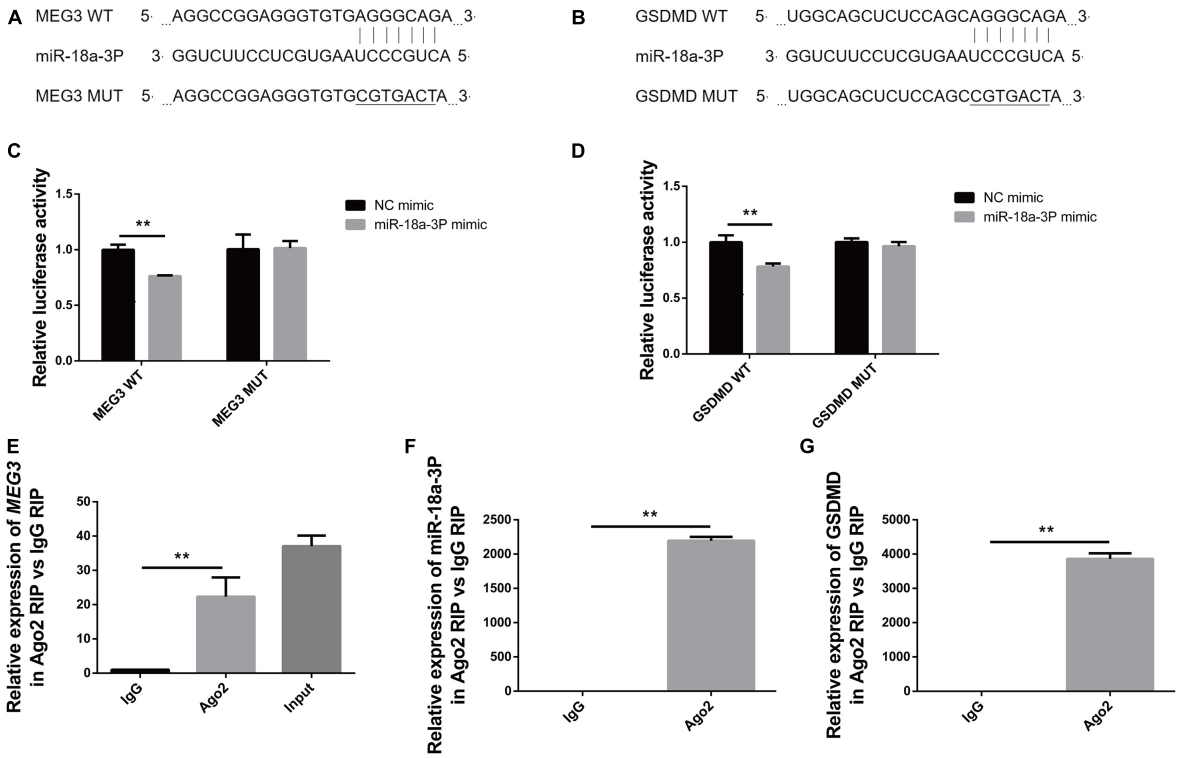

FIGURE 7 | *MEG3* directly binds to miR-18a-3p, and miR-18a-3p directly binds to GSDMD. **(A)** Binding and mutation sites of *MEG3* and miR-18a-3p bases. **(B)** Binding and mutation sites of miR-18a-3p and GSDMD bases. **(C)** Dual-luciferase activity of *MEG3* and miR-18a-3p. **(D)** Dual luciferase activity of miR-18a-3p and GSDMD. **(E)** Relative expression of *MEG3* in RIP assay. **(F)** Relative expression of miR-18a-3p in RIP assay. **(G)** Relative expression of GSDMD in RIP assay. $^{**}P < 0.01$, compared with the respective control group.

can reverse the inhibitory effect of si*MEG3* on pyroptosis in primary human TECs. Finally, we used a luciferase reporter gene and an RIP assay to evaluate the direct target-binding relationship between *MEG3* and miR-18a-3P, and between miR-18a-3P and GSDMD. Our results indicate that *MEG3* regulated GSDMD expression by acting as a ceRNA of miR-18a-3p.

In conclusion, we found that GSDMD-mediated TEC pyroptosis played an important role in the pathophysiological process of septic AKI. To the best of our knowledge, this study is the first to report that lnc can promote TEC pyroptosis by regulating the miR-18a-3p/GSDMD pathway. Our present study provides experimental and theoretical basis for further studies examining the mechanisms of renal TECs death in septic AKI, and provides a potential molecular target for clinical prevention and therapy. However, we only verified and explored the role and mechanism of *MEG3* in LPS-induced TEC pyroptosis. In our future studies, we will investigate this mechanism using additional *in vivo* models and clinical cases.

DATA AVAILABILITY STATEMENT

The original contributions presented in the study are included in the article/supplementary material, further inquiries can be directed to the corresponding author/s.

ETHICS STATEMENT

The animal study was reviewed and approved by Biomedical Ethics Committee of Chongqing Medical University. Written informed consent was obtained from the owners for the participation of their animals in this study.

AUTHOR CONTRIBUTIONS

JD and JY designed the experiments. JY supervised the whole project. JD performed the major research and wrote the manuscript. WT, QL, LL, and LZ provided the technical support. All authors contributed to the article and approved the submitted version.

FUNDING

This research was funded by grant (No. 81770682) from the National Natural Science Foundation of China, Chongqing Basic Research and Frontier Exploration Key Project (cstc2017jcyjBX0014), and Science and by grant from Technology Project of Chongqing Education Commission (KJQN202000439).

REFERENCES

Benetatos, L., Vartholomatos, G., and Hatzimichael, E. (2011). MEG3 imprinted gene contribution in tumorigenesis. *Int. J. Cancer* 129, 773–779. doi: 10.1002/ijc.26052

Bouchard, J., Acharya, A., Cerda, J., Maccariello, E. R., Madarasu, R. C., Tolwani, A. J., et al. (2015). A Prospective International Multicenter Study of AKI in the Intensive Care Unit. *Clin. J. Am. Soc. Nephrol.* 10, 1324–1331. doi: 10.2215/cjn.04360514

Braconi, C., Kogure, T., Valeri, N., Huang, N., Nuovo, G., Costinean, S., et al. (2011). microRNA-29 can regulate expression of the long non-coding RNA gene MEG3 in hepatocellular cancer. *Oncogene* 30, 4750–4756. doi: 10.1038/onc.2011.193

Broz, P., and Dixit, V. M. (2016). Inflammasomes: mechanism of assembly, regulation and signalling. *Nat. Rev. Immunol.* 16, 407–420. doi: 10.1038/nri.2016.58

Ding, B., Xu, S., Sun, X., Gao, J., Nie, W., and Xu, H. (2020). miR-18a-3p Encourages Apoptosis of Chondrocyte in Osteoarthritis via HOXA1 Pathway. *Curr. Mol. Pharmacol.* 13, 328–341. doi: 10.2174/1874467213666200204143740

Doitsh, G., Galloway, N. L., Geng, X., Yang, Z., Monroe, K. M., Zepeda, O., et al. (2014). Cell death by pyroptosis drives CD4 T-cell depletion in HIV-1 infection. *Nature* 505, 509–514. doi: 10.1038/nature12940

Feng, J., Li, M., Wei, Q., Li, S., Song, S., and Hua, Z. (2018). Unconjugated bilirubin induces pyroptosis in cultured rat cortical astrocytes. *J. Neuroinflamm.* 15:23. doi: 10.1186/s12974-018-1064-1

Fink, S. L., and Cookson, B. T. (2019). Pillars Article: Caspase-1-dependent pore formation during pyroptosis leads to osmotic lysis of infected host macrophages. *Cell Microbiol.* 8, 1812–1825.

Gyawali, B., Ramakrishna, K., and Dhamoon, A. S. (2019). Sepsis: the evolution in definition, pathophysiology, and management. *SAGE Open Med.* 7:2050312119835043. doi: 10.1177/2050312119835043

He, D., Zheng, J., Hu, J., Chen, J., and Wei, X. (2020). Long non-coding RNAs and pyroptosis. *Clin. Chim. Acta* 504, 201–208. doi: 10.1016/j.cca.2019.11.035

He, J. H., Han, Z. P., Liu, J. M., Zhou, J. B., Zou, M. X., Lv, Y. B., et al. (2017). Overexpression of Long Non-Coding RNA MEG3 Inhibits Proliferation of Hepatocellular Carcinoma Huh7 Cells via Negative Modulation of miRNA-664. *J. Cell Biochem.* 118, 3713–3721. doi: 10.1002/jcb.26018

Khajevand-Khazaei, M. R., Azimi, S., Sedighnejad, L., Salari, S., Ghorbanpour, A., Baluchnejadmojarad, T., et al. (2019). S-allyl cysteine protects against lipopolysaccharide-induced acute kidney injury in the C57BL/6 mouse strain: involvement of oxidative stress and inflammation. *Int. Immunopharmacol.* 69, 19–26. doi: 10.1016/j.intimp.2019.01.026

Krautwald, S., and Linkermann, A. (2014). The fire within: pyroptosis in the kidney. *Am. J. Physiol. Renal. Physiol.* 306, F168–9. doi: 10.1152/ajprenal.00552.2013

Lei, Z., Guo, H., Zou, S., Jiang, J., Kui, Y., and Song, J. (2021). Long non-coding RNA maternally expressed gene regulates cigarette smoke extract induced lung inflammation and human bronchial epithelial apoptosis via miR-149-3p. *Exp. Ther. Med.* 21:60. doi: 10.3892/etm.2020.9492

Li, B., Bai, L., Shen, P., Sun, Y., Chen, Z., and Wen, Y. (2017). Identification of differentially expressed microRNAs in knee anterior cruciate ligament tissues surgically removed from patients with osteoarthritis. *Int. J. Mol. Med.* 40, 1105–1113. doi: 10.3892/ijmm.2017.3086

Liang, J., Wang, Q., Li, J. Q., Guo, T., and Yu, D. (2020). Long non-coding RNA MEG3 promotes cerebral ischemia-reperfusion injury through increasing pyroptosis by targeting miR-485/AIM2 axis. *Exp. Neurol.* 325:113139. doi: 10.1016/j.expneurol.2019.113139

Liu, Y., Wang, J., Dong, L., Xia, L., Zhu, H., Li, Z., et al. (2019). Long Noncoding RNA HCP5 Regulates Pancreatic Cancer Gemcitabine (GEM) Resistance By Sponging Hsa-miR-214-3p To Target HDGF. *Onco Targets Ther.* 12, 8207–8216. doi: 10.2147/ott.S222703

Liu, Z., Wang, Y., Shu, S., Cai, J., Tang, C., and Dong, Z. (2019). Non-coding RNAs in kidney injury and repair. *Am. J. Physiol. Cell Physiol.* 317, C177–C188. doi: 10.1152/ajpcell.00048.2019

Mahmoud, A. D., Ballantyne, M. D., Miscianinov, V., Pinel, K., Hung, J., Scanlon, J. P., et al. (2019). The Human-Specific and Smooth Muscle Cell-Enriched LncRNA SMILR Promotes Proliferation by Regulating Mitotic CENPF mRNA and Drives Cell-Cycle Progression Which Can Be Targeted to Limit Vascular Remodeling. *Circ. Res.* 125, 535–551. doi: 10.1161/circresaha.119.314876

Miao, N., Yin, F., Xie, H., Wang, Y., Xu, Y., Shen, Y., et al. (2019). The cleavage of gasdermin D by caspase-11 promotes tubular epithelial cell pyroptosis and urinary IL-18 excretion in acute kidney injury. *Kidney Int.* 96, 1105–1120. doi: 10.1016/j.kint.2019.04.035

Na, L., Ding, H., Xing, E., Gao, J., Liu, B., Wang, H., et al. (2020). Lnc-MEG3 acts as a potential biomarker for predicting increased disease risk, systemic inflammation, disease severity, and poor prognosis of sepsis via interacting with miR-21. *J. Clin. Lab. Anal.* 34:e23123. doi: 10.1002/jcla.23123

Pang, X., Feng, G., Shang, W., Liu, L., Li, J., Feng, Y., et al. (2019). Inhibition of lncRNA MEG3 protects renal tubular from hypoxia-induced kidney injury in acute renal allografts by regulating miR-181b/TNF-α signaling pathway. *J. Cell Biochem.* 120, 12822–12831. doi: 10.1002/jcb.28553

Peerapornratana, S., Manrique-Caballero, C. L., Gómez, H., and Kellum, J. A. (2019). Acute kidney injury from sepsis: current concepts, epidemiology, pathophysiology, prevention and treatment. *Kidney Int.* 96, 1083–1099. doi: 10.1016/j.kint.2019.05.026

Poston, J. T., and Koyner, J. L. (2019). Sepsis associated acute kidney injury. *BMJ* 364:k4891. doi: 10.1136/bmj.k4891

Prowle, J. R., and Bellomo, R. (2015). Sepsis-associated acute kidney injury: macrohemodynamic and microhemodynamic alterations in the renal circulation. *Semin. Nephrol.* 35, 64–74. doi: 10.1016/j.semnephrol.2015.01.007

Rhodes, A., Evans, L. E., Alhazzani, W., Levy, M. M., Antonelli, M., Ferrer, R., et al. (2017). Surviving Sepsis Campaign: international Guidelines for Management of Sepsis and Septic Shock: 2016. *Intensive Care Med.* 43, 304–377. doi: 10.1007/s00134-017-4683-6

Sborgi, L., Rühl, S., Mulvihill, E., Pipercevic, J., Heilig, R., Stahlberg, H., et al. (2016). GSDMD membrane pore formation constitutes the mechanism of pyroptotic cell death. *EMBO J.* 35, 1766–1778. doi: 10.15252/embj.201694696

Shi, J., Zhao, Y., Wang, K., Shi, X., Wang, Y., Huang, H., et al. (2015). Cleavage of GSDMD by inflammatory caspases determines pyroptotic cell death. *Nature* 526, 660–665. doi: 10.1038/nature15514

Shum, H. P., Yan, W. W., and Chan, T. M. (2016). Recent knowledge on the pathophysiology of septic acute kidney injury: a narrative review. *J. Crit. Care* 31, 82–89. doi: 10.1016/j.jcrc.2015.09.017

Simion, V., Zhou, H., Haemmig, S., Pierce, J. B., Mendes, S., Tesmenitsky, Y., et al. (2020). A macrophage-specific lncRNA regulates apoptosis and atherosclerosis by tethering HuR in the nucleus. *Nat. Commun.* 11:6135. doi: 10.1038/s41467-020-19664-2

Singer, M., Deutschman, C. S., Seymour, C. W., Shankar-Hari, M., Annane, D., Bauer, M., et al. (2016). The Third International Consensus Definitions for Sepsis and Septic Shock (Sepsis-3). *JAMA* 315, 801–810. doi: 10.1001/jama.2016.0287

Song, P., Ye, L. F., Zhang, C., Peng, T., and Zhou, X. H. (2016). Long non-coding RNA XIST exerts oncogenic functions in human nasopharyngeal carcinoma by targeting miR-34a-5p. *Gene* 592, 8–14. doi: 10.1016/j.gene.2016.07.055

Søvik, S., Isachsen, M. S., Nordhuus, K. M., Tveiten, C. K., Eken, T., Sunde, K., et al. (2019). Acute kidney injury in trauma patients admitted to the ICU: a systematic review and meta-analysis. *Intensive Care Med.* 45, 407–419. doi: 10.1007/s00134-019-05535-y

Wang, H., Zhou, X., Li, H., Qian, X., Wang, Y., and Ma, L. (2017). Transient Receptor Potential Melastatin 2 Negatively Regulates LPS-ATP-Induced Caspase-1-Dependent Pyroptosis of Bone Marrow-Derived Macrophage by Modulating ROS Production. *Biomed. Res. Int.* 2017:2975648. doi: 10.1155/2017/2975648

Xue, Y. L., Zhang, S. X., Zheng, C. F., Li, Y. F., Zhang, L. H., Su, Q. Y., et al. (2020). Long non-coding RNA MEG3 inhibits M2 macrophage polarization by activating TRAF6 via microRNA-223 down-regulation in viral myocarditis. *J. Cell. Mol. Med.* 24, 12341–12354. doi: 10.1111/jcmm.15720

Yang, J. R., Yao, F. H., Zhang, J. G., Ji, Z. Y., Li, K. L., Zhan, J., et al. (2014). Ischemia-reperfusion induces renal tubule pyroptosis via the CHOP-caspase-11 pathway. *Am. J. Physiol. Renal Physiol.* 306, F75–F84. doi: 10.1152/ajprenal.00117.2013

Yang, R., Liu, S., Wen, J., Xue, L., Zhang, Y., Yan, D., et al. (2018). Inhibition of maternally expressed gene 3 attenuated lipopolysaccharide-induced apoptosis through sponging miR-21 in renal tubular epithelial cells. *J. Cell. Biochem.* 119, 7800–7806. doi: 10.1002/jcb.27163

Ye, Z., Zhang, L., Li, R., Dong, W., Liu, S., Li, Z., et al. (2019). Caspase-11 Mediates Pyroptosis of Tubular Epithelial Cells and Septic Acute Kidney Injury. *Kidney Blood Press. Res.* 44, 465–478. doi: 10.1159/000499685

Zha, F., Qu, X., Tang, B., Li, J., Wang, Y., Zheng, P., et al. (2019). Long non-coding RNA MEG3 promotes fibrosis and inflammatory response in diabetic nephropathy via miR-181a/Egr-1/TLR4 axis. *Aging* 11, 3716–3730. doi: 10.18632/aging.102011

Zhang, C. G., Yin, D. D., Sun, S. Y., and Han, L. (2017). The use of lncRNA analysis for stratification management of prognostic risk in patients with NSCLC. *Eur. Rev. Med. Pharmacol. Sci.* 21, 115–119.

Zhang, N., Zhong, Z., Wang, Y., Yang, L., Wu, F., Peng, C., et al. (2019). Competing endogenous network analysis identifies lncRNA Meg3 activates inflammatory damage in UVB induced murine skin lesion by sponging miR-93-5p/epiregulin axis. *Aging* 11, 10664–10683. doi: 10.18632/aging.102483

Zhang, Y., Liu, X., Bai, X., Lin, Y., Li, Z., Fu, J., et al. (2018). Melatonin prevents endothelial cell pyroptosis via regulation of long noncoding RNA MEG3/miR-223/NLRP3 axis. *J. Pineal Res.* 64:12449. doi: 10.1111/jpi.12449

Zhang, Z., Shao, X., Jiang, N., Mou, S., Gu, L., Li, S., et al. (2018). Caspase-11-mediated tubular epithelial pyroptosis underlies contrast-induced acute kidney injury. *Cell Death Dis.* 9:983. doi: 10.1038/s41419-018-1023-x

Zhou, J., Zhang, F., Lin, H., Quan, M., Yang, Y., Lv, Y., et al. (2020). The Protein Kinase R Inhibitor C16 Alleviates Sepsis-Induced Acute Kidney Injury Through Modulation of the NF-κB and NLR Family Pyrin Domain-Containing 3 (NLPR3) Pyroptosis Signal Pathways. *Med. Sci. Monit.* 26:e926254. doi: 10.12659/msm.926254

Zou, D. M., Zhou, S. M., Li, L. H., Zhou, J. L., Tang, Z. M., and Wang, S. H. (2020). Knockdown of Long Noncoding RNAs of Maternally Expressed 3 Alleviates Hyperoxia-Induced Lung Injury via Inhibiting Thioredoxin-Interacting Protein-Mediated Pyroptosis by Binding to miR-18a. *Am. J. Pathol.* 190, 994–1005. doi: 10.1016/j.ajpath.2019.12.013

Conflict of Interest: The authors declare that the research was conducted in the absence of any commercial or financial relationships that could be construed as a potential conflict of interest.

frontiers in Genetics

ORIGINAL RESEARCH
published: 23 September 2021
doi: 10.3389/fgene.2021.736156

Promising Epigenetic Biomarkers Associated With Cancer-Associated-Fibroblasts for Progression of Kidney Renal Clear Cell Carcinoma

Yongke You[1], *Yeping Ren*[1]*, *Jikui Liu*[2]* *and Jianhua Qu*[2]*

[1]Department of Nephrology, Shenzhen University General Hospital, Shenzhen, China, [2]Department of Hepatobiliary Surgery, Peking University Shenzhen Hospital, Shenzhen, China

Kidney renal clear cell carcinoma (KIRC) is the most common malignant kidney tumor as its characterization of highly metastatic potential. Patients with KIRC are associated with poor clinical outcomes with limited treatment options. Up to date, the underlying molecular mechanisms of KIRC pathogenesis and progression are still poorly understood. Instead, particular features of Cancer-Associated Fibroblasts (CAFs) are highly associated with adverse outcomes of patients with KIRC, while the precise regulatory mechanisms at the epigenetic level of KIRC in governing CAFs remain poorly defined. Therefore, explore the correlations between epigenetic regulation and CAFs infiltration may help us better understand the molecular mechanisms behind KIRC progression, which may improve clinical outcomes and patients quality of life. In the present study, we identified a set of clinically relevant CAFs-related methylation-driven genes, NAT8, TINAG, and SLC17A1 in KIRC. Our comprehensive *in silico* analysis revealed that the expression levels of NAT8, TINAG, and SLC17A1 are highly associated with outcomes of patients with KIRC. Meanwhile, their methylation levels are highly correlates with the severity of KIRC. We suggest that the biomarkers might contribute to CAFs infiltration in KIRC. Taken together, our study provides a set of promising biomarkers which could predict the progression and prognosis of KIRC. Our findings could have potential prognosis and therapeutic significance in the progression of KIRC.

Keywords: kidney renal clear cell carcinoma, cancer-associated fibroblasts, epigenetic regulation, DNA methylation, epigenetic biomarkers

OPEN ACCESS

Edited by:
Xiao-ming Meng,
Anhui Medical University, China

Reviewed by:
Qin Zhou,
The First Affiliated Hospital of Sun Yat-sen University, China
Cuiying He,
Fourth Hospital of Hebei Medical University, China

***Correspondence:**
Yeping Ren
renyeping@gmail.com
Jikui Liu
liu8929@126.com
Jianhua Qu
QJH@pkuszh.com

Specialty section:
This article was submitted to Epigenomics and Epigenetics, a section of the journal Frontiers in Genetics

Received: *06 July 2021*
Accepted: *08 September 2021*
Published: *23 September 2021*

Citation:
You Y, Ren Y, Liu J and Qu J (2021) Promising Epigenetic Biomarkers Associated With Cancer-Associated-Fibroblasts for Progression of Kidney Renal Clear Cell Carcinoma. Front. Genet. 12:736156. doi: 10.3389/fgene.2021.736156

INTRODUCTION

The global incidence of kidney cancer is increasing. Approximately 400,000 new cases of kidney cancer are diagnosed worldwide in 2018 (Bray et al., 2018; Hoefflin et al., 2020). KIRC is the most prevalent type of kidney cancer with an increasing prevalence (Frew and Moch, 2015). Among kidney cancers, KIRC is the leading cause of cancer-related death, mainly due to its highly metastatic potential and high relapse rate (Kaelin, 2009; Jemal et al., 2011; Jonasch et al., 2012). Meanwhile, KIRC is relatively resistant to traditional chemotherapy and radiotherapy (Jonasch et al., 2012). Therapeutic options for patients with metastatic KIRC are limited, and the prognosis remains dismal.

Up to now, there is a lack of biomarkers for diagnosis/prognosis prediction and drug targets for therapeutic intervention of KIRC. The overall prognosis of patients with KIRC is still limited, indicating the need for the improvement of therapeutic strategies directed at potential molecular targets (Li et al., 2017). Thus, it is essential and meaningful to identify reliable new biomarkers for better understand the prognosis and progression of KIRC, and further develop novel therapeutic strategies against KIRC.

Recent studies have emphasized the role of the tumor microenvironment or stromal infiltrates in tumor progression and response to various therapies of tumors. Stromal cell infiltration plays a crucial role in tumorigenesis, progression, metastasis, and clinical outcomes. Cancer-associated fibroblasts (CAFs) are of outstanding importance in tumor stromal infiltration. CAFs are the predominant and critical component in the tumor stromal, and their primary function is to provide a microenvironment for promoting tumor cell characteristics associated with increased aggressiveness. Cancer is associated with CAFs at all stages of cancer progression, including initiation, growth, and metastasis of tumor, and they are considered as a niche response to tissue damage caused by cancer cells. CAFs produce various tumor-associated components and play a role in regulating tumor extracellular matrix, tumor cell metabolism, and immune infiltration of the tumor microenvironment (Kalluri, 2016; Curtis et al., 2019). CAFs were proposed to have a protumor effect in kidney cancer. The study by Xu et al. showed that CAFs were involved in tumor progression by influencing cell proliferation, migration, and drug resistance in kidney tumors (Xu et al., 2015; Errarte et al., 2020). In particular, the symbiotic correlation between tumor cells and CAFs was proposed in KIRC, and CAFs seem to be involved in the initial phases of KIRC progression (Bakhtyar et al., 2013; López, 2013; Errarte et al., 2020). However, resulting from a lack of proper experimental models to study CAFs in KIRC, the role of CAFs in KIRC remains to be further explored.

DNA methylation is one of the widely studied epigenetic modifications (Egger et al., 2004; Feinberg, 2007; Bock and Lengauer, 2008) and plays crucial roles in tumorigenesis and progression across tumors. Furthermore, variation of DNA methylation status has been demonstrated to be associated with clinical features of patients with tumor (Morris and Maher, 2010; Morris and Latif, 2017). Previous studies have proposed that DNA methylation status contributes to progression and clinical outcomes of patients with kidney cancers suggesting that DNA methylation has the potential to be prognostic biomarkers and therapeutic targets for KIRC (Ellinger et al., 2011; Ricketts et al., 2014; Eggers et al., 2012; Patrício et al., 2013; Xiao et al., 2013; He et al., 2013). The aberrant DNA methylations have been shown as independent prognostic markers for kidney cancers (Yamada et al., 2006; Morris et al., 2010; Atschekzei et al., 2012; Van Vlodrop et al., 2017). DNA methylation status was proposed to have the potential to improve outcomes of patients with KIRC as well as diagnosis, prognosis, and clinical treatment of KIRC (Evelönn et al., 2019; Angulo et al., 2021). DNA methylation studies relevant to KIRC to date are still limited. No study has reported DNA methylation in CAFs-related genes as prognostic markers for patients with KIRC.

In the present study, we sought to investigate the potential role of CAFs-related DNA methylation genes in clinical outcomes of patients with KIRC. The CAFs-related DNA methylation genes were screened using database-based bioinformatic analysis, and their associations with clinical features were evaluated.

METHODOLOGY

Dataset Download and Processing

The gene expression, DNA methylation and relevant clinical datasets for human KIRC samples were generated by The Cancer Genome Atlas (TCGA). The RNA expression dataset was obtained from Xena UCSC, containing 530 cases (Goldman et al., 2018). The gene expression dataset of normal kidney tissues was downloaded from GTEx database (The Genotype-Tissue Expression project). The DNA methylation dataset was obtained from TCGA database and arranged using R language.

Gene Ontology Analysis

GO analysis was conducted according to differentially expressed genes using the R package clusterprofiler in R language. The GO terms included three categories: Biological process (BP), cellular component (CC) and molecular function (MF).

Stromal and Immune Infiltration Assessment

The stromal and immune infiltrations were evaluated by MCPCounter. Using MCPCounter R package in R, the stromal and immune cell infiltration levels of KIRC samples were calculated.

Eight immune cells and two stromal cells were quantified in human KIRC samples.

Correlation Analysis

To examine the correlation between DNA methylation status of relevant genes and their RNA expression, we performed correlation analysis using datasets from TCGA database. Spearman's correlation coefficient were performed to assess the strength of the relationship between two variables. The analysis was carried out using R language.

Survival Analysis

To examine the clinical significance of DNA methylation status of relevant genes and their RNA expression in KIRC, survival analysis was carried out. For transcriptional regulatory mechanism at epigenetic level, hypermethylation should be accompanied by a reduction of its gene expression. Conversely, hypomethylation should overlap with upregulation of its gene expression. We combined gene expression levels and their methylation status, and then the joint Kaplan-Meier survival analysis of methylation and expression was conducted. Kaplan-Meier analysis was performed and compared using the logrank test. A value of $p < 0.05$ was used to indicate statistical

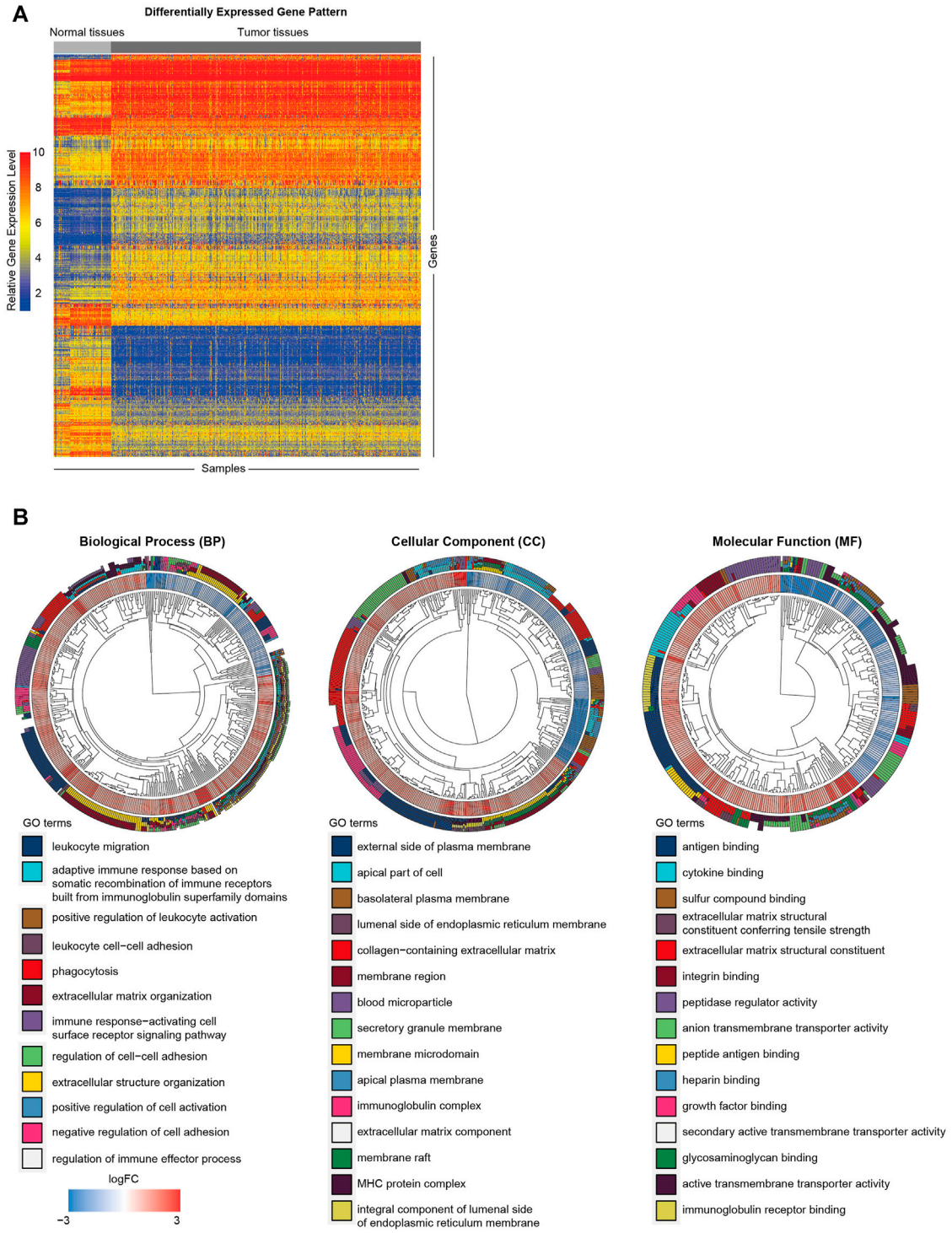

FIGURE 1 | Functional annotation of differentially expressed genes between KIRC tumor and normal tissues. **(A)** Heat map of differentially expressed gene analysis. The ordinate represents the differentially expressed genes while the normal and tumor samples is represented in the abscissa. The blue color indicates lower expression, and the red color indicates higher expression. **(B)** The GO analysis of differentially expressed genes between normal and tumor tissues.

significance. Bioinformatic analyses and statistical analyses were conducted using R language. Survival and survminer packages were used for Kaplan–Meier curves in R language. Survival package was used for computing survival analyses. Survminer package was used for summarizing and visualizing the results of survival analyses.

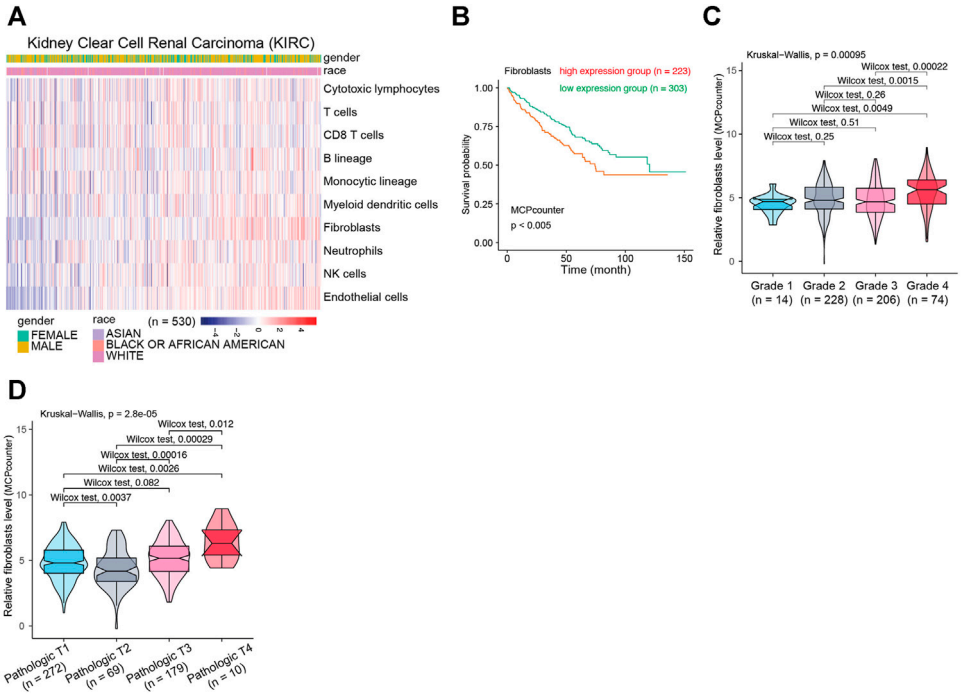

FIGURE 2 | The relationship between CAFs infiltration level and clinical features of patients with KIRC. **(A)** The evaluation of immune and stromal infiltration levels of KIRC based on MCPCounter algorithm. **(B)** Kaplan-Meier survival analysis according to infiltration level of CAFs in KIRC. **(C)** Association between CAFs infiltration level and KIRC histologic grade. **(D)** Association between CAFs infiltration level and KIRC pathological T grade.

Methylation-Driven Gene Screening

The correlations between DNA methylation status of relevant genes and their RNA expression levels were assessed using Spearman's correlation coefficient. $|r| > 0.3$ and $p < 0.05$ served as the screening threshold.

Statistical Analysis

Group comparisons in bioinformatic analysis were carried out by Wilcox test and Kruskal-Wallis test. We performed survival analysis using Kaplan-Meier method with the logrank test. Spearman's correlation test was performed to examine the correlation coefficients in the study. A value of $p < 0.05$ was used to indicate statistical significance.

RESULTS

Evaluation of Clinical Relevance of CAFs in KIRC

To clarify the biological functions of differentially expressed genes (**Figure 1A**) between normal and tumor tissues of KIRC, differential gene analysis was carried out using datasets from GTEx and TCGA databases. The corresponding relationship table between tumor samples and normal samples was downloaded from the differential analysis section of GEPIA database (http://gepia.cancer-pku.cn/help.html). The TCGA tumor samples, TCGA paired adjacent normal samples and GTEX normal samples were arranged and used for the analysis. Then gene ontology (GO) analysis was performed. The R package clusterprofiler was used for the analysis (Yu et al., 2012). As shown in **Figure 1B**, we observed that the tumor microenvironment-related terms (such as cell adhesion and extracellular matrix related terms) were significantly enriched in categories Biological process (BP), Cellular Component (CC) and Molecular Function (MF), respectively. These results suggested that tumor microenvironment changes might contribute to KIRC tumorigenesis. The importance of tumor microenvironment sets the basis for our following CAFs relevant study in KIRC. To specifically study the role of CAFs in KIRC, we firstly evaluated the infiltration level of CAFs in KIRC using MCPCounter (Becht et al., 2016). As shown in **Figure 2A**, the quantification of the abundance of eight immune cells and two stromal cells was performed using KIRC transcriptomic dataset downloaded from the TCGA database. In order to explore the importance of CAFs in KIRC, we performed a series of analyses to examine the relationship between CAFs and clinical features of KIRC. To investigate the correlation between CAFs and survival of patients with KIRC. We then examined the association between CAFs and the survival conditions of patients using Kaplan-Meier survival analysis. The survival analysis showed that the infiltration of CAFs was significantly negatively correlated with the overall survival of KIRC patients (**Figure 2B**, logrank test). We next investigated the relationship between CAFs and histologic grade. As shown in **Figure 2C**, a trend of positive correlation was observed between CAFs infiltration level and the histologic

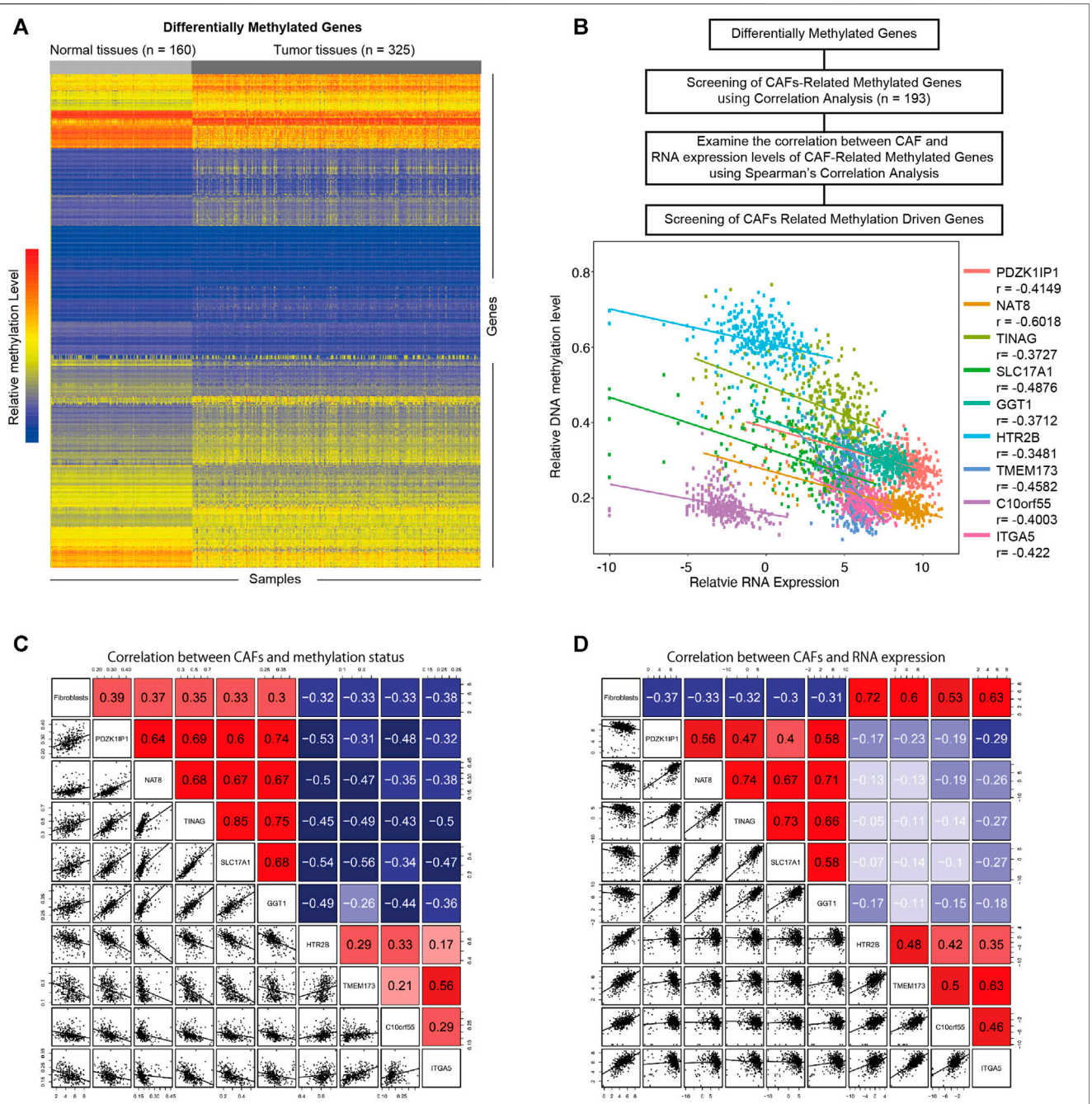

FIGURE 3 | Screening of CAFs related methylation-driven genes. **(A)** Heat map of differentially methylated gene analysis. The ordinate represents the differentially methylated genes while the normal and tumor samples is represented in the abscissa. The blue color indicates lower methylation levels, and the red color indicates higher methylation levels. **(B)** Flowchart of CAFs related methylation-driven genes screening (top). Spearman's correlation between RNA expression level of CAFs related methylation-driven genes and their methylation status (bottom). **(C)** Spearman's correlation between CAFs infiltration level and methylation status of CAFs related methylation-driven genes. **(D)** Spearman's correlation between CAFs infiltration level and RNA expression of CAFs related methylation-driven genes.

grade. Higher infiltration level of CAFs was accompanied by a relative higher tumor histologic grade than lower CAFs infiltration level. Furthermore, we examined the correlation between CAFs infiltration level and tumor stage. The result showed that CAFs infiltration level had a significant positive correlation with tumor T stage, referring to the size and extent of the primary tumor (**Figure 2D**). Meanwhile, the CAFs infiltration in KIRC was also evaluated using XCell (Aran et al., 2017). Similar outcomes were obtained. We observed a negative correlation between CAFs and survival of patients in Kaplan-Meier analysis (**Supplementary Figure S1A**), as well as positive correlations between CAFs and tumor histologic grade/tumor T

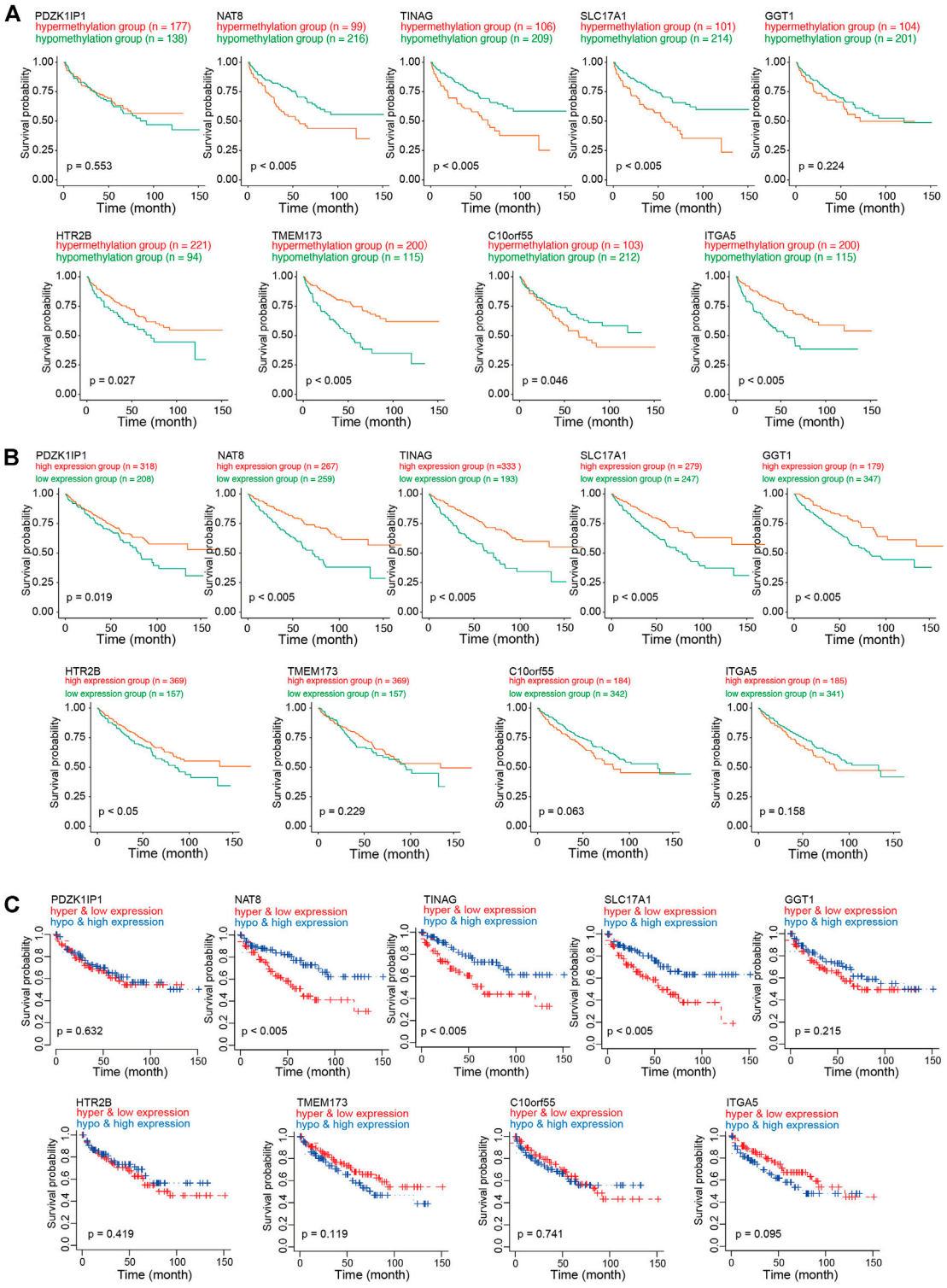

FIGURE 4 | Survival analysis of CAFs related methylation-driven genes in KIRC. **(A)** Kaplan-Meier survival analysis according to methylation status of CAFs related methylation-driven genes. **(B)** Kaplan-Meier survival analysis according to RNA expression of CAFs related methylation-driven genes. **(C)** Kaplan-Meier survival analysis of methylation status combine with RNA expression of CAFs related methylation-driven genes.

stage (**Supplementary Figures S1B,C**). Taken together, these findings suggest that increased CAFs infiltration was associated with aggressive clinical features of KIRC. All in all, results demonstrate that CAFs were involved in the progression and development of KIRC. Therefore, CAFs have potential clinical implication for diagnosis, prognosis, and treatment of KIRC.

Identification of CAFs-Related Methylation-Driven Genes in KIRC

To investigate the influence of DNA methylation on CAFs, we firstly identified differentially methylated genes in KIRC (**Figure 3A**) (|logFC | > 0.2, $p < 0.05$). Through the correlation analysis between methylation status and CAFs infiltration level, we screened the CAFs-related methylated genes. We then examine the correlations between the methylation level of CAFs-related methylated genes and their mRNA expression levels. According to a cutoff value of $r > 0.3$, $p < 0.05$. We identified nine CAFs-related methylation-driven genes (**Figure 3B**). Furthermore, the correlation between CAFs infiltration level and the methylation levels, as well as mRNA expression levels of CAFs-related methylation-driven genes, were shown in **Figures 3C,D**. We observed positive correlations between CAFs infiltration level and methylation status of PDZK1IP1, NAT8, TINAG, SLC17A1, and GGT1. Methylation status of HTR2B, TMEM173, C10orf55, and ITGA5 were negatively correlated with CAFs infiltration level. The correlations between CAFs infiltration level and RNA expression levels of CAFs-related methylation-driven genes were examined. In contrast, RNA expression levels of PDZK1IP1, NAT8, TINAG, SLC17A1, and GGT1 were demonstrated to exhibit negative correlations with CAFs infiltration level. RNA expression levels of HTR2B, TMEM173, C10orf55 and ITGA5 were positively correlated with CAFs infiltration level. Overall, we identified a set of CAFs-related methylation-driven genes that might contribute to the tumor microenvironment via regulating CAFs infiltration.

Survival Significance of CAFs-Related Methylation-Driven Genes

To investigate the role of CAFs-related methylation-driven genes on the survival of patients with KIRC, Kaplan-Meier survival analysis was performed using DNA methylation status of CAFs-related methylation-driven genes. Survival in high methylation and low methylation group was compared using the log-rank test to determine whether the difference was significant. As shown in **Figure 4A**, we observed significant differences in survivals according to the methylation status of NAT8, TINAG, SLC17A1, HTR2B, TMEM173, C10orf55, SLC17A1, and GGT1. The hypermethylation status of NAT8, TINAG, SLC17A1, and C10orf55 were accompanied by worse survival conditions of patients with KIRC. In contrast, we observed that the hypomethylation status of HTR2B, TMEM173, and ITGA5 were accompanied by worse survival conditions of patients with KIRC. We then examined the correlations between RNA expression of CAFs-related methylation-driven genes and survival of patients. As shown in **Figure 4B**, expression levels of PDZK1IP1, NAT8, TINAG, SLC17A1, GGT1, and HT2B were significantly positively associated with survival of patients with KIRC. Furthermore, we integrated the DNA methylation dataset with RNA expression profiling. We then assessed the correlation between methylation status/RNA expression of CAFs-related methylation-driven genes and survival of patients. Patients with hypermethylation status and low expression levels of NAT8, TINAG, and SLC17A1 demonstrated a significantly shorter survival compared with those with hypomethylation status and high expression levels (**Figure 4C**). These results suggest that NAT8, TINAG and SLC17A1 RNA expression levels and DNA methylation status are associated with the survival of patients with KIRC.

Clinical Significance of CAFs-Related Methylation-Driven Genes

To further illustrate the clinical role of NAT8, TINAG and SLC17A1, we assessed the correlations between NAT8, TINAG and SLC17A1, and clinical features. We observed that the DNA methylation levels of NAT8, TINAG and SLC17A1 were significantly associated with histologic grade and T stage of KIRC. The DNA methylation levels of NAT8, TINAG and SLC17A1were significantly higher in high-grade than in the low-grade of tumors (**Figure 5A**). A similar trend of correlation was observed in the T stage. As shown in **Figure 5B**, DNA methylation levels of NAT8, TINAG and SLC17A1 was accompanied by an increasing tumor T stage. We then examined the correlations between RNA expression levels of NAT8, TINAG and SLC17A1, and clinical features. In contrast, an opposite trend was observed for the analysis. RNA expression levels of NAT8, TINAG, and SLC17A1 were negatively correlated with histologic grade and the T stage of KIRC. Decreasing RNA expression levels of NAT8, TINAG, and SLC17A1 were associated with lower tumor grade of KIRC (**Figure 5C**). Meanwhile, a higher tumor T stage was accompanied by reductions of RNA expression levels of NAT8, TINAG, and SLC17A1 (**Figure 5D**). Taken together, We identified three clinically relevant CAFs-related methylation-driven genes containing NAT8, TINAG and SLC17A1. NAT8, TINAG, and SLC17A1 RNA expression levels and DNA methylation status are correlated with the histologic grade and T stage of patients with KIRC. We proposed that manipulation the expression of NAT8, TINAG and SLC17A1 at epigenetic level might contribute to CAFs-mediated KIRC severity.

DISCUSSION

In the present study, we evaluated the infiltration level of CAFs in KIRC based on a databased bioinformatic analysis. We observed the high correlations between CAFs and clinical features in KIRC. By correlating the methylation-driven genes in KIRC, the specific CAFs related methylation-driven genes were identified.

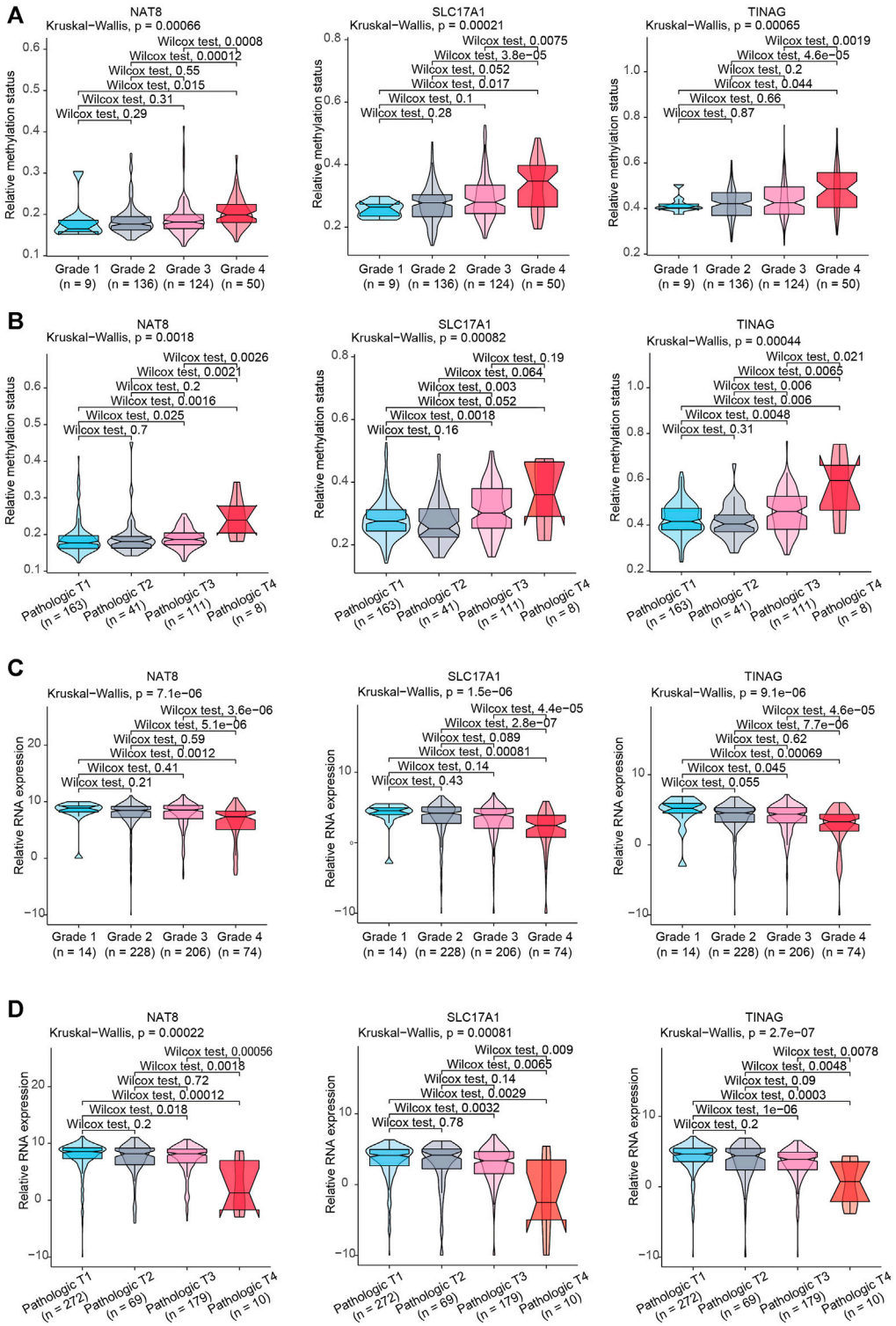

FIGURE 5 | Association between clinical features and NAT8, TINAG, and SLC17A1. **(A)** Association between KIRC histologic grade and methylation status of NAT8, TINAG, and SLC17A1. **(B)** Association between KIRC pathological T grade and methylation status of NAT8, TINAG, and SLC17A1. **(C)** Association between KIRC histologic grade and RNA expression levels of NAT8, TINAG, and SLC17A1. **(D)** Association between KIRC pathological T grade and RNA expression levels of NAT8, TINAG, and SLC17A1.

Furthermore, we identified three clinically relevant CAFs-related methylation-driven genes, NAT8, TINAG, and SLC17A1. The RNA expression and methylation status of NAT8, TINAG, and SLC17A1were highly involved in clinical features of KIRC.

NAT8 belongs to the GCN5-related N-acetyltransferase superfamily (Chambers et al., 2010) that transfer the acetyl group of acetyl-coenzyme A to an acceptor substrate (Dyda et al., 2000). It has been demonstrated that NAT8 was associated with kidney disease (Luo et al., 2021; Juhanson et al., 2008). NAT8 is specifically and almost exclusively expressed in the kidney and liver (**Supplementary Figure S2A**) (dataset from The Human Protein Atlas) (Uhlén et al., 2015). It has been proposed that NAT8 might contribute to kidney injury via influencing acetylation pathways (Chambers et al., 2010). To date, there have been relatively few studies relevant to the biological function of NAT8 in KIRC. In particular, no relevant study identified the biological role of NAT8 in CAFs-mediated tumor microenvironment alteration. In the present study, we identified the significant correlation between NAT8 expression and CAFs infiltration level, and its clinical importance in KIRC.

TINAG encodes an extracellular matrix protein that is expressed in tubular basement membranes. Mutation of the TINAG gene is involved in nephronophthisis via influencing cell survival (Xie et al., 2011). Consistent with the previous study, we observed that TINAG is highly enriched in the kidney at both RNA and protein levels (**Supplementary Figure S2B**; Kanwar et al., 1999). TINAG can interact with extracellular matrix proteins (Kalfa et al., 1994; Kumar et al., 1997; Kanwar et al., 1999). It is able to regulate the adhesion of epithelial cells from kidney tubules suggesting that TINAG is crucial for communication between the cell and extracellular microenvironment (Kalfa et al., 1994; Yoshioka et al., 2002). Our knowledge of the role of TINAG is still incomplete. Particularly, the understanding of its biological function in the tumor microenvironment of KIRC is still vague. This study identified the clinical significance of the TINAG RNA expression pattern and its DNA methylation in KIRC.

SLC17A1 is the solute carrier family 17 member 1 which is expressed on the apical membrane of renal tubular cells. As the first identified member family SLC17 phosphate transporter family, SLC17A1 is proposed to mediate sodium and inorganic phosphate co-transport and believed to be the voltage-driven organic anions transporter which is highly involved in renal insufficiency (Busch et al., 1996; Hollis-Moffatt et al., 2012; Iharada et al., 2010). However, the role of SLC17A1 in the tumor microenvironment is still unknown.

Various therapeutic strategies concentrating on the tumor microenvironment are being developed and implemented in recent years. Indeed, the clinical trials are already showing promising results in KIRC (Nunes-Xavier et al., 2019). Starting from the importance of CAFs in the tumor microenvironment, the analyses of our study explored the potential biomarkers involving CAFs infiltration. In particular, we identified a set of clinically relevant CAFs-related methylation-driven genes. We are not only aim to explore the biomarkers for CAFs infiltration but also more interested in its regulation at the epigenetic level. In conclusion, our study offers a layer of CAFs regulation at the epigenetic level that can change tumor microenvironment, also may provide a therapeutic strategy to affect CAFs infiltration via manipulating clinical relevant CAFs-related methylation-driven genes in KIRC.

We performed the whole analysis based on TCGA dataset, therefore, the limitations of TCGA database should be taken into account. A limitation of the study is the relatively small amount of the cohort of KIRC dataset in TCGA database. Another limitation is that the TCGA used the Illumina 450 k BeadChip array which interrogates only about 450,000 CpG dinucleotides which only partially contains the CpGs in human genome. The incomplete coverage of the data would significantly restrict the relevant epigenetic analysis and a big amount of information of modified genes are missed when we combined the gene expression dataset and DNA methylation dataset. This might result in an analysis bias. Therefore, an improvement is urgently needed to develop analysis strategy to better use the datasets.

DATA AVAILABILITY STATEMENT

The original contributions presented in the study are included in the article/**Supplementary Material**, further inquiries can be directed to the corresponding authors.

AUTHOR CONTRIBUTIONS

YY and JQ designed the study and wrote the manuscript. JQ, YY, and JL performed the bioinformatics analysis. JQ, YY, JL, and YR analyzed and interpreted the data. JL and YR revised the manuscript. All authors contributed to the article and approved the submitted version.

FUNDING

This research was supported by Research Start-up Foundation Shenzhen University (SZU) and Natural Science Foundation of Shenzhen University General Hospital (No. SUGH2020QD011, SUGH2020QD021), the Sanming Project of Medicine in Shenzhen (No. SZSM201612021) and The Science Technology and Innovation Committee of Shenzhen Municipality (20200814071107001).

SUPPLEMENTARY MATERIAL

The Supplementary Material for this article can be found online at: https://www.frontiersin.org/articles/10.3389/fgene.2021.736156/full#supplementary-material

REFERENCES

Angulo, J. C., Manini, C., López, J. I., Pueyo, A., Colás, B., and Ropero, S. (2021). The Role of Epigenetics in the Progression of clear Cell Renal Cell Carcinoma and the Basis for Future Epigenetic Treatments. *Cancers* 13, 2071. doi:10.3390/cancers13092071

Aran, D., Hu, Z., and Butte, A. J. (2017). xCell: Digitally Portraying the Tissue Cellular Heterogeneity Landscape. *Genome Biol.* 18. 220. doi:10.1186/s13059-017-1349-1

Atschekzei, F., Hennenlotter, J., Jänisch, S., Großhennig, A., Tränkenschuh, W., Waalkes, S., et al. (2012). SFRP1CpG Island Methylation Locus Is Associated with Renal Cell Cancer Susceptibility and Disease Recurrence. *Epigenetics* 7, 447–457. doi:10.4161/epi.19614

Bakhtyar, N., Wong, N., Kapoor, A., Cutz, J.-C., Hill, B., Ghert, M., et al. (2013). Clear Cell Renal Cell Carcinoma Induces Fibroblast-Mediated Production of Stromal Periostin. *Eur. J. Cancer* 49, 3537–3546. doi:10.1016/j.ejca.2013.06.032

Becht, E., Giraldo, N. A., Lacroix, L., Buttard, B., Elarouci, N., Petitprez, F., et al. (2016). Estimating the Population Abundance of Tissue-Infiltrating Immune and Stromal Cell Populations Using Gene Expression. *Genome Biol.* 17, 1–20. doi:10.1186/s13059-016-1070-5

Bock, C., and Lengauer, T. (2008). Computational Epigenetics. *Bioinformatics* 24, 1–10. doi:10.1093/bioinformatics/btm546

Bray, F., Ferlay, J., Soerjomataram, I., Siegel, R. L., Torre, L. A., and Jemal, A. (2018). Global Cancer Statistics 2018: GLOBOCAN Estimates of Incidence and Mortality Worldwide for 36 Cancers in 185 Countries. *CA: A Cancer J. Clinicians* 68, 394–424. doi:10.3322/caac.21492

Busch, A. E., Schuster, A., Waldegger, S., Wagner, C. A., Zempel, G., Broer, S., et al. (1996). Expression of a Renal Type I Sodium/phosphate Transporter (NaPi-1) Induces a Conductance in Xenopus Oocytes Permeable for Organic and Inorganic Anions. *Proc. the Natl. Acad. Sci.* 93, 5347–5351. doi:10.1073/pnas.93.11.5347

Chambers, J. C., Zhang, W., Lord, G. M., Van Der Harst, P., Lawlor, D. A., Sehmi, J. S., et al. (2010). Genetic Loci Influencing Kidney Function and Chronic Kidney Disease. *Nat. Genet.* 42, 373–375. doi:10.1038/ng.566

Curtis, M., Kenny, H. A., Ashcroft, B., Mukherjee, A., Johnson, A., Zhang, Y., et al. (2019). Fibroblasts Mobilize Tumor Cell Glycogen to Promote Proliferation and Metastasis. *Cel Metab.* 29, 141–155. doi:10.1016/j.cmet.2018.08.007

Dyda, F., Klein, D. C., and Hickman, A. B. (2000). GCN5-related N-Acetyltransferases: A Structural Overview. *Annu. Rev. Biophys. Biomol. Struct.* 29, 81–103. doi:10.1146/annurev.biophys.29.1.81

Egger, G., Liang, G., Aparicio, A., and Jones, P. A. (2004). Epigenetics in Human Disease and Prospects for Epigenetic Therapy. *Nature* 429, 457–463. doi:10.1038/nature02625

Ellinger, J., Holl, D., Nuhn, P., Kahl, P., Haseke, N., Staehler, M., et al. (2011). DNA Hypermethylation in Papillary Renal Cell Carcinoma. *BJU Int.* 107, 664–669. doi:10.1111/j.1464-410X.2010.09468.x

Errarte, P., Larrinaga, G., and López, J. I. (2020). The Role of Cancer-Associated Fibroblasts in Renal Cell Carcinoma. An Example of Tumor Modulation through Tumor/non-Tumor Cell Interactions. *J. Adv. Res.* 21, 103–108. doi:10.1016/j.jare.2019.09.004

Evelönn, E. A., Landfors, M., Haider, Z., Köhn, L., Ljungberg, B., Roos, G., et al. (2019). DNA Methylation Associates with Survival in Non-metastatic clear Cell Renal Cell Carcinoma. *BMC Cancer* 19. 65. doi:10.1186/s12885-019-5291-3

Feinberg, A. P. (2007). Phenotypic Plasticity and the Epigenetics of Human Disease. *Nature* 447, 433–440. doi:10.1038/nature05919

Frew, I. J., and Moch, H. (2015). A Clearer View of the Molecular Complexity of clear Cell Renal Cell Carcinoma. *Annu. Rev. Pathol. Mech. Dis.* 10, 263–289. doi:10.1146/annurev-pathol-012414-040306

Goldman, M., Craft, B., Hastie, M., Repečka, K., Kamath, A., McDade, F., et al. (2018). The UCSC Xena Platform for Public and Private Cancer Genomics Data Visualization and Interpretation. *bioRxiv*, 326470. doi:10.1101/326470

He, W., Li, X., Xu, S., Ai, J., Gong, Y., Gregg, J. L., et al. (2013). Aberrant Methylation and Loss of CADM2 Tumor Suppressor Expression Is Associated with Human Renal Cell Carcinoma Tumor Progression. *Biochem. Biophysical Res. Commun.* 435, 526–532. doi:10.1016/j.bbrc.2013.04.074

Hoefflin, R., Harlander, S., Schäfer, S., Metzger, P., Kuo, F., Schönenberger, D., et al. (2020). HIF-1α and HIF-2α Differently Regulate Tumour Development and Inflammation of clear Cell Renal Cell Carcinoma in Mice. *Nat. Commun.* 11. 4111, doi:10.1038/s41467-020-17873-3

Hollis-Moffatt, J. E., Phipps-Green, A. J., Chapman, B., Jones, G. T., van Rij, A., Gow, P. J., et al. (2012). The Renal Urate Transporter SLC17A1 Locus: Confirmation of Association with Gout. *Arthritis Res. Ther.* 14, R92. doi:10.1186/ar3816

Iharada, M., Miyaji, T., Fujimoto, T., Hiasa, M., Anzai, N., Omote, H., et al. (2010). Type 1 Sodium-dependent Phosphate Transporter (SLC17A1 Protein) Is a Cl−-dependent Urate Exporter. *J. Biol. Chem.* 285, 26107–26113. doi:10.1074/jbc.M110.122721

Jemal, A., Bray, F., Center, M. M., Ferlay, J., Ward, E., and Forman, D. (2011). Global Cancer Statistics. *CA: A Cancer J. Clinicians* 61, 69–90. doi:10.3322/caac.20107

Jonasch, E., Futreal, P. A., Davis, I. J., Bailey, S. T., Kim, W. Y., Brugarolas, J., et al. (2012). State of the Science: An Update on Renal Cell Carcinoma. *Mol. Cancer Res.* 10, 859–880. doi:10.1158/1541-7786.MCR-12-0117

Juhanson, P., Kepp, K., Org, E., Veldre, G., Kelgo, P., Rosenberg, M., et al. (2008). N-acetyltransferase 8, a Positional Candidate for Blood Pressure and Renal Regulation: Resequencing, Association and In Silico Study. *BMC Med. Genet.* 9. 25. doi:10.1186/1471-2350-9-25

Kaelin, W. G. (2009). Treatment of Kidney Cancer, *Cancer*, 115, 2262–2272. doi:10.1002/cncr.24232

Kalfa, T. A., Thull, J. D., Butkowski, R. J., and Charonis, A. S. (1994). Tubulointerstitial Nephritis Antigen Interacts with Laminin and Type IV Collagen and Promotes Cell Adhesion. *J. Biol. Chem.* 269, 1654–1659. doi:10.1016/s0021-9258(17)42077-1

Kalluri, R. (2016). The Biology and Function of Fibroblasts in Cancer. *Nat. Rev. Cancer* 16, 582–598. doi:10.1038/nrc.2016.73

Kanwar, Y. S., Kumar, A., Yang, Q., Tian, Y., Wada, J., Kashihara, N., et al. (1999). Tubulointerstitial Nephritis Antigen: An Extracellular Matrix Protein that Selectively Regulates Tubulogenesis vs. Glomerulogenesis during Mammalian Renal Development. *Proc. the Natl. Acad. Sci.* 96, 11323–11328. doi:10.1073/pnas.96.20.11323

Kuczyk, M., Steffens, S., Grosshennig, A., Becker, J. U., Hennenlotter, J., Stenzl, A., et al. (2012). Prognostic and Diagnostic Relevance of Hypermethylated in Cancer 1 (HIC1) CpG Island Methylation in Renal Cell Carcinoma. *Int. J. Oncol.* 40, 1650–1658. doi:10.3892/ijo.2012.1367

Kumar, A., Ota, K., Wada, J., Wallner, E. I., Charonis, A. S., Carone, F. A., et al. (1997). Developmental Regulation and Partial-Length Cloning of Tubulointerstitial Nephritis Antigen of Murine Metanephros. *Kidney Int.* 52, 620–627. doi:10.1038/ki.1997.375

Li, J.-K., Chen, C., Liu, J.-Y., Shi, J.-Z., Liu, S.-P., Liu, B., et al. (2017). Long Noncoding RNA MRCCAT1 Promotes Metastasis of clear Cell Renal Cell Carcinoma via Inhibiting NPR3 and Activating P38-MAPK Signaling. *Mol. Cancer* 16. 111. doi:10.1186/s12943-017-0681-0

López, J. I. (2013). Renal Tumors with clear Cells. A Review. *Pathol. - Res. Pract.* 209, 137–146. doi:10.1016/j.prp.2013.01.007

Luo, S., Surapaneni, A., Zheng, Z., Rhee, E. P., Coresh, J., Hung, A. M., et al. (2021). NAT8Variants, N-Acetylated Amino Acids, and Progression of CKD. *Cjasn* 16, 37–47. doi:10.2215/CJN.08600520

Morris, M. R., and Latif, F. (2017). The Epigenetic Landscape of Renal Cancer. *Nat. Rev. Nephrol.* 13, 47–60. doi:10.1038/nrneph.2016.168

Morris, M. R., and Maher, E. R. (2010). Epigenetics of Renal Cell Carcinoma: The Path towards New Diagnostics and Therapeutics. *Genome Med.* 2, 59. doi:10.1186/gm180

Morris, M. R., Ricketts, C., Gentle, D., Abdulrahman, M., Clarke, N., Brown, M., et al. (2010). Identification of Candidate Tumour Suppressor Genes Frequently Methylated in Renal Cell Carcinoma. *Oncogene* 29, 2104–2117. doi:10.1038/onc.2009.493

Nunes-Xavier, C. E., Angulo, J. C., Pulido, R., and López, J. I. (2019). A Critical Insight into the Clinical Translation of PD-1/PD-L1 Blockade Therapy in Clear Cell Renal Cell Carcinoma. *Curr. Urol. Rep.* 20. 1. doi:10.1007/s11934-019-0866-8

Patrício, P., Ramalho-Carvalho, J., Costa-Pinheiro, P., Almeida, M., Barros-Silva, J. D., Vieira, J., et al. (2013). Deregulation of PAX 2 Expression in Renal Cell

Tumours: Mechanisms and Potential Use in Differential Diagnosis. *J. Cel. Mol. Med.* 17, 1048–1058. doi:10.1111/jcmm.12090

Ricketts, C. J., Hill, V. K., and Linehan, W. M. (2014). Tumor-specific Hypermethylation of Epigenetic Biomarkers, Including SFRP1, Predicts for Poorer Survival in Patients from the TCGA Kidney Renal clear Cell Carcinoma (KIRC) Project. *PLoS One* 9, e85621. doi:10.1371/journal.pone.0085621

Uhlén, M., Fagerberg, L., Hallström, B. M., Lindskog, C., Oksvold, P., Mardinoglu, A., et al. (2015). Tissue-based Map of the Human Proteome. *Science* 347, 1260419. doi:10.1126/science.1260419

Van Vlodrop, I. J. H., Joosten, S. C., De Meyer, T., Smits, K. M., Van Neste, L., Melotte, V., et al. (2017). A Four-Gene Promoter Methylation Marker Panel Consisting of GREM1, NEURL, LAD1, and NEFH Predicts Survival of clear Cell Renal Cell Cancer Patients. *Clin. Cancer Res.* 23, 2006–2018. doi:10.1158/1078-0432.CCR-16-1236

Xiao, W., Wang, J., Li, H., Guan, W., Xia, D., Yu, G., et al. (2013). Fibulin-1 Is Down-Regulated through Promoter Hypermethylation and Suppresses Renal Cell Carcinoma Progression. *J. Urol.* 190, 291–301. doi:10.1016/j.juro.2013.01.098

Xie, P., Kondeti, V. K., Lin, S., Haruna, Y., Raparia, K., and Kanwar, Y. S. (2011). Role of Extracellular Matrix Renal Tubulo-Interstitial Nephritis Antigen (TINag) in Cell Survival Utilizing Integrin αvβ3/Focal Adhesion Kinase (FAK)/Phosphatidylinositol 3-Kinase (PI3K)/Protein Kinase B-Serine/Threonine Kinase (AKT) Signaling Pathway. *J. Biol. Chem.* 286, 34131–34146. doi:10.1074/jbc.M111.241778

Xu, Y., Lu, Y., Song, J., Dong, B., Kong, W., Xue, W., et al. (2015). Cancer-associated Fibroblasts Promote Renal Cell Carcinoma Progression. *Tumor Biol.* 36, 3483–3488. doi:10.1007/s13277-014-2984-8

Yamada, D., Kikuchi, S., Williams, Y. N., Sakurai-Yageta, M., Masuda, M., Maruyama, T., et al. (2006). Promoter Hypermethylation of the Potential Tumor suppressorDAL-1/4.1Bgene in Renal clear Cell Carcinoma. *Int. J. Cancer* 118, 916–923. doi:10.1002/ijc.21450

Yoshioka, K., Takemura, T., and Hattori, S. (2002). Tubulointerstitial Nephritis Antigen: Primary Structure, Expression and Role in Health and Disease. *Nephron* 90, 1–7. doi:10.1159/000046307

Yu, G., Wang, L.-G., Han, Y., and He, Q.-Y. (2012). ClusterProfiler: An R Package for Comparing Biological Themes Among Gene Clusters. *OMICS: A J. Integr. Biol.* 16, 284–287. doi:10.1089/omi.2011.0118

Conflict of Interest: The authors declare that the research was conducted in the absence of any commercial or financial relationships that could be construed as a potential conflict of interest.

Publisher's Note: All claims expressed in this article are solely those of the authors and do not necessarily represent those of their affiliated organizations, or those of the publisher, the editors and the reviewers. Any product that may be evaluated in this article, or claim that may be made by its manufacturer, is not guaranteed or endorsed by the publisher.

frontiers in Cell and Developmental Biology

ORIGINAL RESEARCH
published: 23 September 2021
doi: 10.3389/fcell.2021.737498

The RNA N6-Methyladenosine Methyltransferase METTL3 Promotes the Progression of Kidney Cancer via N6-Methyladenosine-Dependent Translational Enhancement of ABCD1

Yue Shi[1,2†], Yanliang Dou[1,2†], Jianye Zhang[3,4,5†], Jie Qi[1,2], Zijuan Xin[1,2], Mingxin Zhang[6], Yu Xiao[7] and Weimin Ci[1,2,8]*

[1] Key Laboratory of Genomic and Precision Medicine, China National Center for Bioinformation, Beijing Institute of Genomics, Chinese Academy of Sciences (CAS), Beijing, China, [2] University of Chinese Academy of Sciences, Beijing, China, [3] Department of Urology, Peking University First Hospital, Beijing, China, [4] Institute of Urology, Peking University, Beijing, China, [5] National Urological Cancer Center, Beijing, China, [6] Department of Urology, The Affiliated Hospital of Qingdao University, Qingdao, China, [7] Department of Pathology, Peking Union Medical College Hospital, Chinese Academy of Medical Sciences, Beijing, China, [8] Institute for Stem Cell and Regeneration, Chinese Academy of Sciences (CAS), Beijing, China

OPEN ACCESS

Edited by:
Xiao-ming Meng, Anhui Medical University, China

Reviewed by:
Carmen Jeronimo, Portuguese Oncology Institute, Portugal
Guihai Feng, Chinese Academy of Sciences (CAS), China

***Correspondence:**
Weimin Ci
ciwm@big.ac.cn

† These authors have contributed equally to this work

Specialty section:
This article was submitted to Epigenomics and Epigenetics, a section of the journal Frontiers in Cell and Developmental Biology

Received: *07 July 2021*
Accepted: *26 August 2021*
Published: *23 September 2021*

Citation:
Shi Y, Dou Y, Zhang J, Qi J, Xin Z, Zhang M, Xiao Y and Ci W (2021) The RNA N6-Methyladenosine Methyltransferase METTL3 Promotes the Progression of Kidney Cancer via N6-Methyladenosine-Dependent Translational Enhancement of ABCD1. Front. Cell Dev. Biol. 9:737498. doi: 10.3389/fcell.2021.737498

The role of N6-methyladenosine (m^6A)-modifying proteins in cancer progression depends on the cell type and mRNA affected. However, the biological role and underlying mechanism of m^6A in kidney cancer is limited. Here, we discovered the variability in m^6A methyltransferase METTL3 expression was significantly increased in clear cell renal cell carcinoma (ccRCC) the most common subtype of renal cell carcinoma (RCC), and high METTL3 expression predicts poor prognosis in ccRCC patients using a dataset from The Cancer Genome Atlas (TCGA). Importantly, knockdown of METTL3 in ccRCC cell line impaired both cell migration capacity and tumor spheroid formation in soft fibrin gel, a mechanical method for selecting stem-cell-like tumorigenic cells. Consistently, overexpression of METTL3 but not methyltransferase activity mutant METTL3 can promote cell migration, spheroid formation in cell line and tumor growth in xenograft model. Transcriptional profiling of m^6A in ccRCC tissues identified the aberrant m^6A transcripts were enriched in cancer-related pathways. Further m^6A-sequencing of METTL3 knockdown cells and functional studies confirmed that translation of ABCD1, an ATP-binding cassette (ABC) transporter of fatty acids, was inhibited by METTL3 in m^6A-dependent manner. Moreover, knockdown of ABCD1 in ccRCC cells decreased cancer cell migration and spheroid formation, and upregulation of ABCD1 acts as an adverse prognosis factor of kidney cancer patients. In summary, our study identifies that METTL3 promotes ccRCC progression through m^6A modification-mediated translation of ABCD1, providing an epitranscriptional insight into the molecular mechanism in kidney cancer.

Keywords: METTL3, kidney cancer, m^6A, ABCD1, cancer progression

INTRODUCTION

Globally, in 2018, there were an estimated 403,000 new cases of renal cell carcinoma (RCC) and 175,000 deaths (Bray et al., 2018). Inactivation of the von Hippel-Lindau tumor suppressor (pVHL) is the best-known oncogenic event in clear cell renal cell carcinoma (ccRCC) (Hsieh et al., 2017). VHL is critical for targeting the α-subunit of hypoxia-inducible factor (HIF) for oxygen-dependent proteolysis (Maxwell et al., 1999; Jaakkola et al., 2001), thus providing a direct molecular link between VHL-associated tumorigenesis and oxygen sensing via HIF. However, *Vhl* deletion in mice failed to elicit tumor formation (Rankin et al., 2006; Kapitsinou and Haase, 2008), suggesting that additional mechanisms are essential. Previous studies including ours have proven that ccRCC is also an epigenetic disease driven by DNA hypermethylation and aberrant histone modifications (Dalgliesh et al., 2010; Cancer Genome Atlas Research Network, 2013; Chen et al., 2016). Very recently, a third component has emerged: the so-called epitranscriptome which is defined as the chemical modifications of RNA that regulate and alter the activity of RNA molecules. It remains largely unknown whether RNA modifications are involved in kidney tumorigenesis. One study has showed that the mutation of *Vhl* and *TP53*, two most important genes in development of ccRCC is associated with the change of N6-methyladenosine (m^6A) regulatory genes (Zhou J. et al., 2019), suggesting that m^6A modification may play an important role in ccRCC. Exploring the epitranscriptomic mechanisms during kidney tumorigenesis may lead to new promising therapeutic strategies.

One of the best-studied RNA modifications linked to cancer is m^6A, which influences a broad spectrum of functions in RNA metabolism, including RNA stability, splicing, processing, localization, and translation initiation (Fu et al., 2014; Roundtree et al., 2017; Huang et al., 2020a). Actually, m^6A installed by the m^6A methyltransferases complex is a dynamical and reversible biological process. m^6A modifications of a transcript are deposited by "writers," the methyltransferase complex, which is composed of two core components METTL3 and METTL14 (Bokar et al., 1997; Liu et al., 2014), and other accessory regulatory subunits, such as WTAP, and KIAA1429 (Ping et al., 2014; Schwartz et al., 2014), and catalyzed by the demethylases, or erasers for depositing and removing them, including FTO and ALKBH5 (Jia et al., 2011; Zheng et al., 2013). And it can be recognized by m^6A-binding proteins known as "readers" such as YTHDF1/2, YTHDC1/2 (Du et al., 2016; Xiao et al., 2016; Hsu et al., 2017).

In addition, METTL3 as the first discovered core methyltransferase subunit, plays a major catalytic role in m^6A methylation process. It was first discovered in 1997 isolated from a HeLa cell nuclear extract that exhibited methyltransferase activity (Bokar et al., 1997; Liu et al., 2014). As the core catalytic component in the methyltransferase complex, loss of METTL3 disrupts numerous physiological processes such as spermatogenesis (Xu et al., 2017), hematopoiesis (Lee et al., 2019), embryonic development (Aguilo et al., 2015), T cell homeostasis (Li H. B. et al., 2017), and memory formation (Zhang et al., 2018). In addition, METTL3 functions as an oncogene or a suppressor gene in many types of cancers by affecting different m^6A levels of target RNAs (Cui et al., 2017; Vu et al., 2017; Chen et al., 2018; Cheng et al., 2019; Lan et al., 2019; Wanna-Udom et al., 2020). Although, Li X. et al. (2017) has reported that low expression of METTL3 was related to activations of adipogenesis and mTOR pathways in ccRCCs, the molecular mechanism of METTL3 in regulating of kidney cancer progression via an m^6A methyltransferase dependent manner remains largely unclear.

Herein, we compared the m^6A mRNA profiles between normal and ccRCC cancer tissues and characterized a significant association between m^6A and kidney cancer progression. Mechanistically, we identified that METTL3 promotes tumor migration and tumor spheroid formation (stem-cell-like tumorigenic cells), and ABCD1 is an m^6A target of METTL3 to treat or prevent kidney cancer metastases. Collectively, our results indicate that METTL3 is a candidate therapeutic target that compromises stem-like tumorigenic cells.

MATERIALS AND METHODS

Clear Cell Renal Cell Carcinoma Specimens and Cell Lines

Primary ccRCC and adjacent kidney tumor samples from two patients involved in this study were obtained from Peking Union Medical College Hospital after pathologic diagnosis. The study was approved by the Ethics Committee of our institutes. Informed consent was obtained from each participant. The ccRCC cell lines used in this study, A498 and 786-O were cultured in DMEM medium (HyClone), 10% fetal bovine serum (FBS, BI), 100 U/ml penicillin, and 100 μg/ml streptomycin in a humidified atmosphere with 5% CO_2 at 37°C.

Establishment of Stable Knockdown and Overexpression Cells

Stable knockdown of target genes was achieved by lentivirus-based short hairpin RNA delivery. The sequences that resulted in successful knock down are shown in **Supplementary Table 1**. Overexpression cells were established by using a modified pLVX-IRES-ZsGreen plasmid. The wild-type and mutant METTL3 plasmids were kindly provided by Pro. Yungui Yang (Beijing Institute of Genomics, Chinese Academy of Sciences) (Yang et al., 2019). Lentiviruses were packaged in HEK293T cells through cotransfecting every shRNA plasmid with packing vectors (PsPAX2, pMD2.G) by X-tremeGENE^{TM} Transfection Reagents (Roche). The lentivirus particles were harvested at 24 and 48 h and directly infected A498 cells under polybrene for 24 h after passage through 0.45 μm syringe filters (Corning). Then, transfected A498 cells were selected for 7 days using 2 μg/ml puromycin or 10 μg/ml blasticidin.

RNA Extraction and Quantitative PCR Analysis

Total RNA was extracted by using TRIzol reagent (Invitrogen) following the manufacturer's protocol. For mRNA expression quantification, 1 μg of total RNA was converted to cDNA

using the RevertAid First Strand cDNA Synthesis Kit (Invitrogen). Quantitative real-time PCR using the KAPA SYBR FAST Universal qPCR Kit (Applied Biosystems) was performed on a 7500 Fast Real-time PCR system (Applied Biosystems). Quantitative PCR primers sequences are listed in **Supplementary Table 1**.

Western Blot Analysis

Western blot analysis was performed following the standard protocol. Total protein from the cell lines was prepared with ice-cold cell lysis buffer (Beyotime Institute of Biotechnology) and quantified using BCA protein assay reagent (Thermo). The primary antibodies used in this study are shown in **Supplementary Table 2**.

Liquid Chromatography-Tandem Mass Spectrometry

In brief, 100–200 ng of mRNA was digested by 0.1 U Nuclease P1 (Sigma) and 1.0 U Calf Intestinal Phosphatase (New England Biolabs) and incubated at 37°C overnight. The sample was then filtered (MW cutoff: 3 kDa, Pall, Port Washington), and subjected to LC-MS/MS. The nucleosides were separated by reversed-phase ultra-performance liquid chromatography on an Agilent C18 column with online mass spectrometry detection using a G6410B triple quadrupole mass spectrometer (Agilent Technologies) in the positive ion mode. The m^6A levels were calculated as the ratio of m^6A to A based on the calibrated concentrations according to the standard curve obtained from pure nucleoside standards running with the same batch of samples.

N6-Methyladenosine ELISA

To detect overall levels of m^6A in different samples, the m^6A ELISA (EpiGentek) was performed according to the manufacturer's instructions. In brief, about 300 ng of total RNA was used as an input. Then RNA samples were captured and detected by spectrophotometer (Bio-Rad) at 450 nm. The level of m^6A methylation was calculated according to the manufacturer's instructions.

Cell Viability Assay

We used CCK8 assay (Lab Lead) to study the impact of METTL3 knock down in A498 and 786-O cell lines. The cells were seeded in 96-well plates in a density of 1000 cells/well and were cultivated at 37°C in 5% CO_2. The cell viability was then measured at 24, 48, and 72 h time point.

Transwell Migration Assay

Transwell migration assays were performed using 24-well Transwell inserts with an 8 μm pore size (Corning). Briefly, in total, 1×10^4 cells in 200 μl of culture medium without FBS were added to the upper chamber, while 500 μl of medium supplemented with 10% FBS was added to the lower chamber and incubated for 12–24 h at 37°C. The cells invading the lower chamber were fixed with 4% paraformaldehyde for 30 min, stained with 0.1% crystal violet solution for 30 min at room temperature, and counted under an upright microscope (five fields per chamber).

Cell Invasion Assay

For cell invasion assay, BioCoat™ Matrigel invasion chamber was used according to the manufacturer's instruction (Corning). Briefly, 2×10^4 cells were resuspended in 200 μl of DMEM medium without FBS, and seeded in the upper portion of the invasion chamber. The lower portion of the chamber contained 500 μl of medium supplemented with 10% FBS. After 16–24 h, non-invasive cells were removed from the upper surface of the membrane with a cotton swab. The invasive cells on the lower surface of the membrane were stained with crystal violet, and counted in four separate areas with an upright microscope.

Three-Dimensional Fibrin Gel Culture of Tumor Cells

A 3D fibrin gel culture was performed according to a previously described method (Liu et al., 2012). Briefly, fibrinogen (Sea Run Holdings) was dissolved in T7 buffer (pH 7.4, 50 mM Tris, 150 mM NaCl) to obtain a concentration of 2 mg/ml. The proper volume of the fibrinogen solution and the cell solution were mixed, resulting in 1 mg/ml (90 Pa) fibrinogen. Fifty microliters of cell/fibrinogen mixtures was seeded into each well of a 96-well plate with 1 μl of thrombin (0.1 U/μl) and then incubated at 37°C for 30 min. Finally, 200 μl of DMEM containing 10% FBS and antibiotics was added to the plate. After culture for 1, 3, or 5 days, the cells were counted by an upright microscope.

Tumor Xenograft Model

A498 cells (1×10^6 cells) were resuspended in 100 μl of PBS and subcutaneously injected into the axillary fossa of nude mice (BALB/c-nude, 4 weeks old). The tumor volume was calculated with the formula $V = 0.5\ ab^2$, where a is the longest tumor axis and b is the shortest tumor axis. The animal protocol was approved by the animal ethics committee of the Beijing Institute of Genomics, Chinese Academy of Sciences.

m^6A-RNA Immunoprecipitation Sequencing and MeRIP-qPCR

The MeRIP experiment was performed according to the reported protocols. Briefly, total RNA was extracted by TRIzol reagent (Invitrogen). mRNA was isolated by a Dynabeads® mRNA Purification Kit (Invitrogen) and fragmented to approximately 100 nt by an RNA fragmentation kit (Ambion). The m^6A primary antibody (Synaptic Systems) was incubated with Pierce™ Protein A Magnetic Beads (Thermo Fisher Scientific) for 1 h at 4°C. The fragmented RNA (∼100 nt) was incubated with the antibody-bead mixture for 4 h at 4°C and then washed five times with IP buffer. The samples were eluted with m^6A nucleotide solution and purified with the phenol-chloroform method. For high-throughput sequencing, the purified RNA fragments from MeRIP and the input RNA were used for library construction with the KAPA Stranded RNA-Seq Library Preparation Kit and sequenced with Illumina HiSeq X Ten. For MeRIP-qPCR, the relevant enrichment of m^6A of ABCD1 in each sample was analyzed by RT-qPCR.

Dual Luciferase Reporter Assay

Cells were seeded into the individual wells of a six-well plate and co-transfected with vectors according to the X-tremeGENE™ Transfection Reagents (Roche) protocol. After 48 h, the firefly and Renilla luciferase activities were measured by a Dual Luciferase Reporter Assay System (Promega). Each group was analyzed in triplicate.

N6-Methyladenosine-miCLIP–Seq

Single-nucleotide-resolution mapping of m^{6}A of A498 cells was carried out according to previously published studies (Chen et al., 2015; Linder et al., 2015) with some modifications. Briefly, the mRNA of A498 cells were purified by Dynabeads mRNA Purification Kit (Life Technologies) and fragmented to about 100 nt by the fragmentation reagent (Life Technologies). 2 μg of fragmented mRNAs were incubated with 5 μg of anti-m6A antibody (Abcam) in 300 μl immunoprecipitation buffer (50 mM Tris, pH 7.4, 100 mM NaCl, 0.05% NP-40) at 4°C for 2 h. The mixture was then irradiated three times with 0.15 Jcm^{-2} at 254 nm by a CL-1000 Ultraviolet Crosslinker (UVP), and then incubated with Dynabeads Protein A (Life Technologies) at 4°C for 2 h. After washing, end-repair and linker ligation, the enriched RNA were isolated from the beads by proteinase K digestion, and extracted by phenol–chloroform. Purified RNAs were reverse transcribed by Superscript III reverse transcriptase (Life Technologies). The cDNA from last step was with size selection on a 6% TBE-Urea gel (Life Technologies), and circularization and re-linearization by CircLigase II (Epicenter) and *Bam*HI (NEB), respectively. Then the cDNA was amplified by AccuPrime SuperMix 1 enzyme (Life Technologies) for 20 cycles and sequenced by Illumina HiSeq X Ten according to the manufacturer's instructions.

Bioinformatic Analysis

In order to measure the variance of gene expression, we calculated the coefficient of expression variation by using the standard deviation divided by the mean (Brown, 1998).

Sequencing reads were aligned to the human genome GRCh37/hg19 by HISAT2, and the m^{6}A peaks were detected by MACS peak-calling software (version 2.1.2) with the default options except for "–nomodel, –keepdup all." A stringent cutoff threshold for a q-value of 1×10^{-5} was used to obtain high-confidence peaks. m^{6}A motifs were identified by using Homer software. Differential gene expression was calculated by R package DEseq2 using HT-seq reads of input samples counted by HT-Seq python package (version 0.9.1), with a fold-change cutoff of 2.0 and a p-value cutoff of 5×10^{-2}. Gene ontology (GO) analysis was performed using Metascape (Zhou Y. et al., 2019), and GO terms with $p < 0.05$ were defined as significant. Network analysis was performed using ConsensusPathDB (CPDB) software (Kamburov et al., 2013; Herwig et al., 2016).

Statistical Analysis

All the data related to cell and animal experiments were evaluated with GraphPad Prism software. Measured data are represented as the mean ± standard deviation (SD). Unpaired parametric two-tailed Student's t-test was used to calculate statistical significance. Overall survival was analyzed with the Kaplan-Meier method using the log-rank test to determine significance. p-values < 0.05, p-values < 0.01 and p-values < 0.001 were considered statistically significant (*, **, ***).

RESULTS

The Expression Variability of N6-Methyladenosine-Modifying Genes, Especially METTL3, Is Increased in Clear Cell Renal Cell Carcinoma

To explore the potential role of m^{6}A modification in ccRCC, we first examined the mean expression of m^{6}A-modifying genes using RNA-seq data from The Cancer Genome Atlas (TCGA). We found that the mean expression of either the m^{6}A-modifying gene set (**Figure 1A**) or each individual gene (data not shown) did not change significantly in the tumor tissues compared to the normal tissues. However, tumors comprise a heterogeneous collection of cells that can differentially promote progression, metastasis and drug resistance. Intratumor and/or intertumor variability in gene expression has been increasingly shown to be functionally important. Consistent with this scenario, the expression variance of multiple m^{6}A-modifying genes especially METTL3, significantly increased during kidney tumorigenesis (**Figures 1B,C**). Indeed, according to Li X. et al. (2017) and Zhou J. et al. (2019) studies, the expression level of METTL3 with high copy number variations showed large heterogeneity in different ccRCC cohorts. To further confirm this finding, we detected the m^{6}A-modifying protein levels of seven pairs of tumor and adjacent normal tissues. The expression of m^{6}A-related proteins between the normal and tumor tissues varied among the patients, and the variance of METTL3 was the most dramatic (**Figure 1D**). Kaplan-Meier analysis showed that patients with increased METTL3 expression had a poor overall survival in TCGA Kidney Clear Cell Carcinoma (TCGA-KIRC) cohort (**Figure 1E**), indicating its role in promoting kidney tumorigenesis.

METTL3 Promotes Clear Cell Renal Cell Carcinoma Progression in an m^{6}A-Methyladenosine Methyltransferase-Dependent Manner

To further investigate the roles of METTL3 in ccRCC, we established a stable METTL3 knockdown cell line in A498 and 786-O cells (**Figure 2A**). Liquid chromatography-tandem mass spectrometry (LC-MS/MS) and ELISA assay confirmed that the level of m^{6}A in the shMETTL3-1 and shMETTL3-2 cells was significantly decreased (**Figure 2B** and **Supplementary Figure 1A**). Functionally, knockdown of METTL3 reduced the cell viability and suppressed their ability in cell migration and invasion (**Supplementary Figures 1B,C** and **Figure 2C**). While overexpression of METTL3 but not the kinase inactive mutant METTL3 promoted (**Figure 2D**). Additionally, stable

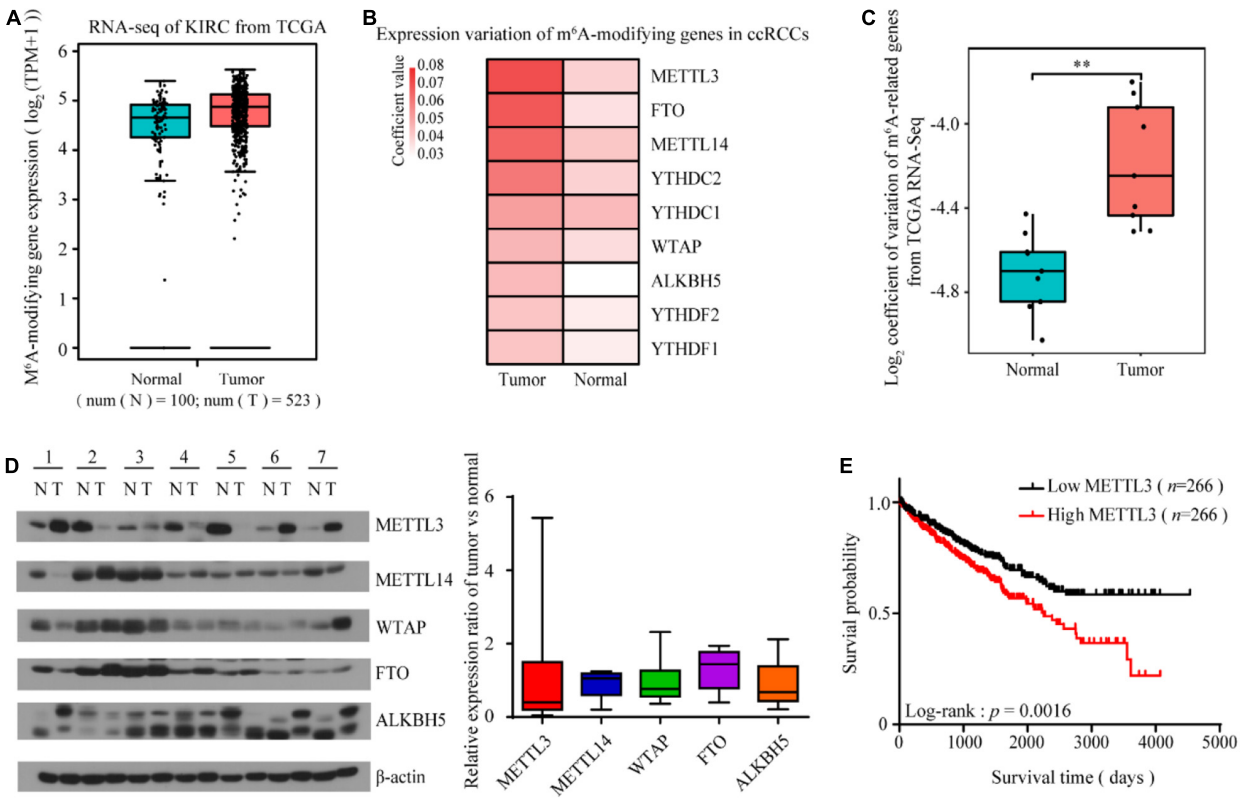

FIGURE 1 | The expression variability of m^{6}A-modifying genes is increased in ccRCC, especially METTL3. **(A)** The mean expression of the m^{6}A-modifying gene set was not significantly changed in the ccRCC tumor tissues compared to the normal tissues from TCGA Data Portal. **(B,C)** The coefficient of expression variation of m^{6}A-modifying genes in the ccRCC tumor tissues compared to the normal tissues (unpaired two samples Wilcoxon test). **(D)** The protein levels of m^{6}A-modifying proteins in seven paired tumor tissues and matched normal tissues from ccRCC patients was determined by western blots (left). β-actin was used as a loading control. The relative expression ratio of m^{6}A-modifying proteins between tumors and normal tissues after normalization to β-actin expression (right). **(E)** Kaplan-Meier survival curves using TCGA Data Portal showed that the expression level of METTL3 can predict the clinical outcome of ccRCC patients. *p*-values were calculated by the log-rank test. *n*, the number of cases. $^{**}P < 0.01$.

knockdown of METTL3 effectively suppressed tumor growth as reflected by the significant reduction of tumor size when compared with the shRNA control (**Figures 2E,F**). But the overexpression of METTL3 rather than the kinase inactive mutant METTL3 could promote the tumor growth *in vivo* xenograft tumor mice models (**Figures 2G,H**). Therefore, METTL3 is required for kidney cancer progression in an m^{6}A methyltransferase-dependent manner.

METTL3 Is Critical for Stem Cell-Like Tumor-Repopulating Cell Maintenance

To further evaluate the functional consequences of the expression variability of METTL3 and identify specific subpopulations that are phenotypically relevant to tumor progression, we used a soft three dimensional (3D) fibrin gel culture system to generate stem cell-like tumor-repopulating cells (TRCs) (Liu et al., 2012; Liu J. et al., 2018). Similarly, A498 ccRCC cells were trapped individually in the gel and grew into spheroid-like shapes resembling stem-like TRCs (**Figure 3A**). Notably, the protein level of METTL3 was higher in the TRCs than in the 2D rigid dish-cultured cells (**Figure 3B**). To further test whether the spheroids formed in the soft 3D fibrin gel may share some features of a stem cell, we examined a panel of stem cell markers by RT-qPCR. Consistently, we found that the gene expression of METTL3 was also upregulated in the cells cultured in the soft 3D fibrin gel (**Figure 3C**). Furthermore, a panel of stem cell makers, Nanog, Nestin, Oct4, and Sox2, were also upregulated in the cells from the soft 3D fibrin gel compared with the control cells (**Figure 3C**). More importantly, knockdown of METTL3 compromised the colony formation of TRC spheroids, and overexpression of METTL3 but not the kinase inactive mutant METTL3 promoted colony formation (**Figures 3D,E**). Therefore, METTL3 is also required for TRC colony formation in an m^{6}A methyltransferase-dependent manner.

M^{6}A-Methyladenosine Methylomes Are Profoundly Reprogrammed During Clear Cell Renal Cell Carcinoma Tumorigenesis

We next sought to determine the m^{6}A-dependent mechanism by which METTL3 loss impedes ccRCC progression. First, we evaluated the genome-wide m^{6}A methylomes during ccRCC tumorigenesis by m^{6}A sequencing (MeRIP-seq) with the tumor

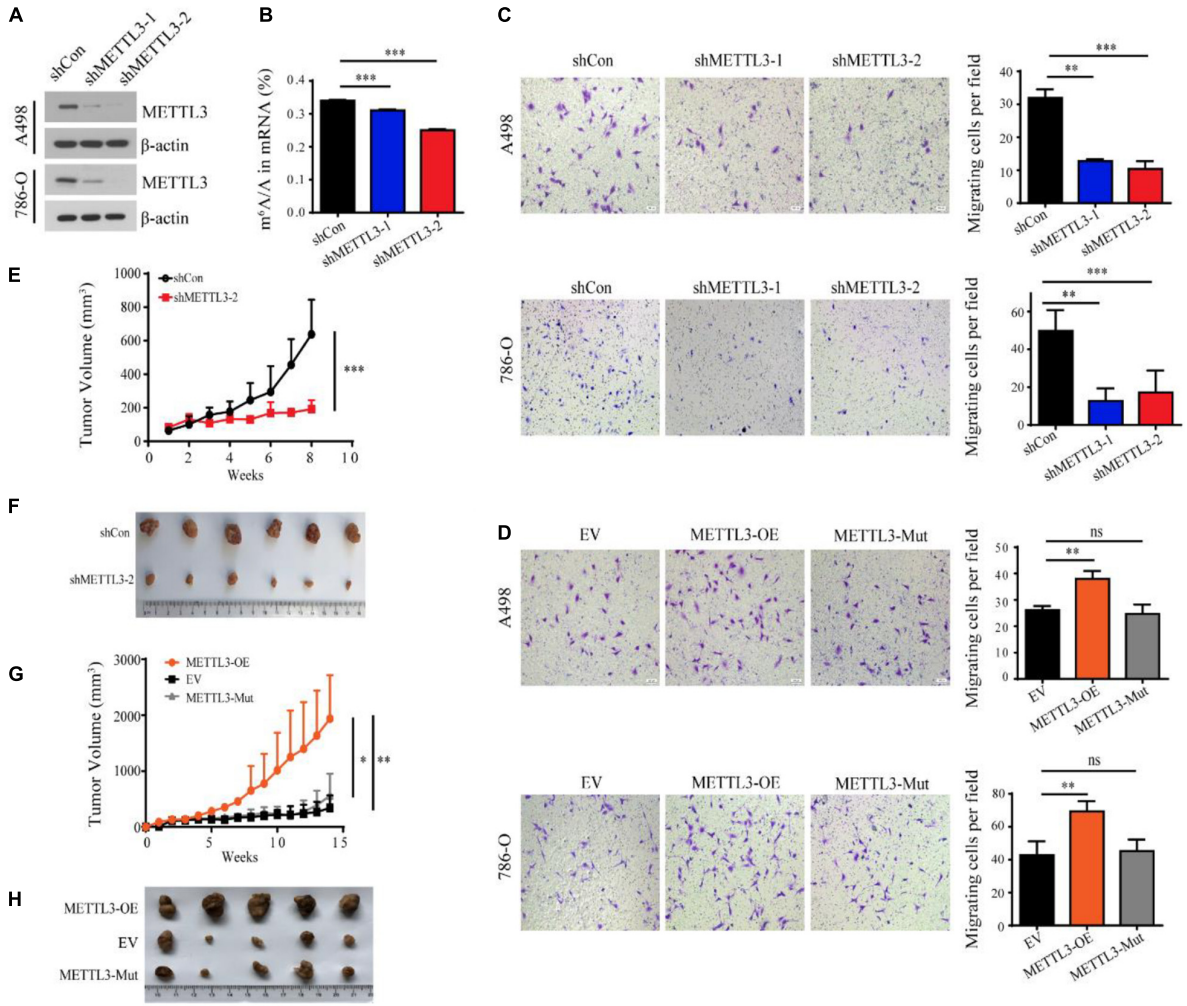

FIGURE 2 | METTL3 promotes ccRCC progression in an m^{6}A methyltransferase-dependent manner. **(A)** Western blot of METTL3 in A498 and 786-O cells transduced with lentiviruses expressing scrambled short hairpin RNA (shCon) and two independent shRNAs targeting METTL3 (shMETTL3-1 and shMETTL3-2). β-actin was used as a loading control. **(B)** m^{6}A ratio determined by LC-MS/MS in the control and METTL3 knockdown A498 cells. Error bars represent the standard deviation (SD) of three biological replicates. **(C,D)** Transwell assays of A498 and 786-O cells transduced with shRNAs targeting METTL3 **(C)** and METTL3-overexpressing virus **(D)** and quantitatively analyzed (right) (scale bar, 500 μm). EV, control empty virus; METTL3-OE, METTL3-expressing virus; METTL3-Mut, methyltransferase inactivated METTL3-expressing virus. Error bars represent the SD of the mean (n = 5). **(E)** Growth curves of xenograft tumors derived from shCon or shMETTL3-2 A498 cells. **(F)** Xenograft tumors formed by shCon or shMETTL3-2 A498 cells in nude mice. **(G)** Growth curves of xenograft tumors derived from A498 cells transduced with METTL3-expressing virus (METTL3-OE), METTL3-Mut-expressing virus (METTL3-Mut) and control empty virus (EV). Error bars represent the SD of the mean (n = 5). **(H)** Xenograft tumors formed by METTL3-OE, EV, or METTL3-Mut A498 cells in nude mice. $^*P < 0.05$, $^{**}P < 0.01$, $^{***}P < 0.001$.

and matched normal tissues from two ccRCC patients except the seven patients in **Figure 1** and **Supplementary Table 3**. In both the tumor tissues and the normal tissues of the two patients, m6A-seq analysis identified high overlapping 10,434–13,169 m^{6}A peaks from 7,038 to 8,214 m^{6}A-modified genes (**Supplementary Table 4**). Consistent with previous studies, the m^{6}A peaks were significantly enriched in the RGACH motif (R = G/A; H = A/C/U) (**Figure 4A**), and were abundant in coding regions (CDSs), 3′UTRs, and near stop codons in all the samples (**Figures 4B,C**). Then, to determine the biological relevance of m^{6}A modification in ccRCC tumorigenesis, we first overlapped the 5,952 m^{6}A genes shared in the normal tissues with the 5,988 modified genes shared in the tumor tissues as shown in **Figure 4D**. And the 1,180 m^{6}A genes that only existed in m^{6}A genes$_{Normal}$ group were regarded as the normal specific genes, while the 1,216 m^{6}A genes that only existed in m^{6}A genes$_{Tumor}$ group were considered as the tumor specific genes (**Figure 4D**). The representative tracks of normal or tumor m^{6}A specific genes were shown in **Figure 4E**. Interestingly, gene ontology (GO) enrichment analysis revealed that the 1,180 normal-specific m^{6}A genes were involved in maintenance of kidney function, such as kidney development, nephron epithelium development, and regulation of body fluid levels (**Figure 4F**). The GO terms of the 1,216 tumor-specific genes with m^{6}A peaks were multiple cancer-related pathways, such as immune-related pathways, regulation of GTPase activity and cell junction assembly (**Figure 4F**). To

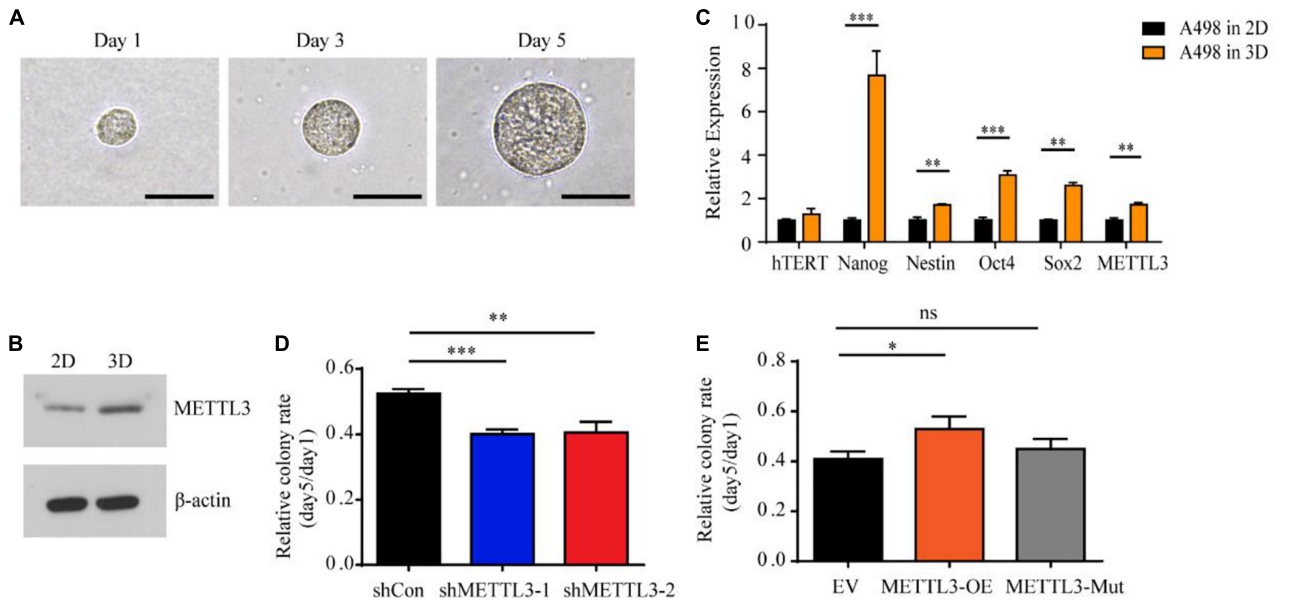

FIGURE 3 | Upregulation of stem cell-associated genes including METTL3 in A498 spheroid cells cultured in 3D fibrin gel. **(A)** A single A498 cell grew into a multicellular tumor spheroid within a 90 Pa 3D fibrin gel during the culture course from Day 1 to Day 5 (scale bar, 500 μm). **(B)** The protein level of METTL3 from A498 cells cultured in 2D rigid dishes or 90 Pa fibrin gels was examined by western blot. β-actin was used as a loading control. **(C)** Stem cell markers and hTERT expression in A498 cells were quantified by RT-qPCR. The same mRNA sample of A498 tumor spheroid cells was used as above. A498 cells cultured in 2D rigid dishes were used as controls. Mean ± SD, $^{*}p < 0.05$, compared with the 2D cells. **(D,E)** Sphere formation analysis of A498 cells transduced with METTL3-targeting virus **(D)** and METTL3-expressing virus **(E)**, normalized to the number of spheroid cells at day 1. Error bars represent the SD of the mean ($n = 3$). $^{**}P < 0.01$, $^{***}P < 0.001$.

test whether the change in m^{6}A modification level is correlated with the change in transcript level, we performed RNA-seq of the two patients (**Supplementary Figure 2A**). There were more downregulated genes in the tumor tissues than in the normal tissues (**Supplementary Table 5** and **Supplementary Figure 2B**). Intriguingly, the downregulated genes also showed significant enrichment in key pathways for maintenance of kidney function, and the upregulated genes showed enrichments in cancer-related pathways (**Supplementary Figures 2C,D**). We next examined whether the changes in transcript levels were correlated with the changes in m^{6}A modification. As shown in **Figure 4G**, we identified a positive correlation between the change in the m^{6}A modification level and that of the mRNA expression level. Thus, m^{6}A targets and transcripts showed dynamically controlled abundance during ccRCC tumorigenesis.

METTL3 Selectively Targets Genes Including Regulators of Fatty Acid Metabolism

To determine which of the deregulated m^{6}A modified transcripts could be direct targets of METTL3, we assessed the transcriptome-wide mRNAs with m^{6}A in the shCon and shMETTL3 ccRCC cells. Consistent with previous studies, the RGACH motif (R = G/A; H = A/C/U) was highly enriched within m^{6}A sites in both the shCon and shMETTL3 cells (**Figure 5A**). M^{6}A peaks in both groups were predominantly located in the CDS, stop codon and 3′UTR (**Figures 5B,C**). Compared to those in the shCon cells, genes with loss of m^{6}A peaks in the shMETTL3 cells were identified as candidate METTL3 targets (shCon-specific genes). In order to obtain the potential targets of METTL3, we overlapped the m^{6}A genes in the shCon group with those in the shMETTL3 group, and there were 583 m^{6}A genes which were only existed in the shCon group regarded as METTL3 targets (shCon-specific genes). As shown in **Figure 5D**, these potential METTL3 targets were significantly enriched in cancer-related terms including phosphate metabolism, mitochondrion organization, apoptosis and cellular response to stress. And some of them have been found to be targets of METTL3 in other studies such as SOCS1, GLI1, MAFA, and MGMT (Li H. B. et al., 2017; Cai et al., 2019; Wang et al., 2020; Shi et al., 2021). Next, we sought to determine whether the candidate METTL3 targets in the ccRCC cell line are relevant to ccRCC patients. Eighty out of 583 candidate METTL3 targets were preferentially methylated in the tumor tissues of ccRCC patients (**Figure 5E**). ConsensusPathDB (Kamburov et al., 2013; Herwig et al., 2016) network analysis of these 80 genes further found enrichment for multiple metabolic pathways, such as fatty acid beta-oxidation, fatty acid catabolic process, and ribonucleotide catabolic process (**Figure 5F** and **Supplementary Tables 6, 7**).

ABCD1 Is a Key Downstream Target of METTL3 in Clear Cell Renal Cell Carcinoma

Among the genes enriched in metabolic pathways, we focused on ABCD1, as ABCD1 was identified from multiple metabolic pathways in the ConsensusPathDB network analysis. ABCD1

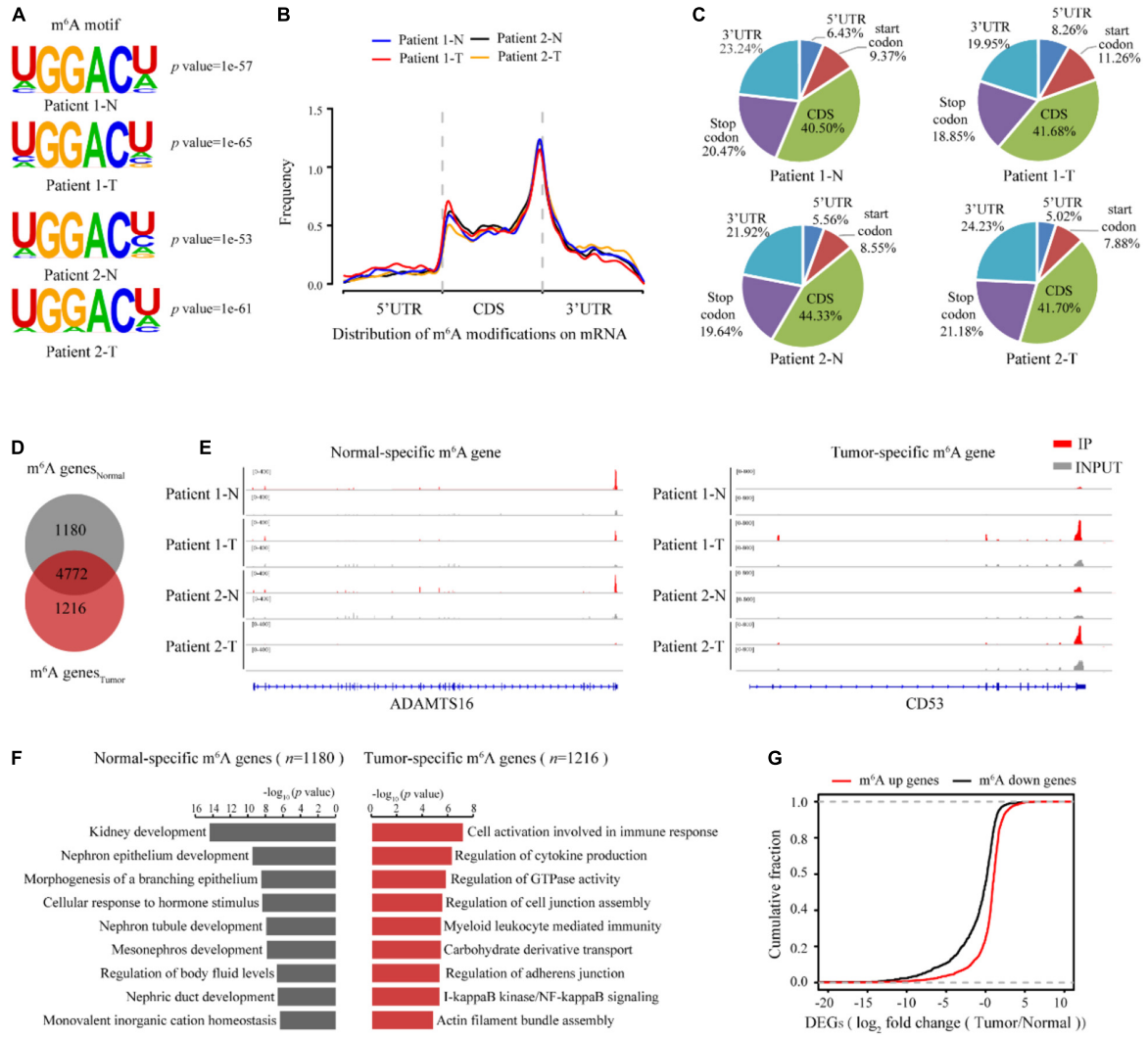

FIGURE 4 | m^{6}A methylomes are profoundly reprogrammed during ccRCC tumorigenesis. **(A)** The consensus motif identified from m^{6}A-seq peaks in the normal and ccRCC tissues. **(B)** The normalized distribution of m^{6}A peaks generated from the normal and tumor tissues across the mRNAs. **(C)** Pie chart of m^{6}A peak proportions in the indicated regions in the normal and tumor tissues. **(D)** Venn diagram of the m^{6}A-modified genes detected in the normal and tumor tissues. **(E)** Profile of IP and input reads of representative normal-specific and tumor-specific m^{6}A peaks in ADAMTS16 and CD53. Levels were normalized by the number of reads in the normal and tumor samples, and the values on the left side of the track represent the range of IP and input level. **(F)** GO pathway analysis of genes with normal-specific and tumor-specific m^{6}A modification. **(G)** Cumulative distribution for the gene expression changes between the normal and tumor tissues for upregulated m^{6}A methylation genes (red) and downregulated m^{6}A methylation genes (black).

is a member of the superfamily of ATP-binding cassette (ABC) transporters that is located in the human peroxisome membrane (Tanaka et al., 2002; Morita et al., 2006). As shown in **Figure 6A**, the m^{6}A-seq data demonstrated that the m^{6}A peak of ABCD1 in the 5′UTR was markedly increased in tumor tissues and diminished upon METTL3 knockdown in the A498 cells. We also confirmed that the m^{6}A abundance decreased after METTL3 knockdown by MeRIP-qPCR in the A498 cells (**Figure 6B**). However, we found that METTL3 knockdown did not significantly change the mRNA level of ABCD1 (**Figure 6C**). Since previous studies have found that m^{6}A modification in the 5′UTR could promote cap-independent translation (Meyer et al., 2015), we measured the protein level of ABCD1. Western blot assays showed that the protein level of ABCD1 decreased upon METTL3 knockdown (**Figure 6D**). To further confirm the reduced ABCD1 protein level is due to the methylation of specific sites, we performed single nucleotide resolution m^{6}A profiling (miCLIP–seq) of A498 cells and found the 7 m^{6}A motifs within the 5′UTR of ABCD1. We then cloned the ABCD1 5′UTR region, including wild-type (WT) or mutant (A-to-T mutation) m^{6}A sites into a luciferase reporter vector to identify the function of these m^{6}A motifs in the regulation of ABCD1 translation (**Figure 6E**). As shown in **Figure 6F**, the luciferase activity was increased in ABCD1 5′UTR wild-type but not in mutant samples. Additionally, knockdown of ABCD1 compromised both tumor migration and tumor sphere formation

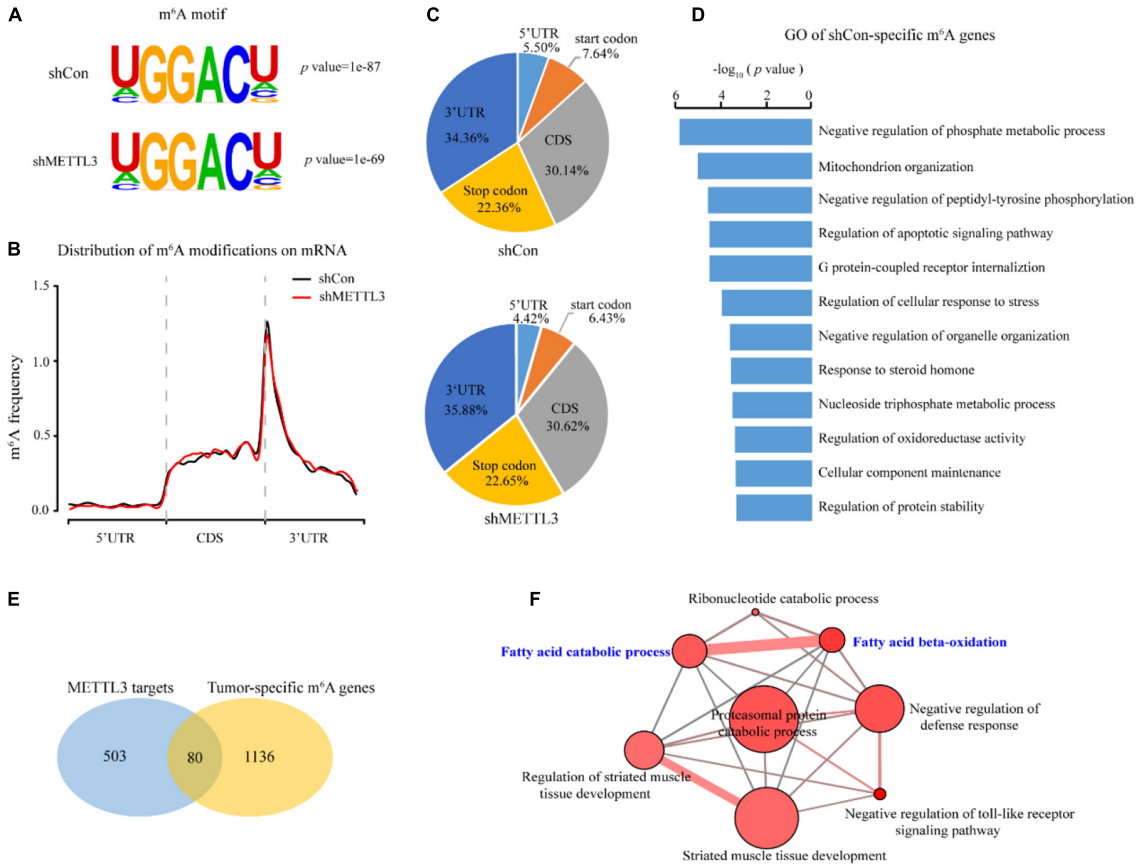

FIGURE 5 | Identification of METTL3 downstream targets in ccRCC. **(A)** Predominant consensus motif identified in the shCon and shMETTL3 A498 cells. **(B)** The normalized distribution of m^{6}A peaks across all mRNA transcripts after METTL3 knockdown. **(C)** The fractions of the m^{6}A peaks in the control and METTL3 knockdown A498 cells within the indicated regions. **(D)** GO pathway analysis of the candidate METTL3 targets in the ccRCC cell line. **(E)** Schematic of the selection for the downstream targets of METTL3 in the ccRCC cell lines and the ccRCC tissues. **(F)** CPDB analysis of 80 candidate targets. *P*-values were calculated according to Fisher's exact test, cutoff $p < 0.01$.

(**Figures 6G–I**), which was phenotypically similar to METTL3 knockdown. Moreover, by using TCGA ccRCC RNA-Seq data, we found patients with high ABCD1 expression were associated with poor overall survival (**Figure 6J**). These results demonstrated that both METTL3 and its downstream targets, such as ABCD1, have potential as therapeutic targets in ccRCC.

DISCUSSION

Paradoxically, the m^{6}A methyltransferase METTL3 was reported to have dual roles in cancer (Huang et al., 2020b), acting as an oncogene in AML (Barbieri et al., 2017), breast (Niu et al., 2019), and liver cancers (Chen et al., 2018), and as a tumor suppressor in glioblastoma (Cui et al., 2017) and endometrial cancers (Liu Y. et al., 2018). However, the direct role of METTL3 via an m^{6}A methyltransferase dependent manner in ccRCC remains unclear. Although there has been a report showing that METTL3 impairs ccRCC progression in Caki-1 and Caki-2 cell lines through epithelial to-mesenchymal transition (EMT) and PI3K-Akt-mTOR pathways (Li X. et al., 2017), other studies identified METTL3 predicts a poor overall survival of ccRCC patients in TCGA datasheet (Chen et al., 2020; Zheng et al., 2020), implying that METTL3 might be an oncogene. In our study, we revealed an important role of METTL3 in regulation of kidney cancer progression. Firstly, we found that the expression variance but not the mean expression level of METTL3 increased significantly during kidney tumorigenesis. Clinical data from TCGA showed that higher expression of METTL3 predicted poor prognosis in ccRCC patients which are consistent with the previously studies. Further functional studies showed that METTL3 was critical for maintaining stem cell-like tumorigenic cells in an m^{6}A-dependent manner. MeRIP-seq and GO analysis showed that the m^{6}A abundance of METTL3 targets related to metabolic processes is dynamically regulated during kidney tumorigenesis. In particular, ABCD1, an ABC transporter, was methylated in its 5′UTR. Consistent with recent findings (Meyer et al., 2015), we demonstrated that depletion of METTL3 decreased the m^{6}A methylation level in the 5′UTR of ABCD1 and reduced the protein level but not the mRNA level. To further demonstrate the regulation of ABCD1 translation efficiency is due to the methylation of specific sites,

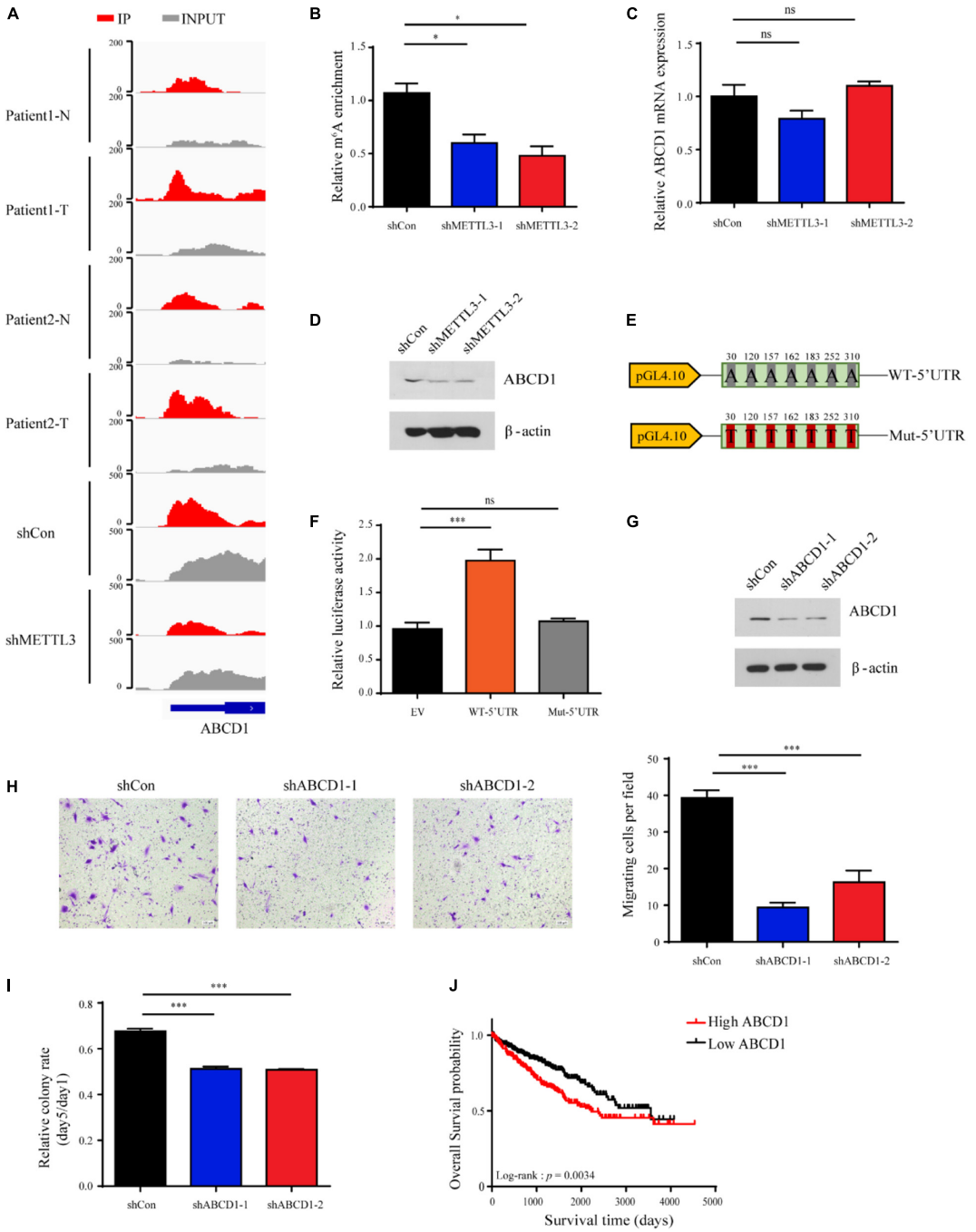

FIGURE 6 | ABCD1 is a key downstream target of METTL3 in ccRCC. **(A)** The read distribution in the 5′UTR of ABCD1 mRNA of the normal and tumor tissues, and the shCon and shMETTL3 A498 cells. The values on the left side of the track represent the range of normalized IP and input levels. **(B)** m^{6}A enrichment in the 5′UTR of ABCD1 mRNA in the METTL3 knockdown A498 cells verified by MeRIP-qPCR. Error bars represent the SD of the mean. **(C)** ABCD1 mRNA expression levels in the shCon and shMETTL3 A498 cells verified by RT-qPCR. Error bars represent the SD of the mean. **(D)** ABCD1 protein levels upon knockdown of METTL3 in A498 cells determined by western blotting. β-actin was used as a loading control. **(E)** pGL4.10 luciferase reporter constructs containing fragments of the human ABCD1 5′UTR with wild-type m^{6}A sites (WT-5′UTR) or mutant (A-to-T mutation) m^{6}A sites (Mut-5′UTR) are shown. The position of the m^{6}A sites is numbered relative to the first nucleotide of the 5′UTR. **(F)** Relative luciferase activity in control constructs (EV) or constructs containing the wild-type 5′UTR of ABCD1 (WT-5′UTR) or mutant m^{6}A sites of ABCD1 (Mut-5′UTR). Firefly luciferase activity for each construct was first normalized to the co-transfected Renilla luciferase construct and then normalized to the control constructs (EV). **(G)** Western blot of ABCD1 in the A498 cells transduced with lentiviruses expressing scrambled short hairpin RNA (shCon) and two independent shRNAs targeting ABCD1 (shABCD-1 and shABCD1-2). β-actin was used as a loading control. **(H)** (left) and quantitatively analyzed (right) (scale bar, 500 μm). Error bars represent (SD) three biological replicates. **(I)** Sphere-formation analysis of A498 cells transduced with ABCD1-targeting virus, normalized to the number of spheroid cells on day 1. Error bars represent the SD of the mean (n = 3). **(J)** Kaplan-Meier survival curves of ccRCC patients based on ABCD1 mRNA expression in TCGA database. Patients were assigned to two subgroups according to the median ABCD1 mRNA expression (log-rank test). *P < 0.05, ***P < 0.001.

we performed miCLIP-seq and found 7 m^6A sites in ABCD1 5′UTR. Mutation of these m^6A sites in the 5′UTR of ABCD1 has no effect on translation efficiency, but the wild-type one increased the reporter protein level. These results suggested that METTL3 promoted kidney tumorigenesis through enhancing of ABCD1 translation in an m^6A dependent manner, providing an epitranscriptional insight into the mechanism of kidney cancer progression.

N6-methyladenosine modification could affect the fate of the modified coding and non-coding RNAs in almost all vital bioprocesses, including cancer promotion and progression (Barros-Silva et al., 2020; Huang et al., 2020b; Yang et al., 2020). This study uncovered the crosstalk between complex cancer-associated metabolic reprogramming and epitranscriptomics in kidney cancer. Previous studies including ours have shown that the oncometabolite R-2-hydroxyglutarate (R-2HG) accumulates at high concentrations in ccRCC (Shim et al., 2014; Chen et al., 2016). R-2HG acts as a competitive inhibitor of α-ketoglutarate (α-KG), binding to the active sites of specific enzymes such as α-KG-dependent dioxygenases including DNA "erasers" (TETs) and histone modifiers (Xu et al., 2011) as well as m^6A "eraser" (FTO and ALKBH5) (Thalhammer et al., 2011; Su et al., 2018). Thus, the m^6A modification level of the transcripts is susceptible to changes in the concentrations of metabolites and/or oncometabolites. Additionally, the genes with m^6A modifications are crucial regulators of cell metabolic pathways such as glycolysis, mitochondrial respiratory chain complex activity, and hypoxia. We found that METTL3 selectively targets multiple genes involved in cell metabolism, such as ABCD1. ABCD1 plays a role in the biosynthesis of fatty acids by beta-oxidation and mitochondrial function (van Roermund et al., 2011; Baarine et al., 2015). Morphologically, ccRCC cells show high levels of lipids and glycogens (Gebhard et al., 1987), indicating altered fatty acid and glucose metabolism in the development of ccRCC. Cell-based assays demonstrated that reductive carboxylation of glutamine generates citrate needed for the growth of mitochondrion-defective tumor cells (Metallo et al., 2011; Mullen et al., 2011), and reductive carboxylation of α-KG to citrate for cell growth can be promoted by hypoxia and HIF1 (Wise et al., 2011). Collectively, the crosstalk between cancer-related metabolic reprogramming and m^6A modifications has a critical role in kidney tumorigenesis.

DATA AVAILABILITY STATEMENT

The data used in this study can be accessed from the National Genomics Data Center, Beijing Institute of Genomics, Chinese Academy of Sciences, under accession numbers HRA000258 and HRA000259 that are accessible at http://bigd.big.ac.cn/gsa-human.

ETHICS STATEMENT

The studies involving human participants were reviewed and approved by the Ethics Committee of Peking University First Hospital. The patients/participants provided their written informed consent to participate in this study. The animal study was reviewed and approved by Ethics Committee of the Beijing Institute of Genomics, Chinese Academy of Sciences.

AUTHOR CONTRIBUTIONS

WC supervised and conceptualized the study. YS and YD performed most of the experiments and bioinformatics analysis. JZ and JQ participated in bioinformatics and statistical analyses. MZ, ZX, and YX were responsible for clinical sample collection and analyses. YS and WC wrote the manuscript. All authors have read and approved the final manuscript.

FUNDING

This work was supported by the CAS Strategic Priority Research Program (XDA16010102 to WC), National Key R&D Program of China (2018YFC2000100 and 2019YFA0110900 to WC), and National Natural Science Foundation of China (31800695 to YS).

ACKNOWLEDGMENTS

We acknowledge Yungui Yang and Ying Yang for their guidance in m^6A-associated experiments. We also appreciate Yusheng Chen for his kind technical support in the bioinformatic analysis.

SUPPLEMENTARY MATERIAL

The Supplementary Material for this article can be found online at: https://www.frontiersin.org/articles/10.3389/fcell.2021.737498/full#supplementary-material

Supplementary Figure 1 | METTL3 promotes ccRCC progression related to **Figure 2**. **(A)** Bar plotting showing the m^6A level in total RNA in the control and METTL3 knockdown cells by using m^6A ELISA assay. Error bars represent the SD of three replicates. **(B)** Cell viability of A498 and 786-O cells transduced with shRNAs targeting METTL3. **(C)** Cell invasion assays of A498 and 786-O cells transduced with shRNAs targeting METTL3 (scale bar, 500 μm), and quantitatively analyzed (right), Error bars represent the SD of the mean. $^*P < 0.05$, $^{***}P < 0.001$.

Supplementary Figure 2 | Gene expression analysis of normal and ccRCC tissues related to **Figure 4**. **(A)** Heatmap showing the correlation of RNA-seq data between normal and ccRCC tissues from the 2 patients. **(B)** The volcano plot of the differentially expressed genes (DEGs) between the normal and ccRCC tissues. **(C,D)** GO pathway analysis of the upregulated genes **(C)** and the downregulated genes **(D)** in the ccRCC tissues.

Supplementary Table 1 | Sequences of the primers used in this study.

Supplementary Table 2 | Antibodies used in this study.

Supplementary Table 3 | MeRIP-seq statistics in this work.

Supplementary Table 4 | m^6A-modified gene summary of the two patients in this study.

Supplementary Table 5 | Differentially expressed gene summary of the two patients in this work.

Supplementary Table 6 | List of the 80 candidates in this work.

Supplementary Table 7 | CPDB analysis results of the 80 candidates in this work.

REFERENCES

Aguilo, F., Zhang, F., Sancho, A., Fidalgo, M., Di Cecilia, S., Vashisht, A., et al. (2015). Coordination of m(6)A mRNA methylation and gene transcription by ZFP217 regulates pluripotency and reprogramming. *Cell Stem Cell* 17, 689–704. doi: 10.1016/j.stem.2015.09.005

Baarine, M., Beeson, C., Singh, A., and Singh, I. (2015). ABCD1 deletion-induced mitochondrial dysfunction is corrected by SAHA: implication for adrenoleukodystrophy. *J. Neurochem.* 133, 380–396. doi: 10.1111/jnc.12992

Barbieri, I., Tzelepis, K., Pandolfini, L., Shi, J., Millan-Zambrano, G., Robson, S. C., et al. (2017). Promoter-bound METTL3 maintains myeloid leukaemia by m(6)A-dependent translation control. *Nature* 552, 126–131. doi: 10.1038/nature24678

Barros-Silva, D., Lobo, J., Guimaraes-Teixeira, C., Carneiro, I., Oliveira, J., Martens-Uzunova, E. S., et al. (2020). VIRMA-dependent N6-methyladenosine modifications regulate the expression of long non-coding RNAs CCAT1 and CCAT2 in prostate cancer. *Cancers* 12:771. doi: 10.3390/cancers12040771

Bokar, J. A., Shambaugh, M. E., Polayes, D., Matera, A. G., and Rottman, F. M. (1997). Purification and cDNA cloning of the AdoMet-binding subunit of the human mRNA (N6-adenosine)-methyltransferase. *RNA* 3, 1233–1247.

Bray, F., Ferlay, J., Soerjomataram, I., Siegel, R. L., Torre, L. A., and Jemal, A. (2018). Global cancer statistics 2018: GLOBOCAN estimates of incidence and mortality worldwide for 36 cancers in 185 countries. *CA Cancer J. Clin.* 68, 394–424. doi: 10.3322/caac.21492

Brown, C. E. (1998). *Applied Multivariate Statistics In Geohydrology and Related Sciences*. New York: Springer, 248.

Cai, J., Yang, F., Zhan, H., Situ, J., Li, W., Mao, Y., et al. (2019). RNA m(6)A Methyltransferase METTL3 promotes the growth of prostate cancer by regulating hedgehog pathway. *Onco Targets Ther.* 12, 9143–9152. doi: 10.2147/OTT.S226796

Cancer Genome Atlas Research Network (2013). Comprehensive molecular characterization of clear cell renal cell carcinoma. *Nature* 499, 43–49. doi: 10.1038/nature12222

Chen, J., Yu, K., Zhong, G., and Shen, W. (2020). Identification of a m(6)A RNA methylation regulators-based signature for predicting the prognosis of clear cell renal carcinoma. *Cancer Cell Int.* 20:157. doi: 10.1186/s12935-020-01238-3

Chen, K., Lu, Z., Wang, X., Fu, Y., Luo, G. Z., Liu, N., et al. (2015). High-resolution N(6) -methyladenosine (m(6) A) map using photo-crosslinking-assisted m(6) A sequencing. *Angew. Chem.* 54, 1587–1590. doi: 10.1002/anie.201410647

Chen, K., Zhang, J., Guo, Z., Ma, Q., Xu, Z., Zhou, Y., et al. (2016). Loss of 5-hydroxymethylcytosine is linked to gene body hypermethylation in kidney cancer. *Cell Res.* 26, 103–118. doi: 10.1038/cr.2015.150

Chen, M., Wei, L., Law, C. T., Tsang, F. H., Shen, J., Cheng, C. L., et al. (2018). RNA N6-methyladenosine methyltransferase-like 3 promotes liver cancer progression through YTHDF2-dependent posttranscriptional silencing of SOCS2. *Hepatology* 67, 2254–2270. doi: 10.1002/hep.29683

Cheng, M., Sheng, L., Gao, Q., Xiong, Q., Zhang, H., Wu, M., et al. (2019). The m(6)A methyltransferase METTL3 promotes bladder cancer progression via AFF4/NF-kappaB/MYC signaling network. *Oncogene* 38, 3667–3680. doi: 10.1038/s41388-019-0683-z

Cui, Q., Shi, H., Ye, P., Li, L., Qu, Q., Sun, G., et al. (2017). m(6)A RNA methylation regulates the self-renewal and tumorigenesis of glioblastoma stem cells. *Cell Rep.* 18, 2622–2634. doi: 10.1016/j.celrep.2017.02.059

Dalgliesh, G. L., Furge, K., Greenman, C., Chen, L., Bignell, G., Butler, A., et al. (2010). Systematic sequencing of renal carcinoma reveals inactivation of histone modifying genes. *Nature* 463, 360–363. doi: 10.1038/nature08672

Du, H., Zhao, Y., He, J., Zhang, Y., Xi, H., Liu, M., et al. (2016). YTHDF2 destabilizes m(6)A-containing RNA through direct recruitment of the CCR4-NOT deadenylase complex. *Nat. Commun.* 7:12626. doi: 10.1038/ncomms12626

Fu, Y., Dominissini, D., Rechavi, G., and He, C. (2014). Gene expression regulation mediated through reversible m(6)A RNA methylation. *Nat. Rev. Genet.* 15, 293–306. doi: 10.1038/nrg3724

Gebhard, R. L., Clayman, R. V., Prigge, W. F., Figenshau, R., Staley, N. A., Reesey, C., et al. (1987). Abnormal cholesterol metabolism in renal clear cell carcinoma. *J. Lipid Res.* 28, 1177–1184.

Herwig, R., Hardt, C., Lienhard, M., and Kamburov, A. (2016). Analyzing and interpreting genome data at the network level with ConsensusPathDB. *Nat. Protoc.* 11, 1889–1907. doi: 10.1038/nprot.2016.117

Hsieh, J. J., Purdue, M. P., Signoretti, S., Swanton, C., Albiges, L., Schmidinger, M., et al. (2017). Renal cell carcinoma. *Nat. Rev. Dis. Prim.* 3:17009. doi: 10.1038/nrdp.2017.9

Hsu, P. J., Zhu, Y., Ma, H., Guo, Y., Shi, X., Liu, Y., et al. (2017). Ythdc2 is an N(6)-methyladenosine binding protein that regulates mammalian spermatogenesis. *Cell Res.* 27, 1115–1127. doi: 10.1038/cr.2017.99

Huang, H., Weng, H., and Chen, J. (2020a). The biogenesis and precise control of RNA m(6)A methylation. *Trends Genet.* 36, 44–52. doi: 10.1016/j.tig.2019.10.011

Huang, H., Weng, H., and Chen, J. (2020b). m(6)A modification in coding and non-coding RNAs: roles and therapeutic implications in cancer. *Cancer Cell* 37, 270–288. doi: 10.1016/j.ccell.2020.02.004

Jaakkola, P., Mole, D. R., Tian, Y. M., Wilson, M. I., Gielbert, J., Gaskell, S. J., et al. (2001). Targeting of HIF-alpha to the von Hippel-Lindau ubiquitylation complex by O2-regulated prolyl hydroxylation. *Science* 292, 468–472. doi: 10.1126/science.1059796

Jia, G., Fu, Y., Zhao, X., Dai, Q., Zheng, G., Yang, Y., et al. (2011). N6-methyladenosine in nuclear RNA is a major substrate of the obesity-associated FTO. *Nat. Chem. Biol.* 7, 885–887. doi: 10.1038/nchembio.687

Kamburov, A., Stelzl, U., Lehrach, H., and Herwig, R. (2013). The ConsensusPathDB interaction database: 2013 update. *Nucleic Acids Res.* 41, D793–D800. doi: 10.1093/nar/gks1055

Kapitsinou, P. P., and Haase, V. H. (2008). The VHL tumor suppressor and HIF: insights from genetic studies in mice. *Cell Death Differ.* 15, 650–659. doi: 10.1038/sj.cdd.4402313

Lan, Q., Liu, P. Y., Haase, J., Bell, J. L., Huttelmaier, S., and Liu, T. (2019). The critical role of RNA m(6)A methylation in cancer. *Cancer Res.* 79, 1285–1292. doi: 10.1158/0008-5472.CAN-18-2965

Lee, H., Bao, S., Qian, Y., Geula, S., Leslie, J., Zhang, C., et al. (2019). Stage-specific requirement for Mettl3-dependent m(6)A mRNA methylation during haematopoietic stem cell differentiation. *Nat. Cell Biol.* 21, 700–709. doi: 10.1038/s41556-019-0318-1

Li, H. B., Tong, J., Zhu, S., Batista, P. J., Duffy, E. E., Zhao, J., et al. (2017). m(6)A mRNA methylation controls T cell homeostasis by targeting the IL-7/STAT5/SOCS pathways. *Nature* 548, 338–342. doi: 10.1038/nature23450

Li, X., Tang, J., Huang, W., Wang, F., Li, P., Qin, C., et al. (2017). The M6A methyltransferase METTL3: acting as a tumor suppressor in renal cell carcinoma. *Oncotarget* 8, 96103–96116. doi: 10.18632/oncotarget.21726

Linder, B., Grozhik, A. V., Olarerin-George, A. O., Meydan, C., Mason, C. E., and Jaffrey, S. R. (2015). Single-nucleotide-resolution mapping of m6A and m6Am throughout the transcriptome. *Nat. Methods* 12, 767–772. doi: 10.1038/nmeth.3453

Liu, J., Dou, X., Chen, C., Chen, C., Liu, C., Xu, M. M., et al. (2020). N (6)-methyladenosine of chromosome-associated regulatory RNA regulates chromatin state and transcription. *Science* 367, 580–586. doi: 10.1126/science.aay6018

Liu, J., Eckert, M. A., Harada, B. T., Liu, S. M., Lu, Z., Yu, K., et al. (2018). m(6)A mRNA methylation regulates AKT activity to promote the proliferation and tumorigenicity of endometrial cancer. *Nat. Cell Biol.* 20, 1074–1083. doi: 10.1038/s41556-018-0174-4

Liu, J., Tan, Y., Zhang, H., Zhang, Y., Xu, P., Chen, J., et al. (2012). Soft fibrin gels promote selection and growth of tumorigenic cells. *Nat. Mater.* 11, 734–741. doi: 10.1038/nmat3361

Liu, J., Yue, Y., Han, D., Wang, X., Fu, Y., Zhang, L., et al. (2014). A METTL3-METTL14 complex mediates mammalian nuclear RNA N6-adenosine methylation. *Nat. Chem. Biol.* 10, 93–95. doi: 10.1038/nchembio.1432

Liu, Y., Liang, X., Dong, W., Fang, Y., Lv, J., Zhang, T., et al. (2018). Tumor-repopulating cells induce PD-1 expression in CD8(+) T cells by transferring kynurenine and AhR activation. *Cancer Cell* 33, 480–494.e7. doi: 10.1016/j.ccell.2018.02.005

Maxwell, P. H., Wiesener, M. S., Chang, G. W., Clifford, S. C., Vaux, E. C., Cockman, M. E., et al. (1999). The tumour suppressor protein VHL targets hypoxia-inducible factors for oxygen-dependent proteolysis. *Nature* 399, 271–275. doi: 10.1038/20459

Metallo, C. M., Gameiro, P. A., Bell, E. L., Mattaini, K. R., Yang, J., Hiller, K., et al. (2011). Reductive glutamine metabolism by IDH1 mediates lipogenesis under hypoxia. *Nature* 481, 380–384. doi: 10.1038/nature10602

Meyer, K. D., Patil, D. P., Zhou, J., Zinoviev, A., Skabkin, M. A., Elemento, O., et al. (2015). 5′ UTR m(6)A promotes cap-independent translation. *Cell* 163, 999–1010. doi: 10.1016/j.cell.2015.10.012

Morita, M., Kurisu, M., Kashiwayama, Y., Yokota, S., and Imanaka, T. A. T. P. - (2006). binding and -hydrolysis activities of ALDP (ABCD1) and ALDRP (ABCD2), human peroxisomal ABC proteins, overexpressed in Sf21 cells. *Biol. Pharmaceut. Bull.* 29, 1836–1842. doi: 10.1248/bpb.29.1836

Mullen, A. R., Wheaton, W. W., Jin, E. S., Chen, P. H., Sullivan, L. B., Cheng, T., et al. (2011). Reductive carboxylation supports growth in tumour cells with defective mitochondria. *Nature* 481, 385–388. doi: 10.1038/nature10642

Niu, Y., Lin, Z., Wan, A., Chen, H., Liang, H., Sun, L., et al. (2019). RNA N6-methyladenosine demethylase FTO promotes breast tumor progression through inhibiting BNIP3. *Mol. Cancer* 18:46. doi: 10.1186/s12943-019-1004-4

Ping, X. L., Sun, B. F., Wang, L., Xiao, W., Yang, X., Wang, W. J., et al. (2014). Mammalian WTAP is a regulatory subunit of the RNA N6-methyladenosine methyltransferase. *Cell Res.* 24, 177–189. doi: 10.1038/cr.2014.3

Rankin, E. B., Tomaszewski, J. E., and Haase, V. H. (2006). Renal cyst development in mice with conditional inactivation of the von Hippel-Lindau tumor suppressor. *Cancer Res.* 66, 2576–2583. doi: 10.1158/0008-5472.CAN-05-3241

Roundtree, I. A., Evans, M. E., Pan, T., and He, C. (2017). Dynamic RNA modifications in gene expression regulation. *Cell* 169, 1187–1200. doi: 10.1016/j.cell.2017.05.045

Schwartz, S., Mumbach, M. R., Jovanovic, M., Wang, T., Maciag, K., Bushkin, G. G., et al. (2014). Perturbation of m6A writers reveals two distinct classes of mRNA methylation at internal and 5′ sites. *Cell Rep.* 8, 284–296. doi: 10.1016/j.celrep.2014.05.048

Shi, J., Chen, G., Dong, X., Li, H., Li, S., Cheng, S., et al. (2021). METTL3 promotes the resistance of glioma to temozolomide via increasing MGMT and ANPG in a m(6)A dependent manner. *Front. Oncol.* 11:702983. doi: 10.3389/fonc.2021.702983

Shim, E. H., Livi, C. B., Rakheja, D., Tan, J., Benson, D., Parekh, V., et al. (2014). L-2-Hydroxyglutarate: an epigenetic modifier and putative oncometabolite in renal cancer. *Cancer Discov.* 4, 1290–1298. doi: 10.1158/2159-8290.CD-13-0696

Su, R., Dong, L., Li, C., Nachtergaele, S., Wunderlich, M., Qing, Y., et al. (2018). R-2HG exhibits anti-tumor activity by targeting FTO/m(6)A/MYC/CEBPA signaling. *Cell* 172, 90.e23–105.e23. doi: 10.1016/j.cell.2017.11.031

Tanaka, A. R., Tanabe, K., Morita, M., Kurisu, M., Kasiwayama, Y., Matsuo, M., et al. (2002). ATP binding/hydrolysis by and phosphorylation of peroxisomal ATP-binding cassette proteins PMP70 (ABCD3) and adrenoleukodystrophy protein (ABCD1). *J. Biol. Chem.* 277, 40142–40147. doi: 10.1074/jbc.M205079200

Thalhammer, A., Bencokova, Z., Poole, R., Loenarz, C., Adam, J., O'Flaherty, L., et al. (2011). Human AlkB homologue 5 is a nuclear 2-oxoglutarate dependent oxygenase and a direct target of hypoxia-inducible factor 1alpha (HIF-1alpha). *PLoS One* 6:e16210. doi: 10.1371/journal.pone.0016210

van Roermund, C. W., Visser, W. F., Ijlst, L., Waterham, H. R., and Wanders, R. J. (2011). Differential substrate specificities of human ABCD1 and ABCD2 in peroxisomal fatty acid beta-oxidation. *Biochim. Biophys. Acta* 1811, 148–152. doi: 10.1016/j.bbalip.2010.11.010

Vu, L. P., Pickering, B. F., Cheng, Y., Zaccara, S., Nguyen, D., Minuesa, G., et al. (2017). The N(6)-methyladenosine (m(6)A)-forming enzyme METTL3 controls myeloid differentiation of normal hematopoietic and leukemia cells. *Nat. Med.* 23, 1369–1376. doi: 10.1038/nm.4416

Wang, Y., Sun, J., Lin, Z., Zhang, W., Wang, S., Wang, W., et al. (2020). m(6)A mRNA methylation controls functional maturation in neonatal murine beta-cells. *Diabetes* 69, 1708–1722. doi: 10.2337/db19-0906

Wanna-Udom, S., Terashima, M., Lyu, H., Ishimura, A., Takino, T., Sakari, M., et al. (2020). The m6A methyltransferase METTL3 contributes to transforming growth factor-beta-induced epithelial-mesenchymal transition of lung cancer cells through the regulation of JUNB. *Biochem. Biophys. Res. Commun.* 524, 150–155. doi: 10.1016/j.bbrc.2020.01.042

Wise, D. R., Ward, P. S., Shay, J. E., Cross, J. R., Gruber, J. J., Sachdeva, U. M., et al. (2011). Hypoxia promotes isocitrate dehydrogenase-dependent carboxylation of alpha-ketoglutarate to citrate to support cell growth and viability. *Proc. Natl Acad. Sci. U.S.A.* 108, 19611–19616. doi: 10.1073/pnas.1117773108

Xiao, W., Adhikari, S., Dahal, U., Chen, Y. S., Hao, Y. J., Sun, B. F., et al. (2016). Nuclear m(6)A reader YTHDC1 regulates mRNA splicing. *Mol. Cell* 61, 507–519. doi: 10.1016/j.molcel.2016.01.012

Xu, K., Yang, Y., Feng, G. H., Sun, B. F., Chen, J. Q., Li, Y. F., et al. (2017). Mettl3-mediated m(6)A regulates spermatogonial differentiation and meiosis initiation. *Cell Res.* 27, 1100–1114. doi: 10.1038/cr.2017.100

Xu, W., Yang, H., Liu, Y., Yang, Y., Wang, P., Kim, S. H., et al. (2011). Oncometabolite 2-hydroxyglutarate is a competitive inhibitor of alpha-ketoglutarate-dependent dioxygenases. *Cancer Cell* 19, 17–30. doi: 10.1016/j.ccr.2010.12.014

Yang, X., Liu, Q. L., Xu, W., Zhang, Y. C., Yang, Y., Ju, L. F., et al. (2019). m(6)A promotes R-loop formation to facilitate transcription termination. *Cell Res.* 29, 1035–1038. doi: 10.1038/s41422-019-0235-7

Yang, X., Zhang, S., He, C., Xue, P., Zhang, L., He, Z., et al. (2020). METTL14 suppresses proliferation and metastasis of colorectal cancer by down-regulating oncogenic long non-coding RNA XIST. *Mol. Cancer* 19:46. doi: 10.1186/s12943-020-1146-4

Zhang, Z., Wang, M., Xie, D., Huang, Z., Zhang, L., Yang, Y., et al. (2018). METTL3-mediated N(6)-methyladenosine mRNA modification enhances long-term memory consolidation. *Cell Res.* 28, 1050–1061. doi: 10.1038/s41422-018-0092-9

Zheng, G., Dahl, J. A., Niu, Y., Fedorcsak, P., Huang, C. M., Li, C. J., et al. (2013). ALKBH5 is a mammalian RNA demethylase that impacts RNA metabolism and mouse fertility. *Mol. Cell* 49, 18–29. doi: 10.1016/j.molcel.2012.10.015

Zheng, Z., Mao, S., Guo, Y., Zhang, W., Liu, J., Li, C., et al. (2020). N6methyladenosine RNA methylation regulators participate in malignant progression and have prognostic value in clear cell renal cell carcinoma. *Oncol. Rep.* 43, 1591–1605. doi: 10.3892/or.2020.7524

Zhou, J., Wang, J., Hong, B., Ma, K., Xie, H., Li, L., et al. (2019). Gene signatures and prognostic values of m6A regulators in clear cell renal cell carcinoma - a retrospective study using TCGA database. *Aging* 11, 1633–1647. doi: 10.18632/aging.101856

Zhou, Y., Zhou, B., Pache, L., Chang, M., Khodabakhshi, A. H., Tanaseichuk, O., et al. (2019). Metascape provides a biologist-oriented resource for the analysis of systems-level datasets. *Nat. Commun.* 10:1523. doi: 10.1038/s41467-019-09234-6

Conflict of Interest: The authors declare that the research was conducted in the absence of any commercial or financial relationships that could be construed as a potential conflict of interest.

Publisher's Note: All claims expressed in this article are solely those of the authors and do not necessarily represent those of their affiliated organizations, or those of the publisher, the editors and the reviewers. Any product that may be evaluated in this article, or claim that may be made by its manufacturer, is not guaranteed or endorsed by the publisher.

Advantages of publishing in Frontiers

OPEN ACCESS
Articles are free to read for greatest visibility and readership

FAST PUBLICATION
Around 90 days from submission to decision

HIGH QUALITY PEER-REVIEW
Rigorous, collaborative, and constructive peer-review

TRANSPARENT PEER-REVIEW
Editors and reviewers acknowledged by name on published articles

Frontiers
Avenue du Tribunal-Fédéral 34
1005 Lausanne | Switzerland

Visit us: www.frontiersin.org
Contact us: frontiersin.org/about/contact

REPRODUCIBILITY OF RESEARCH
Support open data and methods to enhance research reproducibility

DIGITAL PUBLISHING
Articles designed for optimal readership across devices

FOLLOW US
@frontiersin

IMPACT METRICS
Advanced article metrics track visibility across digital media

EXTENSIVE PROMOTION
Marketing and promotion of impactful research

LOOP RESEARCH NETWORK
Our network increases your article's readership